TECHNISCHE UNIVERSITÄT MÜNCHEN
TUM School of Engineering and Design

Agricultural irrigation demand modelling and assessment of membrane ultrafiltration alone or hybridized with inline dosed powdered activated carbon for non-potable water reuse applications

Christoph Johann Schwaller

Vollständiger Abdruck der von der TUM School of Engineering and Design der Technischen Universität München zur Erlangung des akademischen Grades eines

Doktors der Ingenieurwissenschaft (Dr.-Ing.)

genehmigten Dissertation.

Vorsitzende:	Prof. Dr. Sonja Berensmeier
Prüfer der Dissertation:	1. Prof. Dr.-Ing. Jörg E. Drewes 2. Prof. Dr. Tzahi Y. Cath, Colorado School of Mines, USA 3. apl. Prof. Dr. rer. nat. habil. Brigitte Helmreich

Die Dissertation wurde am 27.07.2022 bei der Technischen Universität München eingereicht und durch die TUM School of Engineering and Design am 07.12.2022 angenommen.

Qui putat se aliquid esse, aliquid assequi desiit

Sokrates

ABSTRACT

Climate change will have a drastic impact on our already overexploited freshwater resources. The rapid increase in global population, urbanization, changes in land use and increasing industrialization, especially in the agricultural sector, have resulted that half of the global freshwater resources are already being used by humans. On a global scale, the agricultural sector consumes 70 % of all freshwater resources accessible to humans and by 2030 it is projected that global water consumption will exceed availability by 40 %. Enormous use conflicts in the water sector will be the result of the associated gap in the water supply. In order to alleviate water scarcity and conflicts due to competing needs between the drinking water sector, agriculture and the energy sector, water must be managed much more efficiently and sustainably. The motto is '*from a linear water management to a paradigm of circular water management*'. Particularly, the reuse of water could represent an important solution and water reuse is already part of the 17 Sustainable Development Goals (SDG 6). In particular, through increased efficiency and water recycling in agriculture, substantial amounts of conventional water resources (groundwater and surface water) could be saved and preserved for purposes such as drinking water supply. However, water recycling, i.e. the reclamation and subsequent reuse of water, is coupled with a number of challenges: What is the demand to be met, what quality requirements must be fulfilled, what are the associated costs, what are suitable operator models, where are the responsibilities defined, how is the legal framework designed, and how is public acceptance gained? In the context of this thesis, two of the aforementioned challenges were addressed:

For the planning and implementation of non-potable water reuse projects for agricultural purposes a comprehensive understanding of the irrigation demand is required. However, this information is frequently not readily available. Thus, a modeling approach based on the CROPWAT software was adapted and further developed, with which the plant-specific agricultural irrigation demand could be calculated. Based on this, the daily, monthly and annual peak demand for a complete agricultural region in Lower Franconia (Gochsheim) could be computed. In particular, the daily peak demand is an essential planning variable for water reuse projects and was an important part of a concept study that was elaborated for the region around Schweinfurt in Lower Franconia, Germany.

Secondly, a treatment strategy was conceptualized and implemented that is likely to meet the existing and future quality requirements for water reuse in Germany for agricultural purposes. Both, the microbial (e.g. viruses, bacteria, protozoa) as well as physicochemical water quality (e.g. salinity, heavy metals, trace organic chemicals such

as pharmaceuticals or industrial chemicals) has to be sufficient for a safe agricultural and urban irrigation applications: Ceramic or polymeric membrane ultrafiltration combined with powdered activated carbon was identified as a promising treatment approach to produce an adequate water quality. For a compact implementation, the powdered activated carbon was dosed inline prior to the membrane.

As part of this second section of the present thesis, it was initially examined which factors influenced the removal performance of MS2 phages, antibiotic resistance genes (ARGs) or bacteria when ultrafiltration alone was employed. The removal efficiency of viruses such as MS2 phages strongly depends on operational parameters, such as flux and transmembrane pressure (TMP) conditions during ultrafiltration. Hence, within a laboratory-scale study effects of varying flux and TMP conditions during ceramic ultrafiltration on the infectivity and retention of MS2 bacteriophages were investigated. The laboratory-scale study showed that the retention of MS2 phage increased with increasing membrane fluxes. Presumably, increasing concentration polarization led to increased aggregation and thus to improved size exclusion of MS2 phages. Within the laboratory-scale study it could also be shown that despite high flux or TMPs the infectivity of the MS2 phages was not impaired.

Within the pilot-scale study low-pressure membrane filtration was investigated with regard to its removal performance of ARGs (sul1, ermB, vanA) present in the effluent after conventional secondary wastewater treatment. Key operational parameters influencing ARG removal during ultrafiltration were examined. Special focus was laid on the effects of initial ARG concentrations and the formation of a ‘fouling layer’ on the removal performance of a polymeric ultrafiltration membrane. Increased ARG concentrations in the ultrafiltration permeate were found at increased ARG concentrations in the feed water. Moreover, the results revealed that the fouling layer forming during ultrafiltration acted as an additional barrier against some ARGs (such as vanA), while for some other ARGs (such as sul1 and ermB) no significant effects were observed. Surprisingly, in the context of the pilot-study, living and dead bacterial cells (carrying ARGs) could be detected in the permeate of the ultrafiltration.

After the thorough investigation of the removal performance of ultrafiltration alone, experiments were conducted in which powdered activated carbon was dosed inline prior to the ultrafiltration membrane. In addition to optimizing the removal of trace organic chemicals (TOrCs), special focus was laid on an improved operational stability. The simultaneous and continuous dosing of powdered activated carbon and polyaluminium chloride as coagulant resulted in comparatively low membrane fouling, but had clearly detrimental effects on the adsorption performance of the powdered activated carbon. On the other hand, mere ‘pre-coating’ of the ultrafiltration membrane with polyaluminium

chloride with continuous addition of powdered activated carbon ensured both efficient TOrC removal performance and stable operation.

For a safe water reuse practice, ARGs have to be considered in addition to TOrCs. Since ARGs are transferred by so called mobile genetic elements (e.g. plasmids, MS2 phages), in the last study it was investigated, whether and to what extent a 'cake layer' consisting of powdered activated carbon could affect the potential transmission of mobile genetic elements. Using a flow simulation (CFD simulation), the hydrodynamic flow fields above an ultrafiltration membrane were simulated with and without a particle cake layer. Despite the particle cake layer, no relevant changes in strain rates were observed. This led to the conclusion that the adsorptive removal of a particle cake consisting of powdered activated carbon would outweigh the removal due to the modified hydrodynamic flow fields.

The critical discussion of the results elaborated in this doctoral thesis revealed further interesting findings: Estimating agricultural irrigation demand applying the developed model is not only a helpful planning variable in the context of water reuse projects. A comprehensive understanding of irrigation demand will also play an important role in the context of a more sustainable, demand-oriented water management. During the studies dealing with the removal of MS2 phages or ARGs during membrane ultrafiltration effects of operating conditions (such as flux, feed concentrations of ARGs or MS2 phages, fouling layer) on the removal performance of the ultrafiltration membrane could be observed. Despite that some results from the lab-scale study were partially contradicting the results obtained during the pilot-scale study, a particularly important conclusion could be drawn: The EU regulation 2020/741/EU requires for water reuse an adequate validation monitoring. However, the impact of different operating conditions and their influence on the removal performance of viruses or bacteria are not accounted for. Based on our findings it is recommended to account for different operational conditions on the overall treatment efficiency in order to obtain for e.g. a proper evaluation of the UF treatment efficiency. The hybridization of ultrafiltration with powdered activated carbon showed promising results in terms of the removal efficiency of well adsorbable trace organic chemicals and also had some operational advantages. However, in order to produce a water quality that allows both, hygienic and chemically safe irrigation in the future, alternative treatment options (e.g., ultrafiltration combined with ozonation, biological activated carbon and final UV disinfection) should be considered and investigated. Despite of employing an advanced treatment, some assume that accumulation of certain contaminants in the environment will occur. In the last section of this dissetation it is discussed that this risk is negligible as long as appropriate treatment and management practices are applied.

ZUSAMMENFASSUNG

Der Klimawandel wird drastische Auswirkungen auf unsere ohnehin schon übernutzten Frischwasserressourcen haben. Denn der schnelle Zuwachs der Weltbevölkerung, Urbanisierungsdruck, veränderte Landnutzungen und eine zunehmende Industrialisierung, vor allem im Agrarsektor, haben dazu geführt, dass bereits heute die Hälfte der globalen Frischwasserressourcen vom Menschen genutzt werden. Auf globaler Ebene verbraucht der Agrarsektor 70 % aller dem Menschen zugänglichen Frischwasserressourcen und bis 2030 wird befürchtet, dass der weltweite Wasserverbrauch die Verfügbarkeit um 40 % übersteigen wird. Enorme Nutzungskonflikte im Wassersektor werden die Folge der damit einhergehenden Lücke in der Wasserversorgung sein. Um Wasserknappheit und Konflikte aufgrund konkurrierender Bedürfnisse zwischen dem Trinkwassersektor, der Landwirtschaft und der Energiewirtschaft abzumildern, muss Wasser deutlich effizienter und nachhaltiger bewirtschaftet werden. „*Von einem linear gedachten Wassermanagement, hin zu einem Paradigma einer zirkulären Wasserwirtschaft*“ lautet die Devise und die Wiederverwendung von Wasser könnte einen wichtigen Lösungsansatz darstellen. Wasserwiederverwendung ist bereits Teil der 17 Ziele für nachhaltige Entwicklung (SDG 6). Insbesondere durch eine Effizienzsteigerung und Wasserrecycling in der Landwirtschaft könnten substantielle Mengen an konventionellen Wasserressourcen (Grundwasser und Oberflächenwasser) eingespart und für Zwecke, wie die Trinkwasserversorgung bereitgestellt werden. Wasserrecycling, also die Wiedergewinnung und anschließende Wiederverwendung von Wasser, ist allerdings mit einigen Herausforderungen gekoppelt: Was ist der zu bedienende Bedarf, welche Qualitätsanforderungen müssen eingehalten werden, wie hoch sind die damit verbundenen Kosten, was sind passende Betreibermodelle, wo werden die Verantwortlichkeiten definiert, wie ist der rechtliche Rahmen gestaltet, und wie gewinnt man die Akzeptanz der Öffentlichkeit? Im Kontext der vorliegenden Arbeit wurde sich zwei der zuvor genannten Herausforderungen angenommen:

Für die Planung und Umsetzung von Projekten zur Wasserwiederverwendung für landwirtschaftliche Zwecke ist ein umfassendes Verständnis des Bewässerungsbedarfs erforderlich. Diese Informationen sind jedoch häufig nicht ohne Weiteres verfügbar. Deshalb, wurde ein Modellierungsansatz basierend auf der CROPWAT Software adaptiert und weiterentwickelt, mit welchem der pflanzenspezifische landwirtschaftliche Bewässerungsbedarf berechnet werden konnte. Basierend darauf konnte der tägliche, monatliche sowie jährliche Spitzenbedarf für eine komplette landwirtschaftlich genutzte Region in Unterfranken (Gochsheim) kalkuliert werden. Insbesondere der Tagesspitzenbedarf ist eine essentiell wichtige Planungsgröße für

Wasserwiederverwendungsprojekte und war wichtiger Bestandteil einer Konzeptstudie die für die Region um Schweinfurt in Unterfranken, Deutschland erstellt wurde.

Zweitens wurde eine Aufbereitungsstrategie konzipiert und umgesetzt, die den bestehenden und zukünftigen Qualitätsanforderungen an die Wasserwiederverwendung in Deutschland für landwirtschaftliche Zwecke gerecht werden soll. Sowohl die mikrobielle (z. B. Viren, Bakterien, Protozoen) als auch die physikalisch-chemische Wasserqualität (z. B. Salzgehalt, Schwermetalle, organische Spurenstoffe wie Pharmazeutika oder Industriechemikalien) muss für eine sichere landwirtschaftliche und städtische Bewässerungsanwendung ausreichend sein: Ultrafiltration mit Keramik- oder Polymer-Membranen kombiniert mit Pulveraktivkohle wurde als ein vielversprechende Ansatz zur Wasseraufbereitung ausgewählt, um eine adäquate Wasserqualität zu erzeugen. Für eine kompakte Umsetzung wurde die Pulveraktivkohle inline vor der Membran dosiert.

Im Rahmen dieses zweiten Abschnitts der vorliegenden Arbeit wurde eingangs untersucht, welche Faktoren beim alleinigen Einsatz einer Ultrafiltration die Entfernungsleistung von MS2 Phagen, Antibiotikaresistenzgenen (ARGs) oder Bakterien beeinflussen. Die Entfernungseffizienz von Viren wie MS2-Phagen hängt stark von Betriebsparametern wie Flux- und Transmembrandruck (TMP)-Bedingungen während der Ultrafiltration ab. Daher wurden im Rahmen einer Studie im Labormaßstab die Auswirkungen unterschiedlicher Flux- und TMP-Bedingungen während der Keramik-Ultrafiltration auf die Infektiosität und Retention von MS2-Bakteriophagen untersucht. Die im Labormaßstab durchgeführte Studie zeigte, dass der Rückhalt von MS2 Phagen mit zunehmenden Membrandurchflüssen zunahm. Vermutlich hat zunehmende Konzentrationspolarisation zu einer verstärkten Aggregation und damit zu einem verbesserten Größenausschluss der MS2 Phagen geführt. Im Rahmen der Studie im Labormaßstab konnte auch gezeigt werden, dass trotz hoher Flux oder TMPs die Infektiosität der MS2-Phagen nicht beeinträchtigt wurde.

Im Rahmen der Pilotstudie wurde die Niederdruck-Membranfiltration hinsichtlich ihrer Entfernungsleistung von ARGs (sul1, ermB, vanA) untersucht, die im Ablauf nach konventioneller sekundärer Abwasserreinigung vorhanden sind. Die wichtigsten Betriebsparameter, die die ARG-Entfernung während der Ultrafiltration beeinflussen, wurden untersucht. Besonderes Augenmerk wurde auf die Auswirkungen anfänglicher ARG-Konzentrationen und die Bildung einer „Fouling-Schicht“ auf die Entfernungsleistung einer polymeren Ultrafiltrationsmembran gelegt. Erhöhte ARG-Konzentrationen im Zulaufwasser resultierten in erhöhten ARG-Konzentrationen im Ultrafiltrationspermeat. Darüber hinaus zeigten die Ergebnisse, dass der „Fouling-Layer“, der sich während der Ultrafiltration aufbaute, als verstärkende Barriere für

manche ARGs (z. B. vanA) wirkte, während für einige andere ARGs (z. B. sul1 und ermB) keine signifikanten Auswirkungen beobachtet wurden. Überraschenderweise konnten im Rahmen der Pilotstudie lebende und tote Bakterienzellen (mit ARGs) im Permeat der Ultrafiltration nachgewiesen werden.

Nach der eingängigen Untersuchung der Entfernungsleistung der Ultrafiltration, wurden Versuche durchgeführt, im Rahmen welcher Pulveraktivkohle inline vor der Ultrafiltrationsmembran dosiert wurde. Neben der Optimierung der Entfernung von organischen Spurenstoffen (TOrCs), wurde besonderer Fokus auf eine verbesserte Betriebsstabilität gelegt. Die gleichzeitige und kontinuierliche Dosierung von Pulveraktivkohle und Polyaluminiumchlorid als Fällmittel resultierte zwar in einem vergleichsweise geringen ‚Fouling' der Membran, hatte aber deutlich nachteilige Auswirkungen auf die Adsorptionsleistung der Pulveraktivkohle. Dahingegen konnte durch das bloßes ‚Precoating' der Ultrafiltrationsmembran mit Polyaluminiumchlorid bei kontinuierlicher Zugabe von Pulveraktivkohle sowohl eine effiziente Entfernungsleistung als auch ein stabiler Betrieb gewährleistet werden.

Für eine sichere Wasserwiederverwendung müssen neben einer Entfernung von TOrCs auch ARGs berücksichtigt werden. Da ARGs durch sogenannte mobile genetische Elemente (z. B. Plasmide, MS2-Phagen) übertragen werden, wurde in der letzten Studie untersucht, ob und in welchem Ausmaß sich eine ‚Kuchenschicht' bestehend aus Pulveraktivkohle auf die potenzielle Transmission von mobilen genetischen Elementen (z. B. Plasmide, MS2 Phagen) auswirken könnte.. Mithilfe einer Strömungssimulation (CFD Simulation) wurden die hydrodynamischen Strömungsfelder oberhalb einer Ultrafiltrationsmembran mit und ohne einem Partikelkuchen simuliert. Trotz des Partikelkuchens waren keine relevanten Änderungen von Dehnungsraten zu beobachtet. Dies ließ den Schluss zu, dass die adsorptive Entfernungsleistung eines Partikelkuchens bestehend aus Pulveraktivkohle, die Entfernungsleistung bedingt durch die veränderten hydrodynamischen Strömungsfelder überwiegen würde.

Die kritische Auseinandersetzung mit den Ergebnissen dieser Promotionsarbeit offenbarte weitere interessante Erkenntnisse: Die Abschätzung des landwirtschaftlichen Bewässerungsbedarfs mithilfe des entwickelten Models ist nicht nur eine hilfreiche Planungsgröße im Kontext von Wasserwiederverwendungsprojekten: Auch im Kontext eines nachhaltigeren bedarfsorientierten Wassermanagements wird das umfassende Verständnis des Bewässerungsbedarfs eine wichtige Rolle spielen. Während der Studien, die sich mit der Entfernung von MS2-Phagen oder ARGs während der Membran-Ultrafiltration befassten, konnten Auswirkungen der Betriebsbedingungen (wie Flux, Konzentrationen von ARGs oder MS2-Phagen im Zulauf, Fouling-Layer) auf die Entfernungsleistung der Ultrafiltrationsmembran beobachtet werden. Obwohl einige

Ergebnisse der Laborstudie teilweise den Ergebnissen der Pilotstudie widersprachen, konnte eine besonders wichtige Schlussfolgerung gezogen werden: Die EU Verordnung 2020/741/EU fordert für die Wasserwiederverwendung ein adäquate Validierungsuntersuchungen. Allerdings werden die Auswirkungen unterschiedlicher Betriebsbedingungen und deren Einfluss auf die Entfernungsleistung von Viren oder Bakterien nicht berücksichtigt. Basierend auf unseren Erkenntnissen wird empfohlen, unterschiedliche Betriebsbedingungen auf die Gesamtentfernungseffizienz zu berücksichtigen, um z. B. um eine korrekte Bewertung der UF-Behandlungseffizienz zu erhalten. Die Hybridisierung der Ultrafiltration mit Pulveraktivkohle zeigte zwar vielversprechende Ergebnisse bezüglich der Entfernungsleistung von gut adsorbierbaren organischen Spurenstoffen und auch einige betriebliche Vorteile. Um zukünftig jedoch eine Wasserqualität zu produzieren, die sowohl eine hygienisch als auch eine chemisch besorgnisfreie Bewässerung zulässt, sollten alternative Behandlungsoptionen (z. B. Ultrafiltration kombiniert mit einer Ozonung, biologisch aktivierter Aktivkohle und abschließende UV-Desinfektion) in Erwägung gezogen und untersucht werden. Trotz einer weitergehenden Aufbereitung wird teilweise befürchtet, dass es zu einer Anreicherung bestimmter Schadstoffe in der Umwelt kommen kann. Im letzten Abschnitt dieser Disseration wird daher diskutiert, dass dieses Risiko vernachlässigbar ist, solange angemessene Behandlungs- und Managementpraktiken angewendet werden.

DANKSAGUNG

Wer hätte gedacht, dass man, nachdem man gerade von einer Expedition von einem 7000er im Himalaya zurückkehrt, die Entscheidung trifft, eine Promotion am Lehrstuhl für Siedlungswasserwirtschaft an der TU München zu machen…oder vielleicht gerade deshalb? Zwar war das Bergsteigen an der ein oder anderen Stelle etwas mehr lebensbedrohlich, aber im Vergleich zur Promotion ja doch eher nur ein Spaziergang: Aber genug der Scherze: Größten Dank Dir, Prof. Dr.-Ing. Jörg E. Drewes, dafür dass Du mich in Leh zu einer Promotion überzeugt hast, mir die Möglichkeit gegeben hast, in Deinem Team am SIWAWI-Lehrstuhl zu promovieren und natürlich für Deine Betreuung: Eine super Erfahrung, eine extrem arbeitsintensive und damit lehrreiche Zeit, ein inspirierendes Arbeitsumfeld, große Gestaltungsfreiheit und definitiv das mit Abstand coolste Promotionsprojekt, das ich mir nicht spannender hätte vorstellen können: ‚*Nutzwasser rocks*!' Hier will ich mich auch gleich ganz herzlich bei Dir, Prof. Dr. Brigitte Helmreich bedanken: Deine Geduld und Dein offenes Ohr zu jeder Zeit und Wurscht, wie doof die Frage auch war: Deine Bürotür war stets offen und stets ist man zuversichtlicher rausgekommen, als man hineingegangen ist! Soft Skills in der Wissenschaft...Ja auch das ist drin: Vielen Dank Dir, Dr.-Ing. Konrad Koch, für Dein Mentoring und Deine freundschaftlichen Ratschläge, Deinen Humor und Deine Zeit…definitiv musste ich viel Lachen mit Dir, aber irgendwie auch ein dickeres Fell anlegen…schadet sicherlich nicht! And many thanks to Prof. Dr. Tzahi Y. Cath for being the third member in the Scientific Committee for this dissertation thesis: It was a pleasure meeting you in person in Golden at the Colorado School of Mines…thanks for your hospitality and the cool tour through your pilots!

Hubert Moosrainer, jo mei, wos hat i gmocht ohne Di…do war I ned weit kemma, des sog I da! Merci für Dei Geduld: jo ab und zua bin I wahrscheinlich ab und zua zu oft in Dei Werkstatt eine glaffen! Merci fürs zam basteln, merci für de ganzen supa Tips, merci fürs zama lachen und merci fürs zama Brotzeiten und Bier trinka! Da ‚Juck Hubert Norris' am Leahstui! Ein herzliches Vergelts Gott natürlich auch an Dich, Susanne Wießler und Dich, Marianne Lochner: Ohne Euch wärs ein schwerer Weg durch den Uni-Bürokratie-Dschungel gwesen! Was wäre unsere Forschung ohne den echten Experten im Labor? Ein verzweifelter Versuch, Daten über Monte-Carlo-Simulationen am Computer zu erfinden, um das nächste Paper zu schreiben…Vielen, vielen Dank Dir Myriam Reif, vielen Dank Dir, Wolfgang Schröder, vergelts Gott Dir, Heidi Mayrhofer, und vielen Dank Dir, Uschi Wallentits, für all Eure Geduld, Eure Hilfsbereitschaft und Euer unendlich wertvolles Wissen…sogar ich habe schlussendlich das Pipettieren und Titrieren gelernt und die Daten ham sogar glangt fürs Paperschreiben.

Ein Jahr lang Planung und Bau haben sich gelohnt: Das Nutzwassertier, es keucht und kracht, zischt und bläst, spritzt und sprudelt und leuchtet dann auch noch…endlich steht es nun in Schweinfurt auf dem Betriebsgelände der Kläranlage Schweinfurt. Ein herzliches Dankeschön hier an Dich, Bastjan Kebinger, für die spannende Zusammenarbeit bei der Tiefbauplanung zur Multibarrieren-Nutzwasser-Aufbereitungsanlage, bestehend aus einer keramischen Ultrafiltration, nachgeschalteten Ozonung und BAK-Filtration sowie einer abschließenden UV-Desinfektion, oder eben einfach kurz, das Nutzwassertier. Vielen Dank Dir, Jens Gebhardt, für Deine stets optimistische und richtige Einschätzung bei der Hydraulikplanung...ja irgendwie muss das Wasser dann ja auch durch die Anlagen fließen, gell. Sehr dankbar bin ich Dir, Dr.-Ing. Nadine Scheyer: Eine Anlage aufs Blatt Papier zu malen ist das eine….aber ohne Deine Unterstützung, unendliche Geduld und immerwährenden Zuversicht, wäre die schöne Nutzwasseranlage nicht mal ein Viertel so schön…und laufen täte sie auch nicht. Ja und dann noch die 1001 Fittinge: Thomas Barthel, einfach nur klasse und vielen Dank Dir für die mindestens 1001 Bestellungen. Fabian Freund und Erik Mantel, meine lieben Freunde aus Schweinfurt: Vergelts Gott für die lustige Zeit mit Euch, egal wo, ob in Oldenburg oder Schweinfurt, und ein noch größeres Dankeschön an Euch für die Rund-um-die-Uhr-Betreuung des doch ein wenig hilflosen und störanfälligen Nutzwassertieres. Vielen Dank Dir, Stefan Rose, Dir, Edgar Hehn, und dem ganzen Werkstatt-Elektrotechnik-Klärwerk-Labor-Team in Schweinfurt: Schorsch, Mano, Andi, Anne, Klaus, Miriam, Steffen, Enrico, Birgit, Tim, Werner (das Bier war vorzüglich) und sorry an alle die ich vergessen habe: Da sieht man erst wie aufwändig so eine Anlage im Demonstrationsmaßstab ist…zusammen bringt ihr locker 1001 Stunden auf die Waage, die Ihr investiert habt, damit das Nutzwassertier so märchenhaft läuft wie es läuft. Und zu guter Letzt an dieser Stelle: Ein herzliches Dankeschön an die Damen aus Unterfranken: Susanne, Dank für Deinen grünen Daumen, ohne Dich wäre der Kohlrabi im Gewächshaus vertrocknet, bevor er gewachsen wäre, und vielen Dank an Euch Anja und Christine für die super Gastfreundschaft mit all der Verpflegung, die wir stets genießen durften in Schweinfurt auf der Kläranlage bei Euch!

Ich danke der Regierung von Unterfranken und dem Bundesministerium für Bildung und Forschung für die Förderung der beiden Nutzwasserprojekte. Die Konzeptstudie (finanziert seitens der Regierung von Unterfranken) war Voraussetzung für das derzeit laufende Demonstrationsprojekt ‚*Nutzwasserbereitstellung und Planungsoptionen für die urbane und landwirtschaftliche Bewässerung*‘ (finanziert seitens BMBF, FKZ 02WV1563A).

Keinen meiner Kollegen oder Kolleginnen am Lehrstuhl werde ich je vergessen: Danke Euch für die super lustige, freundschaftliche und hilfsbereite Atmosphäre am Lehrstuhl. Jonas Aniol, vielen Dank Dir für die ganzen Handwerkerhacks, die ich bitter

nötig hatte beim Bau der Labor- und Pilotanlagen. Vielen Dank Dir, Dr.-Ing. Johann Müller, für Deine Freundschaft, Geduld und Hilfe beim Auffinden der Spurenstoffe…eine echte Detektivarbeit. Спасибо, Вероника Житенева, за помощь в моделировании потенциальной производительности очистных сооружений. Vielen Dank Dir, Dr. Oliver Knoop, für die super Kaffeepausen und Deine Unterstützung im Spurenstofflabor. Vielen Dank Dir, Philipp Sperle, für die unzähligen Labor-Tips, die geduldige Statistik-Beratung und die inspirierenden Diskussionen und vor allem für die hammer Zeit in USA…ein Trip den ich nicht vergessen werde, zumindest das was ich noch weiß! Vielen Dank auch an Dich, Javad Ahmadi: Begonnen haben wir als, ich, der unerfahrene Doktorand und Du, der fleißige Student im Mikroplastikprojekt. Und nun, best Buddies und super Kollegen im Nutzwasserprojekt…alles hat riesig Spaß mit Dir gemacht, egal ob das viele Mikroskopieren und Mikroplastikpartikelzählen oder dann das Basteln und Probeziehen in Schweinfurt an der Nutzwasseranlage oder einfach die super Zeit im Büro oder die Nachschichten beim Schmieden einer Unternehmensidee mit literweise Kaffee und Schokolade…vielen Dank für Deine super Freundschaft und große Hilfe!

Ein herzliches Dankeschön an all die Studenten und Studentinnen die mich während meiner Promotion in ihrer Bachelor-, Studien-, oder Masterarbeitszeit begleitet haben. Die vielen Ideen, die einem während der Promotion kommen, ließen sich nur durch die hervorragende Zusammenarbeit mit Euch umsetzen. Deshalb ganz vielen Dank an Euch, Ayaa Al-areqi, Manoel Stauner, Javad Ahmadi, Poojesh Bertram, Elizaveta Akhimova, Clara Lehrer, Felix Bergmann, Kevin Fokkens, Kim Lange, Magdalena Knabl, Natacha Heymes, Christina Kordetzky, und Yvonne Keller…ich habe viel von Euch gelernt…und hoffentlich auch ihr von mir!

Man glaubt es kaum: Es gibt auch noch Freizeit neben der Promotion...hier will ich meinen Freunden danken, denn hier spielt die Musik, oder es wird Berg gegangen, oder einfach mal gequatscht. Danke Euch Christian Urban, Christian Probst, Seppi Braun, Simon Hutzler, Michi Hilmer, Thomas Schandl, Sebastian Konrad, Timmy Binder, Rick Schneider, Kevin Keim, Leonardo Titzschkau, Stefan Knilling, Johannes Rothe, Flo Schöttl…ihr begleitet mich nun schon Jahre oder gar Jahrzehnte und seid ein unentbehrlicher Bestandteil in meinem Leben geworden.

Unendlicher Dank gilt natürlich meinen Großeltern und meinen Eltern, meinem Bruder Mahatma Andi, meinen Schwestern Anna und Nina, meiner Frau Anastasiya und meinem Sohn Jakob für alle Unterstützung, Ermutigung, Liebe, Geduld, und Glück, denn die lustigsten und glücklichsten Stunden, die man sich nur wünschen kann, kann man nur mit euch haben…in diesem Sinne: hakuna matata, pitau minau!

CONTENTS

LIST OF FIGURES

LIST OF TABLES

ABBREVIATIONS AND ACRONYMS

ALB	Arbeitsgemeinschaften für Landtechnik und Bauwesen
AMR	Antimicrobial resistance
ANSI	American national standards institute
AOC	Assimilable organic carbon
AOP	Advanced oxidation processes
ARB	Antibiotic resistant bacteria
ARG	Antibiotic resistance gene
B	Blank sample
BAC	Biological activated carbon
BBCH	Biologische Bundesanstalt für Land- und Forstwirtschaft, Bundessortenamt und Chemische Industrie
BC	Boundary conditions
BDOC	Biodegradable dissolved organic carbon
BGR	Bundesanstalt für Geowissenschaften und Rohstoffe
BGS	Brandt Gerdes Sitzmann Umweltplanung GmbH
BLZ	Bundesinformationszentrum Landwirtschaft
BMBF	German Federal Ministry of Education and Research
BNR	Biological nutrient removal (e.g. CAS)
CAS	Conventional activated sludge treatment
CEB	Chemical enhanced backwash
CFD	Computational fluid dynamics
CFP	Centrifugal feed pump
COD	Chemical oxygen demand
cont. coag.	continuous coagulation
d_{50}	Median diameter
DIN	Deutsches Institut für Normung
DNA	Deoxyribonucleic acid
DOC	Dissolved organic carbon
DPB	Disinfection by-product
dPCR	digital polymerase chain reaction
dsDNA	double stranded DANN
DWA	Deutsche Vereinigung für Wasserwirtschaft, Abwasser und Abfall
DWD	Deutscher Wetterdienst
eARG	Extracellular ARG
EC	Electrical conductivity
EPS	Extracellular polymeric substances
ET0	Potential evapotranspiration
EU	European Union
EU WRRL	Europäische Wasserrahmenrichtlinie
FAO	United Nations' Food and Agriculture Organization
FC	Filtration cycle
FI	Flow indicator
FT	Feed tank
GAC	Granulated activated carbon
GrwV	Grundwasserverordnung
GWRL	Grundwasserrichtlinie
H_2SO_4	Sulphuric acid
HCl	Hydrochloric acid
HGT	Horizontal gene transfer
HMP	Hybrid membrane process
HNAC	High nucleic acid count
HNO_3	Nitric acid
IACS	Integrated administration and control system
iARG	Intracellular ARG
ICE	Integrative and conjugative elements
ID	Identification number
IoT	Internet of things

ISO	International Organization for Standardization
kDa	Kilo Dalton
LAWA	Bund/Länder-Arbeitsgemeinschaft Wasser
LC–MS/MS	Liquid chromatography coupled with tandem mass spectrometry
LfL	Bayerische Landesanstalt für Landwirtschaft
LfU	Landesamt für Umwelt
LMH	Liters per square meter per hour
LNAC	Low nucleic acid count
LOD	Limit of detection
LOQ	Limit of quantification
LoRaWAN	Long range wide area network
LR	Leaching requirement
LRV	Log removal values
LTE	Long term evolution
Max	Maximum
MBR	Membrane bioreactor
MDa	Mega Dalton
MF	Microfiltration
MGE	Mobile genetic element
Min	Minimum
MWCO	Molecular weight cut-off
n	Number of observations/measurements
NaOCl	Sodium hypochlorite
NaOH	Sodium hydroxide
NC	Negative control
NDMA	N-nitrosodimethylamine
NF	Nanofiltration
NO_3^--N	Nitrate-nitrogen
NOM	Natural organic matter
NSF/ANSI	National science foundation
NWRI	National Water Research Institute
O_3	Ozonation
OWID	Our world in data
PAC	Powdered activated carbon
PACl	Polyaluminium chloride
PAW	Plant available water
PBS	Phosphate-buffered saline
PC	Positive control
PCR	Polymerase chain reaction
PES	Polyethersulfone
PFAS	Per- and polyfluoroalkyl substances
PFU	Plaque forming units
PI	Pressure indicator
PO_4^{3-}-P	Phosphate-phosphorus
ppm	Parts per million
precoat.	precoating
PTFE	Polytetrafluoroethylene
PVDF	Polyvinylidene fluoride
qPCR	real-time quantitative digital polymerase chain reaction
Re	Reynolds number
RNA	Ribonucleic acid
RO	Reverse osmosis
rRNA	Ribosomal ribonucleic acid
RUF	District Government of Lower Franconia (Regierung von Unterfranken)
RZ	Rooting depth
SDG	Sustainable development goal
SE	Secondary effluent (after conventional wastewater treatment)
SEM	Scanning electron microscope
SF	Sand filtration
SMP	Soluble microbial products

std	Standard deviation
TCC	Total cell count
TE	Tertiary effluent (secondary effluent after PAC adsorption and sand filtration)
TMP	Transmembrane pressure
TOC	Total organic carbon
TOrC	Trace organic chemical
TSA	Tryptic soy agar
TSB	Tryptic soy broth
UBA	Umweltbundesamt
UF	Ultrafiltration
UMTS	Universal mobile telecommunications system
UN	United Nations
UNESCO	United Nations Educational, Scientific and Cultural Organization
US EPA	United States Environmental Protection Agency
UV	Ultraviolet
UV_{254}	Ultraviolet absorbance at 254 nm
v %	volume percent
VGT	Vertical gene transfer
WFD	Water Framework Directive
WHO	World Health Organisation
Wi	Weissenberg number
WRI	World Resources Institute
WWTP	Wastewater treatment plant

1 INTRODUCTION

The rapid growth of global population, changes in land use, increasing urbanization, progressive industrialization, and industrial agriculture have resulted in the fact that around 50 % of the planet's fresh water resources are already being used by humans (Dodds et al. 2013; Myers 2017). Since 1901, the global water demand has increased exponentially by over 600 % (OWID 2020). It is estimated that around 4,600 km^3 of fresh water is ‘consumed’ every year (Boretti and Rosa 2019). With about 70 %, the largest part is used for agricultural irrigation (AQUASTAT 2016; UNESCO 2020). By 2050, the global population is expected to increase by around 22–32 % to around 9.4–10.2 billion people, with two-thirds of the total population is expected to live in cities (UNESCO 2020). As a result, total global water demand is expected to increase by around 20–30 % to 5,500–6,000 km^3 by 2050 (Burek et al. 2016). It is feared that urban water demand will increase by as much as 80 % by 2050 and that the water demand of around 27 % of all cities worldwide will exceed the local availability of surface water (Flörke et al. 2018). It is even projected that by 2030 water demand will exceed supply by 40 % on a global scale (UN Programme, International Resource Panel 2015). According to an analysis by the World Resources Institute (WRI) already a quarter of the world's population lives in regions characterized by acute and extreme water shortages (WRI 2019). The situation is likely to worsen worldwide in the next few decades especially due to climate change impacts (van Vliet et al. 2017; Greve et al. 2018; Flörke et al. 2018; O'Neill et al. 2017; UNESCO 2020). Hence, our global fresh water resources are being put progressively more under enormous stress and it is expected that serious water use conflicts will arise (Vörösmarty et al. 2010; European Commission 2012; Holland et al. 2015c; Rosa et al. 2018; Greve et al. 2018).

Germany is still considered a country in which water is available in sufficient quantity and quality (Seis et al. 2016; UBA 2021c). This is why the established paradigm of a linear water management in which water is used once, treated via conventional wastewater treatment and discharged to receiving streams is still prevailing in Germany. However, due to climate change even in Germany progressively more regions experience water shortage, extended droughts, and increasing conflicts over water (LfU 2009; RUF 2010; LAWA 2017). These conflicts may arise when in the context of scarce surface and groundwater resources the simultaneous water demand for agricultural irrigation, public drinking water supply, urban landscape irrigation, cooling water demand for energy production, industrial and commercial requirements, or maintaining minimum ecological base flows exceed the water availability. These conflicts occur often seasonally in the

spring and summer for several weeks to months when water demand in the various sectors is disproportionately high. According to the findings of several studies (Altmayer et al. 2017; LAWA 2017), even in Germany extreme weather events such as long-lasting dry periods may occur more often to more severe extent and longer duration. With an average annual precipitation of approximately 450–650 mm/year the region Würzburg-Schweinfurt-Kitzingen in Lower Franconia is one of the driest areas in Germany (DWD 2018c; LfU 2020). In order to ensure an integrated and sustainable management of the locally overexploited groundwater by agriculture (RUF 2006, 2010), the development of alternative options for the extraction, distribution and potential use of stormwater and reclaimed water, in particular for the purpose of urban landscape and agricultural irrigation, are urgently needed. This is especially important in order to secure groundwater as the primary source for drinking water supply (2000/60/EC), to provide sufficient and reliable irrigation water for agricultural production in the high-price segment (i.e., fruit and vegetable cultivation), and to preserve urban green areas during prolonged droughts in the spring and summer months. It is expected that the irrigation demand in regions that experience progressively more periods of water shortage will not be covered in the future without the use of alternative water resources such as reclaimed water. Thus, the reuse of reclaimed water in Germany is of growing importance to overcome future bottlenecks in water supply.

In order to alleviate water scarcity and conflicts due to competing needs between the drinking water sector, agriculture and the energy sector, water must be managed far more efficiently and sustainably (Mantovani et al. 2001; Daigger 2009; Maczulak 2010; Vollmer et al. 2018; Greve et al. 2018). In the near future water use conflicts between urban and agricultural areas are expected for increasingly more watersheds. By improving the water use efficiency in agriculture enough water for urban use could be released in 80 % of these watersheds (Flörke et al. 2018). Investing in a more efficient and sustainable water management in agriculture could therefore serve as an important strategy to adapt to global change such as the climate and food crisis. In addition to improved efficiency of agricultural irrigation practices and optimized storage systems, the reclamation of (municipal) wastewater and its reuse for agricultural and landscape irrigation purposes represent a promising approach for a more sustainable water management (Iglesias and Garrote 2015; Bixio et al. 2006; WRI 2019). Water recycling, i.e. the reclamation and reuse of water may efficiently and sustainably address water challenges and overcome periods of water shortage as effects of climate change by creating new sources of high-quality water supplies. (Alcalde-Sanz and Gawlik 2014; Iglesias and Garrote 2015; Garrote 2017; Water Reuse Europe 2018; 2020/741/EU). Yet, in the European Union (EU), only around 2.4 % of the treated municipal wastewater is currently reused (Alcalde-Sanz and Gawlik 2014). Of this, 52 % is used for irrigation

(Water Reuse Europe 2018). Hence, in most EU countries and in many countries worldwide, the potential for expanding water reuse and the use of appropriate technologies is substantial (Khan et al. 2017; Drewes et al. 2019). For Germany, an estimated water reuse potential of 144 million m^3/year by 2025 is assumed, which corresponds to a tripling of today's use (Water Reuse Europe 2018). Moreover, the reuse of reclaimed water has become a key goal in several Sustainable Development Goals (SDGs), especially in the areas of 'Clean Water' and 'Sanitation' (UN 2015, SDG 6). The importance of water reuse for agricultural irrigation in the European Union was also emphasized within a new regulation of the European Parliament and of the Council on minimum requirements for water reuse (2020/741/EU).

However, water reuse as an integrated concept of water management involves the convergence of diverse areas such as engineering, governance, health risks, regulation, and public perception. This represents a significant challenge to water reuse projects (Miller 2006). For instance, a challenge exists that the reuse of reclaimed water for irrigation purposes is only necessary during the irrigation season during which particularly the peak demand has to be reliably covered. Furthermore, water reuse for irrigation purposes requires investment in a separate water distribution and storage infrastructure. Hence, the implementation of a water reuse project for seasonal application is only economically viable if it enables potential savings or additional income elsewhere, or if the associated expenses can be redistributed or passed on. At the end it is important for a successful implementation of a water reuse project that the associated benefits outweigh the potential opportunity costs of the business as usual (i.e., conventional water management). Therefore, before implementing water reuse it has to be carefully weighed against conventional water management options. Water reuse has to be adapted to local conditions and should be able to react dynamically to fluctuations of the water demand and the inflow water quality. This requires highly flexible, safe and robust treatment systems as well as adequate operational and monitoring strategies. The protection of public health and the environment such as groundwater, surface water or soil has to be guaranteed anytime while practicing water reuse (US EPA 600-R-12-618). Concluding, potable as well as non-potable water reuse is associated with various (engineering) challenges that have to be addressed for an economically, socially and ecologically feasible implementation.

Firstly, for the planning and dimensioning of treatment and storage systems required for water reuse for agricultural purposes the long- as well as short-term irrigation demands are important (Asano and Mills 1990; Asano 1991; Urkiaga et al. 2008). Hence, this dissertation aimed to determine site specific agricultural irrigation demand via modelling: In addition to the determination of crop specific demand, also overall gross irrigation

requirements on an annual, monthly and daily basis were estimated for an entire agricultural area.

Secondly, wastewater treatment plant effluents intended for water reclamation can contain a wide spectrum of constituents of concern such as salts, nutrients, heavy metals, trace organic chemicals (TOrCs), pathogens, or antibiotic resistance genes (ARGs) (Chen et al. 2013a). When reusing reclaimed water, the microbiological parameters are of upmost importance in addition to the usual standard parameters used for quality control during conventional municipal wastewater treatment. Pathogens present in water reused for agricultural irrigation can pose an acute risk for human health via direct ingestion or inhalation or via the consumption of crops eaten raw. Humans or animals also might be exposed to pathogens by using groundwater that has been impacted by reclaimed water (Chen et al. 2013a; Lonigro et al. 2016; Cui et al. 2020). In addition to microbiologically concerning constituents, a broad range of TOrCs occur in wastewater treatment plant effluents. TOrCs comprise industrial and household chemicals (such as solvents, plasticizers, pesticides, monomers, complexing agents), personal care products, hormonally active chemicals as well as pharmaceuticals (and their active metabolites) (Ternes 2007a; Dong et al. 2015). This resulted in the fact that TOrCs are widely detected in various environmental compartments such as soil, groundwater and surface water bodies (Nikolaou et al. 2007; Vieno et al. 2007; Wu et al. 2009; Li 2014b; Sui et al. 2015; Lin et al. 2015; Biel-Maeso et al. 2018) or even crops that are irrigated with reclaimed water (Sharma et al. 2020). Due to their biological activity, aquatic toxicity and indications of potentially adverse interactions with the endocrine system, the presence of TOrCs in municipal wastewater poses with the microbial risk another public health challenge during reuse of reclaimed water (Drewes et al. 2018). Hence, water reuse requires both technical and regulatory requirements in order to adequately reduce the microbiological as well as chemical risk for human health (National Research Council 2012). Advanced water treatment is one viable technical measure in order to ensure a hygienically as well as chemically safe reuse of the reclaimed water for non-potable applications. Thus, within this dissertation thesis, an advanced treatment strategy was conceptualized and implemented that was expected to meet the existing and future quality requirements for water reuse for agricultural purposes in Germany. Ceramic or polymeric membrane ultrafiltration combined with inline dosed powdered activated carbon (PAC) was chosen as promising treatment approach for the production of a microbial as well as chemically adequate water quality. Ultrafiltration membranes (UF) are considered as reliable barrier against microorganisms such as bacteria, protozoa, viruses or partially even antibiotic resistance genes (ARGs) (Di Zio et al. 2005; Iannelli et al. 2014; Ferrer et al. 2015; Cordier et al. 2020; Hembach et al. 2019; Böckelmann et al. 2009), while PAC can be used for the efficient removal of a broad range of trace organic chemicals (TOrCs)

such as pharmaceuticals, industrial, or household chemicals (Worch 2012). This thesis aimed to assess UF without PAC with regard to its removal efficiency of microbial constituents (e.g. viruses such as MS2 phages, antibiotic resistance genes, bacteria) or combined with inline dosed PAC with regard to TOrCs removal. During the investigations of the PAC/UF hybrid membrane process, special focus was also laid on the identification of an operational mode with minimum TMP built-up at maximum TOrCs removal efficiency.

2 STATE-OF-THE-ART

2.1 Estimation of water demand via modelling

For the planning and dimensioning of treatment and storage systems required for water reuse for agricultural purposes the long- as well as short-term irrigation demands are decisive (Asano and Mills 1990; Asano 1991; Urkiaga et al. 2008). In this context, in addition to an understanding of crop specific demand, also overall gross irrigation requirements, in particular the daily peak demand, are important parameters (Watts 1968; Wright and Jensen 1972; Khadra and Lamaddalena 2006; Mariño et al. 1993; Gallichand et al. 1991).

Despite the fact that farmers in Germany are usually obliged to record their water demand for irrigation purposes, the corresponding data are often incomplete, have insufficient temporal resolution, are lacking transparency with regard to the area-specific requirement, or are not readily available. Thus, irrigation demand modelling is a promising approach to compensate for the lack of field data on irrigation demand. Modelling represents a fast and cost-effective approach to evaluate irrigation demand where respective field data are incomplete, poor in temporal resolution or not available at all. Many studies have already dealt with the estimation of the irrigation demand via modelling (Foster et al. 2019; Le Page et al. 2020; Li et al. 2020a; Li et al. 2020b; Zambrano-Vaca et al. 2020). However, either the determination of only crop specific irrigation demand was performed (Zambrano-Vaca et al. 2020), only annually or monthly resolved demand data were determined (Shen et al. 2013; Shi et al. 2018; Le Page et al. 2020; Li et al. 2020a; Li et al. 2020b; López-Lambraño et al. 2020), the determination of the crop water requirement was based (solely) on soil moisture data that are not easily available (Abolafia-Rosenzweig et al. 2019), or the focus was only laid on the estimation of crop coefficients (Seidel et al. 2019).

In order to obtain temporally high resolved estimations of the irrigation demand, the Penman-Montheith equation (Allen et al. 1998; Savva et al. 2002) can be employed. However, for this approach accurate meteorological data are required (Droogers and Allen 2002; Feng et al. 2017; Seidel et al. 2019). If sufficient meteorological data are available, reference evaporation ET_0 can be computed according to Penman-Montheith:

$$ET_0 = \frac{0.408\,\Delta\,(R_n - G) + \gamma \frac{900}{T + 273}\,u_2(e_s - e_a)}{\Delta + \gamma\,(1 + 0.34\,u_2)} \quad (2\text{-}1)$$

Where:

ET_0 = Reference crop evapotranspiration [mm/day]
R_n = Net radiation at the crop surface [MJ/m^2 per day]
G = Soil heat flux density [MJ/m^2 per day]
T = Mean daily air temperature at 2 m height [°C]
u_2 = Wind speed at 2 m height [m/sec]
e_s = Saturation vapor pressure [kPa]
e_a = Actual vapor pressure [kPa]
$e_s - e_a$ = Saturation pressure deficit [kPa]
Δ = Slope of saturation vapor pressure curve at temperature T [kPa/°C]
γ = Psychometric constant [kPa/°C]

The crop water requirement is mainly determined by the crop evapotranspiration ET_c (Allen et al. 1998; Savva et al. 2002):

$$ET_c = ET_0 * K_c \quad (2\text{-}2)$$

Where:

ET_c = crop evapotranspiration [mm/day]
ET_0 = reference evapotranspiration [mm/day]
K_c = crop coefficient

Crop evapotranspiration ET_c applies under standard conditions, which is equivalent to no water stress for the plant. In order to account for a water stress situation, the crop evapotranspiration should be calculated for non-standard conditions ET_a according to the following formula using the water stress coefficient k_s (Allen et al. 1998):

$$ET_a = ET_c * k_s \quad (2\text{-}3)$$

Where:

ET_a = crop evapotranspiration under non-standard conditions [mm/day]
ET_c = crop evapotranspiration [mm/day]
k_s = water stress coefficient = 1

The net irrigation requirement is derived from the field balance equation according to Savva et al. (2002):

$$IR_n = ET_c - \left(P_{eff} + G_e + W_b\right) + LR_{mm} \quad (2\text{-}4)$$

Where:

IR_n = net irrigation requirement [mm]
ET_c = crop evapotranspiration [mm/day] = ET_a, since $k_s = 1$
P_{eff} = effective dependable rainfall [mm]
G_e = groundwater contribution from water table [mm]
W_b = water stored in the soil at the beginning of each period [mm]
LR_{mm} = leaching requirement [mm]

Since during irrigation usually water losses occur due to e.g. leaking pipes, the efficiency of the irrigation system also has to be accounted for when determining the

gross irrigation requirements. Consequently, the gross irrigation requirement IR_g can be determined according to Savva et al. (2002):

$$IR_g = \frac{IR_n}{E} \quad (2\text{-}5)$$

Where:

IR_g = gross irrigation requirements [mm]
IR_n = net irrigation requirements [mm]
E = overall irrigation project efficiency [-]

The entire computational procedure is implemented e.g. in CROPWAT 8.0 software, freely available from the United Nations' Food and Agriculture Organization (FAO). However, the CROPWAT 8.0 software is only capable to compute the water demand of a specific crop cultivated on a specific soil type in a specific cultivation period. This represents a clear drawback of using CROPWAT 8.0 for the estimation of the agricultural irrigation demand for an entire agricultural area with varying soil conditions, crop cultivation periods and a broad spectrum of different crops. To estimate the overall irrigation demand for an entire agricultural area, many different crops, soils and cultivation periods have to be accounted for. By modifying and implementing the procedure of the CROPWAT 8.0 software in Python, many different scenarios (different crops, different soils, different cultivation periods) can be accounted for simultaneously.

2.2 Water quality challenges associated with water reuse

2.2.1 Pathogens

Waterborne pathogens include bacteria such as *E. coli*, *Legionella*, or *Campylobacter jejuni*, viruses such as adeno-, rota- or noroviruses, and protozoa such as *Cryptosporidium parvum* or *Giardia lamblia*. *E. coli* is one of the most frequently utilized indicator organisms, together with Enterococci (Kulkarni et al. 2018). Besides *E. coli* and *Enterococci* other microorganisms such as *Aeromonas* spp. or *Legionella* spp. are monitored as relevant pathogens in reclaimed water (Kulkarni et al. 2018; Dingemans et al. 2020). However, the presence of indicator bacteria does not always correlate with the occurrence of pathogenic viruses (Carducci et al. 2008; Costán-Longares et al. 2008). This is why, e.g. bacteriophages become increasingly more popular as indicator viruses and are used for risk assessments for the occurrence of viruses in water (Selinka et al. 2011). Bacteriophages such as the MS2 phage are not pathogenic to humans, ubiquitously present in our anthropogenically affected environment (Calero-Cáceres et al. 2019; Zarei-Baygi and Smith 2021; Debroas and Siguret 2019) and are often more persistent than pathogenic viruses (Schijven and Hassanizadeh 2000; Nasser et al. 1993). Thus, their uncomplicated handling and fast detection makes them useful indicator organisms for water related health risk assessments. Furthermore, adenovirus is also regarded as an suitable fecal indicator organism in reclaimed water (Rusiñol et al. 2020). Adenoviruses has a higher tenacity than the classic indicator bacteria and are therefore also useful to indicate fecal contamination of the water that occurred longer ago (Selinka et al. 2011). Among pathogens, viruses have the highest mobility and persistence in the environment. In addition, viruses are the most difficult to remove during engineered water treatment processes. The most common enteric viruses include norovirus, rotavirus, adenovirus and enterovirus (Leclerc et al. 2000; WHO 2017).

Table 2-1 summarizes some of the most relevant (indicator) pathogenic microorganisms that are possible present and have to adequately removed by water treatment.

Table 2-1: (Indicator) pathogens or pathogen groups relevant for water reuse applications (Rusiñol et al. 2020; Chhipi-Shrestha et al. 2017)

Pathogen type	Examples
Bacteria	Fecal Indicator Bacteria (*E. coli* + *Intestinal Enterococci*)
	Heterotrophic bacteria
	Legionella spp.
	Aeromonas spp.
	Arcobacter spp.
	Campylobacter
	Shigella
	Salmonella
	Vibrio cholera
	Heliobacter pylori
Viruses	Human adenoviruses (Fecal indicator)
	Noroviruses, genogroup I & II
	Human enteroviruses
	Rotavirus
	Hepatitis A virus, hepatitis E virus
	Different polyomaviruses e.g. Human JC Polyomaviruses, Merkel cell Polyomavirus
	Bacteriophages
Protozoa	Fecal Indicator protozoa (*Giardia Duodenalis cysts* + *Cryptosporidium parvum oocysts*)
	Blastocysts sp.
	Acanthamoeba castellanii
Helminths	*Taenia* (tapeworm)
	Ascaris (roundworm)
	Trichuris (whipworm)
	Ancylostoma (hookworm)

2.2.2 Antibiotic resistant bacteria and genes

Antibiotics and their metabolites are ubiquitously present in the environment (Munir et al. 2011; Hong et al. 2013; Alexander et al. 2015; Hiller et al. 2019). The selective pressure induced by the exposure of bacteria to this potpourri of antibiotics has resulted in a substantial increase of occurrences of antibiotic resistant bacteria (ARB) (Lan et al. 2019). The World Health Organization (WHO) has identified the spreading of ARB and their associated antibiotic resistance genes (ARG) as a growing public health concern, especially since antimicrobial resistance (AMR) threatens the effective prevention and treatment of infections caused by bacteria, parasites, viruses and fungi (WHO 2014, 2015).

In the environment ARGs are present either as intracellular (iARG) or extracellular (eARG) fractions of DNA. In nutrient rich environments iARGs constitute the main fraction of ARGs, while in receiving aquatic environments eARGs are predominant (Zarei-Baygi and Smith 2021). In general, ARGs can be spread via vertical gene transfer (VGT) or horizontal gene transfer (HGT). Especially HGT plays a key role in spreading of ARGs. Transformation, conjugation and transduction are described as the main forms for the intercellular movement of DNA and therefore the transmission of eARGs or

iARGs in prokaryotes (Frost et al. 2005; Thomas and Nielsen 2005). Especially important agents that effect the DNA movement or ARG transmission are plasmids, bacteriophages and transposons (Frost et al. 2005). For instance, iARGs or eARGs are often encoded in plasmids and can be horizontally transferred via conjugation or transformation, respectively (Matsui et al. 2001; Matsui et al. 2003; Frost et al. 2005; Johnston et al. 2014). On the other hand, phages are suspected to facilitate the exchange of genetic material between bacteria via transduction. By transduction phages enable bacterial adaptation and evolution since they can inject DNA accidentally acquired of a host into new host bacteria (Calero-Cáceres et al. 2019) where the injected DNA can recombine with the cellular chromosome and can there be inherited (Frost et al. 2005; Thomas and Nielsen 2005). Moreover, ARGs carried by phages have shown high persistence against conventional wastewater treatment and disinfection with chlorine, UV irradiation, or ozonation due to their protection inside the protein capsid. Given this and that phages are the most abundant and diverse biological entity in the world, phages play a major role in the acquisition, maintenance, and spread of AMR (Calero-Cáceres et al. 2019; Zarei-Baygi and Smith 2021; Debroas and Siguret 2019). Thus, both phages and plasmids represent relevant mobile genetic elements (MGEs) enabling the acquisition, maintenance, and spread of ARGs.

In addition, the extended-spectrum β-lactamase *E. coli* can already be found in high concentrations in our environment (Dingemans et al. 2020). Other examples for ARB are *E. coli* species resistant to ampicillin and chloramphenicol. Moreover, there even exist bacteria that are resistant to a variety of pharmaceuticals known as multidrug-resistant (MDR) bacteria. Examples for ARGs are $bla_{CTX\text{-}M}$, *tetO, tetQ, qnrB, dfrA12, ermB, vanA, blaVIM1, sul1* or *sul2* (Krzeminski et al. 2019).

Wastewater treatment plant (WWTP) effluents have been recognized as significant sources of AMR with substantial dissemination of AMR to the receiving water body (Kumar and Pal 2018). Within various studies AMR was detected in hospital as well as residential/municipal wastewater (Sigala and Unc 2012; Li et al. 2015; Rizzo et al. 2013; Szczepanowski et al. 2009; Rodriguez-Mozaz et al. 2015). Even though a large part of the ARBs are retained during wastewater treatment, still a substantial amount of ARBs ends up in the receiving water with the treated wastewater (Rizzo et al. 2013; Rodriguez-Mozaz et al. 2015). The occurrence of antibiotic resistance in anthropogenically impacted surface waters has already been observed and described elsewhere (Pei et al. 2006; Stoll et al. 2012; Li et al. 2014a; Zhang et al. 2014; Hiller et al. 2019). Thus, the aquatic environment plays an important role in the development and spread of AMR. Advanced wastewater treatment is one way to control or reduce the spread of ARBs and ARGs in the aquatic environment. Bürgmann et al. (2018) emphasized the urgent need for a more holistic approach described as ‘One Water’ in order to comprehend the fate of ARB and

ARGs not only in various waste management systems, but also the interconnections as well as interdependencies between our food (including irrigation of crops), sanitation and potable water systems. Therefore, when using reclaimed water (e.g. for agricultural irrigation purposes) it is of utmost importance to remove AMR to an extent that an environmentally safe and hygienic application is ensured.

2.2.3 Heavy metals

Heavy metals, such as arsenic (As), cadmium (Cd), copper (Cu), chromium (Cr), molybdenum (Mo), nickel (Ni), lead (Pb), and zinc (Zn) can also be present in raw municipal wastewater. Their potential accumulation in the soil or crop that is irrigated with reclaimed water can result in their enrichment in the food chain to a toxicity level that poses a health risk to end consumers. However, usually heavy metals are removed sufficiently during conventional wastewater treatment as they adsorb to sewage sludge (Chen et al. 2013a; Asano et al. 2007).

2.2.4 Trace organic chemicals (TOrCs) and transformation products

TOrCs comprise industrial and household chemicals (such as solvents, plasticizers, pesticides, monomers, complexing agents), personal care products, hormonally active chemicals as well as pharmaceuticals (and their active metabolites). TOrCs are usually only insufficiently removed during conventional biological wastewater treatment and a broad range of TOrCs occurs in wastewater treatment plant effluents (Ternes 2007a; Dong et al. 2015). This resulted in the fact that TOrCs are widely detected in various environmental compartments such as soil, groundwater and surface water bodies (Nikolaou et al. 2007; Vieno et al. 2007; Wu et al. 2009; Li 2014b; Sui et al. 2015; Lin et al. 2015; Biel-Maeso et al. 2018) or even crops that are irrigated with reclaimed water (Sharma et al. 2020). Just to name a few, typical examples for TOrCs present in wastewater or reclaimed water are for instance 4-formylaminoantipyrine, atenolol, benzotriazole, carbamazepine, diclofenac, diphenhydramine, erythromycin, fluoxetine, ibuprofen, ketoprofen, meprobamate, primidone, sulfamethoxazole, trimethoprim, or venlafaxine. Typical pesticides, possibly present in wastewater or reclaimed water are atrazine and DEET (N,N-diethyl-meta-toluamide) (Park and Lee 2018; Sharma et al. 2020).

Due to their biological activity, aquatic toxicity and indications of potentially adverse interactions with the endocrine system, the presence of TOrCs in municipal wastewater poses with the microbial risk another public health challenge during reuse of reclaimed water (Drewes et al. 2018; Petrie et al. 2015). Hence, water reuse requires both technical

and regulatory requirements in order to significantly reduce the risk for human health originating from TOrCs (National Research Council 2012).

2.2.5 Disinfection and oxidation by-products (DBPs)

DBPs are chemicals that are formed when a chemical disinfection or oxidizing agent reacts with water constituents besides the targeted pathogens or chemicals. The formation of DBPs is primarily facilitated by the presence of effluent organic matter (EfOM) or bromide (Br^-) and at high concentrations of disinfectant or oxidizing agents. An increasing dosage of disinfectant or oxidizing agent, will usually also result in higher DBPs concentrations. Thus, the ideal amount of disinfectant or oxidizing agent has to be identified to ensure hygienically safe reclaimed water without an excess DBP formation. Typical DBPs that are likely to form during chlorination or ozonation are, for instance, N-nitrosodimethylamine (NDMA), chlorate, perchlorate, bromate or trihalomethanes (Criquet et al. 2015). This is especially of concern since NDMA and bromate have carcinogenic effects on humans (Crittenden and Harza 2005).

2.2.6 Nutrients and salts

Reclaimed water contains different essential plant nutrients such as nitrogen (N), phosphorus (P) and potassium (K), as well as required micronutrients such as the metals boron (B), cobalt (Co), copper (Cu), iron (Fe), manganese (Mn), molybdenum (Mo), nickel (Ni), and zinc (Zn). The actual concentrations depend on the feed water quality and the preceding treatment train (Chen et al. 2013a; Asano et al. 2007).

Municipal wastewater may contain elevated levels of dissolved salts, such as calcium (Ca^{2+}), magnesium (Mg^{2+}), potassium (K^+), sodium (Na^+), chloride (Cl^-), sulphate (SO_4^{2-}), nitrate (NO_3^-), and bicarbonate (HCO_3^-). During conventional wastewater treatment these ions are usually insufficiently retained. Consequently, reclaimed water may exhibit salinity levels 1.5 to 2 times higher than the tap water used in the service area. This could result in salinization of the agricultural soil where reclaimed water is used for extensive irrigation. Elevated concentrations of Na^+, Cl^- and HCO_3^- can deteriorate the soil and are toxic to certain crops (Chen et al. 2013a; Erel et al. 2019).

2.2.7 Pathways and risk of exposure to contaminants possibly present in reclaimed water

Humans or the environment can be exposed to the aforementioned contaminants via different pathways. Humans might be exposed to potential contaminants via a direct contact to the reclaimed water, e.g. during irrigation application by spraying or aerosols. By the consumption of crops that were irrigated with reclaimed water humans might also get in contact with contaminants present in reclaimed water. Another pathway exists in the consumption of groundwater that possibly has been impacted by reclaimed water due to leaching and infiltration (Figure 2-1).

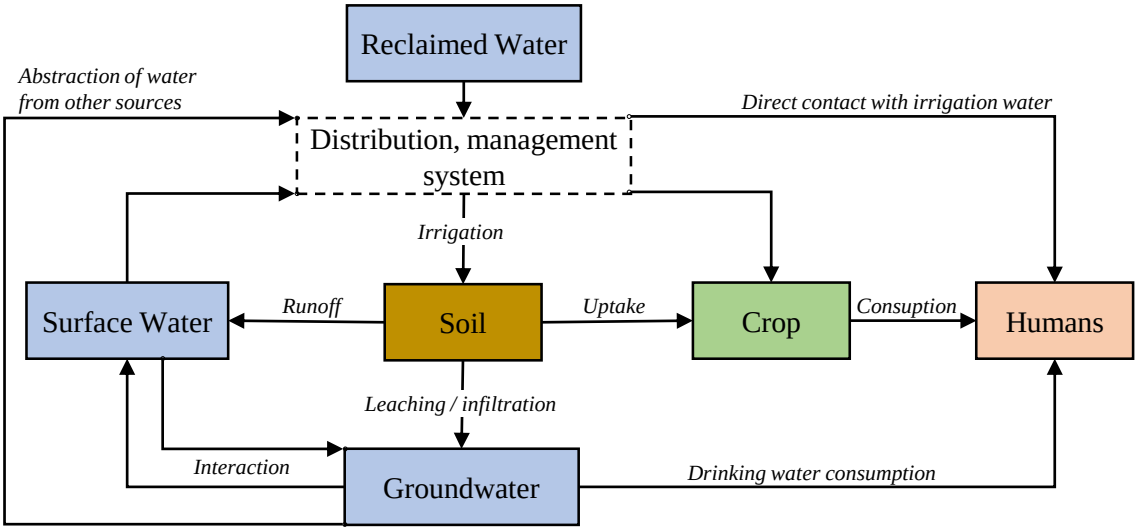

Figure 2-1: Potential pathways of human exposure to contaminants possibly present in reclaimed water, adapted from Carter et al. (2019)

2.3 Legal requirements relevant for water reclamation and reuse

For the application of reclaimed water (reclaimed wastewater, stormwater, etc.) for agricultural or urban irrigation, it is of utmost importance to define water quality requirements in order to ensure hygienically safe and environmentally sound practices. In this context, soil, groundwater, surface water, irrigated crops and human health are particularly important to be protected. Furthermore, the various transfer paths between these different compartments or entities have to be considered (cf. Figure 2-1). Based thereon, legal areas of environmental protection, consumer and health protection as well as product liability are affected (Seis et al. 2016). For water reuse applications that take place indirectly through groundwater recharge (e.g. irrigation) where best agricultural practice is not followed, trace organic chemicals (household and industrial chemicals, pharmaceuticals), and other compounds (nitrate, nitrite, etc.) also have to be sufficiently removed that adverse impacts on groundwater quality can be excluded. Negative consequences for soil, groundwater, surface water and especially human health have to be minimized or completely prevented.

In order to ensure environmental as well as human health protection, some countries where water reuse has a long tradition (e.g. Australia, USA, some southern EU member states) have already established legislative requirements for water reuse. For instance, the *'Guidelines for Water Reuse'* developed by the US Environmental Protection Agency, provides planning and management considerations, discusses types of reuse applications, gives an overview on state regulatory programs for water reuse, or summarizes treatment technologies for protecting public and environmental health (US EPA 600-R-12-618). Other important guidelines or regulations that have to be accounted for in the context of agricultural water reuse are DIN 19650, DIN 19684-10, GrwV (2010), EU WFD 2000/60/EC, or ISO 16075. A summary of those can be found in Table 2-2.

The most recent regulation with respect to quality requirements for water reuse has been passed by the European Commission in 2020, named '*EU Regulation 2020/741 of the European Parliament and of the Council on minimum requirements for water reuse*' (2020/741/EU). This EU regulation will apply in all EU member states from 26th of June 2023 onwards (German Environmental Protection Agency or Umweltbundesamt, abbreviated as UBA 2021b) and it addresses water reuse solely for agricultural irrigation purposes. The regulation 2020/741/EU defines four classes of reclaimed water quality (A, B, C, D) and specifies the permitted agricultural use and irrigation method. Each water quality class requires at least secondary treatment and disinfection. Filtration is additionally needed only for the reclaimed water quality class A which allows the irrigation of all food crops consumed raw. Concrete water quality requirements provided within this regulation are limited to thresholds for *E. coli*, BOD_5, TSS, turbidity and Legionella where there exists risk of aerosolization, or for intestinal nematodes for irrigation of pastures or forage. Risk management requirements are set out in Appendix II of the regulation. The proposed risk management comprises i.a. the description of the entire water reuse system, including the wastewater origin, treatment barriers, the supply, and distribution system, as well as storage infrastructure. The risk assessment shall address both, environmental as well as human and animal health risks associated with water reuse. Furthermore, preventive measures concerning heavy metals, pesticides, disinfection by-products, pharmaceuticals, other concerning substances, or anti-microbial resistance are roughly specified. Preventive measures may include access control, additional disinfection or pollutant removal technologies, irrigation methods, etc. (2020/741/EU). However, for instance the important topic of an adequate salt management is not elaborated (Drewes et al. 2018).

According to the UBA, the '*Minimum requirements for water reuse*' by the European Commission (2020/741/EU) are neither specific nor strict enough. The specified minimum requirements for the four classes of reclaimed water quality only apply at the point where the water is passed on from the treatment plant. Subsequent quality changes

are not considered (UBA 2021a). This means that the EU regulation only aims at the operators of the treatment plant, while operators of the water conveyance or storage system and the end user (e.g. farmer) are not directly obligated by the regulation (Spieler et al. 2021b).

Consequently, the regulation does not oblige the EU member states to require separate authorizations for storage, distribution and use. It is also critical that risk management does not allow for a harmonized approach and requires further elaboration by the Commission and the Member States (UBA 2021a). The UBA therefore, strongly recommends that the national requirements for water reuse should not only specify but should clearly exceed the requirements proposed by the 2020/741/EU. For instance, specific minimum requirements are necessary for the advanced treatment (after conventional wastewater treatment), disinfection as well as filtration. Treatment combinations should be specified and disinfection by-products should be considered. Validation of disinfection requirements is also suggested for classes A to C of reclaimed water quality. The contamination with pathogens of irrigated food should be monitored. While the minimum requirements only relate to the so-called point of compliance, where the water is passed on by the operators of the treatment plant, risk management should encompass the entire system. The possible additional requirements in risk management are also vague. For instance, the preventive measures concerning heavy metals, pesticides, disinfection by-products, pharmaceuticals, other concerning substances, or anti-microbial resistance are only mentioned. Concrete technical or management measures and threshold values are not specified (Spieler et al. 2021a). Groundwater, soil and drinking water protection areas should also be specially protected and monitored (UBA 2021a). So far there are no European regulations on quality requirements for the reclaimed water applied on soils. Furthermore, the EU regulation falls short of the regulations for site-specific surface and groundwater protection in German water law (Spieler et al. 2021a). The irrigation with reclaimed water in drinking water protection zones is suggested to be banned at all. The implementation of water reuse can also involve high administrative and infrastructural costs. Responsibility for bearing the costs must be clarified (UBA 2021a). Despite that the EU regulation for minimum requirements for water reuse (2020/741/EU) is an important first step, it is not yet sufficient in qualitative terms. It is expected that responsible authorities in Germany are guided by national water law requirements due to for precautionary reasons. Therefore, there is a great need for action in Germany for the creation of a technical set of rules that specifies these requirements for different water reuse applications (Spieler et al. 2021a, 2021b).

In order to implement the regulation by the 2020/741/EU into German law until June of 2023, at the end of 2020 a working group of the Bund/Länder-Arbeitsgemeinschaft Wasser (LAWA) was established. Questions on the legal scope, exclusion of use,

approval requirements, material requirements, the design of risk management and monitoring are addressed. In addition to the legal anchoring and specification of the EU regulation, a technical set of rules of the DWA (DWA-M 1200) is elaborated (UBA 2021a; LAWA 2021).This guideline is intended to support the implementation of the regulation 2020/741/EU into German law and consists of the three parts. The first part deals with water reuse principles for different user, the second part elaborates the requirements for advanced wastewater treatment prior to water reuse, and the third part examines the reuse of reclaimed water for irrigation in agriculture, horticulture and green spaces with regard to its impact on the entire ecosystem (cf. Table 2-2).

Table 2-2: Overview of national and international requirements/regulations/guidelines relevant in the context of reuse of reclaimed water for agricultural or urban irrigation purposes

Legal scope	**Guideline/ regulation**	**Summary**
Germany	DIN 19650	• Hygienic requirements for irrigation water in agriculture, horticulture, landscaping, as well as park and sports facilities • Quality requirements for irrigation water taken from the naturally occurring surface and ground water. • In addition, rainwater, drainage water and drinking water can be used for irrigation. • Use of treated wastewater is possible
	DIN 19684-10	• Specification of qualitative and quantitative requirements for irrigation water depending on the application conditions (climate, soil, plants)
	GrwV (2010)	• Groundwater protection against pollution from certain dangerous substances such as nitrate, pesticides, arsenic, cadmium, lead, mercury, etc.
	DWA-M 1200	• Guideline for the planning and operational tasks that arise with water reuse, as well as the official approval procedures. • Intended to support the implementation of the 2020/741/EU regulation in Germany • Consists of the three parts o Part 1: Water reuse principles for different user o Part 2: Requirements for advanced wastewater treatment o Part 3: Use of reclaimed water for irrigation in agriculture, horticulture and green areas
Europe	EU water frame-work directive 2000/60/EC	• Commitment to achieve good qualitative and quantitative status of all water bodies (including marine waters up to one nautical mile from shore) by 2015.
	EU minimum requirements for water reuse 2020/741/EU	• Definition of four different classes of reclaimed water quality as well as the permissible use and irrigation methods for each class. • Definitions particularly based on microbial water quality parameters • Minimum frequencies and performance targets for monitoring the reclaimed water • Proposal of specific preventive measures to limit risk are also proposed as part of this regulation.
	ISO 16075	Divided into three parts • 1st part ('The basis of a reuse project for irrigation'): Comparable to the descriptions DIN 19684-10, but in contrast to this specifically refer to the use of reclaimed wastewater for irrigation • 2nd part ('Development of the project'): Suggestions on the water quality of reclaimed wastewater depending on the wastewater quality or the potential use. Based on the guidelines of the US EPA 600-R-12-618 and WHO (2006) → multi-barrier concept. These (redundant) barriers minimize the health risks posed by the pathogens associated with the consumption of products irrigated with reclaimed water or with access to areas irrigated with reclaimed water. • 3rd part ('Components of a reuse project for irrigation'): Description of components required for a water reuse project, e.g. water storage, additional treatment technologies, piping systems and irrigation facilities.
United States	US EPA 600-R-12-618	• Planning and management considerations • Types of reuse applications • State regulatory programs for water reuse • Regional variations in water reuse • Treatment technologies for protecting public and environmental health • Funding water reuse systems • Public outreach, participation, and consultation • Global experiences in water reuse
Globally	WHO (2006)	• Assessment of health risk • Health based targets • Health protection measures • Monitoring and system assessment • Sociocultural aspects • Environmental aspects • Economic and financial considerations • Policy aspects • Planning and implementation

2.4 Treatment technologies for water reclamation

When the minimum requirements for water reuse will be implemented into German law until 2023 (cf. section 2.3), it has to be expected that these requirements will substantially exceed the requirements proposed within 2020/741/EU. In addition to microbiological organisms, further constituents such as TOrCs, PFAS, ARBs as well as ARGs have to be sufficiently removed during water reclamation in order to prevent any risk to public or environmental health. Thus, in order to comply with qualitative requirements (cf. section 2.3), a water treatment will be required which, in addition to hygienic parameters such as microbial pathogens, also effectively removes TOrCs (cf. section 2.2). Due to seasonal water demand which is usually typical for agricultural irrigation and the need for short-term coverage of (daily) peak demand, flexible, compact and modular treatment trains will be required that can also withstand longer shut-down periods.

Conventional wastewater treatment consists of preliminary treatment (e.g., rakes, screens), primary wastewater treatment (e.g., sedimentation, flotation), and secondary wastewater treatment (e.g., conventional aerobic sludge system or anaerobic microbial system). Often the secondary treatment is the final stage of a wastewater treatment plant before discharging the effluent into a receiving water body (Akinsemolu 2020; Osundeko et al. 2019; Chen et al. 2013a). TOrCs, hormones, or endocrine disrupting substances are usually insufficiently removed during conventional wastewater treatment and a broad range of TOrCs occurs in the corresponding secondary effluents (Ternes 2007a; Dong et al. 2015; K'oreje et al. 2020). Conventional municipal wastewater treatment plants, therefore, represent major point sources of TOrCs to the environment (González et al. 2015; Bui et al. 2016). Moreover, pathogens such as viruses are also not completely retained during conventional wastewater treatment (Bosch 1998; Fleischer and Hambsch 2007; Botzenhart and Fleischer 2009). Even in combination with sand filtration conventional activated sludge treatment removes only around 1.6 log of enterovirus or 0.9 log of norovirus (Ottoson et al. 2006). Because of this, water reuse of reclaimed secondary effluent is only allowed after at least a disinfection step, or disinfection after filtration according to the EU regulation 2020/741/EU (cf. section 2.3).

However, via advanced wastewater treatment (e.g., advanced biological processes, coagulation, filtration, micro-, ultra- or nanofiltration, reverse osmosis, adsorption on activated carbon, chlorine or UV disinfection or ozonation) organic constituents including TOrCs, nutrients such as N and P, metals, pathogens, or turbidity can be further removed from a secondary/tertiary effluent (Osundeko et al. 2019; Rizzo et al. 2020). Especially in high income countries advanced treatment is becoming the standard for the final wastewater treatment (Akinsemolu 2020; Osundeko et al. 2019). Some of the most

promising and widely applied advanced water treatment technologies are introduced within the subsequent sections:

2.4.1 Oxidative and advanced biological water treatments

Oxidative processes such as ozonation or advanced oxidation processes (AOPs) represent a promising option for the treatment of wastewater prior to reuse. Ozone and UV-based advanced oxidation processes do not only result in the oxidation of a broad range of relevant water constituents (e.g., TOrCs, odor, color, etc.) but also offer an effective disinfection of reclaimed water. In addition, oxidation with ozone leads to an improved biodegradability of organic carbon, which can be measured as assimilable organic carbon (AOC) or biodegradable dissolved organic carbon (BDOC) (Yavich et al. 2004; Hammes et al. 2006). For this reason, a combination with a downstream biological (and sometimes adsorptive) stage is often recommended. Sand filters being applied downstream of an ozonation or AOP treatment step have shown effective removal of organic micropollutants (Hollender et al. 2009). Ozonation followed by biological activated carbon (BAC) filters (Reungoat et al. 2012) or artificial groundwater recharge (Hübner et al. 2012; Zucker et al. 2015) also resulted in high abatement of TOrCs. Besides enhancing the biological degradation of DOC, another benefit of combining ozone and downstream biological active (carbon) filters is the potential removal of transformation products and oxidation-by-products due to biodegradation and adsorption (Hübner et al. 2014; Scheurer et al. 2012).

2.4.2 Adsorption processes for advanced water treatment

Granular activated carbon (GAC) and powdered activated carbon (PAC) are traditionally used for the adsorptive removal of organic contaminants (Worch 2012). A large spectrum of TOrCs can be efficiently removed with activated carbon (Altmann et al. 2014), especially from pre-treated water with relatively low residual concentrations of competing water constituents (Zietzschmann et al. 2014). In principle, adsorption by activated carbon represents an effective way to reduce the concentrations of many TOrCs, unless of some very polar substances that are poorly adsorbable, such as iodinated X-ray contrast media or artificial sweeteners and complexing agents (Jekel et al. 2015). In order to optimize TOrCs removal, often oxidative processes such as ozonation are combined with a downstream adsorptive treatment via GAC or PAC. When PAC is used downstream of an advanced water treatment such as ozonation, an additional process stage is required in order to reliably separate the PAC loaded with TOrCs. Because of the higher technical effort associated with the use of PAC, usually GAC is preferred over PAC after treatment via ozonation as a downstream biological active adsorber (BAC).

2.4.3 UV disinfection for advanced water treatment

Disinfection by ultraviolet irradiation (UV) is a commonly used technology for water disinfection (Hassen et al. 2000; Zhuang et al. 2015; Gibson et al. 2017). UV disinfection can effectively inactivate microorganisms such as bacteria, viruses, or protozoa. Even some TOrCs can be degraded at high UV dosages and an inactivation of ARB as well as ARGs was also observed during UV irradiation (Rizzo et al. 2020). According to the German drinking water directive for drinking water disinfection a fluence of 400 J/m^2 (40 mJ/cm^2) at a wavelength of 254 nm is required (Trinkwasserverordnung 2020). For adequate inactivation of MS2 phages and adenovirus in potable water treatment, the National Water Research Institute suggests a fluence of 20 mJ/cm^2 or 180 mJ/cm^2, respectively. For water reuse applications a fluence of 100 mJ/cm^2 is recommended (National Research Council 2012). In general, UV fluences applied for the disinfection of wastewater treatment plant effluents can range from 60 to 200 mJ/cm^2 (Bourrouet et al. 2001).

Besides the disinfection directly by UV radiation, UV light can be combined with radical promoters to generate highly reactive radicals. The radicals that are formed during UV-AOP processes effectively oxidize and ‘remove’ organic compounds such as TOrCs or also color, taste and odor (Gerrity et al. 2013; Gerrity et al. 2011; Miklos et al. 2018; Miklos et al. 2019).

2.4.4 Membrane ultrafiltration for advanced water treatment

Depending on the pore size, different membrane separation processes can be distinguished comprising microfiltration (MF), ultrafiltration (UF), nanofiltration (NF) and reverse osmosis (RO). These membrane processes can be operated separately or in combination with other processes as a part of integrated technologies (Rizzo et al. 2020). In particular, UF membrane applications are gaining attention within the scientific research community. Nowadays, UF technology is employed in many sectors, such as the food, beverage, healthcare product, or bioengineering sector, or for industrial, municipal wastewater, or drinking water treatment or also as pretreatment prior to desalination processes (Al Aani et al. 2020).

2.4.4.1 Relevant characteristics of UF membranes

Pore sizes of UF membranes typically range between 2 to 100 nm (van der Bruggen et al. 2003). The molecular weight cut-off (MWCO) of membranes is another relevant parameter for the characterization of UF membranes, especially when UF is employed for the separation of proteins and other biological compounds by their molecular weight. At a specific MWCO, 90 % of molecules within the corresponding molecular weight are

retained (Singh 2015). The properties of membranes are strongly influenced by their surface charge, measured as the zeta potential which is affected by the pH of the filtered media. A negative zeta potential (unit in [mV]) indicates a negative surface charge (Bellona et al. 2004; ElHadidy et al. 2013a).

UF membranes are usually manufactured of polymeric and ceramic materials. Typical polymeric membrane materials are polysulfone, polyvinylidene fluoride, cellulose acetate, polyethersulfone, acrylate or polypropylene. Ceramic membranes can consist of various metal oxides such as aluminium oxide (Al_2O_3), zirconium oxide (ZrO_2) or titanium dioxide (TiO_2). In comparison to ceramic membranes, polymeric membranes are less stable especially with respect to high temperature, chemicals, or mechanical stress (Goswami and Pugazhenthi 2020). Ceramic membranes show an excellent resistance against high temperatures and chemicals and they exhibit a longer lifetime than polymeric membranes (up to 10 years). Ceramic membranes are more rigid than polymeric membranes which 5 to 10 times elevated fluxes in comparison to polymeric membranes. Due to their stronger mechanical tenacity, ceramic membranes also keep their integrity longer than polymeric ones (Gitis and Rothenberg 2016; Werner et al. 2014; Ng et al. 2018). Furthermore, the higher mechanical strength and physical as well as chemical resistance of ceramic membranes allows more frequent and aggressive hydraulic as well as chemical enhanced backwashes than it is feasible for polymeric membranes. This enables a more stable overall operation since higher recovery rates after hydraulic as well as chemical enhanced backwash can be achieved (Singh 2015). However, ceramic membranes are more expensive, are brittle and have a higher weight than polymeric membranes (Werner et al. 2014).

2.4.4.2 Mechanisms of and influencing factors on UF removal efficiency

Removal of particles during membrane filtration such as UF is influenced mainly by three parameter groups: membrane properties, feed water characteristics and properties of the particles to be removed (Bellona et al. 2004). Typical membrane properties that affect rejection include molecular weight cut-off, pore size, surface charge (measured as zeta potential), hydrophobicity/hydrophilicity (measured as contact angle), and surface morphology (measured as roughness) (Bellona et al. 2004). In addition to the aforementioned membrane properties, feed water characteristics strongly influence the rejection of particles: pH, ionic strength, hardness, the presence of organic matter, water temperature, or particle concentration can be named as crucial influencing feed water parameters (Bellona et al. 2004; Furiga et al. 2011; Gerba and Betancourt 2017; Langlet et al. 2007; Langlet et al. 2008; Jacquet et al. 2021). Membrane fouling which is a function of the feed water quality as well as membrane characteristics also affects removal efficiency during UF. Fouling can be beneficial for the UF rejection efficiency due to

clogging of pores and reducing their diameter as well as formation of a cake layer (Cheng and Hong 2017; ElHadidy et al. 2014). Finally, particle characteristics such as particle concentration, particle weight, particle size and geometry as well as hydrophobicity/hydrophilicity affect particle rejection during UF (Jacquet et al. 2021; Bellona et al. 2004).

The complex interactions of the aforementioned key parameters affecting the removal efficiency result in a few main mechanisms for the retention of particles or microorganisms such as bacteria, or viruses during UF: size exclusion, adsorption on the membrane surface due to opposite charges, hydrophobic interactions between the particles and the membrane surface, and electrostatic repulsion of particles by the membrane due to identical electrical charges are the most relevant removal mechanisms during UF (ElHadidy et al. 2013a; Goswami and Pugazhenthi 2020).

In addition to pathogens, there are other contaminants of concern that have to be addressed when reusing water (cf. section 2.2). These contaminants include, but are not limited to, ARBs, ARGs, and TOrCs (Dong et al. 2015; Ternes et al. 2007b; Ternes 2007a; Drewes et al. 2018; Hembach et al. 2019; Hiller et al. 2019). TOrCs removal solely by UF membranes can be neglected, since the UFs' pore sizes are too large for a physical separation of TOrCs (Yoon et al. 2006; Yoon et al. 2007). Hence, for a sufficient reduction of concerning TOrCs, UF has to be combined with processes that are capable to remove TOrCs (cf. 2.5). In contrast, UF membranes can act as reliable physical barriers against turbidity, pathogenic bacteria, bacterial indicators, partially even viruses or ARGs due to size exclusion/physical separation (Madaeni 1999; Di Zio et al. 2005; Gómez et al. 2006; Ferrer et al. 2015; Iannelli et al. 2014; Werner et al. 2014).

Contrary to studies that regard UF membranes as reliable barrier against pathogens, other studies reported extracellular plasmids (possibly carrying ARGs), viruses including phages or even bacteria permeating through membrane pores with diameters much smaller than the sizes of the corresponding plasmids, bacteria or viruses (Arkhangelsky and Gitis 2008; Arkhangelsky et al. 2008; Arkhangelsky et al. 2011; Latulippe et al. 2007; Latulippe and Zydney 2009; Latulippe and Zydney 2011; Slipko et al. 2019; Larson et al. 2006). Wick and Patrick (1999a) observed MS2 phages with a molecular weight of 2 MDa penetrating membranes with MWCOs of 750, 500, and 300 kDa. Even bacteria were reported to break through UF membranes with a nominal pore size of 100 nm (Liu et al. 2019) or a MWCO of 100 kDa (Ren et al. 2018). For solution-diffusion based tight nanofiltration or reverse osmosis membranes transmission of free DNA was also reported (Slipko et al. 2019; Arkhangelsky et al. 2011). There are different explanations for the penetration of viruses, bacteria, or plasmids through membrane pores smaller than their expected radius. Each membrane has **a pore size distribution**, hence there always exist

pores that are large than the nominal pore size. For instance, UF membranes with a nominal pore size of 40 nm can have pores as large as 90 nm (ElHadidy et al. 2013b). Thus, a small fraction of particles that are larger than the reported nominal pore size can pass the UF membranes via UF membrane. In addition, for polymeric membranes a positive correlation between applied flux/TMP and breakthrough of viruses, or bacteria was measured. **Pore enlargement** due to increasing hydrodynamic forces associated with increasing TMP was causing a higher transmission of the viruses (Arkhangelsky and Gitis 2008). But also the **deformation of bacteria, viruses or plasmids** due to the extensional forces that form in the converging flow fields above membrane pores can result in their increased transmission through an UF membrane (Arkhangelsky et al. 2011; Slipko et al. 2019; Latulippe and Zydney 2009; Latulippe et al. 2007). It was even observed that the degree of cell deformation depends on cell-wall properties. Gram-positive bacteria with their thicker and more rigid peptidoglycan layer were better rejected during MF than gram-negative bacteria since their thinner peptidoglycan layer resulted in stronger deformation and thus transmission through MF pores (Lebleu et al. 2009). During the deformation of bacterial cells, it is assumed that some intracellular liquid is pressed out of the bacterial cells resulting in a reduced effective cell diameter (Suchecka et al. 2003). In another study, an increasing **concentration polarization** was found to cause a decreased retention or increased breakthrough of polyethylene glycol during UF right after the TMP was elevated. However, with ongoing filtration the retention increased again, which was associated with the decreasing flux with time at constant TMP. Apparently, the tightening of the formed concentration polarization layer with continuous filtration time led to this effect (Kallioinen et al. 2007). Farahbakhsh and Smith (2004) observed a more complex behavior during separation of coliphages with an polymeric UF. Initially, log removal values (LRVs) increased with increasing flux/TMP but at certain point the LRV decreased with increasing flux. The **formation of a cake layer** that is progressively compressed was assumed to cause an increasing retention of the coliphages with increasing flux. At a critical flux the associated elevated **strain rates** were expected to cause the remobilization of the coliphages retained in the cake layer possibly explaining the decreasing LRVs with increasing flux (Farahbakhsh and Smith 2004). In some other studies dealing with polymeric UF, viruses were also slightly better retained at elevated TMP (Tsurumi et al. 1990; Hirasaki et al. 1994). However, an explanation of the observed phenomenon was not provided.

Due to seasonal water demand which is usually typical for agricultural irrigation and the need for short-term coverage of (daily) peak demand, flexible, compact and modular treatment trains will be required that can also withstand longer shut-down periods. These requirements favor (ceramic) ultrafiltration membranes due to their robustness and long lifetime (2.4.4.1). Besides technologies such as ozonation, UV disinfection, or

chlorination, ultrafiltration is also recommended by Seis et al. (2016) for water reclamation for non-potable purposes. The recent guideline with respect to quality requirements for water reuse adopted by the 2020/741/EU recommends to perform validation monitoring of reclaimed water for agricultural irrigation: Performance targets of ≥ 5.0 LRVs for *E. coli* and ≥ 6.0 LRVs for coliphages are proposed. For an adequate validation monitoring and since it is expected, that quality requirements for reused water will be more stringent than the EU guidelines are implemented into German law (cf. section 2.3), it is of utmost importance to gain a comprehensive and deep understanding of the mechanisms that affect the treatment efficiency of UF membranes. Based on the previous review of studies dealing with mechanisms and factors influencing UF removal efficiency, the following open aspects requiring a deeper investigation can be inferred:

1. Most of the studies reviewed were focusing on removal efficiency of polymeric UF membranes. Investigation of the removal efficiency of bacteria or viruses during ceramic UF are still quite rare. Phages could be inactivated due to the higher fluxes and associated strain rates that are possible during ceramic UF. This would have an impact on the required validation monitoring of the UF treatment. Thus, firstly it is of relevance to elucidate potential deformation or damage (and thus inactivation) of MS2 phages during ceramic membrane UF.
2. Secondly, the effects of varying flux and TMP conditions on the removal efficiency of MS2 phages during ceramic ultrafiltration are not well understood, yet. If the removal efficiency of viruses including phages, or bacteria is a function of applied flux/TMP this has also has consequences for the validation monitoring suggested by the 2020/741/EU.
3. Often key factors that influence the removal efficiency of antimicrobial resistance (AMR) during membrane UF are insufficiently described. Hence, the influence of the microbial load in the feed water, the pore size of membranes, and the effect of the formation of a fouling layer on ARG removal efficiencies need to be elucidated.

2.5 A promising combination: PAC/UF hybrid membrane processes

Due to seasonal demand, water reuse for agricultural irrigation requires a water treatment that reliably enables the coverage of short-term peak demand (cf. section 2.1). In order to meet this requirement, technical solutions are needed that are flexible, compact, robust, modular, can be switched on and off spontaneously, and can withstand longer shut-down periods. These requirements favor for instance (ceramic) ultrafiltration membranes, which represent a reliable physical barrier against pathogens including antibiotic resistance (Ng et al. 2018). Beside operational flexibility and robustness, the

removal of pathogens as well as TOrCs is important where water reuse with high water quality requirements is practiced. This is the case for irrigation in agriculture of crops intended for raw consumption or if it is planned to recharge groundwater by reclaimed water (cf. section 2.3). However, TOrCs removal solely by UF membranes is ineffective, since the UF pore sizes are too large for a physical separation of TOrCs and the TOrCs retention by adsorption on the UF membrane surface can be neglected (Yoon et al. 2006; Yoon et al. 2007). Hence, for an adequate reduction of concerning TOrCs, UF has to be combined with processes that are capable to remove TOrCs.

For fouling control, membrane UF is usually hybridized with pretreatment processes such as coagulation, adsorption or pre-oxidation. Powdered activated carbon (PAC) as adsorbent and ozone for oxidation are widely used for fouling mitigation during UF. In few cases also permanganate or chlorine are applied as oxidants prior to UF for fouling reduction (Gao et al. 2011). Ozone oxidation and PAC adsorption are both widely applied processes for water treatment since they are easily commercially available technologies. In addition to benefits for operational stability, the hybridization of UF with oxidation via ozone or adsorption via PAC are likely to guarantee a safe water quality allowing water reuse for irrigation of food crops or even groundwater recharge.

Several studies have investigated a combination of UF with PAC with respect to TOrCs removal (Snoeyink et al. 2000; Snyder et al. 2007; Ivancev-Tumbas et al. 2008; Campinas and Rosa 2010; Ivancev-Tumbas and Hobby 2010; Stoquart et al. 2012; Margot et al. 2013; Löwenberg et al. 2014; Rodriguez et al. 2016; Ivancev-Tumbas et al. 2018). These studies differ clearly with respect to the PAC/UF process configurations and operating procedures, which in turn significantly affect not only the overall adsorptive removal efficiency of TOrCs but also operational conditions, such as reversible as well as irreversible membrane fouling (Stoquart et al. 2012).

Three main different configurations of the hybrid membrane process (HMP) PAC/UF can be distinguished (Stoquart et al. 2012):

1. HMP with PAC pre-treatment;
2. HMP with PAC post-treatment, and
3. HMP with integrated PAC treatment.

In order to maintain longer hydraulic retention times PAC is often employed within a carbon contact reactor. This maintains higher adsorption performance of natural organic matter (NOM) and TOrC as well as better membrane fouling mitigation (Ivancev-Tumbas et al. 2008; Margot et al. 2013; Löwenberg et al. 2014; Sheng et al. 2016). However, by dosing PAC inline, directly prior to UF a more compact implementation of the PAC/UF hybrid membrane process can be realized since the PAC contact reactor is spared

(Ivancev-Tumbas et al. 2008; Ivancev-Tumbas et al. 2018). Typically applied PAC concentrations were ranging between 5 to 100 mg/l. The studies investigating PAC/UF hybrid membrane processes focused either solely on removal potential (Ivancev-Tumbas et al. 2008; Ivancev-Tumbas and Hobby 2010; Ivancev-Tumbas et al. 2018) or on effects on operational stability only (Yu et al. 2014). However, for the economically feasible application of the PAC/UF hybrid membrane process, both the treatment efficiency as well as the operational stability (transmembrane pressure) have to be considered and optimized simultaneously.

In addition to the abatement of TOrCs or pathogens, antimicrobial resistance including ARGs and ARBs have to be properly addressed during water reclamation (cf. sections 2.2 and 2.3). This means that the research on the hybrid membrane process PAC/UF even has to be expanded to its effects on ARG/ARB removal. Many studies have already investigated the effect of membrane filtration on ARB/ARGs removal. Some studies investigating the effect of membrane filtration on the removal of extracellular plasmids, viruses including phages or bacteria (possibly carrying ARGs) reported the ability of these entities to permeate through membrane pores with diameters much smaller than the sizes the corresponding plasmids, bacteria or viruses (Arkhangelsky and Gitis 2008; Arkhangelsky et al. 2008; Arkhangelsky et al. 2011; Latulippe et al. 2007; Latulippe and Zydney 2009; Latulippe and Zydney 2011; Slipko et al. 2019; Larson et al. 2006). Furthermore, it is known, that adsorption to activated carbon such as PAC does not represent a viable disinfection process, but nevertheless a reduction of AMR is expected due to possible adsorption or entrapment of ARB/ARGs inside the pores of PAC (Zhang et al. 2017; Ashbolt et al. 2018; Bürgmann et al. 2018; Rizzo et al. 2020). Calderón-Franco et al. (2020) also observed adsorptive removal of ARGs and mobile genetic elements by biochar. However, the combination of PAC adsorption and UF was not investigated with regard to ARG separation. Since the permeation of ARGs through UF membranes is governed by hydrodynamic forces during UF, it would be of importance to analyzed how the flow fields in UF processes are modified by the presence of PAC particles. Besides the adsorption or entrapment of AMR inside the PAC pores, it can be assumed that the hybridization of UF with PAC will have an effect on AMR separation in comparison to UF treatment alone due to the hydrodynamic effects of the formed PAC cake layer.

3 RESEARCH OBJECTIVES, HYPOTHESES AND DISSERTATION STRUCTURE

Beside the estimation of the local irrigation demand which is important for planning of water reuse projects, this thesis also aimed to assess membrane UF alone or combined with PAC with regard to treatment efficiency and operational stability. For that purpose, five main research objectives are proposed:

3.1 Research objective #1

Development of a modelling approach for estimating the agricultural irrigation demand for planning of non-potable water reuse projects.

For the proper planning and dimensioning of treatment and storage systems required for water reuse for agricultural purposes, in particular the determination of overall daily peak gross irrigation requirements is necessary. Modelling represents a fast and cost-effective approach to evaluate irrigation demand where respective field data are incomplete, poor in temporal resolution or not available at all. In order to obtain these temporally high resolved estimations of the irrigation demand, the computational approach implemented in CROPWAT 8.0 software can be applied. However, the CROPWAT 8.0 software is only capable to compute the water demand of a specific crop cultivated on a specific soil type in a specific cultivation period. This represents a clear drawback of using CROPWAT 8.0 for the estimation of the agricultural irrigation demand for an entire agricultural area with varying soil conditions, crop cultivation periods and a broad spectrum of different crops. To compute the overall irrigation demand for an entire agricultural area, many different crops, soils and cultivation periods have to be accounted for.

Therefore, **research objective #1** aimed to estimate site specific agricultural irrigation demand via modelling. Thus, **hypothesis #1** was proposed:

> ***Research hypothesis #1:*** *The local overall daily peak gross irrigation requirement for an entire agricultural area cultivated with different crops on different soils can be estimated via a modelling approach implemented in Python based on the Penman-Monteith equation and a modified computational procedure of the CROPWAT 8.0 software.*

Research hypothesis #1 is elaborated within **Chapter 4**. Putting it into a nutshell, research hypothesis #1 was tested by simulating a broad range of different possible cultivation scenarios implemented in Python and comparing the modeled results with corresponding field data of monthly and annual irrigation demand. Thereby the applied

simulation approach could be validated. Based thereon and a statistical analysis of the modelled data, it was possible to determine the overall daily peak gross irrigation requirement for an entire agricultural area cultivated with different crops on different soils.

3.2 Research objective #2

Investigation of effects of varying flux and transmembrane pressure (TMP) conditions during ceramic ultrafiltration on the infectivity and retention of MS2 phages.

Despite the broad spectrum of studies dealing with the removal of bacteria, or viruses such as MS2 phages during polymeric membrane UF or MF, investigations elucidating the removal efficiency of MS2 phages by ceramic UF membranes are rare. Phages could be inactivated due to the higher fluxes and associated strain rates that are possible during ceramic UF. In addition, the effects of varying flux and TMP conditions on the removal efficiency of MS2 phages during ceramic ultrafiltration are not well understood, yet.

For the investigation of effects of varying flux and transmembrane pressure (TMP) conditions during ceramic ultrafiltration on the infectivity and retention of MS2 phages two sub-hypotheses were proposed:

> ***Research hypothesis #2.1:*** *Increasing fluxes/TMPs during ceramic membrane UF can lead to the damage or inactivation of MS2 phages due to elevated hydrodynamic strain rates.*
>
> ***Research hypothesis #2.2:*** *Increasing fluxes/TMPs during ceramic membrane UF will cause a decreasing retention of MS2 phages due to the elongation of the MS2 phages in the converging flow field or due to enlargement of the UF pores.*

Research hypotheses #2.1 as well as **#2.2** are addressed within **Chapter 5**. For testing research hypothesis #2.1, we analyzed the ratios of plaque forming units (PFU) indicating infectious MS2 phages and the total amount (infectious and non-infectious) of MS2 phages measured via digital polymerase chain reaction (dPCR) at varying flux/TMP conditions. Research hypothesis #2.2 was investigated by performing a trend analysis of plaque forming units (PFUs) and dPCR results during varying flux/TMPs conditions. It was found that despite high fluxes and TMP during ceramic membrane UF, the infectivity of MS2 phages was not impaired. Furthermore, and contrary to what was initially hypothesized, the physical separation of MS2 phages significantly increased with increasing flux and TMP.

3.3 Research objective #3

Investigation of key factors influencing antimicrobial resistance (AMR) removal efficiency during membrane UF.

There are plenty of studies focusing on the reduction of ARB and ARGs during membrane filtration. Nevertheless, key operational parameters are usually insufficiently reported. Often key factors that influence the antimicrobial resistance (AMR) removal efficiency during membrane UF for wastewater treatment are poorly described. Hence, the influence of the microbial load in the feed water, the pore size of membranes, and the effect of the formation of a fouling layer on ARG removal efficiencies during UF are important to be analyzed in more depth. Three sub-hypotheses were proposed for elaborating research objective #3:

> ***Research hypothesis #3.1:*** *Higher ARG abundances in the feed water will result in higher ARGs abundances in the corresponding UF filtrates.*
>
> ***Research hypothesis #3.2:*** *The built-up a fouling layer during UF will lead to a higher AMR removal efficiency.*
>
> ***Research hypothesis #3.3:*** *Despite nominal pore sizes of UF membranes being smaller than the diameter of bacteria, intact bacteria and AMR will break through UF membranes.*

Research hypotheses #3.1, #3.2 and **#3.3** are elucidated in **Chapter 6**: Pilot-scale membrane studies were performed. It was found that the determining factor for AMR removal was the pore size of the membrane. The formation of the fouling layer during membrane UF resulted in a slightly increased removal of intra- and extrachromosomal ARG or partially had only negligible effects. The study revealed that higher ARG abundance in the feed resulted in higher ARG abundance in the filtrate. Live-dead cell counting in UF filtrate showed intact bacteria breaking through the UF membrane.

3.4 Research objective #4

Optimization of pilot-scale UF membrane processes hybridized with inline dosed powdered activated carbon with regard to TOrC removal and fouling mitigation.

Membrane ultrafiltration combined with inline dosing of powdered activated carbon represents a promising hybrid membrane process (HMP) for the production of microbiological and chemically safe reclaimed water. When employing this HMP it is crucial to optimize the operational stability (mitigation of membrane fouling) while simultaneous maintaining its removal efficiency of for instance TOrCs. Especially, questions regarding the optimization of the operational stability by the employment of coagulation and its interferences with inline dosed PAC, have not yet been comprehensively investigated. So far, the effects of inline dosed coagulant on TOrC adsorption by PAC are unclear and to date no investigations have been conducted to elucidate a possible optimum operational mode for improved TOrCs removal with concomitantly maintaining operational stability. To address this research gap, the following hypothesis was proposed:

> ***Research hypothesis #4:*** *Precoating the UF membrane with a cake layer using polyaluminium chloride (PACl) as coagulant with continuous inline dosing of PAC prior to UF achieves a significant better TOrC removal efficiency as well as mitigated TMP built-up than an operational mode with simultaneous and continuous inline dosing of coagulant and PAC.*

Research hypotheses #4 is elaborated within **Chapter 7**: Within the scope of this study, ten different operational modes, including: a) UF with or without addition of coagulant (polyaluminium chloride PACl) prior to UF treatment, b) UF only with inline dosing of PAC prior to the membrane, c) UF with continuous inline PAC and coagulant dosing, and d) precoating of the UF with coagulant with continuous inline PAC dosing, were investigated at pilot-scale. It was found that the simultaneous and continuous inline dosing of PACl coagulant and PAC prior to the UF had detrimental effects on TOrC removal efficiency. However, precoating with coagulant with continuous inline dosing of PAC prior to UF showed particularly beneficial effects on the reduction of TOrCs and mitigation of TMP built-up. Besides guaranteeing a high hydraulic backwash efficiency, this specific operational mode slightly but significantly attenuated membrane fouling and the hydraulic resistance of the cake layer formed during the filtration cycles.

3.5 Research objective #5

Evaluation of the effect of a particle cake layer on hydrodynamic strain rates and its consequences for the permeation of mobile genetic elements through UF membrane pores.

In addition to the abatement of TOrCs or pathogens, antimicrobial resistance including ARGs and ARBs have to be properly addressed during water reclamation. The presence of a PAC particle cake layer might have the potential to affect the separation efficiency of ARGs during UF since in particular hydrodynamic strain rates are responsible for their transmission through UF pores smaller than the diameter of the entities possibly carrying ARGs. In order to analyze how the flow fields in UF processes are modified by the presence of PAC particles and if the removal of mobile genetic elements possibly carrying ARGs is improved by the altered flow fields, the following hypothesis was stated:

> ***Research hypothesis #5:*** *The formation of a PAC particle layer will act like a funnel, thereby increasing the distance over which flow accelerates prior to entering the UF pore and hence decreasing the fluid strain rate, which would result in less deformation of MGEs and therefore less permeation through the UF membrane.*

Research hypotheses #5 is elaborated within **Chapter 8**. Computational Fluid Dynamics (CFD) simulations of the flow fields inside UF membranes were performed on scales where hydrodynamic effects which are relevant to MGEs could be observed. Baseline information on flow fields without any PAC cake layer was first obtained through modelling. The flow fields were then modelled with the presence of a cake layer in order to gain better understanding of the physical effects that would evolve from the particle cake layer specifically with regard to hydrodynamic effects. Based on our investigations it could be concluded that the presence of the PAC particle cake layer only had negligible effects on the hydrodynamic strain rates relevant for MGE deformation. Therefore, the potential adsorption onto PAC or entrapment of AMR inside the PAC pores in a hybrid PAC-UF process is expected to be the prevailing abatement mechanism of AMR while hydrodynamic effects can be neglected.

3.6 Dissertation structure

This dissertation is based on a cumulative collection of five peer-reviewed research articles, each representing an individual chapter of this dissertation thesis. **Chapter 4** representing **Paper I** addresses research objective #1 (section 3.1) wherein a modelling approach for the determination of site-specific agricultural demand was developed, validated and applied in order to estimate overall daily gross irrigation demand for an entire agricultural area cultivated with different crops on different soils.

Chapter 5 and **6** comprise **Paper II** and **Paper III** and address research objectives #2 (section 3.2) and #3 (section 3.3), respectively. Basically, within the context of these two chapters, factors that influence the removal efficiency of viruses such as MS2 phages, antibiotic resistance genes (ARGs), or bacteria during membrane ultrafiltration were investigated.

Paper IV and **Paper V** represent **chapters 7** and **8** addressing research objectives #4 (section 3.4) and #5 (section 3.5). These chapters analyzed the hybrid membrane process PAC combined with UF. Focus is laid on TOrC removal, operational stability measured as TMP built-up and effects of the PAC cake layer on the hydrodynamic flow fields during UF.

The overall summary of the structure of the cumulative dissertation with the corresponding chapters, applied methods, underlying research objectives and hypotheses as well as elaborated publications is provided in Table 3-1.

Table 3-1: Dissertation structure summarizing research objectives, hypotheses, and corresponding publications.

Chapter	Research objective	Research hypothesis	Method	Publication
4	**Objective #1:** Development of a modelling approach for estimating the agricultural irrigation demand for planning of non-potable water reuse projects.	**Hypothesis #1:** The local overall daily peak gross irrigation requirement for an entire agricultural area cultivated with different crops on different soils can be estimated via a modelling approach implemented in Python based on the Penman-Monteith equation and a modified computational procedure of the CROPWAT 8.0 software.	Python modelling	**Paper I:** Schwaller, C.; Keller, Y.; Helmreich, B.; Drewes, J. E. (2021). Agricultural Water Management 244, p. 106529.
5	**Objective #2:** Investigation of effects of varying flux and transmembrane pressure (TMP) conditions during ceramic ultrafiltration on the infectivity and retention of MS2 phages.	**Hypothesis #2.1:** Increasing fluxes/TMPs during ceramic membrane UF can lead to the damage or inactivation of MS2 phages due to elevated hydrodynamic strain rates. **Hypothesis #2.2:** Increasing fluxes/TMPs during ceramic membrane UF will cause a decreasing retention of MS2 phages due to the elongation of the MS2 phages in the converging flow field or due to enlargement of the UF pores.	Lab-scale experiments	**Paper II:** Schwaller, C.; Knabl, M. A.; Helmreich, B.; Drewes, J. E. (2022). Separation and Purification Technology, p. 121709.
6	**Objective #3:** Investigation of key factors influencing antimicrobial resistance (AMR) removal efficiency during membrane UF.	**Hypothesis #3.1:** Higher ARG abundances in the feed water will result in higher ARGs abundances in the corresponding UF filtrates. **Hypothesis #3.2:** The built-up a fouling layer during UF will lead to a higher AMR removal efficiency. **Hypothesis #3.3:** Despite nominal pore sizes of UF membranes being smaller than diameter of bacteria, during UF intact bacteria and AMR will break through UF membranes.	Pilot-scale experiments	**Paper III:** Hiller, C. X.; Schwaller, C.; Wurzbacher, C.; Drewes, J. E. (2022). Science of The Total Environment, p. 156052.
7	**Objective #4:** Optimization of pilot-scale UF membrane processes hybridized with inline dosed powdered activated carbon with regard to TOrC removal and fouling mitigation.	**Hypothesis #4:** Precoating the UF membrane with a cake layer using polyaluminium chloride (PACl) as coagulant with the continuous inline dosing of PAC prior to UF achieves a significant better TOrC removal efficiency as well as mitigated TMP built-up than an operational mode with simultaneous and continuous inline dosing of coagulant and PAC.	Pilot-scale experiments	**Paper IV:** Schwaller, C.; Hoffmann, G.; Hiller, C. X.; Helmreich, B.; Drewes, J. E. (2021). Chemical Engineering Journal 414, p. 128801.
8	**Objective #5:** Evaluation of the effect of a particle cake layer on hydrodynamic strain rates and its consequences for the permeation of mobile genetic elements through UF membrane pores.	**Hypothesis #5:** The formation of a PAC particle layer will act like a funnel, thereby increasing the distance over which flow accelerates prior to entering the UF pore and hence decreasing the fluid strain rate, which would result in less deformation of MGEs and therefore less permeation through the UF membrane.	CFD modelling	**Paper V:** Schwaller, C.; Fokkens, K.; Helmreich, B.; Drewes, J. E. (2022). Chemical Engineering Science 254, p. 117606.

4 ESTIMATING THE AGRICULTURAL IRRIGATION DEMAND FOR PLANNING OF NON-POTABLE WATER REUSE PROJECTS

The following chapter presents investigations related to ***research hypothesis #1***: *The local overall daily peak gross irrigation requirement for an entire agricultural area cultivated with different crops on different soils can be estimated via a modelling approach implemented in Python based on the Penman-Monteith equation and a modified computational procedure of the CROPWAT 8.0 software.*

This chapter has been published with some editorial changes as follows:

Schwaller, Christoph; Keller, Yvonne; Helmreich, Brigitte; Drewes, Jörg E. (2021): Estimating the agricultural irrigation demand for planning of non-potable water reuse projects. In Agricultural Water Management 244, p. 106529. DOI: https://doi.org/10.1016/j.agwat.2020.106529

Author contributions: Christoph Schwaller and Jörg E. Drewes developed the research objective. Christoph Schwaller and Yvonne Keller established the required data basis for the modelling approach. Yvonne Keller implemented a first version of the modelling approach within Excel. Christoph Schwaller implemented the modelling approach in Python, analyzed the data and wrote the manuscript. Jörg E. Drewes and Brigitte Helmreich supervised the study and reviewed the manuscript. All authors approved the final version of the manuscript.

4.1 Abstract

Water reclamation and reuse represent a promising approach to mitigate water related use conflicts especially in the agricultural sector where challenges with regard to water management are increasingly exacerbated by the effects of climate change. However, for the conceptualization and implementation of non-potable water reuse projects for agricultural purposes a comprehensive understanding of the irrigation demand is required. However, this information is frequently not readily available. Within the scope of this study a mathematical modelling approach based on the Penman-Monteith equation and a modified computational procedure of the CROPWAT 8.0 software was applied in order to determine the irrigation demand for an entire agricultural area in Gochsheim, Lower Franconia (Germany) since locally recorded data were missing, inconsistent or incomplete. Particularly important for the planning of a water reuse project was the determination of the overall daily peak gross irrigation requirement.

Keywords: Non-potable water reuse project planning; irrigation infrastructure planning; agricultural irrigation requirement modelling; crop specific irrigation requirements; overall daily peak irrigation requirements

4.2 Introduction

In August 2019, the World Resources Institute (WRI) published an analysis of water resource availability in 189 countries worldwide. According to this assessment, a quarter of the world's population lives in regions where there is an acute water shortage (WRI 2019). The situation is likely to worsen worldwide in the next few decades. Especially the rapid growth of population, increasing urbanization, progressive industrial and agricultural activities, exacerbated by the effects of climate change, are putting enormous stress on our global water resources (Marcotullio 2007; Zimmerman et al. 2008; Vörösmarty et al. 2010; McDonald et al. 2014; Drewes and Khan 2015). The associated need for increased food and energy production also has a significant 'water footprint' (Drewes et al. 2012). Therefore, communities across the world face water supply challenges due to increasing demand, drought, depletion and contamination of groundwater, and dependence on single sources of supply (Miller 2006; Wada et al. 2012). In the context of increasing use conflicts in the water sector, growing uncertainty regarding the availability of already constrained water resources as a consequence of climate change impacts, rising energy prices, and the need to mitigate for greenhouse gas emissions, cities and whole regions will be required to use and manage water resources far more efficiently and sustainably than today's systems (Mantovani et al. 2001; Daigger 2009; Maczulak 2010).

Despite a generally moderate climate, even some regions in Germany are characterized by increasing use conflicts in the water sector (Jacob et al. 2008; LfU 2009; RUF 2010). These conflicts may arise when in the context of scarce surface and groundwater resources the simultaneous water demand for agricultural irrigation, public drinking water supply, urban landscape irrigation, cooling water demand for energy production, industrial and commercial requirements, or the requirement to maintain minimum ecological flows exceed the water availability. These conflicts occur often seasonally in the spring and summer for several weeks to several months, when the water demand in the various sectors is disproportionately high. In 2017, the 'German Working Group on water issues of the Federal States and the Federal Government' published a report on the effects of climate change on water management in Germany (LAWA 2017). The impact of climate change on the flow regime of surface waters (e.g. rivers and streams) in a water-scarce region such as Lower Franconia has also been extensively studied (Altmayer et al. 2017). According to the findings of these two studies, extreme weather events such as heavy rainfall that can lead to floods and long-lasting droughts may occur more often in more severe extents and longer duration. With an average annual precipitation of approximately 450–650 mm/year, the region around Würzburg-Schweinfurt in Lower Franconia is one of the driest areas in Bavaria, Germany (DWD 2018c; LfU 2020). Especially in the region around the city of Schweinfurt (Figure 11-1)

the limited water resources are causing increasing use conflicts in the water sector, whereby particularly the local agriculture is affected. It is representative for other regions in Lower Franconia, other parts of Bavaria but also other regions in Germany with similar challenges (RUF 2010). Moreover, the area is characterized by low groundwater recharge rates (<25 mm/year) and by rivers with limited discharge. In Lower Franconia, special efforts have always been necessary to ensure the drinking water supply as far as possible from local and well-protected groundwater resources.

In order to ensure an integrated and sustainable management of the locally overexploited groundwater by agriculture (RUF 2010), the development of alternative options for the extraction, distribution and potential use of stormwater and reclaimed water, in particular for urban landscape and agricultural irrigation purposes, are urgently needed. This is especially important to secure groundwater as the prime source for drinking water supply. Options that have been neglected in these regions around Schweinfurt to compensate for these conflicts are to expand the portfolio of available water resources with so far unused water resources and to replace high-quality water resources such as groundwater through local, semi-decentralized multiple non-potable water reuse strategies, thereby keeping water in a region longer overall. This could substantially reduce the pressure on constrained groundwater resources and is already practiced on large scale in other regions with similar boundary conditions (Bixio et al. 2006; Nakamoto 2010; Bischel et al. 2012; Shishkina et al. 2012; van Houtte and Verbauwhede 2012; Burgess 2015; Drewes et al. 2018). Reclamation of stormwater runoff or wastewater effluents and their reuse can effectively alleviate challenges associated with increasing water-use conflicts by resolving water resource issues and creating new sources of high-quality water supplies (Bixio et al. 2006; Helmreich and Horn 2009; Trinh et al. 2013; Libutti et al. 2018). The future potential of using reclaimed water is substantial (Bixio et al. 2006; Alcalde-Sanz and Gawlik 2014). The inclusion of water reuse in integrated water resources planning represents a promising approach for a sustainable water resource management (Miller 2006; Alcalde-Sanz and Gawlik 2014).

However, for proper planning of water reuse projects, a reliable estimation of the respective demand is required (Asano and Mills 1990; Asano 1991; Urkiaga et al. 2008). Thus, for an adequate conceptualization and a proper design of the associated infrastructure for a non-potable water reuse strategy for agricultural areas such as the region around Schweinfurt, besides the determination of the crop specific irrigation requirements, it is of utmost importance to gain an understanding of the overall gross irrigation requirements. In this context, particularly the daily peak demand is an important parameter (Watts 1968; Wright and Jensen 1972; Khadra and Lamaddalena 2006; Mariño et al. 1993; Gallichand et al. 1991). The local irrigation association of Gochsheim (neighboring municipality of Schweinfurt, Figure 11-1) is obliged to record its respective

irrigation quantities and to report to the local state agency. However, since the recorded data were partially incomplete, were characterized by low temporal resolution (recording of complete annual or monthly irrigation demand but not of daily peak demand), and were lacking transparency with regard to the area-specific requirement, it was necessary to conduct modelling to determine temporal sufficiently resolved water demand data for agricultural irrigation. This situation is a common shortcoming and other studies also have reported of lacking consistent information on irrigation water use and highlighted the importance of modelling to compensate for this uncertainty (Wriedt et al. 2009; Shen et al. 2013; Wu et al. 2017b; Shi et al. 2018; Abolafia-Rosenzweig et al. 2019; Seidel et al. 2019; López-Lambraño et al. 2020; Mansour et al. 2020a; 2020b). Within these and also further studies (Foster et al. 2019; Le Page et al. 2020; Li et al. 2020a; Li et al. 2020b; Zambrano-Vaca et al. 2020) the estimation of irrigation water requirements has been comprehensively addressed. However, either the determination of the irrigation requirements of only a single crop was performed (Zambrano-Vaca et al. 2020), only annually or monthly resolved demand data were determined (Shen et al. 2013; Shi et al. 2018; Le Page et al. 2020; Li et al. 2020a; Li et al. 2020b; López-Lambraño et al. 2020), the determination of the crop water requirement was based (solely) on soil moisture data that are not easily available (Abolafia-Rosenzweig et al. 2019), or the focus was only laid on the estimation of crop coefficients (Seidel et al. 2019). The determination of overall daily peak gross irrigation requirements which are especially crucial for planning of non-potable water reuse projects is not properly elaborated, yet.

Therefore, within the scope of this study a modelling approach was developed to determine the crop specific net irrigation demands as well as the overall annual, monthly and daily gross irrigation requirements for the local practice of agriculture, using the town of Gochsheim as a case study. The analysis of the modelled data provided the basis for the development of a non-potable water reuse project for agricultural purposes, adapted to the local conditions.

4.3 Material and methods

4.3.1 Study site

The study site with a total area of about 55–60 hectares was located near Schweinfurt (50.049206° N, 10.219422° E) in Lower Franconia in Northern Bavaria (Germany) at an altitude of 210–240 m above sea level (Figure 11-1).

4.3.2 Computational approach for the estimation of the irrigation demand

Modelling of the agricultural irrigation requirement was performed by using the general-purpose programming language Python and was based on the same computational procedure as applied in the CROPWAT 8.0 software, freely available from the United Nations' Food and Agriculture Organization (FAO). The implementation of the CROPWAT 8.0 software into Python allowed modelling of the irrigation demand for a broader range of many different possible growing scenarios. The method was based on the Penman-Montheith equation (Allen et al. 1998; Savva et al. 2002) and is the recommended methodology for calculations of the required reference evapotranspiration if accurate meteorological data are available (Droogers and Allen 2002; Feng et al. 2017; Seidel et al. 2019). For a more detailed description of the input data for the model refer to Table 11-1. Details on the computational approach for the crop specific net irrigation requirements based on Allen et al. (1998) and Savva et al. (2002), in which i.a. also the effective rainfall is taken into account, are given within section 11.3.3 (*'Details on computational approach for estimation of the crop specific irrigation requirements'*).

For the modelling of the crop specific irrigation demand, some simplifications or assumptions were made, namely:

- Since within the modelling approach the prevention of any water stress for the crops was intended, irrigation took place as soon as the critical depletion was reached; a water stress coefficient k_s of 1 was chosen. This represented a conservative approach for the determination of the irrigation requirements.
- The full saturation of the soil with water at the beginning of the planting season was assumed. This translated into an initial soil moisture depletion ρ_{ini} of 0 % (water stored in the soil at the beginning of each period W_b = soil water content at full saturation = field capacity of the soil = PAW = 100 mm/m).
- Since in the study area around Gochsheim the mean groundwater table during the irrigation season (April–October) was usually ~1.5–4 m below ground surface (Figure 11-6), it was assumed that capillary ascent of water into the effective rooting zone did not happen. Thus, groundwater contribution from water table (G_e) was neglected ($G_e = 0$).
- Leaching requirement was neglected ($LR_{mm} = 0$) since based on reports by the local farmers irrigation is performed according to 'best management practices'. This is tantamount to the effort to prevent infiltration.
- Irrigation scheduling is also a determining factor effecting the irrigation demand. In practice, farmers irrigate their crops according to subjective assessment, mainly based on their personal experience. Since it was not possible to account for the individual irrigation scheduling of the local farmers, it was

assumed for modelling that irrigation was performed when the soil water content reached the critical depletion. Consequently, this approach represented an ideal irrigation with regard to crop yield preventing any water stress for the crop and thus, preventing any water stress induced crop loss.

- Beside the irrigation scheduling also the exact amount of applied irrigation water depends on the subjective irrigation methodology of the local farmers. However, this could not be reflected in the model. Hence, modelling of irrigation requirements was based on the assumption of full recharge of the field capacity of the soil.
- The overall efficiency of the local irrigation system in Gochsheim was estimated by farmers to be approximately 75–85 %, which was in accordance with the irrigation efficiency of the commonly used stationary irrigation systems (sprinklers) given in Savva et al. (2002) or LfL (2008). Based thereon, for modelling purposes an overall irrigation efficiency of 80 % was assumed.

Beside the computation of the (crop specific) net irrigation requirements also the overall gross irrigation requirements were determined. Being more specifically, the intention was the estimation of the gross irrigation demand for the whole agricultural area in Gochsheim. For that purpose, it was necessary to weight the respective crop specific gross irrigation requirements according to the respective shares of the fields cultivated with the corresponding crops in the total agricultural area in Gochsheim in a specific year (Table 11-2). Finally, the sum total of the weighted crop specific gross irrigation requirements was calculated:

$$IR_{g,overall} = \sum_{i,k=1}^{N} f_i * IR_{g,k} \quad (4\text{-}1)$$

$$f_i = \frac{Area\ of\ field\ i\ cultivated\ with\ crop\ k}{Total\ agricultural\ area\ in\ Gochsheim}$$

Where:

$IR_{g,\ overall}$	= overall gross irrigation requirements
f_i	= share of agricultural field cultivated with specific crop in total agricultural area
N	= number of different crops in agricultural area
IR_{gki}	= crop specific gross irrigation requirements of crop cultivated on specific field

4.3.3 Climate data

The climate data for the 47-year period from 1973 to 2019 recorded from the German Meteorological Service (DWD) at the climate station located in Bad Kissingen (Lower Franconia, Germany) were fed into the model for a representative as well as comprehensive estimation of the agricultural irrigation requirement (DWD 2018b). The climate station ‘Bad Kissingen’ (distance to the planning area approximately 28 km)

provided a comprehensive climate record (precipitation, temperature, wind speed, sunshine duration, humidity, etc.) over a sufficiently long period from 1946 to the present.

Climate data were required for the computation of the reference evapotranspiration ET_0 according to the Penman-Monteith equation (Allen et al. 1998; Savva et al. 2002):

$$ET_0 = \frac{0.408\,\Delta\,(R_n - G) + \gamma \frac{900}{T+273}\,u_2(e_s - e_a)}{\Delta + \gamma\,(1 + 0.34\,u_2)} \quad (4\text{-}2)$$

Where:

ET_0	= reference crop evapotranspiration [mm/day]
R_n	= net radiation at the crop surface [MJ/m^2 per day]
G	= soil heat flux density [MJ/m^2 per day]
T	= mean daily air temperature at 2 m height [°C]
u_2	= wind speed at 2 m height [m/sec]
e_s	= saturation vapor pressure [kPa]
e_a	= actual vapor pressure [kPa]
$e_s - e_a$	= saturation pressure deficit [kPa]
Δ	= slope of saturation vapor pressure curve at temperature T [kPa/°C]
γ	= psychometric constant [kPa/°C]

4.3.4 Soil parameters

In addition to climate, soil parameters are determining factors influencing the agricultural irrigation demand (Savva et al. 2002). Gleysol and gleyic cambisol consisting of silt, loam or clay but also stagnic luvisol (pseudogley) and cambisol-pseudogley consisting of sand to loamy sand were predominant in the agricultural area of Gochsheim (Figure 11-2). The topsoil in the agricultural area of Gochsheim consisted mainly of loamy sands as well as (loamy) clay (Figure 11-3). Based on the knowledge of the soil type the soil specific characteristics (Table 4-1) were deduced according to Amelung et al. (2018).

Table 4-1: Mean effective rooting zone (RZe) in Central European arable soils, plant-available water (PAW), plant available water in the effective rooting zone (PAW*RZe) for commonly occurring soil textures (medium bulk density) and for peat horizons/moors adapted from Amelung et al. (2018) based on Ad-hoc-AG Boden (2005).

Soil texture and abbreviation	**RZ_e (m)**	**PAW (% vol.)**	**PAW * RZ_e (mm)**
Loamy sand (Sl3)	0.8	15	120
Silt and loamy clay (Tu2, Tl)	1.0	12	120

The values in Table 4-1 were in accordance with results regarding the effective rooting zone RZ_e as well as the plant-available water PAW obtained from the BGR-Geoviewer (2020) (Figure 11-4). With an average depth of RZ_e of ~0.9 m, the PAW ranged between 100 mm/m–155 mm/m (Table 4-1 and Figure 11-4). In order to make conservative and therefore not too optimistic assumptions with regard to PAW and for

the modelling of the irrigation requirements, a PAW of 100 mm/m was used for further calculations.

With 73.3 mm the maximum daily precipitation in the planning area (in the period from 1973–2019) was smaller than the assumed maximum rain infiltration rate of approximately 90–96 mm (according to Maniak (2016) for medium deep sandy soils, loess or loamy sand soils; Figure 11-3). Thus, this parameter could be neglected for further calculations.

Since the largest part of the agricultural area in Gochsheim could be characterized by a maximum rooting depth RZ_{max} of ≥2 m (Figure 11-5), it was assumed that crop-roots did not reach this depth and therefore crops were not limited in their physiological/potential rooting depth.

With regard to the initial soil moisture no data were available. However, an initial soil moisture depletion ρ_{ini} of 0 % was assumed, which is equivalent to a full saturation of the available field capacity of the soil. This in turn meant that the initial available soil moisture PAW_{ini} corresponded to total available soil moisture.

4.3.5 Crop data and parameters

The Bavarian State Research Center for Agriculture (‘Bayerische Landesanstalt für Landwirtschaft’) provided information on area-specific/sectoral agricultural use in form of data extracted from the ‘Integrated administration and control system (IACS)’. From 2016 to 2019, various types of vegetables such as cabbage, lettuce, sugar beet, onions, potatoes and ornamental plants were grown. Prior to 2016, no distinction was made between the certain types of vegetables. It was merely given that the agricultural land was mainly cultivated with vegetables. However, it was unknown which specific crops have been grouped together under the collective term vegetables. Sugar beets, ornamental plants and potatoes were also cultivated, and in the years before 2012 aromatic, medicinal and culinary plants such as herbs. For the period prior to the year 2005, no information was available regarding the agricultural land management. Thus, based on IACS data, assumptions had been made on the cultivated crops and their corresponding area fractions (for a detailed overview of the cultivated crops and their respective area fractions for the period from 2005–2019, Table 11-2).

The lengths of the growth stages of the different crops were inferred from Savva et al. (2002) for the region Europe. If data were specifically lacking for Europe the most plausible data from other regions were chosen instead (Table 11-3). Most of the required crop coefficients (K_c) were obtained from Hochschule Geisenheim (2019) or BBCH

(2001). Where the respective data were missing, the crop coefficients according to Allen et al. (1998) or Savva et al. (2002) were used.

The initial rooting depths of the various crops (~0.25 m) were also taken from Allen et al. (1998) or Savva et al. (2002). The maximum values of the rooting depths, if available, were obtained from information provided by the DWD (2018a), otherwise also from the information given by Allen et al. (1998) or Savva et al. (2002). The values for the critical depletion $\rho_{critical}$ required for modelling were obtained from Savva et al. (2002) and BLZ (2017) (Table 11-3).

The intention of the applied modelling approach was the conservative estimation of agricultural irrigation demand. Therefore, within the applied modelling approach ideal irrigation was assumed, which is equivalent to no occurrence of any crop loss. Thus, the yield response factor, which accounts for reduction in crop yield when crop stress would be caused by shortage of soil water (Savva et al. 2002), was neglected for model computations.

According to the local farmers in Gochsheim, the growing period in the region was from April to October. No information was available on the individual planting and harvesting data of the individual crops cultivated in the past on the various agricultural fields. Therefore, assumptions had to be made in this regard. These assumptions were based on a literature review for the individual crops that were considered in the model. According to this, most of the cultivated crops were planted in the period from beginning of April to mid of May. For most crops harvesting was assumed to take place mid/end of October, occasionally end of November/beginning of December. The temporal distribution of recorded groundwater pumping rates for agricultural irrigation further confirmed this assumption (Figure 11-7). The study area of Gochsheim was characterized by numerous individual, independent and separate agricultural fields. On each of these fields, crops were cultivated during different periods. Furthermore, occasionally, during a season (e.g. April–November) different crops on the same field were grown. Thus, in order to account for the effects of different cultivation start times, the irrigation demand was modelled for 45 different cultivation start times per year. Beginning from April and ending with mid of May (~45 days) every day was assumed as start of the respective cultivation in order to cover the specified main cultivation period from April to mid of May. More detailed information to all crop specific assumptions required for modelling the agricultural irrigation demand in Gochsheim are summarized in Table 11-3.

4.3.6 Groundwater pumping rates for agricultural irrigation

Recorded irrigation data required for the validation of the model were obtained directly from the local farmers. Monthly resolved groundwater extraction rates for

irrigation purposes as well as the irrigated land area were available for the years 2014–2018. Since the recorded data had been documented manually by the individual farmers they often lacked transparency or consistency. Therefore, a range was calculated within that the recorded irrigation demand data most probably laid.

4.4 Results and discussion

4.4.1 Validation of the modelling approach

When comparing the range of irrigation demands determined by the model with the recorded actual irrigation demands for the years 2014 to 2018, two different scenarios could be identified, characterized as average (2014, 2016, 2017) and dry (2015, 2018) years, respectively (Figure 4-1). For the first scenario, comprising the years 2014, 2016 and 2017, the ranges but also the medians as well as arithmetic means of the modelled data were in accordance with the respective recorded actual data. For all of these years the modelled irrigation demand ranged between 175–240 mm, with a median and arithmetic mean irrigation demand of approximately 200–230 mm (Figure 4-1). In the second scenario, consisting of the years 2015 and 2018, the modelled irrigation demands were significantly higher than for the other years and exceeded the respective recorded actual data consistently by a factor of about 1.3–1.4 with regard to the respective arithmetic means. The modelled mean irrigation demand for both years were 320 and 340 mm, respectively, while the yearly mean value of the recorded actual demand data for both years was about 240 mm (Figure 4-1). In general, for both years, 2015 as well as 2018, relatively high modelled but also recorded actual irrigation requirements were observed. This substantial difference between the recorded actual and modelled data for these years could be attributed to the fact that both years (2015 and 2018) had low precipitation (~200 mm), relatively high temperatures (above average, horizontal lines in Figure 4-2) and thus, high ET_0 rates during crop season from April–October (mean temperature in 2015 ~14.5 °C and ET_0 of 700 mm, mean temperature in 2018 ~16.5 °C and ET_0 of 800 mm; Figure 4-2). 2018 had been an extremely dry and hot year (Marx 2019). Consequently, the overall annual gross irrigation requirement computed by the model was significantly higher than that of the other years. However, the recorded actual demand did not follow this particular pattern, thus the corresponding overall annual gross irrigation requirement was less high than it would be expected for such a dry and hot year. The mean of the modelled overall annual gross irrigation requirement therefore, ‘overestimated’ the respective recorded actual value by ~42 %. When displaying the modelled overall gross irrigation demand in monthly resolution for both years, 2015 and 2018 and by the simultaneous comparison with the respective recorded actual demand values (Figure 4-3), it was obvious that the modelled overall monthly gross irrigation data

consistently ‘overestimated’ the recorded actual monthly data for the period from April to August. Only the month of September did not fit into that pattern since in this month the modelled irrigation requirement was less than the recorded actual demand. However, the local farmers reported that during hot and dry years, such as 2015 and 2018, even for the month of September irrigation was necessary to soak the dry and hard soil with water in order to soften it and enable harvesting, particularly for root crops. Consequently, groundwater was extracted not for compensating the deficit of the crop water requirement, but for harvesting reason.

The reasons for the overestimation and differences between the irrigation demand determined by the model approach and the recorded actual irrigation demand, particularly for the hot and dry years 2015 as well as 2018, were likely caused by the following reasons:

- **Scheduling of the irrigation:** The irrigation schedule of farmers with regard to the irrigation frequency and extent was unknown. The irrigation scheduling in the model was based on the soil moisture balance and always irrigated to full, therefore ideal soil water saturation capacity. In contrast, in reality farmers irrigate purely according to subjective measurements, i.e. not according to the idealized model irrigation.
- **Crop losses:** According to the board of the irrigation association in Gochsheim, at least 15–20 % crop losses were reported for 2018 due to insufficient irrigation. This means that an optimal irrigation for the prevention of the corresponding crop losses would also have required correspondingly higher amounts of irrigation in reality. In the model calculation, this optimal/ideal irrigation was assumed without any crop loss, and therefore resulted in higher irrigation demands. Assuming the reported crop loss as a corresponding reduction in supply security by ~15–20 % allowed the comparison of the actual irrigation demand of ~210–275 mm for 2018 (Figure 4-1) with the range between the 80 and 85 %-quantile of the annual modelled irrigation demand of ~218–240 mm (Figure 4-7). Accordingly, the modelled irrigation requirement for ensuring an 80–85 % supply security was in very good agreement with the respective recorded irrigation demand for the year 2018 during which a crop loss of about 15–20 % had been experienced. This finding further provided a strong indication of the validity of the model.

Based on these results, the modelled irrigation requirement represented a good approximation of the actual overall annual gross irrigation demand for years characterized by sufficient rainfall and moderate temperatures, such as the years 2014, 2016 and 2017.

During these years no crop losses occurred which meant that the applied irrigation quantity was sufficient for preventing any water stress for the crops. For years with high temperatures and insufficient precipitation, thus increased ET_0 during the main irrigation season from April–October (Figure 4-2), the reported crop losses could have been mitigated by sufficient, ideal irrigation as it was computed by the model. Therefore, the modelled overall annual gross irrigation demand for these years also represented a good approximation of the actual needed overall annual gross irrigation requirements. Based thereon, the modelling of a broader database for a holistic estimation of the annual, but in particular of the daily irrigation demand was possible. Along with the comprehensive discussion of the other model results, even additional aspects confirming the validity of the applied model approach were elaborated within the sections 4.4.2 and 4.4.3; however, these were omitted for this section.

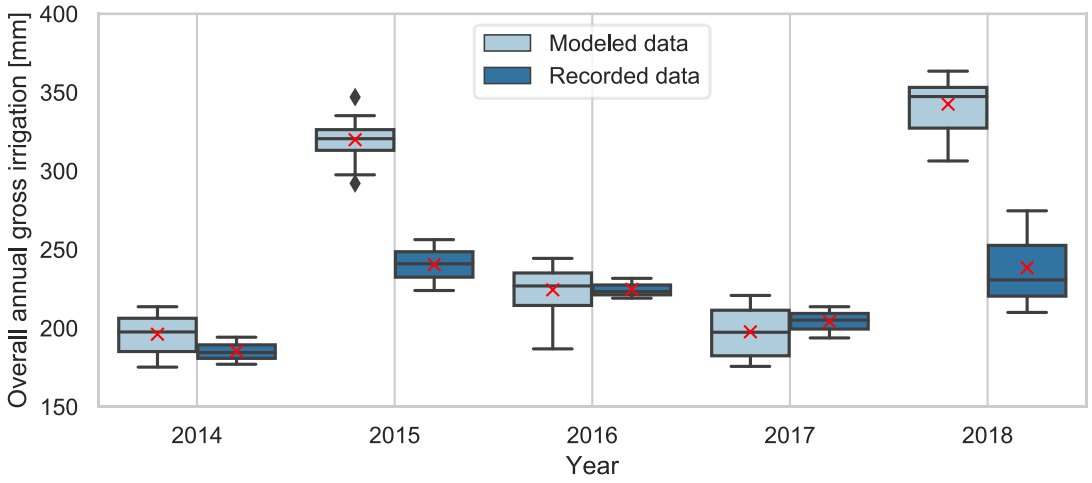

Figure 4-1: Overall annual gross irrigation demand in Gochsheim (comparison of modelled demand data – recorded demand data); the box shows the quartiles (25 %- and 75 %-quantile) of the dataset while the whiskers extend to show the rest of the distribution, except for points that are determined to be 'outliers' using the method that is a function of the 1.5 inter-quartile range; the median is indicated by the horizontal line within the box and the arithmetic mean is represented by the red cross.

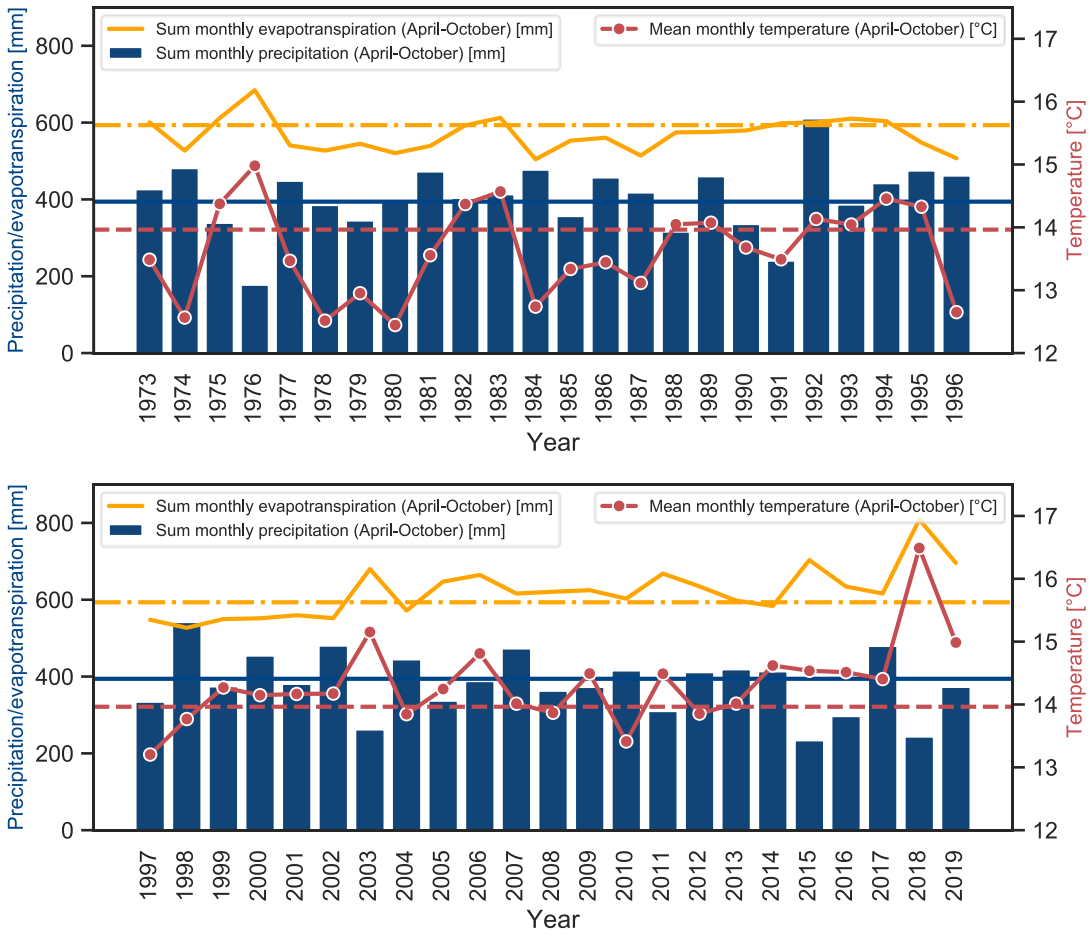

Figure 4-2: Temperature, potential evapotranspiration ET_0 and precipitation during the irrigation season (April–October); the horizontal lines indicate the arithmetic means over the period of 1973–2019 of the respective parameters.

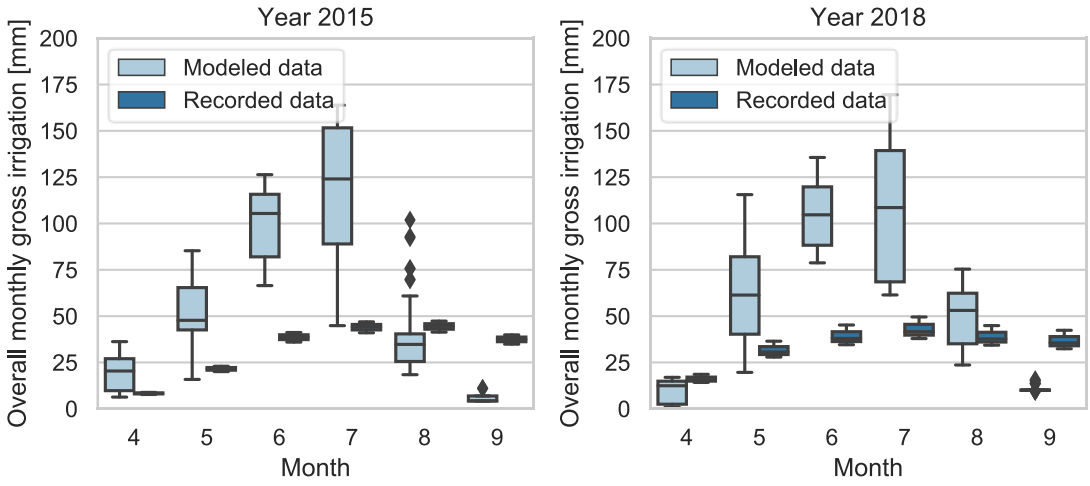

Figure 4-3: Overall monthly gross irrigation requirement in Gochsheim (comparison of modelled demand data – recorded demand data); the box shows the quartiles (25 %- and 75 %-quantile) of the dataset while the whiskers extend to show the rest of the distribution, except for points that are determined to be 'outliers' using the method that is a function of the 1.5 inter-quartile range; the median is indicated by the horizontal line within the box.

4.4.2 Crop specific net irrigation requirements

The crop specific annual net irrigation requirements for ten different crops were modelled (Figure 4-4). These modelled irrigation requirement data were statistically analyzed and compared with irrigation requirement data adapted from Paschold and Beltz (2010) as well as Zinkernagel et al. (2017) (Table 4-2). For the simulation period from 1973–2019 the most water intensive crop was celery with a mean and maximum annual net irrigation demand of ~371 mm and 602 mm, respectively. Onions had the second highest annual net irrigation requirement with a corresponding mean and maximum of ~242 mm and 427 mm, respectively. The discrepancies in the annual net irrigation requirements of the various crops were mainly due to their different crop coefficients (K_c). Because the higher the K_c, the higher the crop specific evapotranspiration and consequently the corresponding crop specific irrigation required (Allen et al. 1998; Savva et al. 2002; Hochschule Geisenheim 2019). For instance, with the highest crop specific annual net irrigation requirement of 228–602 mm/year, celery (Table 4-2) is simultaneously characterized by the highest K_c-value ranging between 0.5–1.4 (K_c, Table 11-3). The results with regard to the crop specific annual net irrigation demands were comparable to the findings given by Paschold and Beltz (2010) as well as Zinkernagel et al. (2017). Within their studies they determined e.g. for celery, onion as well as potato arithmetic mean annual net irrigation requirements with 300–320 mm, 259–304 mm and 138–172 mm, respectively (Table 4-2). In addition, the maximum values of the crop specific annual net irrigation demands, determined by the model (Table 4-2), were also in good agreement with the corresponding results presented by Paschold and Beltz (2010) and Zinkernagel et al. (2017). The estimations with regard to the crop specific annual net irrigation demand by Paschold and Beltz (2010) as well as Zinkernagel et al. (2017) were again just recently (November 2019) confirmed within the German Technical Guidance Document DWA-M 590.

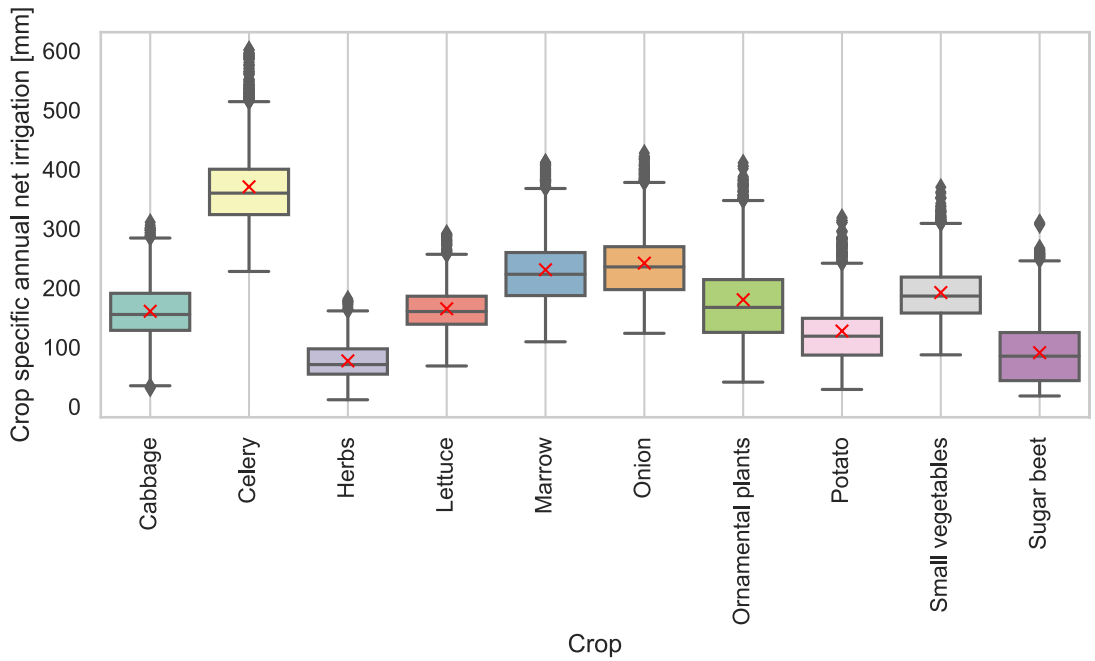

Figure 4-4: Modelled crop specific annual net irrigation requirements for the period from 1973–2019; Table 4-2 for statistical analysis; the box shows the quartiles (25 %- and 75 %-quantile) of the dataset while the whiskers extend to show the rest of the distribution, except for points that are determined to be 'outliers' using the method that is a function of the 1.5 inter-quartile range; the median is indicated by the horizontal line within the box and the arithmetic mean is represented by the red cross.

Table 4-2: Statistical analysis of the crop specific annual net irrigation requirements, modelled data for the period 1973–2019 and data adapted from Zinkernagel et al. (2017) for (loamy) sand soils in the region of Nuremberg (closest to study area) and Paschold and Beltz (2010) for sandy soils in the region of Geisenheim where similar soils are typical (BGR-Geoviewer 2020).

Data origin		Cabbage	Celery	Herbs	Lettuce	Marrow	Onion	Ornamental plants	Potato	Small vegetables	Sugar beet
Model	**n**	2115	2115	2115	2115	2115	2115	2115	2115	2115	1920
	Minimum	31	228	11	68	109	123	41	29	87	18
	25 %-Quantile	128	324	55	139	187	197	125	87	158	44
	Median	155	360	71	160	223	236	167	119	186	85
	Arithmetic mean	161	371	77	165	231	242	180	127	192	91
	75 %-Quantile	191	400	97	186	260	270	214	149	218	125
	95 %-Quantile	246	521	127	242	357	362	330	249	287	211
	Maximum	311	602	181	292	412	427	411	319	370	310
Paschold and Beltz (2010), Zinkernagel et al. (2017)	**Minimum**	39–69	115–182	-	7–26	144–173	92–124	-	13–37	-	-
	Arithmetic mean	171–179	320–371	-	131–149	290–335	259–304	-	138–172	-	-
	Maximum	284–316	525–549	-	232–271	445–505	427–521	-	251–330	-	-

Beside the annual crop specific net irrigation demand also the daily crop specific net irrigation requirements were determined (Figure 4-5, Table 4-3). The most water intensive crop on a daily basis constituted 'ornamental plants' with a minimum, arithmetic mean and maximum daily irrigation requirement of 15 mm, 41 mm and 64 mm, respectively. The relatively high daily net irrigation demand for this crop in comparison to the remaining crops was attributed to the relatively high critical depletion at the middle (critical depletion = 0.45) and the end of the crop development (critical depletion = 0.8, Table 11-3). Since irrigation was assumed to always take place as soon as the critical depletion of the crop had been reached, the following applied: The lower the critical depletion, the sooner and more often irrigation was required. For higher critical depletion values, however, more irrigation was required in fewer days (Allen et al. 1998; Savva et al. 2002). The same explanation applied for the relatively high net irrigation demand of sugar beet or in reverse logic for the relatively low net irrigation demand, e.g. typical for lettuce, celery or onions (Table 11-3 for crop specific critical depletion values) and became also obvious by analyzing the number of irrigation days n in Table 4-3. By comparing the modelled daily net irrigation requirement data with corresponding data from literature (Table 4-3), again the similarity became obvious and by that the validity with regard to daily net irrigation requirement was confirmed. For instance, the arithmetic means of the modelled daily net irrigation requirements for cabbage, celery or potato were 19 mm, 12 mm and 28 mm, respectively, while the corresponding data given by Gallichand et al. (1991) were 14–24 mm, 6–14 mm and 18–30 mm, respectively.

The overall good agreement of the modelled crop specific annual irrigation requirement data with corresponding data from the literature (annual as well as daily) further supported the validity of the model. On the other hand it might allow an assessment of the crop specific irrigation demand for future planning purposes by the local farmers and might even provide a useful tool for decision making on the choice of crops in the context of climate change effects, or in general as guide for designing irrigation equipment and reservoirs (Gallichand et al. 1991).

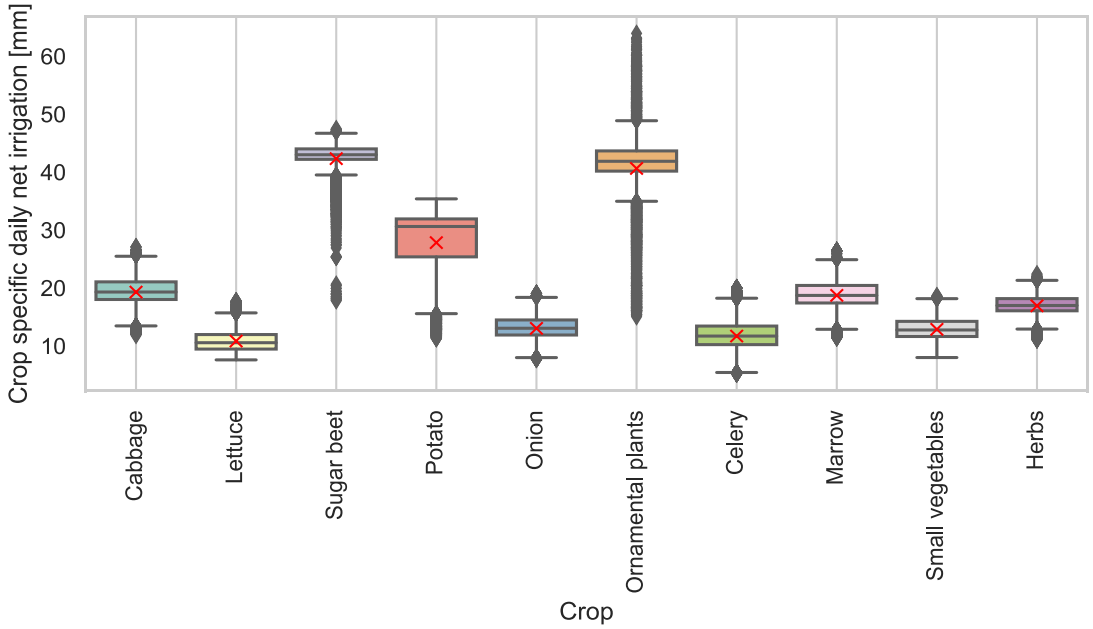

Figure 4-5: Modelled crop specific daily net irrigation requirements for the period from 1973–2019; the box shows the quartiles (25 %- and 75 %-quantile) of the dataset while the whiskers extend to show the rest of the distribution, except for points that are determined to be 'outliers' using the method that is a function of the 1.5 inter-quartile range; the median is indicated by the horizontal line within the box and the arithmetic mean is represented by the red cross.

Table 4-3: Statistical analysis of the crop specific daily net irrigation requirements, modelled data for the period 1973–2019 and data adapted from Gallichand et al. (1991) for (loamy) sand soils and with similar modelling conditions; since Gallichand et al. (1991) calculated within their study only weekly net irrigation requirements, for an adequate comparison with the own model data, it was assumed that the weekly requirements were irrigated on one day per week. Since for the own model i.a. broccoli was summarized within the group 'cabbage', for comparison the values of broccoli by Gallichand et al. (1991) were chosen.

Data origin		**Cabbage**	**Celery**	**Herbs**	**Lettuce**	**Marrow**	**Onion**	**Ornamental plants**	**Potato**	**Small vegetables**	**Sugar beet**
Model	**n**	17614	66954	9600	32167	26049	39260	9380	9675	31599	4124
	Minimum	12	5	11	8	11	8	15	11	8	18
	25 %-Quantile	18	10	16	9	17	12	40	25	12	42
	Median	19	12	17	11	19	13	42	31	13	43
	Arithmetic mean	19	12	17	11	19	13	41	28	13	42
	75 %-Quantile	21	13	18	12	20	14	44	32	14	44
	95 %-Quantile	24	16	20	14	23	16	47	34	16	45
	Maximum	27	20	22	18	26	19	64	35	19	47
Gallichand et al. (1991)	**Minimum**	10	6	-	2	-	4	-	17	-	-
	Arithmetic mean	14–24	6–14	-	2–8	-	5–12	-	18–30	-	-
	Maximum	25	15	-	9	-	13	-	36	-	-

4.4.3 Overall gross irrigation requirements

The overall gross irrigation requirements for the past 47 years (1973–2019) were derived from the modelling results (according to section 4.3.2) in order to create the broadest possible database for estimating the overall irrigation demand in the agricultural area in Gochsheim. The range of the overall annual gross irrigation requirements determined by the model for this period for Gochsheim is visualized in Figure 4-6 in form of box-whisker plots.

A close relationship between climate characteristics and the corresponding quantitative (overall) irrigation requirements exits, as can be inferred from Figure 4-2 and Figure 4-6: years with a high mean temperature (>15 °C) and low precipitation (~<250–300 mm) during the main irrigation season, such as the years 1976, 2003, 2015 and 2018, tended to have relatively high irrigation demands with ~290–360 mm. This close interdependence between the irrigation demand and the climate data further confirmed the plausibility of the irrigation requirement results generated by the model. For 50 % of the modelled scenarios, an annual overall gross irrigation of ~171 mm (median) would have been sufficient (Table 4-4, Figure 4-7, upper right panel). The median was similar to the arithmetic mean of the annual overall gross irrigation requirement of ~181 mm (Table 4-4). According to Figure 4-1 these values (median and arithmetic mean of modelled data) were close to the recorded overall gross irrigation demand of about 185 mm for the year 2014. With its precipitation and its mean temperature during the main irrigation season being nearly the same as the long term mean (1973–2019) the year 2014 was actually representative for a ‘normal’ year. This again proofed the validity of the model approach. According to the modelled data, the overall annual gross demand would have been covered with a 95 % certainty if ~322 mm had been supplied and by providing 367 mm per year even the maximum of the modelled irrigation demand could have been sufficiently met/covered. This upper range of the annual irrigation requirements (322–367 mm) was in close agreement with an estimate of the overall annual gross irrigation demand for an extreme hot and dry year by the engineering consulting firm BGS Umwelt GmbH, a collaborating partner within the project for which this model was performed. Furthermore, the results were in good agreement with modelling results for that area by Wriedt et al. (2009) having determined a range (Min–Max) of the net irrigation requirements between 122–239 mm (simulation period 1995–2002), which translated to a gross irrigation requirements of 153–299 mm under the assumption of an overall irrigation efficiency of 80 %. In summary, according to the modelling results as well as recorded irrigation requirement data for a normal year, e.g. represented by 2014, an overall annual gross irrigation requirement of about 170–190 mm will be sufficient, while during an extreme hot as well as dry year, such as 2015 or 2018, the overall annual gross irrigation demand might double (322–367 mm), in order to

guarantee an adequate irrigation of the local crops in Gochsheim and preventing any crop loss.

Table 4-4: Statistical analysis of modelled overall gross irrigation requirement data.

Temporal resolution	n	Unit	Min	25 %-Quantile	Median	Arithmetic mean	75 %-Quantile	95 %-Quantile	Max
Annually	2115		74.6	142	171	181	208	322	367
Monthly	10453	mm	0.4	13.9	28.5	36.7	52.7	98.3	169
Daily	87154		0.3	0.9	3	4.4	5.3	14.3	38.7

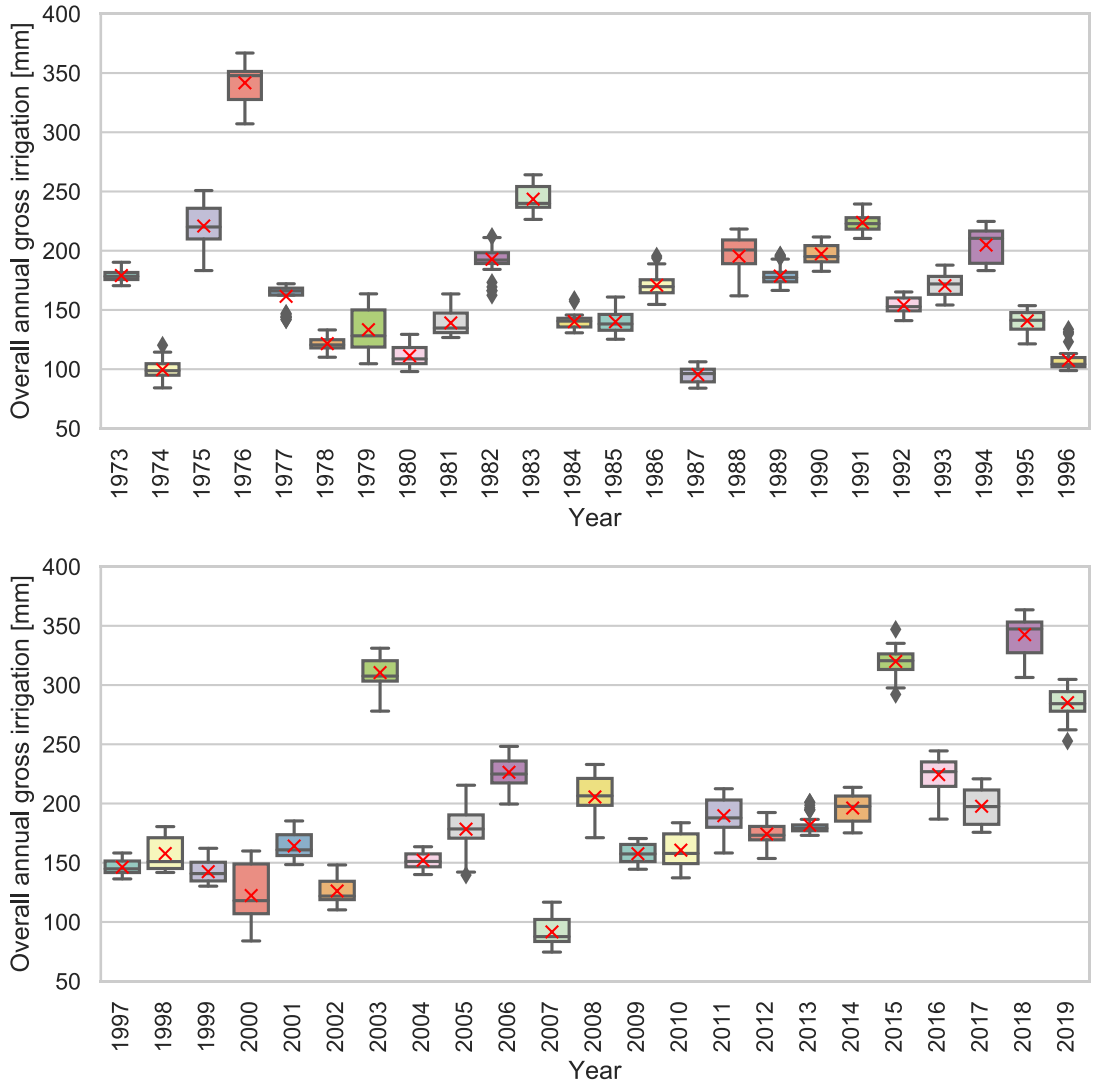

Figure 4-6: Modelled overall annual gross irrigation requirement in Gochsheim for the years 1973–2019; the box shows the quartiles (25 %- and 75 %-quantile) of the dataset while the whiskers extend to show the rest of the distribution, except for points that are determined to be 'outliers' using the method that is a function of the 1.5 inter-quartile range; the median is indicated by the horizontal line within the box and

The implementation of non-potable water reuse projects including required infrastructure for a whole agricultural area such in Gochsheim needs a comprehensive understanding of the respective local water demand (Asano and Mills 1990; Asano 1991; Urkiaga et al. 2008). Especially the (overall) daily peak (gross) irrigation demand is of utmost importance for the planning and design of pumps, storage, irrigation systems und water treatment facilities for non-potable water reuse (Watts 1968; Wright and Jensen 1972; Khadra and Lamaddalena 2006; Gallichand et al. 1991). Therefore, based on the previous confirmation of the validity of the modelling approach and in addition to the overall annual gross irrigation requirements, a higher temporal resolution was created by computing overall daily gross irrigation requirements for the whole agricultural area in Gochsheim. According to the (cumulative) frequency distribution (Figure 4-7, bottom two panels) and the corresponding statistical analysis (Table 4-4), 50 % (median) of the modelled overall daily gross irrigation requirements were less than 3.0 mm. The arithmetic mean with 4.4 mm was ~47 % higher than the median. By a provision of ~38.7 mm even the maximum of the overall daily gross irrigation requirements could have been covered. However, the provision of the maximum overall daily gross irrigation requirement of 38.7 mm would not have been feasible. The complete agricultural area in Gochsheim to be irrigated, summed up to about 55–60 ha. Assuming that a maximum of ~20 ha had been irrigated at one day, this would have translated into a demand of 7740 m^3/day. If this amount had been applied in 4 hours, which was a common time for the local irrigation applications in Gochsheim, a water flow of 1,935 m^3/hour would have been required. With a technically common flow velocity of 0.8–1 m/sec within the main supply pipe, this would have resulted into a corresponding pipe diameter of 100 cm. Not only the costs of the construction of the corresponding pipe trench but also the costs for the pipes itself or the corresponding treatment plant (if wastewater reclamation had been considered) would not be economically feasible in the context of the local conditions in Gochsheim. Furthermore, the probability of the event that the maximum of 38.7 mm was needed, could be neglected ($1.15*10^{-5}$). In contrast, the 95 %-quantile of the overall daily gross irrigation requirement of 14.3 mm (Table 4-4, Figure 4-7) represented a more economically as well as technically feasible benchmark. Moreover, the value was also comparable to not only the overall daily gross peak irrigation requirement reported by the local farmers, but also to an estimation derived from BGS Umwelt.

Apparently, for planning of non-potable water reuse projects and in the case of lacking recorded data, modelling based on the CROPWAT 8.0 approach (Allen et al. 1998) combined with statistical analysis constituted a helpful approach for estimating useful and plausible benchmarks of the overall daily peak irrigation requirement.

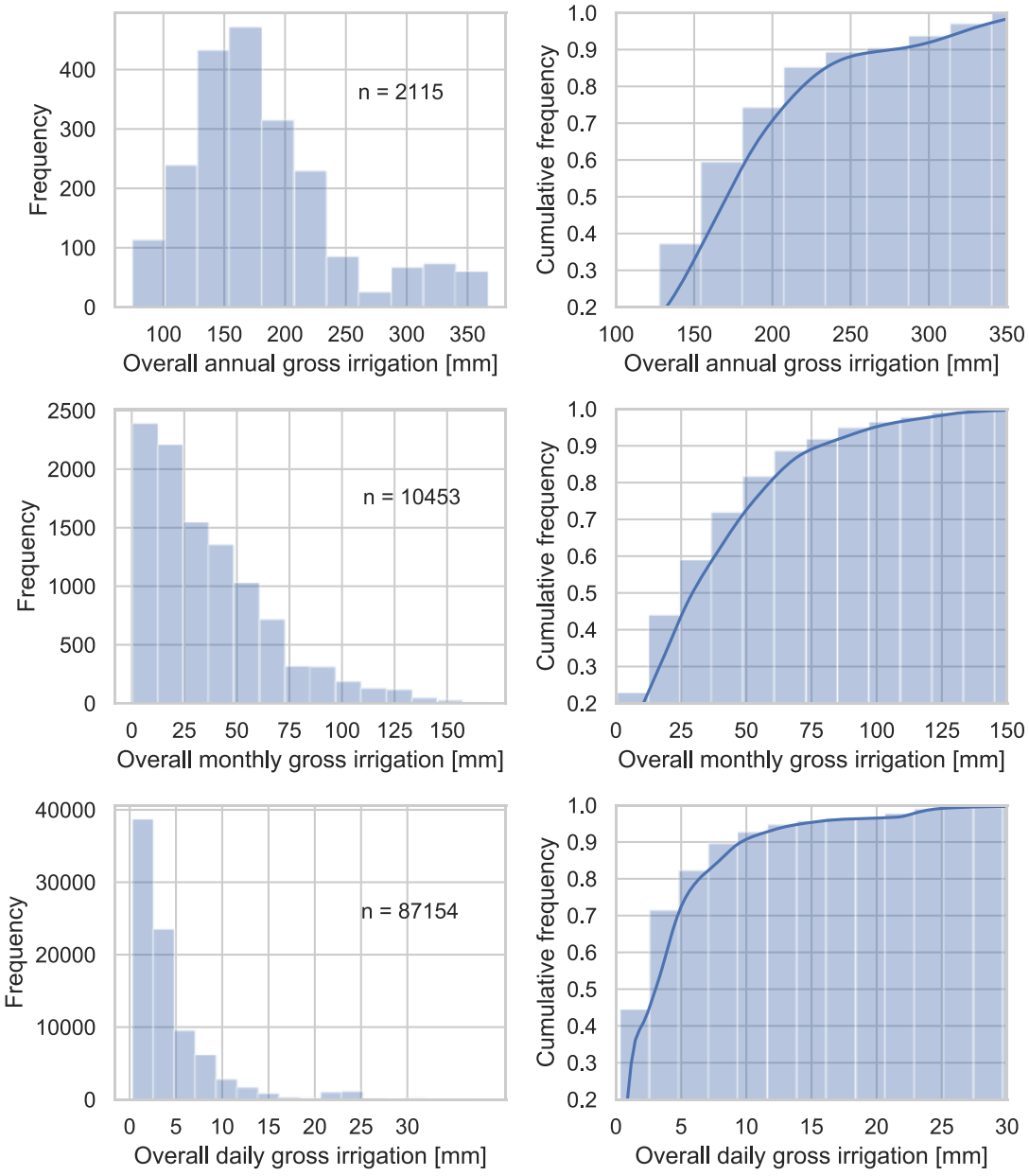

Figure 4-7: Histograms and cumulative frequency plots of the overall annual, monthly and daily gross irrigation requirement in Gochsheim for the years 1973–2019; the upper two panels show distribution of annual irrigation requirements, the middle two panels show the distribution of the monthly irrigation requirements and the bottom two panels show the distribution of the daily irrigation requirements.

4.5 Conclusion

Modelling is a viable and cost-effective approach for estimating irrigation demand data for a proper planning of non-potable water reuse projects. So far, most studies in this field focus on the determination of annually or monthly resolved crop requirement data. The proper estimation of overall daily peak demand data crucial for planning of agricultural water-reuse projects is usually not addressed. If accurate meteorological data are available, the computational approach on which the CROPWAT 8.0 is based on (a software provided by the FAO), constitutes an easy to implement model. By a simulation of a broad range of different possible growing scenarios and a comprehensive visual as well as statistical analysis of the modelled data i.a. the crop specific irrigation requirements, which are useful measures for the irrigation and water management planning of individual farmers, can be evaluated. Furthermore, by this modelling approach and a corresponding weighting of the calculated crop specific gross irrigation requirements, even the more important overall daily (monthly, or annual) peak gross irrigation requirements for a whole agricultural area can be estimated. In particular, the overall daily peak gross irrigation requirements represent the basis for adequate design of a non-potable water reuse infrastructure. The approach for the determination of this value utilized in this study can also be easily as well as cost-effectively applied to other comparable projects since only a limited and usually well available data set (meteorological, soil and crop data) is required. However, since this applied modelling approach constitutes a rather conservative assessment of the overall daily peak irrigation demand, the technically and economically most feasible demand value should be determined based on a statistical analysis taking into account the local desired security of supply. The results within this study revealed that the 95 %-quantile of the modelled daily irrigation demand with ~14.3 mm represented a viable benchmark for the design of infrastructure required for the non-potable water reuse project for agricultural purposes in Gochsheim, a municipality in Lower Franconia.

As a final conclusion, this approach and the results constitute a viable as well as helpful basis not only for the agricultural management of individual local farmers but in particular an essential prerequisite for the planning of non-potable water reuse projects for agricultural purposes adapted to the local conditions.

4.6 Acknowledgements

This work was funded by the Government of Lower Franconia (RUF), Germany. We are grateful for the support by Dr. Heiko Gerdes, BGS Umwelt GmbH and all stakeholders in the case study region for technical support and valuable discussions.

5 EFFECTS OF VARYING FLUX AND TRANSMEMBRANE PRESSURE CONDITIONS DURING CERAMIC ULTRAFILTRATION ON THE INFECTIVITY AND RETENTION OF MS2 BACTERIOPHAGES

The following chapter presents investigations related to ***research hypothesis #2.1***: *Increasing fluxes/TMPs during ceramic membrane UF can lead to the damage or inactivation of MS2 phages due to elevated hydrodynamic strain rates.*

Furthermore, ***research hypothesis #2.2*** is addressed: *Increasing fluxes/TMPs during ceramic membrane UF will cause a decreasing retention of MS2 phages due to the elongation of the MS2 phages in the converging flow field or due to enlargement of the UF pores.*

This chapter has been published with some editorial changes as follows:

Schwaller, Christoph; Knabl, Magdalena; Helmreich, Brigitte; Drewes, Jörg E. (2022): Effects of varying flux and transmembrane pressure conditions during ceramic ultrafiltration on the infectivity and retention of MS2 bacteriophages. In Separation and Purification Technology 299, p. 121709. DOI: https://doi.org/10.1016/j.seppur.2022.121709

Author contributions: Christoph Schwaller developed the research objective, constructed the laboratory membrane skid and designed the experiments. Christoph Schwaller and Magdalena Knabl conducted the experiments, analyzed the samples and data. Christoph Schwaller wrote the original manuscript. Magdalena Knabl partially wrote the original manuscript and reviewed the manuscript. Jörg E. Drewes and Brigitte Helmreich supervised the study and reviewed the manuscript. All authors approved the final version of the manuscript.

5.1 Abstract

Membrane ultrafiltration (UF) constitutes a promising technology to remove viruses including phages from water. However, the removal efficiency of viruses such as MS2 phages strongly depends on operational parameters, such as flux and transmembrane pressure (TMP) conditions during UF. Initially, we investigated during this lab-scale study if the infectivity of MS2 phages was impaired at very high fluxes and the associated high TMPs during ceramic membrane UF: The ratio of plaque forming units (PFU) indicating infectious MS2 phages and the total amount (infectious and non-infectious) of MS2 phages measured via digital polymerase chain reaction (dPCR) remained constant at varying fluxes. Hence, we concluded that the infectivity of MS2 phages was not significantly affected. Secondly, a trend analysis of PFUs and dPCR results during varying flux/TMP conditions was performed: It was found that with increasing fluxes/TMPs, the retention of MS2 phages significantly increased: Enhanced aggregation of the MS2 phages was expected to improve the size exclusion effect during ceramic UF while enlargement of ceramic membrane pores could be ruled out. Our findings partially contradict investigations with polymeric UF membranes. Possible underlying mechanisms were comprehensively discussed.

Keywords: Ceramic membrane ultrafiltration; transmembrane pressure; flux conditions; MS2 phage retention; MS2 phage integrity

5.2 Introduction

Antibiotic resistance genes (ARGs) carried by phages have shown high persistence against conventional wastewater treatment and disinfection with chlorine, UV irradiation, or ozonation due to their protection inside the protein capsid. Given this and that phages are the most abundant and diverse biological entity in the world, phages play a major role in the acquisition, maintenance, and spread of antimicrobial resistance (AMR) (Calero-Cáceres et al. 2019; Zarei-Baygi and Smith 2021; Debroas and Siguret 2019). Furthermore, due to their icosahedral shape, their size of roughly 30 nm and their contained single stranded RNA, MS2 phages are very similar to some enteric viruses such as the hepatitis A (≈27 nm) and poliovirus (≈28 nm). This and their relatively simple analysis make MS2 phages suitable as surrogates to investigate the pathogenic virus retention during water treatment processes (Fiksdal and Leiknes 2006; ElHadidy et al. 2013a; Furiga et al. 2011).

Wastewater treatment plant (WWTP) effluents have been identified as relevant sources of AMR, e.g. carried by phages with substantial dissemination of ARB as well as ARGs to the receiving aquatic environment (Kumar and Pal 2018; Hiller et al. 2019; Calero-Cáceres et al. 2019; Sigala and Unc 2012; Li et al. 2015; Rizzo et al. 2013). Since phages or plasmids are not efficiently removed or inactivated by conventional secondary wastewater treatment (Bürgmann et al. 2018; Hembach et al. 2019), membrane ultrafiltration (UF) can be applied downstream to provide a barrier against viruses such as phages, plasmids or bacteria possibly carrying ARGs, which are removed by means of size exclusion and adsorption to the membrane surface (Hembach et al. 2019).

However, some studies investigating the effect of membrane filtration on the removal of extracellular plasmids, viruses including phages or bacteria reported the ability of these entities to permeate through membrane pores with diameters much smaller than the sizes the corresponding plasmids, bacteria or viruses (Arkhangelsky and Gitis 2008; Arkhangelsky et al. 2008; Arkhangelsky et al. 2011; Latulippe et al. 2007; Latulippe and Zydney 2009; Latulippe and Zydney 2011; Slipko et al. 2019; Larson et al. 2006). Transmission of free DNA was even observed for solution-diffusion based tight nanofiltration or reverse osmosis membranes (Slipko et al. 2019; Arkhangelsky et al. 2011). It was demonstrated that transmission of plasmid DNA, independent of its conformation (supercoiled, open-circular or linear), can occur by elongation of the flexible plasmids in the highly converging and thus accelerating flow fields that form above the membrane pore openings (Arkhangelsky et al. 2011; Latulippe et al. 2007; Latulippe and Zydney 2009; Latulippe and Zydney 2011; Hirasaki et al. 1995). Moreover, Wick and Patrick (1999b) observed that MS2 phages with a rough molecular weight of 2000 kDa were able to pass membranes with molecular weight cut-off (MWCO) of 750,

500 and 300 kDa. A flux dependent retention of plasmids, viruses of bacteria was observed during polymeric membrane UF or MF: The transmission of plasmids (Slipko et al. 2019; Arkhangelsky et al. 2011), viruses (Arkhangelsky and Gitis 2008; Wick and Patrick 1999b) or even bacteria (Suchecka et al. 2003) increased with increasing fluxes or transmembrane pressures (TMPs). The penetration of bacteria, plasmids or viruses through membrane pores smaller than their expected radius was e.g. explained by membrane pore enlargement induced by high TMPs (Arkhangelsky and Gitis 2008) or by a possible deformation of (bacterial) cells due to the TMP (Suchecka et al. 2003). Elsewhere, the extensional forces that form in the converging flow fields that form above membrane pores were found to be in the order of magnitude, where the damage of plasmids (Meacle et al. 2007; Lengsfeld and Anchordoquy 2002; Simon et al. 2011) or of proteins, such as the capsid proteins of MS2 phage is likely to occur (Schwaller et al. 2022). All of the previously mentioned studies were investigating the removal of bacteria, viruses such as MS2 phages only during polymeric membrane UF or MF. Investigation of the removal efficiency of bacteria or viruses during ceramic UF are still quite rare or completely lacking.

The higher mechanical strength and physical as well as chemical resistance of ceramic membranes allows more frequent and aggressive hydraulic as well as chemical enhanced backwashes than it is feasible for polymeric membranes. This enables a more stable overall operation since higher recovery rates after hydraulic as well as chemical enhanced backwash can be achieved (Werner et al. 2014; Gitis and Rothenberg 2016; Singh 2015) which is especially important since ceramic membranes are increasingly more operated in dead end filtration mode (Ng et al. 2018; Fan et al. 2014). Due to their longer lifetimes and chemical as well as mechanical resistance, ceramic membranes are, despite their higher costs, progressively more used also for full scale applications (Ng et al. 2018).

Especially in the context of the ‘Regulation of the European Parliament and of the Council on minimum requirements for water reuse’ it is important to be aware of effects of varying operational conditions (e.g. flux or TMP) on the removal of (indicator) microorganisms. This regulation requires a validation monitoring of reclaimed water for agricultural irrigation before the reclamation plant is put into operation, when equipment is upgraded, and when new equipment or processes are added. For example, for total coliphages a performance target of ≥ 6 log is suggested (2020/741/EU). However, the operational conditions during validation monitoring are not further specified. More importantly, it is not specified how the log removal values (LRVs) should be determined (Polaczyk et al. 2008; Ikner et al. 2011). Independent of whether ceramic membranes are intended to be applied as main water treatment step or for purpose of concentration of viruses such as MS2 phages it has to be considered that during ceramic ultrafiltration

higher fluxes are possible compared to polymeric UF (Ng et al. 2018). Phages could be inactivated due to the higher fluxes and associated strain rates that are possible during ceramic UF. This would have an impact on the required validation monitoring of the UF treatment. Moreover, the effects of varying flux and TMP conditions on the removal efficiency of MS2 phages during ceramic ultrafiltration are not well understood, yet. If the removal efficiency of viruses including phages, or bacteria is a function of applied flux/TMP this has also consequences for the validation monitoring suggested by the European Commission (2020/741/EU).

To our knowledge no studies exists that elucidate possible negative effects of high fluxes or TMPs during ceramic membrane UF on the infectivity of MS2 phages. Hence, within this study we investigated the effects of varying flux and TMP conditions during ceramic UF on the retention of MS2 phages. Initially, special focus was laid on potential deformation or damage (and thus inactivation) of MS2 phages during membrane UF. We hypothesized that at very high fluxes/TMPs an impairment of the MS2 phage infectivity could occur: We analyzed the ratios of plaque forming units (PFU) indicating infectious MS2 phages and the total amount (infectious and non-infectious) of MS2 phages measured via digital polymerase chain reaction (dPCR) at varying flux/TMP conditions. Furthermore, the hypothesis was stated that increasing fluxes/TMPs during ceramic membrane UF will cause a decreasing retention of MS2 phages due to the elongation of the MS2 phages in the converging flow field or due to enlargement of the UF pores. To address the second hypothesis, a trend analysis of plaque forming units (PFUs) as well as dPCR results during varying flux/TMPs conditions was performed.

5.3 Experimental

5.3.1 Experimental setup of the ceramic lab-scale UF membrane system

The schematic set-up of the employed lab-scale UF membrane system is illustrated in Figure 5-1. The lab-scale membrane system consisted of a pressure driven ceramic UF membrane (type CA0250-A3T30G) provided by inopor®. In total three membranes from the same type but originating from different batches were used during the experimental procedures. All membranes had a cylindrical geometry with a cross section diameter of 25 mm, which contained 19 individual channels arranged evenly in cross section. The total membrane area of each of the employed ceramic membranes was about 0.05225 m^2. The support structure of the membrane consisted of aluminum oxide (α-Al_2O_3). Titan dioxide (TiO_2) acted as active filtration layer coated on top of the support structure. Further membrane specifications are summarized in Table 5-1. The UF membrane was operated at an inside-out, dead-end filtration mode. Backwash for the removal of particles separated by the membrane during filtration was possible. The piping system was made

from stainless steel pipes and PTFE hoses. Feed tank, backwash tank, membrane housing and all relevant valves consisted also of stainless steel. Both, the feed pump as well as the backwash pump were eccentric screw pumps.

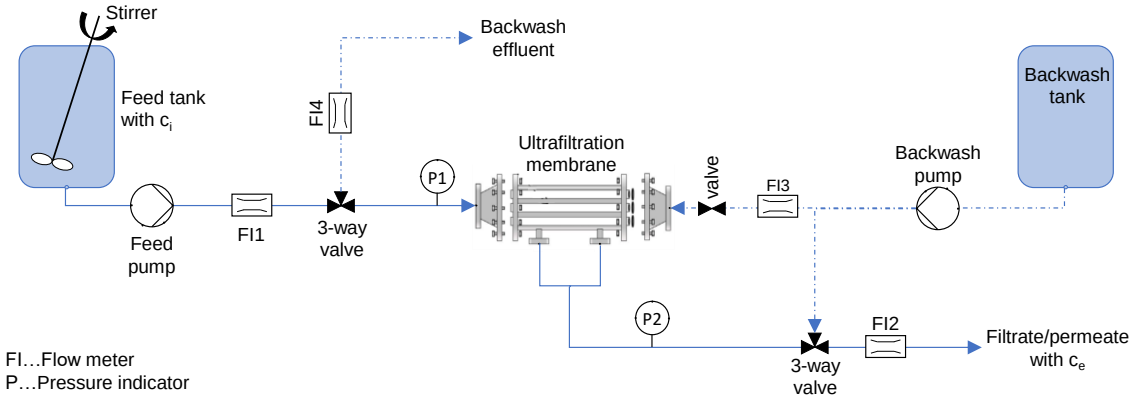

Figure 5-1: Experimental set-up of lab-scale UF system. Flow path during normal filtration operation is indicated by the solid line, while backwash flow is indicated by the dashed line. FI stands for a flow meter, PI for a pressure gauge.

Table 5-1: Specifications of employed ceramic UF membrane (type CA0250-A3T30G) provided by inopor®, active filtration layer made of TiO_2. SEM micrographs of the ceramic membrane can be found in section 11.4 (Figure 11-9, Figure 11-10, Figure 11-11).

Parameter	**Unit**	**Value**
Channel diameter	mm	3.5
Median pore size (d_{50})	nm	30
Module length	mm	250
Molecular weight cut-off	kDa	100
Number of channels	-	19
Outer diameter	mm	25
Specific membrane area	m^2	0.05225
Permeability	$L \cdot m^{-2} \cdot h^{-1} \cdot bar^{-1}$	Between 60 – 120[x]
Dead end volume of module	L	0.05
Zeta potential at pH 7	mV	5 – 6.2

[x] depending on membrane batch (for details refer to Figure 11-12 in section 11.4.8)

5.3.2 Preparation of MS2 phage stock and phage suspension used as feed water characteristics

The MS2 phage stock solution was prepared according to the standard procedure ISO 10705-1:2001 (1995), Annex C. The MS2 phage stock solution had an initial titer of roughly $3.9 \cdot 10^{11}$ PFU·mL^{-1} stock. For all experiments always the same MS2 phage stock was utilized.

The initial MS2 phage stock was then diluted in phosphate buffered saline solution (PBS) to produce a final MS2 phage suspension with a concentration of about $6 \cdot 10^{6}$ - $9 \cdot 10^{6}$ PFU·mL^{-1} or $1.7 \cdot 10^{7}$ PFU·mL^{-1}. The MS2 phage suspension with the concentration of $6 \cdot 10^{6}$ - $9 \cdot 10^{6}$ PFU·mL^{-1} was used as feed water for the first four experiments while the MS2 phage suspension with a concentration of $1.7 \cdot 10^{7}$ PFU·mL^{-1} was used for experiment five (cf. description of experimental procedure section 5.3.3.2). PBS with MS2 phages was thoroughly stirred. The PBS was prepared following NSF/ANSI 55 (2019) and the pH value of the PBS was always adjusted to about 7.0. The composition of the initially prepared PBS is summarized in Table 11-8. Before adding the MS2 phages to the PBS, the PBS was autoclaved at 121 ± 1 °C and 1.034 bar for 20 min in order to provide proper sterilization. Stabilizing viruses, including MS2 phages in a PBS solution was also recommended elsewhere (Langlet et al. 2009). Furthermore, the MS2 phage suspension had a temperature of about 20.0 °C and an electrical conductivity (EC) of about 13 mS·cm^{-1} during the experimental runs.

5.3.3 General experimental preparations, procedures and sampling conditions

5.3.3.1 Cleaning of UF lab-scale system prior to experiment and sterilization of equipment

One day prior to each experiment the whole UF lab-system was flushed with ultrapure water (Milli-Q water). Thereafter the UF lab-system without the membrane was flushed and soaked alternately with 1 v % solutions of sodium hydroxide (NaOH) and hydrochloric acid (HCl) with intermediate flushing the system with Milli-Q water and PBS for neutralizing the applied acids or the base. The ceramic membrane was stored in 80 v % ethanol. Details regarding the chemical cleaning protocol and applied chemicals can be found in the sections 11.4.2 and 11.4.5. The preparation of the utilized PBS was previously described (section 5.3.2).

In order to guarantee sterile sampling conditions, all required sampling equipment was autoclaved at 121 ± 1 °C at 1.034 bar for 20 min before running the experiment. Permeability tests were conducted before, during and after the experiments with Milli-Q

water and PBS. During each experiment the TMP, flow, EC, pH, as well as temperature were continuously monitored and recorded.

5.3.3.2 Experimental procedure and sampling

Initially, the ceramic UF membrane module was conditioned by filtering Milli-Q water for 30 min. Then the whole lab-scale system with integrated UF membrane was again alternately cleaned with nitric acid (HNO_3), followed by Milli-Q flush, and autoclaved PBS.

In order to investigate the effect of flux and TMP on the removal efficiency of MS2 phages and potential impacts on their integrity, in total **five experiments** with varying flux or TMP conditions and two different MS2 phage concentrations in the feed water were performed: The filtration experiments one to four were conducted with similar initial MS2 phage concentrations in the feed tank ($\approx 6 \cdot 10^6$ - $9 \cdot 10^6$ PFU·mL^{-1}). For experiment five, the feed water was spiked with about the two- to threefold initial MS2 phage concentration ($1.7 \cdot 10^7$ PFU·mL^{-1}) compared to the initial MS2 phage feed water concentration applied during experiments one to four. Within each experiment a triplicate (**replicate 1, 2,** and **3**) of pre-defined fluxes was performed. Within each triplicate, the sequence of set fluxes was randomized. An overview of the applied fluxes, the order of replicates within each experimental run and the corresponding samples is given in Table 5-2.

Table 5-2: Overview of applied flows, resulting fluxes ($A_{Membrane}$ = 0.05225 m^2) with corresponding sample identification within one experimental run. For each of the five experiments these 3 replicates were conducted.

Replicate	Applied flow [L·h^{-1}]	Resulting flux [LMH]	Applied TMP range [bar]$^+$	Sample ID
1	30	574	4.4 – 8.8	1S30
	4.8	92	0.8 – 2.1	1S4.8
	24	459	3.5 – 6.5	1S24
	12.6	241	2.0 – 4.0	1S12.6
2	4.8	92	0.8 – 2.1	2S4.8
	24	459	3.5 – 6.5	2S24
	12.6	241	2.0 – 4.0	2S12.6
	30	574	4.4 – 8.8	2S30
3	24	459	3.5 – 6.5	3S24
	12.6	241	2.0 – 4.0	3S12.6
	30	574	4.4 – 8.8	3S30
	4.8	92	0.8 – 2.1	3S4.8
Blank (without UF membrane)	30	No flux since no membrane integrated		B-0

$^+$ Applied TMP is given as a range since depending on the membrane batch different TMPs were required to achieve the corresponding flux or flow

Samples for PFU and dPCR analysis of the MS2 phages were drawn from the feed tank prior and after the experiment (feed tank before and feed tank after, respectively). Negative control samples were taken from the Milli-Q and PBS before and after these water qualities were applied for flushing the system in order to monitor for potential cross contamination (caused for instance by remaining MS2 phages inside the system).

A positive control sample (blank) was obtained after the experiment was terminated: For this the ceramic UF membrane was removed from the system and only the feed water spiked with the MS2 phages (cf. section 5.3.2) was pumped through the system. Following this procedure allowed to check if the MS2 phages within their flow path were removed (e.g. by adsorption) or damaged (e.g. by mechanical shear stress inside of the eccentric screw pump).

5.3.4 Analytical methods: Quantification of MS2 phages

The detection and quantification of MS2 phages was achieved via PCR and by using cell-culture based approaches. PCR methods cannot distinguish between viable/infectious and nonviable/noninfectious phages. Therefore, to quantify the amount of infectious phages it was necessary to perform a cell-culture analysis as well (Lee et al. 2017). Hence, by applying PCR and PFU it was possible to analytically distinguish between viable/infectious and nonviable/noninfectious MS2 phages.

5.3.4.1 Plaque forming units

Regarding the cell-culture method, the double-agar-layer procedure is most commonly applied, following ISO 10705-1:2001 (1995) or NSF/ANSI 55 (2019). The principle of the method is that above a layer of agar a second volume of agar mixed with (diluted) sample and an Escherichia coli (*E. coli*) suspension is poured. During the incubation the *E. coli* bacteria grow on the agar, leaving empty spots, so called plaques, wherever a MS2 phage infected an *E. coli*. The number of plaques corresponds to the number of infectious MS2 phages in a sample (Furiga et al. 2011). Therefore, PFU analysis was conducted in order to quantify the amount of infectious MS2 phages. The PFU analysis was performed according to the NSF/ANSI 55 (2019) standard. As recommended in NSF/ANSI 55 (2019), an 1.5 % tryptic soy agar (TSA) was used as bottom agar. As top agar an 1 % TSA was applied. The composition of the TSA for bottom and top agar is summarized in Table 11-9. The pH of the final TSA was set to 7.3 ± 0.2, for both the bottom as well as the top agar.

E. coli were cultivated in tryptic soy broth (TSB, cf. CASO-Bouillon Table 11-4 and Table 11-10 in section 11.4). The pH of the final TSB was around 7.3 ± 0.2. Prior to the experiments, the TSA as well as the TSB were autoclaved at 121 ± 1°C at 1.034 bar for

20 min. After preparation, the top agar TSA was stored with tightened screw cap in a heating cabinet at 55 °C and the TSB was pipetted as aliquots of 8 mL into autoclavable PP test tubes with screw cap and stored at 4 °C in the fridge. The bottom agar was poured into petri dishes. After the solidification, the plates were stored upside down at 4 °C in the fridge as well.

5.3.4.2 Digital PCR

In general, PCR is a method that allows the precise quantification of defined targets of DNA or RNA. In order to quantify the total amount of MS2 phages digital PCR was conducted. Hence, by applying dPCR both, active/infectious as well as defective MS2 phages are measured. The protocol for the dPCR analysis was adapted from elsewhere (QIAGEN 2021). The respective details can be found in the supplementary information (cf. 11.4.4). The required substances are specified in Table 11-6. Details on the specific RNA sequences that are targeted by the employed primers and the probe are visualized in 11.4.1. Briefly, initial lysis of the phage protein capsid was induced by heating the prepared PCR pre-plate to 95 °C for 5 min. Then 36 µL of reaction mix (cf. Table 11-13) were added to the heated sample aliquots and well mixed via vortexing and centrifuging. The total 40 µL volume was then transferred to a dPCR nanoplate and analyzed in the dPCR device. Thereby a reverse transcription step (40 min at 50°C) was followed by a PCR initial heat activation (2 min at 95 °C). Subsequently, 40 two-step cycles were performed, consisting each of a denaturation step (5 s at 95 °C) and a combined annealing/extension step (30 s at 61.5°C). A negative (NC) and positive control (PC) were added to each PCR plate, in order to monitor the process reliability and the method's consistency between the different analyzed plates.

5.3.5 Data analysis, statistics and visualization

The flux J (in $L \cdot m^{-2} \cdot h^{-1}$ or **LMH**) was calculated according to equation (8-1) as the ratio of the observed flow Q (in $L \cdot h^{-1}$) and membrane area $A_{Membrane}$ (in m^2) (Gitis and Rothenberg 2016; Mehta and Zydney 2005):

$$J = \frac{Q}{A_{Membrane}} \tag{5-1}$$

Membrane permeability can be expressed as the flux J (in LMH) divided by the corresponding transmembrane pressure TMP (in bar) (equation (5-2)) (Mehta and Zydney 2005; Gitis and Rothenberg 2016):

$$M = \frac{J}{TMP} \tag{5-2}$$

The log removal values LRVs (unitless) for the MS2 phages measured either via PFU (in PFU·mL^{-1}) or dPCR (in gene copies·mL^{-1}) method was computed according to equation (5-3). c_i represents the influent concentration, and c_e is effluent = permeate concentration of MS2 phages (measured as PFU·mL^{-1} or via dPCR as gene copies·mL^{-1}) (Crittenden and Harza 2005):

$$LRV = \log(\frac{c_i}{c_e}) \tag{5-3}$$

The ratio of the PFU (in PFU·mL^{-1}) to the dPCR (in gene copies·mL^{-1}) was calculated via equation (5-4):

$$Ratio\ PFU/dPCR = \frac{c_{PFU}}{c_{dPCR}} \tag{5-4}$$

In order to test linear regression (e.g. linear regression for the observed PFU or dPCR results as a function of the applied flux) with respect to statistical significance, the F-Test for linear regression was applied. This test is used to check whether the null hypothesis, which states that an identified relationship (via linear regression) between two data sets is statistically insignificant, is true or not (Morrison 2009; Heiberger and Burt Holland 2015). The level of significance α for the F-Test was set to 0.05. For the p-value <α = 0.05, the results of the F-Test can be regarded as statistically significant.

Cook's distance D_i was used to evaluate how much a predictive model, for example a fitted trend line, changes when a specific data point is removed from the data set that acts as basis for building that model. D_i evaluates the unusualness of both the predictive (x) and responding (y) variables. It can thus be seen as a parametrical combination of the leverage and studentized deleted residuals. The respective mathematical description of Cook's distance for a certain data point *i* is presented in equation (5-5).

$$D_i = \frac{e_i^2}{k \cdot \mathrm{MSE}} \cdot \left(\frac{h_i}{(1-h_i)^2}\right) \tag{5-5}$$

e_i represents the residual of the observed to the predicted y-value and *k* gives the number of independent variables. MSE is the mean square error of the predictive model and h_i is the leverage of the observation *i*. It was stated that only data points where the D_i is exceeding 1 should be considered as unusual, even though other sources give thresholds of 4/n or 4/(n – k – 1) (Heiberger and Burt Holland 2015).

Spearman correlation was applied to describe the relation between LRVs and the filtration time in order to determine filtration time dependent change of the LRV. The Spearman correlation coefficient, an alternative correlation coefficient to the Bravais-Pearson, is obtained by changing from the original values to their ranks. Thereby each value is ranked by the rank position which is obtained after sorting the values in ascending

order (Morrison 2009). The Spearman correlation coefficient is defined as the Bravais-Pearson correlation coefficient applied to the ranked pairs $(rg(x_i), rg(y_i), i = 1, \dots, n)$:

$$r_{SP} = \frac{\sum_{i=1}^{n}(rg(x_i) - \overline{rg}_X)(rg(y_i) - \overline{rg}_Y)}{\sqrt{\sum_{i=1}^{n}(rg(x_i) - \overline{rg}_X)^2} * \sqrt{\sum_{i=1}^{n}(rg(y_i) - \overline{rg}_Y)^2}} \quad (5\text{-}6)$$

Where the mean values of the ranks are given by:

$$\overline{rg}_X = \frac{1}{n}\sum_{i=1}^{n} rg(x_i) = \frac{1}{n}\sum_{i=1}^{n} i = \frac{n+1}{2} \quad (5\text{-}7)$$

$$\overline{rg}_Y = \frac{1}{n}\sum_{i=1}^{n} rg(y_i) = \frac{1}{n}\sum_{i=1}^{n} i = \frac{n+1}{2} \quad (5\text{-}8)$$

The Spearman correlation coefficient was applied to examine the strength and direction of the monotonic (nonlinear) relationship between two continuous or ordinal variables (Morrison 2009).

In addition, two-sample t-test with dependent samples with a significance level $\alpha = 0.05$ was performed in order to compare LRVs of experiments 1, 2, 3 and 4 with the LRVs of experiment 5 (section 5.4.3).

Data were visualized and statistically analyzed using Python 3.8 within Spyder as interface. The modules ‘pandas’, ‘seaborn’, ‘matplotlib’ and ‘matplotlib.pyplot’ as well as ‘numpy’ were applied. The packages ‘FormatStrFormatter’ of the module ‘matplotlib.ticker’, ‘stats’ of the module ‘scipy’ and the package ‘statsmodels.api’ were imported.

5.4 Results and discussion

5.4.1 Absolute MS2 phage concentrations and effects of storage and conveyance in piping on MS2 phages

Initially, it was investigated whether or not the storage of the feed water spiked with MS2 phages or the conveyance in the piping of the UF system had caused any observable effects on the MS2 phages. For that, the initial MS2 phage concentrations (determined by PFU as well as dPCR) in the feed water tank (feed tank before, feed tank after) and blank samples as well as the respective data from UF permeate during varying flux conditions were visualized in Figure 5-2.

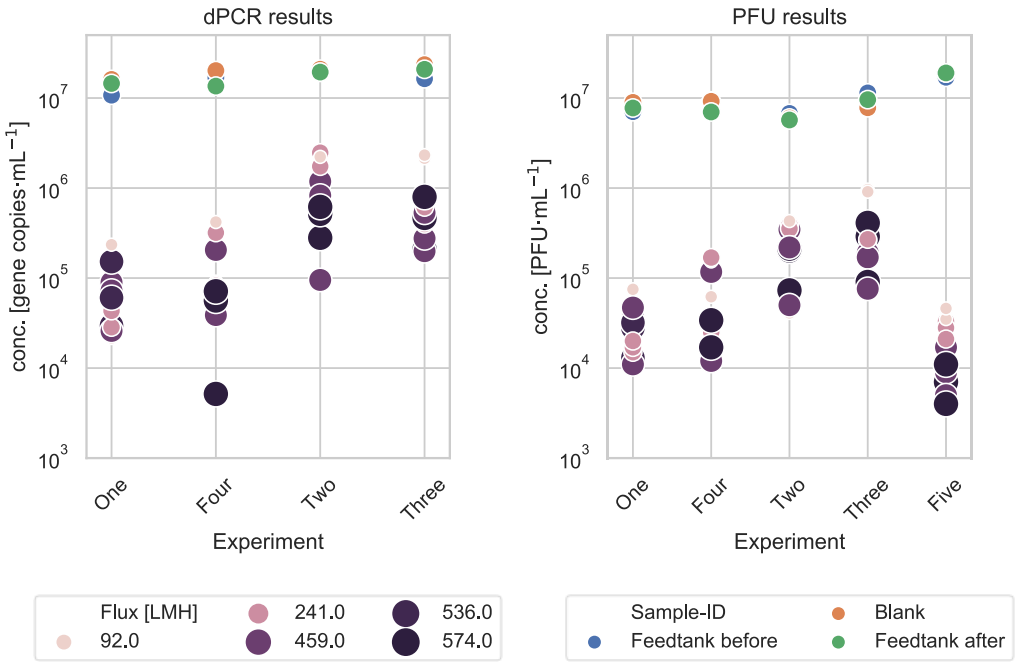

Figure 5-2: Scatterplots of MS2 phage concentrations in the feed water, the blank and the permeate during varying flux conditions. Feed water was sampled before (feed tank before) and after (feed tank after) the experiments. The blank samples for the MS2 phage concentration were drawn without a membrane being integrated.

For all experiments both, the dPCR as well as the PFU results from samples drawn from the feed tank before as well as after the experiments were comparable (Figure 5-2). This suggests that the MS2 phage concentration and therefore the infectivity of the MS2 phages in the feed tank stayed stable during the experimental procedure. The PFU or dPCR concentration results of MS2 phages from the blank sample (system without UF ceramic membrane) was in the range of the respective feed tank concentrations for all experiments. Based on these observations it could be concluded that neither the storage in the feed tank nor the conveyance in the piping of the UF system did have any observable effects on the MS2 phages (such as inactivation, adsorption, mechanical destruction, dilution by dead volume, etc.). This basis was important to be laid in order to distinctly assign later potential effects of the variable flux or TMP on the MS2 phage concentration in the permeate of the ceramic UF process and to neglect possible effects of storage and conveyance on the MS2 phages.

Samples were drawn from the permeates during varying flux conditions ranging between 92 - 574 LMH. The absolute concentrations of the dPCR and PFU results are depicted in Figure 5-2. During experiment one and four the initial MS2 phage concentrations in the feed water of about $8 \cdot 10^6$ PFU·mL^{-1} were reduced to concentrations of about $5 \cdot 10^3$ - $4 \cdot 10^5$ PFU·mL^{-1} in the permeate depending on the flux. During experiments two and four the initial MS2 phage concentrations in the feed water of about $8 \cdot 10^6$ PFU·mL^{-1} were reduced less efficiently to concentrations ranging between $4 \cdot 10^4$ –

$9 \cdot 10^5$ PFU·mL^{-1} in the permeate depending on the flux. The difference between the removal efficiencies between experiments one/four and two/three can be explained by the fact that experiments one/four were conducted with ceramic membranes of similar permeability characteristics (cf. section 11.4.8, Table 11-17), and for experiments two/three ceramic membranes originating from another batch were used. During experiment 5, a higher initial feed MS2 phage concentration ($1.7 \cdot 10^7$ PFU·mL^{-1}) resulted in lower MS2 phage concentrations in the permeate ($4 \cdot 10^3$ – $4 \cdot 10^6$ PFU·mL^{-1}). The MS2 phage concentrations measured via dPCR showed a similar pattern as the MS phage concentrations measured as PFU. The detailed analysis and discussion of the effect of varying flux on the retention of MS2 phages are provided in section 5.4.4.

5.4.2 Effects of varying flux and transmembrane pressure on the integrity or infectivity of MS2 phages

The extensional forces that form in the converging flow fields above membrane pores could be in the order of magnitude where damages of plasmids (Meacle et al. 2007; Lengsfeld and Anchordoquy 2002; Simon et al. 2011) or of proteins, such as the capsid proteins of MS2 phages, are likely to occur (Schwaller et al. 2022). Therefore, inter alia this study investigated possible effects of varying flux or TMP conditions on the infectivity of MS2 phages. In addition to the results within section 5.4.1, these results represent an important basis for the discussion of the subsequent investigations of effects of varying flux or TMP conditions during ceramic UF on the retention of MS2 phages.

By means of PFU, viable or infectious MS2 phages were measured while via dPCR the total amount of MS2 phages in the permeate samples taken at varying fluxes (cf. Table 5-2) were quantified. If MS2 phages were damaged during the filtration process due to increasing strain associated with increasing flux, decreasing PFU results would be observed in the permeate samples with increasing fluxes. At the same time, the total amount of the MS2 phages in the corresponding permeate samples (measured by dPCR) should stay constant or even increase since the inactivated MS2 phages would add up. Thus, the ratio of corresponding PFU and dPCR measurements would shrink with increasing flux or TMP.

However, it was found that the ratio of PFU and dPCR results did not show a statistically significant change with increasing flux. This is visualized in Figure 5-3, where none of the 95 % confidence intervals of the individual boxplots of the PFU/dPCR ratios are overlapping. Hence, based on a 95 % confidence interval all the PFU/dPCR ratios at the different fluxes are statistically similar or not significantly different. Apparently, increasing fluxes or TMPs had no significant or only negligible effects on the integrity of the MS2 phages. The PFU and the dPCR results have developed almost

parallel confirming that a decrease of PFUs was associated with the concurrent decrease of dPCR. The parallel slopes of the absolute MS2 concentrations or LRVs measured via PFU and dPCR are also observable in Figure 5-5 or Figure 11-15, respectively. Hence, it can be concluded that during ceramic UF the integrity of MS2 phages was not impaired by the elevated strain rates at high fluxes or TMPs. Apparently, the capsid of MS2 phages is stable enough to withstand elevated strain rates: The rigidity of global proteins or viruses has already been noted elsewhere (Hirasaki et al. 1994; Hirasaki et al. 1995; Tsurumi et al. 1990).

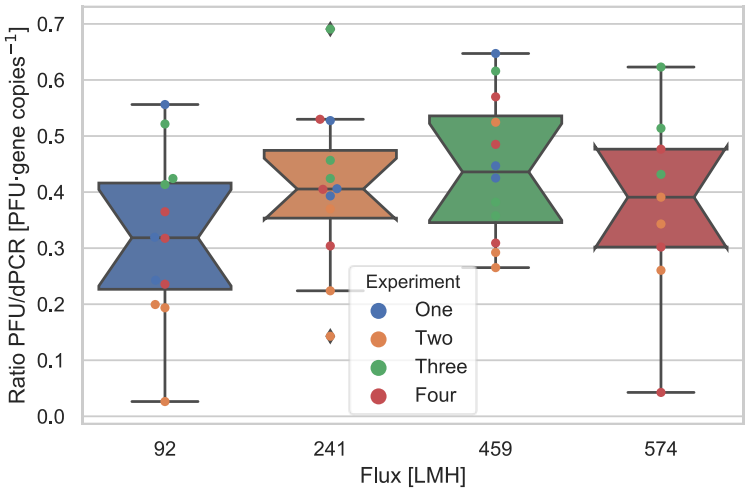

Figure 5-3: Boxplots of PFU/dPCR ratios of the MS2 phage measurement. The notches of the box plots indicate the 95 % confidence interval of the corresponding data sets. Each box shows the 25 %- and 75 %-quantiles of the dataset, while the whiskers extend to show the rest of the distribution, except for points that are determined to be 'outliers' using the method that is a function of the 1.5 inter-quartile range. The median is indicated by the horizontal line within the box. Since the data were roughly normally distributed, the arithmetic mean was close to the median.

5.4.3 Effect of MS2 phage concentration in the feed water on their retention

The filtration experiments one to four were conducted with similar initial MS2 phage concentrations in the feed tank ($\approx 6 \cdot 10^6$ - $9 \cdot 10^6$ PFU·mL^{-1}). For experiment five, the feed water was spiked with about the two- to threefold initial MS2 phage concentration ($1.7 \cdot 10^7$ PFU·mL^{-1}) compared to the initial MS2 phage feed water concentration applied during experiments one to four. According to Figure 5-2, higher initial MS2 phage concentrations in the feed tank during experiment five resulted in lower MS2 phage concentrations in the respective permeate samples that were taken at varying flow conditions. This meant that the higher initial MS2 phage concentration in the feed caused a significantly increased median and mean LRV of PFUs (LRV $\approx$ 3) compared to all other experiments (LRV $\approx$ 1.5 - 2.5) (Figure 5-4). The statistical t-test data confirmed the

statistical significance of this assessment: The arithmetic mean LRV during experiment five (high MS2 phage concentration) was significantly higher compared to the experiments one to four (two-sample t-test with dependent samples with $p = 2 \cdot 10^{-9}$ - $6 \cdot 10^{-3}$, for details cf. section 11.4.11, Table 11-18 - Table 11-21). The higher removal which resulted from the higher initial MS2 phage concentration in the feed tank during experiment five compared to all other experiments (Figure 5-4), was most likely due to the fact that the increased MS2 phage concentration promoted its aggregation (Jacquet et al. 2021). Consequently, bigger MS2 phage clusters that form during the aggregation could be removed more efficiently via size exclusion. It can be concluded from this investigation that an increased initial MS2 phage feed concentration leads to an enhanced separation due to improved size exclusion during membrane UF. This conclusion is going to be an important premise for the discussion within section 5.4.4.

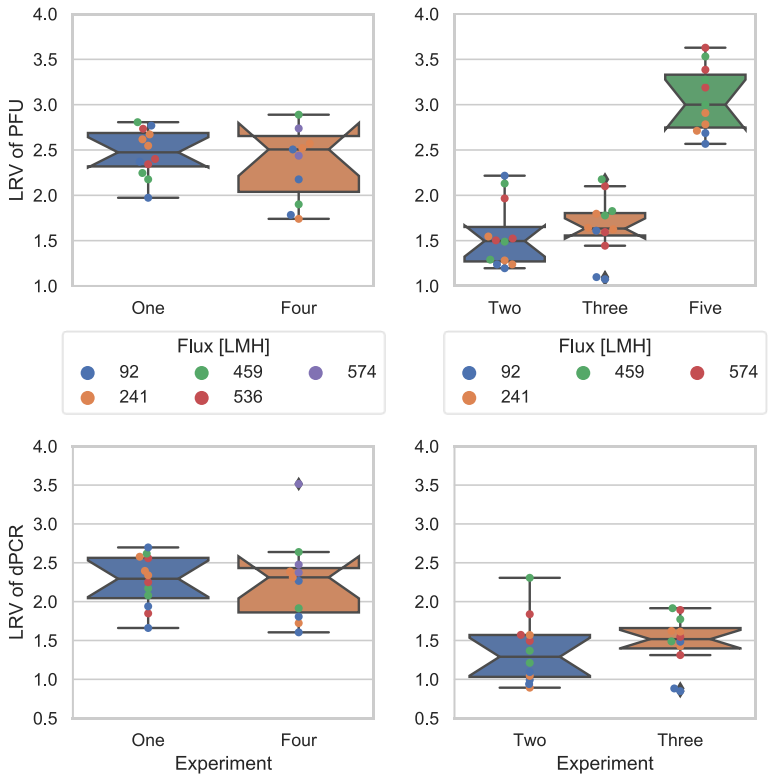

Figure 5-4: Boxplots of LRVs of experiments one to five for MS2 phages measured either by PFU (upper panels) or by dPCR (bottom panels). For experiments one and four, ceramic membrane originating from different batches but with similar permeability characteristics (cf. SI 8, Table S13) were used. For the remaining experiments two, three and five a ceramic membrane originating from another batch was employed. During the experiments one to four, an initial MS2 phage concentration of $6 \cdot 10^6$ – $9 \cdot 10^6$ PFU·mL^{-1} was used while for experiment five a higher MS2 phage concentration of $1.7 \cdot 10^7$ PFU·mL^{-1} was applied. The notches of the box plots indicate the 95 % confidence interval of the corresponding data sets. Each box shows the 25 %- and 75 %-quantiles of the dataset, while the whiskers extend to show the rest of the distribution, except for points that are determined to be ‘outliers’ using the method that is a function of the 1.5 inter-quartile range. The median is indicated by the horizontal line within the box. Since the data were roughly normally distributed the arithmetic mean was close to the median.

5.4.4 Effects of varying flux and transmembrane pressure on the retention of MS2 phages

LRVs measured via dPCR and PFU were ranging from 1 to 4 within our experiments (cf. Figure 5-4). Despite the fact that within our study ceramic UF membranes were employed, our results were in good agreement with MS2 phage LRVs during UF with polymeric membranes reported elsewhere (Arkhangelsky and Gitis 2008; Langlet et al. 2009; Boudaud et al. 2012). These studies also conducted their UF experiments in dead-end filtration mode, using membranes with comparable pore sizes or MWCOs (for details refer to section 11.4.14, Table 11-22). Apparently, ceramic and polymeric membranes can achieve similar LRV of MS2 phages as long as their key characteristics such as pore size or MWCO are comparable.

However, when it comes to impacts of operational conditions (e.g. varying flux or TMP) during UF on the removal of MS2 phages, distinct differences were observed between our study employing a ceramic UF membrane and similar studies conducted with polymeric membranes: For instance, Arkhangelsky and Gitis (2008) reported that with increasing TMP during UF with polymeric membranes made of polyether sulfone (PES) the LRVs of MS2 phages decreased from 3.8 at a TMP of 1 bar to a LRV of about 2.8 at a TMP of 4 to 5 bar. It was suggested that pore enlargement induced by the increasing TMP facilitated this phenomenon (Arkhangelsky and Gitis 2008). Elsewhere, during investigations with polymeric UF membranes increasing transmission meaning decreasing retention of plasmids (Slipko et al. 2019; Arkhangelsky et al. 2011), viruses (Arkhangelsky and Gitis 2008; Wick and Patrick 1999b) or even bacteria (Suchecka et al. 2003) with increasing fluxes/TMP during filtration was reported. The increased transmission or reduced retention (reduced LRVs) in these studies was explained as side effect of the deformation and the associated reduction of the diameter of the plasmids, viruses or bacteria cells (Slipko et al. 2019; Arkhangelsky et al. 2011; Suchecka et al. 2003).

Contrary to the findings from the previously mentioned studies, in our study we observed statistically significantly increasing LRVs measured via dPCR with increasing flux or TMP (panels on the left side in Figure 5-5, $p < \alpha = 0.05$). The LRVs measured via PFU also positively correlated with the increasing flux or TMP, however less statistically significant (panels on the right side in Figure 5-5). The trend line of the LRVs measured via PFUs during experiment 5 could be characterized by the steepest ascend with the strongest statistical significance ($p = 2.76 \cdot 10^{-4} << \alpha = 0.05$, cf. Figure 5-5). Apparently, the two- to threefold increased initial MS2 phage concentration in the feed for experiment 5 further promoted the increase of the LRVs with increasing flux or TMP.

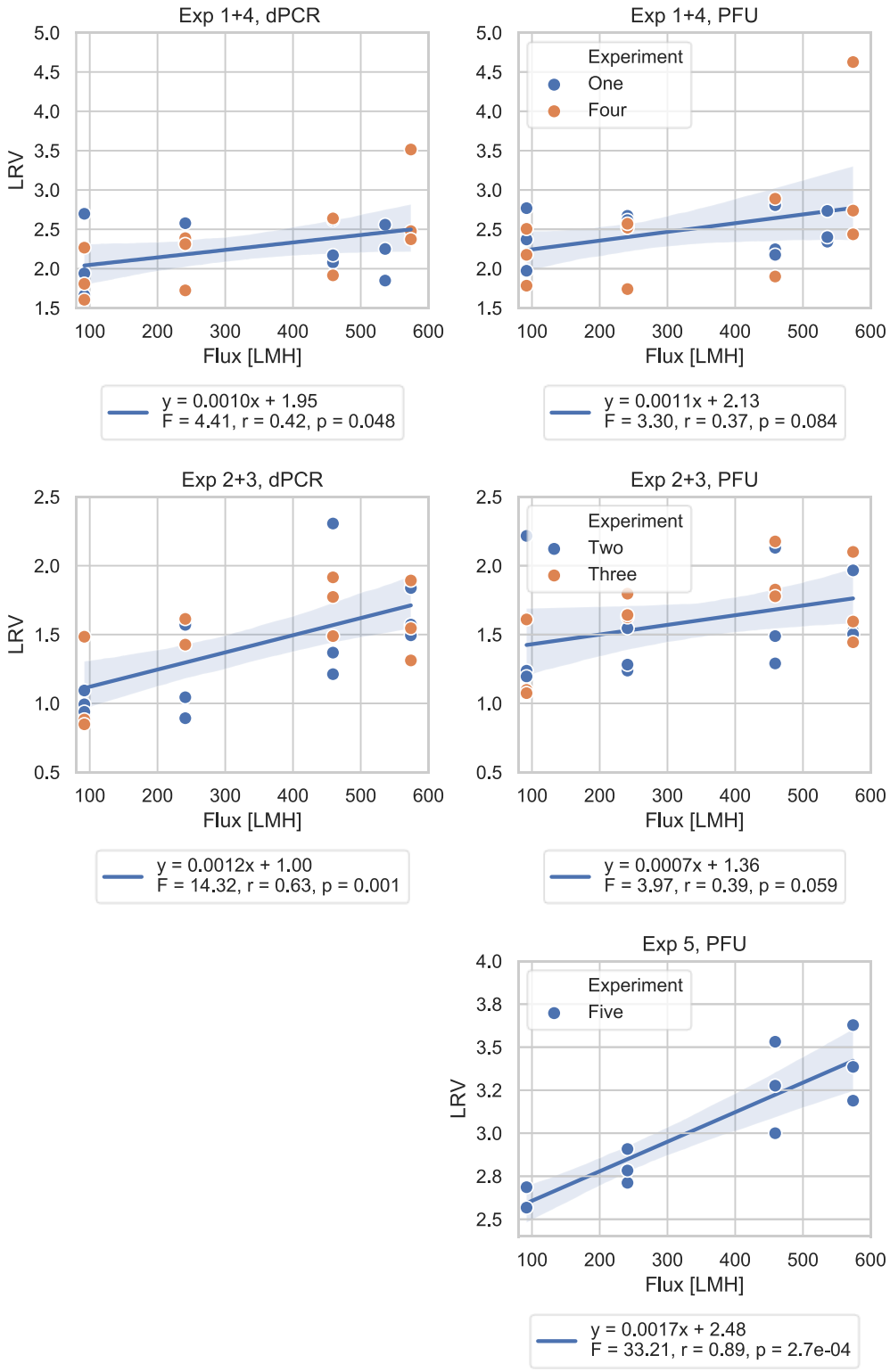

Figure 5-5: Linear regression models fitting the increasing LRVs of MS2 phages with increasing flux or TMP measured by dPCR as well as PFU. The shaded areas around the fitted lines indicate the 95 % confidence interval of the regression lines. y describes the equation of the trend line equation. r represents the Pearson correlation coefficient. For $p < \alpha = 0.05$ the corresponding observed trend can be regarded as statistically significant. The underlying absolute values are displayed in section 11.4.12 (Figure 11-15). Data points that had a Cook's distance of ≈0.5 were identified as outliers and excluded (cf. section 11.4.10, Figure 11-14).

Our results contradict findings of decreasing LRVs with increasing flux or TMP during UF with polymeric membranes. Hence, it has to be assumed that the mechanisms explaining decreased retention of viruses during polymeric membrane UF may not directly be transferred to explain virus removal during ceramic ultrafiltration. Or in other words, it has to be expected that at elevated fluxes or TMPs, ceramic membranes partially behave in a opposite way than polymeric membranes with regard to some key virus removal mechanisms. As reported elsewhere, the main mechanisms for virus retention during UF are size exclusion, adsorption of viruses on the membrane due to opposite charges, hydrophobic interactions between virus and membrane and electrostatic repulsion of viruses by the membrane due to identical electrical charges (ElHadidy et al. 2013a; Goswami and Pugazhenthi 2020). Subsequently, possible removal mechanisms explaining the enhanced removal of viruses such as MS2 phages with increasing fluxes or TMPs during ceramic UF are discussed:

Adsorption due to opposite charges was likely to happen since MS2 phages have a negative zeta potential of around -20 to 30 mV at a pH of 7 (ElHadidy et al. 2013a; Langlet et al. 2007), while the ceramic membrane had a slightly positive zeta potential of about 6 ± 0.85 mV (cf. Table 5-1). However, if the increasing flux rates had an effect on the adsorption of MS2 phages on the ceramic membrane surface, it would rather be expected that the higher associated forces during increased TMP conditions would counteract the adsorption instead of enhancing it. Electrostatic repulsion and hydrophobic interactions due to the opposite charges of the MS2 phages and the ceramic membrane material were also excluded as reasons for increasing LRVs.

Hence, size exclusion is left as the mechanism that was affected by the varied flux/TMP. The question was whether characteristics of the MS2 phages or the membrane itself were influenced by varying flux or TMP conditions leading then to different size exclusion efficiencies. Since an increasing TMP was accompanied by an increasing retention of MS2 phages (Figure 5-5) during UF with the tested ceramic membranes, it can be concluded that pore enlargement as observed for polymeric membranes (Arkhangelsky and Gitis 2008) was not occurring in our case. Otherwise it would have increased the transmission of MS2 phages.

Membrane compaction which might actually explain the increasing retention of MS2 phages with increasing TMP was also not expected to be the reason for the improved retention of MS2 phages at higher TMPs. It has to be noted that ceramics such as Al_2O_3 or TiO_2 are quite brittle/inflexible (Liu et al. 2020; Werner et al. 2014) and relevant deformation of this material will not happen at the applied TMPs of maximum 8 bars. For instance, Kalatur et al. (2014) examined the mechanical properties of porous ZrO_2 ceramics and found relevant deformation of the material not until mechanical stresses

larger than 50 MPa (≈500 bars) were employed. Furthermore, the compaction of the membrane surface by increased TMPs would have caused an reduced permeability (Persson et al. 1995; Bohonak and Zydney 2005; Kallioinen et al. 2007). However, during our experiments the permeability of the employed ceramic membranes remained constant independent of the applied flux/TMP (Figure 5-6, for details refer to section 11.4.8, Table 11-17). Hence, it was unlikely that relevant membrane compaction occurred during our experiments. The constant permeability indicated also that no or negligible fouling by cake layer formation happened. This was plausible since synthetically produced solution (PBS) did not contain any particulate matter nor other typical foulants such as organic matter (Jacquet et al. 2021).

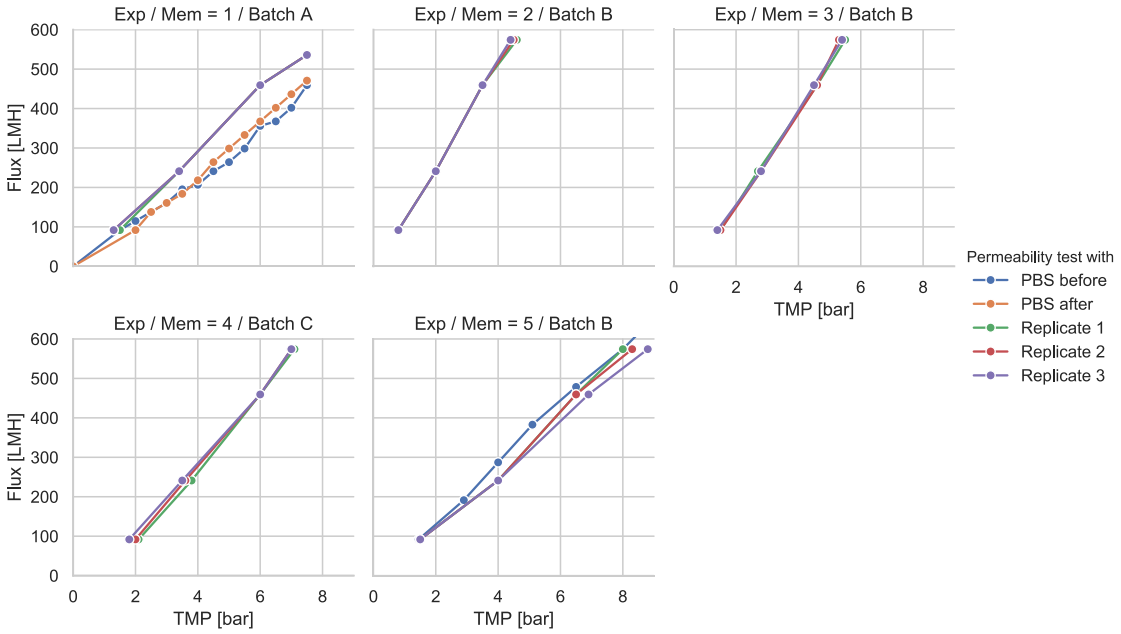

Figure 5-6: Permeability data of utilized ceramic UF membranes. Permeability was tested with different water qualities and at different stages of the respective experiment: PBS (phosphate buffered saline solution) before and after the experiments (PBS before and after), with PBS spiked with MS2 phages (replicate 1, 2, 3). The captions of the individual panels indicate the experiment (exp) and membrane batch.

Since relevant changes of the ceramic membrane (such as compaction or pore enlargement) due to elevated flux/TMP conditions could be excluded, it has to be assumed that rather some characteristics of the MS2 phages were changed during the varying flux/TMP conditions. pH, ionic strength, or temperature can effect MS2 phage characteristics and therefore their behavior in water (Furiga et al. 2011). However, all these parameters stayed constant during all experimental procedures and as expected, ceramic ultrafiltration did not alter the ionic strength measured as EC (cf. section 11.4.8, Table 11-17).

Increasing elongational strain rates due to increasing fluxes/TMPs can be in the order of magnitude where proteins, plasmids or bacteria get deformed or damaged (Slipko et al. 2019; Arkhangelsky et al. 2011; Suchecka et al. 2003; Schwaller et al. 2022). Firstly however, deformation due to elongation that lead to the reduction of diameter resulting in an increased transmission did not occur since with increasing flux/TMP the MS2 removal increased (cf. Figure 5-5 or Figure 11-15 in section 11.4.12). Secondly, decreasing PFU numbers with increasing fluxes (cf. Figure 5-5) resulting from a partial inactivation of MS2 phages due to large elongational strain rates during ceramic UF, could also be excluded (cf. previous section 5.4.2). The quite parallel and congruent trend of the dPCR results and the PFU results further confirmed the assumption that MS2 phage inactivation was not the reason for the decreasing PFU trend (Figure 5-5).

The most probable and accurate explanation for the increased LRVs during elevated flux or TMP conditions during our experiments is that elevated fluxes or TMPs caused aggregation of the MS2 phages improving thereby their size exclusion during ceramic UF. Particularly, two main mechanisms can account for this:

- The first important mechanism promoting MS2 phage aggregation could be the following: Meng and Li (2019) investigated the effect of varying TMPs (0.5, 1.0 and 1.5 bar) and feed nanoparticle concentrations (20, 70 and 100 ppm) on the particle concentration of the concentration polarization layer. They found that both, an increase in the feed concentration as well as increased TMP resulted in an increased concentration in the boundary layer in front of the membrane. For our study this means that elevated TMP/flux could have led to an increased MS2 phage concentration in the boundary layer in front of the membrane. The increased MS2 phage concentration in the boundary layer and elevated TMPs would allow MS2 phages to more easily overcome electrostatic repulsion forces between the individual phages and promote their aggregation and thereby their physical separation via size exclusion (Jacquet et al. 2021). Within our own study higher initial MS2 phage concentrations in the feed water resulted also in overall significantly enhanced LRVs (cf. section 5.4.3) and in a more prominent and statistically significant increasing LRV trend of MS2 phages with increasing flux (Figure 5-5, Experiment 5). This supports the explanation that increased concentrations, likely caused by elevated TMPs, can result in enhanced LRVs. Finally, Farahbakhsh also observed that with increasing TMP the retention of coliphages was improving: The formation of a gel layer that is progressively compressed was assumed to cause an increasing retention of the coliphages with increasing flux (Farahbakhsh and Smith 2004). In summary we can conclude that elevated TMP/flux conditions can result in increasing

MS2 phage concentrations in front of the UF membrane (Meng and Li 2019) and that these elevated MS2 phage concentrations can cause increased LRVs due to enhanced aggregation promoting therefore size exclusion (Jacquet et al. 2021).

- The converging flow fields in the vicinity of the membrane pore openings (Arkhangelsky and Gitis 2008; Arkhangelsky et al. 2011; Latulippe et al. 2007; Latulippe and Zydney 2009; Latulippe and Zydney 2011; Slipko et al. 2019; Larson et al. 2006) represent the second relevant mechanism facilitating MS2 phage aggregation (Simon et al. 2011): The higher the flux, the more converging the respective flow field and the higher the associated extensional and shear strain rates (Schwaller et al. 2022). Even though this has not led to a relevant deformation/inactivation of the MS2 phages (cf. section 5.4.2), it has likely resulted in an improved aggregation by an enhanced compression of the MS2 phages to each other. For instance, Simon et al. (2011) observed that the aggregation of the protein bovine serum albumin increased with increasing extensional flow. As partial conclusion it can be stated that increasing fluxes/TMPs can also lead to enhanced aggregation due to associated increasing strain rates and progressively stronger converging flow fields.

It has to be assumed that especially the second mechanism during which higher flux/TMP conditions facilitated the MS2 phage aggregation due to elevated strain rates and stronger converging flow fields outweighs the first mechanism (increasing concentration in front of the membrane at elevated fluxes/TMPs). This is based on the following observation: With progressing filtration time, the absolute numbers of MS2 phages retained by the ceramic UF membrane increased in the vicinity of the membrane. This resulted in a progressively increasing MS2 phage concentration in the boundary layer of the membrane. Despite the growing MS2 phage concentration in the boundary layer, the LRVs slightly decreased with progressing filtration time: Nearly all LRVs of the first replicates were found to be larger than the LRVs of the second replicates and most of the LRVs of the second replicates were larger than the LRVs of the third replicates (Figure 11-16). This correlation is highlighted by Figure 5-7: A strong and significant Spearman correlation existed between the ranked PFU LRVs and the corresponding replicates ($r = -0.76$, $p = 3.1 \cdot 10^{-12}$). Maybe the increasing concentration polarization resulted in an increasing concentration gradient between the concentrate retained on the UF surface and the permeate. This might have resulted in the decreasing LRVs due to enhanced diffusion of MS2 phages with progressing filtration time (Jönsson et al. 2006; Meng and Li 2019), thereby slightly counteracting MS2 phage aggregation due to the converging flow fields.

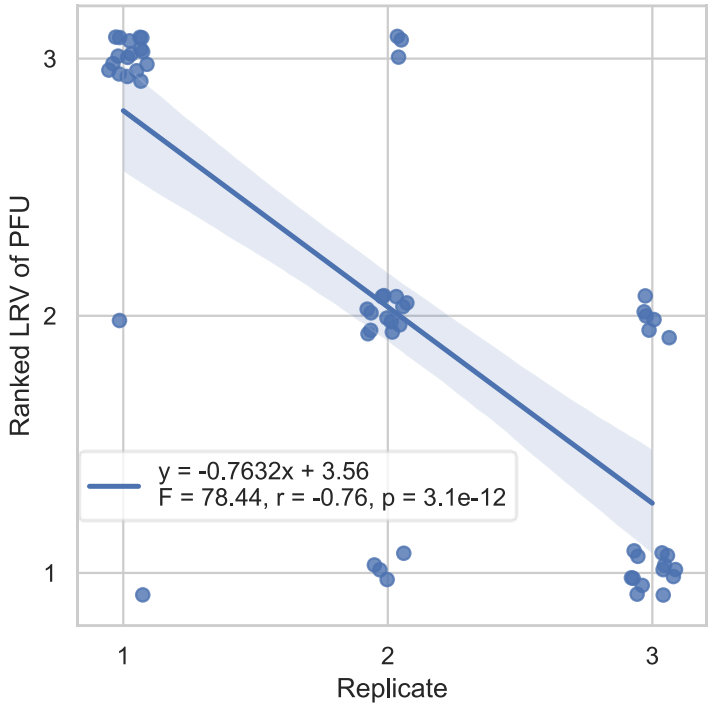

Figure 5-7: Spearman rank correlation of the order of replicates (as means of the filtration time) and the corresponding ranked LRVs. The ranks of the LRV range between 1 and 3 since the flows were tested in triplicates. Linear regression models fitting the decreasing ranked PFU LRVs of MS2 phages with progressing filtration time (the replicate number increases with progressing filtration time). The shaded area around the fitted line indicates the 95 % confidence interval of the regression line. y describes the equation of the trend line equation. r represents the Pearson correlation coefficient. For $p < \alpha = 0.05$ the corresponding observed trend can be regarded as statistically significant.

5.5 Conclusion

Investigation of the removal efficiency and relevant removal mechanisms of bacteria or viruses such as MS2 phages during ceramic UF are still quite rare. Hence within this study, we partially addressed this research gap by stating two main research hypotheses:

- Firstly, we stated that increasing fluxes/TMPs during ceramic membrane UF can lead to the damage or inactivation of MS2 phages due to elevated hydrodynamic strain rates: Contrary to what was hypothesized, high fluxes and TMPs during ceramic membrane UF have not impaired the infectivity of MS2 phages. This conclusion was based on the fact that the ratio of plaque forming units (PFU) indicating infectious MS2 phages and the total amount (infectious and non-infectious) of MS2 phages measured via dPCR remained constant at varying fluxes.

- Secondly, we hypothesized that increasing fluxes/TMPs during ceramic membrane UF will cause a decreasing retention of MS2 phages due to the elongation of the MS2 phages in the converging flow field or due to enlargement of the UF pores. However, we observed that with increasing flux and TMP the physical separation of MS2 phages during ceramic UF was significantly enhanced. Most likely enhanced aggregation of the MS2 phages due to increasingly stronger converging flow fields and strain rates promoted the size exclusion effect during ceramic UF. Moreover, relevant enlargement of UF pores of the ceramic membrane did not occur.

Our mechanistic findings are especially interesting, e.g. in the context of the most recent guideline with respect to quality requirements for water reuse adopted by the European Commission (2020/741/EU). It is recommended to perform validation monitoring of reclaimed water for agricultural irrigation and a performance target of ≥ 6.0 log removal values is proposed. Therefore, we recommend that for validation monitoring of ceramic UF, but also when viruses have to be concentrated, e.g. via ceramic membrane UF, the effect of varying operational conditions such as flux or TMP should be accounted for.

5.6 Acknowledgements

This work was funded by the German Federal Ministry of Education and Research (BMBF), which we especially acknowledge (Grant number: 02WV1563D). We would like to express our gratitude to Rauschert Distribution GmbH, Business Unit Inopor for the donation of the ceramic UF membrane and the provision of necessary specifications on the UF membrane. Moreover, we acknowledge the support and valuable advice by our colleagues Dr. Christian Wurzbacher, Heidrun Mayrhofer and Ursula Wallentits during the PFU and dPCR analysis. We also acknowledge the support by Hubert Moosrainer when constructing the ultrafiltration membrane laboratory unit. Finally, we are grateful to Javad Ahmadi and Poojesh Bertram for their support during the fifth experimental run.

6 REMOVAL OF ANTIBIOTIC MICROBIAL RESISTANCE BY MICRO- AND ULTRAFILTRATION OF SECONDARY WASTEWATER EFFLUENTS AT PILOT SCALE

The following chapter presents investigations related to ***research hypothesis #3.1***: *Higher ARG abundances in the feed water will result in higher ARGs abundances in the corresponding UF filtrates.*

Furthermore, ***research hypothesis #3.2*** is addressed: *The built-up a fouling layer during UF will lead to a higher AMR removal efficiency.*

Lastly, ***research hypothesis #3.3*** is elucidated: *Despite nominal pore sizes of UF membranes being smaller than the diameter of bacteria, intact bacteria and AMR will break through UF membranes.*

This chapter has been published with some editorial changes as follows:

Hiller, Christian X.; Schwaller, Christoph; Wurzbacher, Christian; Drewes, Jörg E. (2022): Removal of antibiotic microbial resistance by micro-and ultrafiltration of secondary wastewater effluents at pilot scale. In Science of The Total Environment, p. 156052. DOI: https://doi.org/10.1016/j.scitotenv.2022.156052

Author contributions: Christian Hiller developed the research objective, conducted the experiments and wrote the manuscript as first author. Christoph Schwaller supported partially during the writing of the manuscript, analyzed the data, prepared the graphs and reviewed the manuscript. Christian Wurzbacher supported partially during the writing of the paper and reviewed the manuscript. Jörg E. Drewes supported the funding acquisition, supervised the study and reviewed the manuscript. All authors approved the final version of the manuscript.

6.1 Abstract

Low-pressure membrane filtration was investigated at pilot scale with regard to its removal of ARGs in conventional secondary treated wastewater plant effluents. While operating microfiltration (MF) and ultrafiltration (UF) membranes, key operational parameters for AMR studies and key factors influencing AMR removal efficiencies of low-pressure membrane filtration processes were examined. The main factor for AMR removal was the pore size of the membrane. The formation of the fouling layer on capillary membranes had only a small additive effect on intra- and extrachromosomal ARG removal and a significant additive effect on mobile ARG removal. Using feeds with different ARGs abundances revealed that higher ARG abundance in the feed resulted in higher ARG abundance in the filtrate. Live-Dead cell counting in UF filtrate showed intact bacteria breaking through the UF membrane. Strong correlations between 16S rRNA genes (as surrogate for bacteria quantification) and the *sul1* gene in UF filtrate indicated ARBs likely breaking through UF membranes.

Keywords: microfiltration; ultrafiltration; standard filtration mode; antibiotic resistance genes; 16S rRNA gene, total cell counts

6.2 Introduction

Antibiotics, antibiotic resistant bacteria (ARB), and antibiotic resistance genes (ARGs) present in wastewater effluents can contribute to elevated levels of those constituents in the receiving aquatic environment (Alexander et al. 2015; Kristiansson et al. 2011; Rizzo et al. 2013). This can result in an increase in the abundance of AMR in surface waters after receiving conventional WWTP effluents (Hiller et al. 2019). This topic has been intensively studied in the past for urban and low impacted surface water analyzing either ARB by cultivation method or ARGs by qPCR technique (Hiller et al. 2019). The spread of AMR in the environment is facilitated by horizontal gene transfer, which describes the gene transfer by conjugation, transformation and transduction (Giedraitienė et al. 2011). The horizontal gene transfer is occurring naturally, not only between similar bacterial strains and between gram-negative and gram-positive bacteria, but also between pathogenic and non-pathogenic bacteria (Courvalin 1994). That is the reason why both ARB and ARGs promote the increase of antibiotic resistance in the aquatic environment. Therefore, release of ARB and ARGs into the aquatic environment should be reduced.

Advanced wastewater treatment processes are capable to remove AMR to levels similar to ‘low impacted surface water’ concentrations (Hiller et al. 2019). One possible technical solution is the use of membrane filtration such as microfiltration (MF) and ultrafiltration (UF). These technologies have been established predominantly as membrane bioreactor (MBR) process applications (Du et al. 2020). Here, low-pressure membrane filtration is applied to replace the secondary clarifier as the solids separating step of the biological treatment stage. The implementation of a full-scale membrane filtration process in a conventional biological nutrient removal facility concerning ARB and ARGs removal requires a mechanistic understanding of the membrane filtration process. Most ARB are larger (0.2 to 2 µm) than MF or UF pores and therefore should be efficiently retained by MF or UF. In contrast, mobile ARGs which can be encoded in mobile genetic elements such as plasmids, integrons, transposons, or bacteriophages are usually too small to be sufficiently removed by size exclusion alone (Slipko et al. 2019; Breazeal et al. 2013). While previous studies confirmed the penetration of mobile ARGs through the membrane pores the question is raised if all bacteria and all intracellular ARGs are retained by UF or is it possible that intact bacteria including ARB can pass the membrane pores. Furthermore, the fact of mobile ARGs breaking through the membrane pores hypothesizes whether higher ARGs abundance in the feed can result in higher ARGs abundance in the filtrate. Certainly, the term low-pressure membranes significantly differ in their pore size distribution ranging from MF (e.g., 450 nm) to UF (e.g., 20 nm) resulting in different AMR removal efficiencies (Breazeal et al. 2013). Beside different pore sizes of MF and UF, filtration processes applied differ from cross flow mode with

continuous water- or air-cross-flow to dead-end filtration mode with separate backwash mode to minimize the build-up of a fouling layer. However, the fouling layer could cover pores potentially resulting in an increased ARGs removal.

While plenty information is available on the reduction of ARB and ARGs in different membrane filtration studies, key operational parameters (e.g., sampling protocols, dry or wet weather conditions, wastewater constituents, or operational parameters like flux, TMP, membrane integrity confirmation etc.) are not comprehensively reported. For example, the ARG studies of Munir et al. (2011) and Böckelmann et al. (2009) examined the membrane filtration process of full-scale WWTPs for ARG removal efficiencies whereas no flux, TMP, operation mode and weather conditions were reported. Therefore, key operational parameters and target genes should be determined for AMR examinations of membrane filtration processes. Only uniform testing methods enable a comparison of AMR removal efficiencies of membrane filtration studies.

Previous mechanistic studies on AMR removal during membrane filtration have investigated ARGs predominantly in bench scale systems, and studies investigating AMR retention of MF and UF by employing capillary membranes in parallel operation mode at pilot scale are missing. Bench scale studies investigated the effect of different pore sizes on ARGs removal was evaluated by Breazeal et al. (2013). While UF with a cut-off of 100 kDa demonstrated a 1.7 log unit rejection of *bla* genes/100 mL, a 3 log greater abatement of *bla* genes was achieved by using a UF with a cut-off of 10 kDa (Breazeal et al. 2013). Further, Chaudhry et al. (2015) reported of beneficial effects of an increasing fouling layer on virus removal. Within their study they observed an additional pathogenic virus removal between 0.5 and 1.6 log units in a full-scale membrane bioreactor (pore size 0.04 µm). However, studies on the effect of the fouling layer on AMR removal using capillary membranes are still missing. Further membrane filtration studies with respect to the abatement of mobile ARGs and their penetration through UF membranes were conducted by Slipko et al. (2019) and Krzeminski et al. (2020), whereas membranes with a molecular weight cut-off (MWCO) smaller than 5 kDa (UF, NF and RO) were applied resulting in removal efficiencies of more than 99 % of free DNA. Further UF studies resulted in bacteria removal between 36 to 98.9 % using cultivation method (Morales-Morales et al. 2003; Ren et al. 2018). In this UF study flow cytometry is applied for a more accurate bacteria removal analysis (Cheswick et al. 2019).

In this study, MF and UF were investigated as efficient technologies to reduce the dissemination of ARB and ARGs. The objective of this study was to mechanistically examine key factors that influence the AMR removal efficiency during the membrane filtration processes for wastewater treatment in standard filtration mode. We specifically investigated the influence of the microbial load in the feed, the pore size of the capillary

membranes, and the effect of the fouling layer on removal efficiencies. It was hypothesized that the smaller pore size of the UF membranes lead to higher AMR removal. Furthermore, it was tested whether feed waters with higher ARGs abundances would result in higher ARGs abundances in the corresponding filtrates. Besides, while employing capillary membranes, it was expected that a fouling layer will result in a higher AMR removal efficiency. Finally, it was investigated to what extent intact bacteria as well as AMRs from feed water break through UF membranes at pilot scale.

6.3 Materials and methods

6.3.1 WWTP Steinhäule and membrane filtration pilot unit

Pilot-scale membrane studies were performed at the wastewater treatment plant Steinhäule in Neu-Ulm, Germany with a treatment capacity of 445.000 population equivalents. The WWTP Steinhäule is designed for 2,600 L/s (flow at wet weather conditions), which is double the dry weather flow. At this facility, wastewater is treated by four treatment stages – mechanical, biological, chemical, and physical stages. After secondary treatment, the physical stage is comprised of a contact reactor where 10 mg/L of powdered activated carbon (PAC) is continuously fed in order to remove trace organic chemicals. A subsequent clarifier is employed to separate the PAC followed by a tertiary filtration step. Settled activated carbon from the clarifier is returned to the contact reactor for better utilization of the PAC. Secondary effluent (SE) as well as tertiary effluent (SE+PAC+SF) were used as feed water qualities for subsequent membrane filtration studies. The overall wastewater treatment process at WWTP Steinhäule is illustrated in Figure 6-1A. Feed water constituents are presented in Table 11-23. All AMR examinations were executed using a membrane filtration pilot plant. The membrane filtration pilot plant consisted of two parallel trains. Every train comprised of four pre-filters (400 µm cut-off), feed tank (reservoir), membrane module, and by-pass filtrate/ backwash tank. Pump and flocculant tank enabling continuous flocculant dosing. Chemical enhanced backwash (CEB) was performed with one acid tank and pump as well as two base tanks and two pumps (Figure 6-1B).

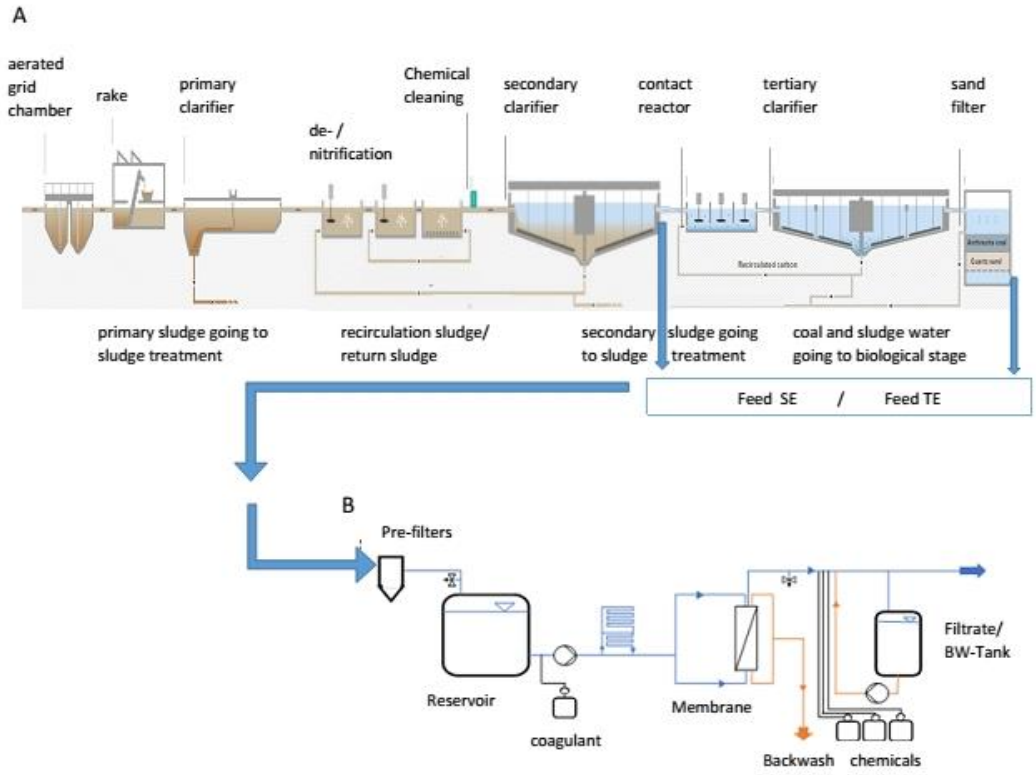

Figure 6-1: Schematic diagram of the overall wastewater treatment at WWTP Steinhäule (1A). Schematic flow diagram of one train of the membrane filtration pilot plant is shown in Figure 6-1B.

Membrane modules with pore sizes of 20 nm (UF, 80 m² surface are) and 450 nm (MF, 22 m² surface area) were selected for AMR studies. Both membrane modules were made of hydrophilized polyethersulfone and had a contact angle of 52°. While UF membrane module had 7 capillaries per fiber, the MF membrane module consisted of one capillary per fiber. Both membrane modules were operated in an inside-out, dead-end filtration mode in parallel. Microfiltration operated at a flux of 70 LMH. The ultrafiltration operated at fluxes of 40 and 70 LMH during the AMR studies.

The filtration cycle of the membrane filtration process is described in the following section: The standard operation mode of the membrane filtration process was 60 minutes. In this mode, the pilot plant operated at constant sustainable flux at 40 or 70 LMH under reversible fouling conditions, whereas feed wastewater was pumped from the reservoir through the membrane module to the filtrate side (Figure 6-1). A final coagulant (polyaluminium chloride solution, DIN 883, PLUSPAC FD ACH, Feralco Deutschland GmbH, Germany) dose of 2 mg/L was continuously fed into the feed line directly prior to the feed side of the membrane module. The continuous coagulant dosing was applied as fouling control. Coagulation reduces the occurrence of reversible fouling and increases the filtration efficiency (Yoo 2018). After 60 minutes, the standard operation mode ended and both feed pump and coagulation pump were switched off. Standard backwash mode

was activated, whereas hydraulic backwashing was executed by applying filtrate water from the backwash-tank to the module at an outside-in mode. The backwash mode lasted for 45 seconds at a flux of 230 LMH. After 23 backwash modes, a chemical enhanced backwash (CEB) mode was performed. The CEB mode consisted of injecting and rinsing the UF for 90 seconds with 150 ppm sodium hydroxide at an intake flux of 120 LMH. After that, the UF module was soaked for 15 min with the injected sodium hydroxide. A final (hydraulic) backwash rinsed the chemical out at a flux of 230 LMH for 70 s. A short backwash at 70 LMH for 900 s with only filtrate was conducted directly after the sodium hydroxide CEB. Finally, the CEB procedure was repeated with sulfuric acid. After CEB procedure with sulfuric acid and a backwash to rinse the chemical out of the membrane module, the standard operation mode was initiated again.

6.3.2 Experiments and sampling conditions

In section 6.4.1, key operational parameters for membrane filtration studies were examined. AMR examinations were executed only at dry weather conditions and during standard filtration mode of the membrane filtration process. Other filtration modes, such as backwash and chemical enhanced backwash modes, were not considered. The standard filtration mode in this study is defined as the time of the membrane filtration operation, whereas the membrane filtration operates at a certain steady flux (e.g. 70 LMH) and at constant filtrate quality. In experiment I continuous filtrate quality analyses were executed in filtrate using the total cell count (TCC) as quality parameter. After 60 minutes, the filtration cycle was terminated and the backwash mode was activated in order to remove the fouling layer. In addition to the TCC analyses the transmembrane pressure (TMP) was employed as surrogate parameter for the built-up of a fouling layer within 3 and 60 minutes of standard filtration mode (experiment II). For long-term TCC measurement, one flow cytometry measurement device (Sigrist company) was connected to the feed line and one to the filtrate line of the membrane filtration pilot plant to automatically sample and measure TCC values over a period of 3 days before and after the AMR studies (experiment III). To compare the treatment variability of UF trains 1 and 2 in experiment IV, the two flow cytometry measurement devices were connected at the filtrate sides of both UF trains to automatically sampling and measuring TCC values for 2 days.

The fouling layer was examined as layer with additional AMR removal in experiment V in section 6.4.2. In order to account for possible effects of the fouling layer on AMR removal efficiency, sampling was conducted of feed and of UF filtrate after 5 and 55 minutes during standard filtration mode.

In section 6.4.3, following key factors for AMR removal were studied: Experiment VI intended to investigate for the effect of the AMR abundance in the feed and its consequences to AMR abundance in the filtrate. To analyze the relation of AMR abundance in feed and filtrate, samples were taken from the feed and filtrate side of the pilot plant. In addition, secondary effluent and tertiary effluent of WWTP Steinhäule were used as feed waters with different qualities and AMR abundances.

Pore size as an influencing factor on AMR removal efficiency of the membrane filtration process was examined in section 6.4.4 (experiment VII). The comparison of MF and UF removal efficiencies were performed by sampling filtrate qualities of both trains during parallel operation mode in consistent conditions (same flux, same material PES, same hydrophilicity of the membrane, inside-out operation, same feed, same coagulation dose, same standard filtration mode, backwash and CEB conditions). Samples for ARGs and 16S rRNA genes as well as flow cytometry analyses were taken from feeds and corresponding UF filtrates.

In section 6.4.5, breakthrough of intact bacteria was examined as further factor influencing AMR removal efficiency. In experiment VIII, samples were taken from the feed and the corresponding filtrate from the pilot-scale UF membrane filtration (pore size of 20 nm) whereas a virgin membrane module was applied. In parallel to the pilot-scale membrane filtration, the dead and living bacteria analysis was also conducted with sterile syringe filter (Whatman® Anatop®) with a pore size of 20 nm. Both UF samples were taken and compared to exclude possible contaminations at the filtrate side. The dead and living bacteria analysis was performed using another flow cytometry from Beckman Coulter whereas gating considered all events that were larger than the added 0.2 µm beads.

To maintain sterile sampling conditions, sampling taps were flamed and stagnant water was removed prior to sampling. Grab samples for qPCR were taken and were frozen immediately after sampling at minus 20°C. Grab samples for flow cytometry (Sigrist GmbH) were manually or automatically taken and immediately analyzed at the membrane filtration pilot plant. Grab samples for flow cytometry measurement (Beckman Coulter) were manually taken and were analyzed in the laboratory within three hours.

6.3.3 AMR and microbial biomass analyses

Pre-screening studies confirmed sufficient abundances of *ermB* and *sul1* genes in the two feed water qualities in order to demonstrate ARGs removal of at least 2 log units. *VanA* gene exhibited lower abundances in the feed waters, but due to its role as antibiotic of last resort it was included in this study. Hence, the following antibiotic resistance genes were selected for AMR analyses: *ermB, sul1* and *vanA* genes. In addition, the *16S rRNA*

gene was selected as a surrogate parameter for total cells present in samples. *16S rRNA* gene quantification is practiced for bacteria quantification (Clarridge III 2004; Revetta et al. 2010; Hembach et al. 2019).

In the laboratory, samples were thawed and an aliquot of 20 mL of the sample were freeze-dried to concentrate cells and DNA. The pellet was dissolved in 500 µl Water and extracted using the Power Soil DNA extraction kit (Qiagen), following the manufacturers protocol. The DNA was then subjected to quantitative PCR (CFX 96, Bio-Rad) with primer sets for *sul1* (Pei et al. 2006), *ermB* (Alexander et al. 2015), *16S* (López-Gutiérrez et al. 2004), and a primer probe combination for *vanA* (primer VnF and VnR from Lata et al. (2009) with probe vanAPr from Furukawa et al. (2015). For *sul1*, *ermB*, and *16S*, we employed the GoTaq qPCR Master Mix (Promega), following the reaction guidelines for a total volume of 21 µl with 1 µl of template DNA. DNA was diluted if necessary with nuclease-free water. Amplification products of the qPCR were inspected by investigating the melt-curve of each reaction. For *vanA* we used the SsoAdvanced Universal Probes Mix (Bio-Rad) following the reaction guidelines for a total volume of 16 µl. The qPCR results were calibrated using a ten-fold dilution series of a linearized plasmid (obtained by cloning using the pGEM-T easy system (Promega)) that contained a single copy variant of the listed genes across at least five orders of magnitude resulting in following efficiencies: *16S* (E = 91.9, R^2 = 0.99, slope = -3.54, intercept = 38.2), *ermB* (E = 94.6, R^2 = 0.99, slope = -3.46, intercept = 38.8), *sul1* (E = 83.4, R^2 = 0.99, slope = -3.82, intercept = 42.2), *vanA* (E = 89.3, R^2 = 0.99, slope = -3.61, intercept = 40.3). The detection limit of *vanA* and *ermB* genes were 1,000 gene copies per 100 mL, for *sul1* gene 1,750 gene copies per 100 mL as well as for *16S rRNA* gene the detection limit was 10,000 gene copies per 100 mL. The given detection limits were all above the calculated limit of detection, and were adjusted by the respective PCR efficiency and by setting a minimum of four gene copies per PCR reaction. ARG values that were below these detection limits were accounted for by using half the value of the detection limit in the bar plots. For the correlation analysis values below the detection limit were excluded.

Cell count and cell status were investigated using flow cytometry (Sigrist GmbH, Switzerland) revealing total cell count (TCC), low nucleic acid count (LNAC), and high nucleic acid count (HNAC). TCC is the sum of LNAC and HNAC. LNAC represents cells with low nucleic acid amounts, whereas HNAC provides information about cells with high nucleic acid amounts. The relation of LNAC and HNAC sample describes the microbiological fingerprint of a water sample. Santos et al. (2019) investigated in a flow cytometry study of different sampling sites of a river. Bacteria community analysis exhibited high HNAC density sampling downstream of the WWTP discharge due to high amounts of organic and nutrient from the wastewater. A higher LNAC density was analyzed sampling river headwater with an oligotrophic environment. Even disruptions

in the microbiological system can be observed analyzing LNAC and HNAC (Kötzsch and Sinreich 2014). TCC, HNAC and LNAC values were analyzed using main fluorescent channels between 525 and 545 nm (FL1) and low pass fluorescent channels of more than 715 nm (FL2). Samples were stained with the fluorescent dye SYBR® Green. The gating was fixed to quantify LNAC, HNAC and background signals by using recommended values by the manufacturer. The detection limit of the flow cytometry was 10,000 cells per 100 mL. The fluorescent dye SYBR® Green binds to double stranded DNA (dsDNA). Hence, low nucleic acid amounts (LNA) is a sum parameter whereas double stranded DNA of small bacterial cells and virus with DNA genome (dsDNA) can be counted by flow cytometry (Kötzsch et al. 2012; Brown et al. 2015). Therefore, 16S rRNA gene was compared to HNAC values as surrogates for bacteria quantification in wastewater.

To distinguish between live and dead cells in UF filtrate the following dyes were applied: SYTO 9 nucleic acid stain showed intact cell membranes and fluoresces bright green. The applied fluorescent channel was 525 nm (FITC-H). Propidiumiodide indicates damaged membrane cells and fluoresces red (LIVE/DEAD™ BacLight™ Bacterial Viability and Counting Kit, for flow cytometry, Thermo Fisher). The applied fluorescent channel was 690 nm (PC5.5-H). Cell analyses were differentiated by using the Sub-micron Particle Size Reference Kit (Thermo Fisher) with 0.2 µm beads. To quantify living and dead bacteria the gating was adjusted to cells that are larger than 0.2 µm. These measurements were taken by a CytoFlex instrument (Beckman Coulter, USA).

6.3.4 Statistical data analyses

Statistical data evaluation was conducted using pair samples two-tailed t-test and independent samples two-sided t-test with a significant threshold $\alpha = 0.05$. The t-test requirements were normality and homogeneity of variances. To examine the significance of mean values of different data series of 5 minutes samples and 55 minutes samples to quantify AMR removal of the fouling layer, the pair samples t-test was applied. Based on corresponding values (5 and 55 minutes of a filtration cycle), the two data series should have good correlation values.

The statistical data analyses of the examinations of different AMR abundance of the feeds resulting in different AMR abundance in filtrates were performed using independent samples t-test. Independent samples t-tests for significance analyses were also applied for AMR studies analyzing different pore sizes of MF and UF resulting in different AMR abundance in the filtrates. Pearson correlation was used in order to show the relation between 16S rRNA genes (surrogate for bacteria quantification) and ARGs of feed and filtrate samples in experiment IX.

6.4 Results and discussion

6.4.1 Assessing standard filtration mode, fouling layer build-up, membrane integrity confirmation and treatment variability at pilot scale

To analyze particle removal during standard filtration mode operated at a constant flux of 70 LMH using tertiary effluent from a full-scale wastewater treatment plant as feed, TCC values were determined in samples collected within the first 5 minutes and after 55 minutes of the membrane filtration cycle (Figure 6-2). The analysis of the UF filtrate revealed higher TCC values within the first and second minute compared to the third, fourth, and fifth minute. Lower filtrate quality at the early start of a membrane filtration cycle was in agreement with observations reported by Chaudhry et al. (2015) observing significant higher turbidity and particle counts during the first minutes directly after completion of either backwash or chemical enhanced backwash modes. The reason for this reduced filtrate quality could be the result of particle breakthrough or might have been caused by an impaired water quality used as backwash water. The phenomenon of reduced filtrate quality occurs within the first two minutes of standard filtration mode. The reasons for this reduced filtrate quality could be the backwash mode with low quality backwash water, a reduced fouling layer on the feed side enabling higher turbidity and particle concentration, or a contamination of the UF membrane at filtrate side. However, the low filtrate quality ended within the third minute of standard filtration mode so that low filtrate quality is not a long-lasting event. Constant filtrate quality was achieved at 5 and 55 minutes of standard filtration mode. These statements can be confirmed due to a statistical evaluation. While TCC abundance was significantly different comparing UF filtrate within 1 and 5 minutes of standard filtration mode (pair samples t-test, TCC: $R = 0.999$; $dF = 2$; $p = 0.012$), the UF filtrate after 5 and 55 minutes of standard filtration mode in Figure 2 exhibited no significant differences of TCC abundances (pair samples t-test, TCC: $R = 0.794$; $dF = 2$; $p = 0.199$).

In order to quantify contaminations of the UF membrane at the filtrate side that could result in lower filtrate quality, *16S rRNA* gene analyses were compared at the beginning of the membrane filtration studies using a virgin membrane module (August 2018), after 2 months of continuous UF operation (November 2018), and after 12 months of continuous UF operation (September 2019). 16S rRNA gene abundances of $2.40 \cdot 10^5$ per 100 mL were measured at the beginning of the membrane filtration studies within 5 and 55 minutes of standard filtration mode (August 2018). After two months and 12 months of continuous UF operation, the arithmetic mean values of 16S rRNA gene of 5-minute samples (October 2018: $1.67 \cdot 10^5$ per 100 mL; 2019: $1.52 \cdot 10^5$ per 100 mL) and of 55-minute samples (October 2018: $2.31 \cdot 10^5$ per 100 mL; 2019: $1.80 \cdot 10^5$ per 100 mL)

showed no significant difference compared to the values measured at the beginning of the UF study. It can be concluded that the UF filtrate within 5 and 55 minutes of standard filtration mode showed no increasing 16S rRNA gene abundance. Therefore, a secondary contamination of ultrafiltration membrane can be excluded.

Including these events during sampling would result in a more appropriate assessment of the membrane filtration performance. According to this MF and UF study to analyze AMR removal, sampling was not executed before the first 3 minutes of a filtration cycle.

Furthermore, the transmembrane pressure was used as a surrogate parameter to assess fouling layer build-up. The results of experiment II revealed that the TMP decreased during the first 5 minutes of the standard filtration mode. After 5 minutes, the TMP continuously increased (Figure 6-2). This observation further justifies the choice of a consistent sampling procedure between 5 and 55 minutes during this membrane filtration study to assess AMR removal efficiencies during the continuous build-up of a fouling layer.

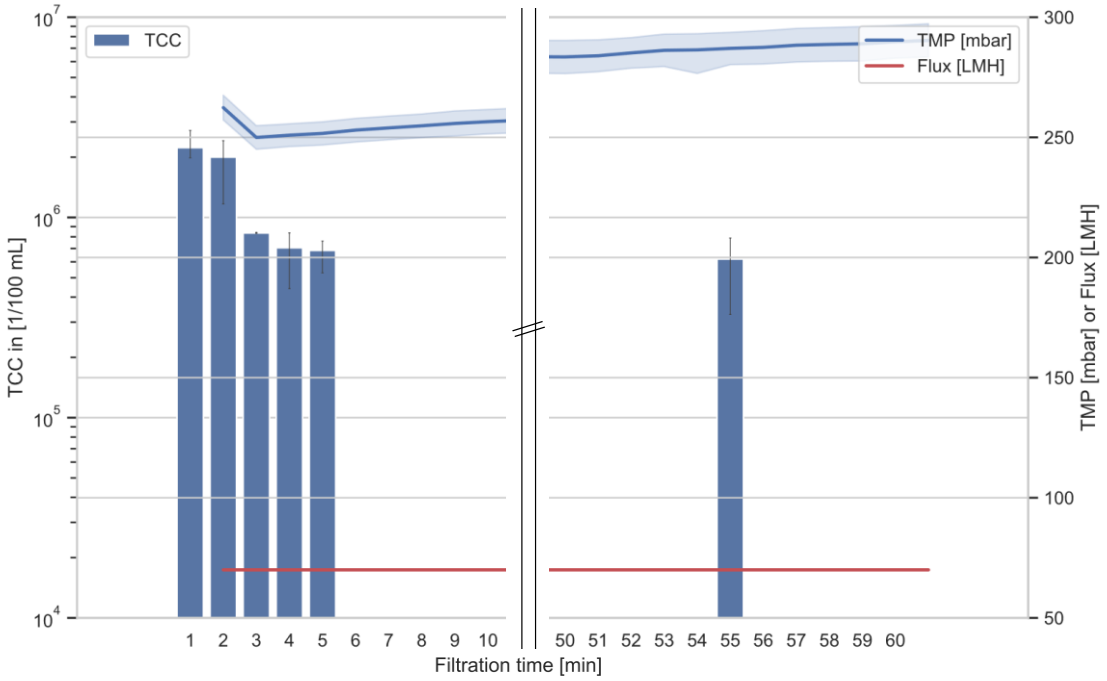

Figure 6-2: Arithmetic mean values of TCC of UF filtrate within the first 5 minutes and after 55 minutes of standard filtration cycle using tertiary effluent as feed (experiment I, n = 3).

In experiment III, long-term flow cytometry measurements were automatically analyzed in feed and UF filtrate for membrane integrity tests. While the results of the flow cytometry analysis of tertiary effluent as feed water was relatively constant (TCC $3.1 \cdot 10^8$–$3.9 \cdot 10^8$ per 100 mL; HNAC $5.0 \cdot 10^7$–$9.1 \cdot 10^7$ per 100 mL), the results of the UF filtrate resulted in a higher deviation compared to the feed (TCC $1.8 \cdot 10^5$–$8.4 \cdot 10^5$ per

100 mL; HNAC $4.9 \cdot 10^4$–$3.1 \cdot 10^5$ per 100 mL). All in all, the flow cytometry analysis performed over 3 days during continuous UF operation suggested that the TCC removal efficiency by the UF membrane was relatively constant resulting in a reduction of about 3 log units (Figure 6-3). At the end of the entire study, the TCC analyses of feed and corresponding filtrate confirmed a 3-log removal of TCC and therefore confirming that the UF membrane was not compromised while investigating the efficacy of AMR removal. Similar TCC removal results of the UF using surface water as feed are reported by Adomat et al. (2020), who operated a UF with a pore size of 20 nm and observed about 2 log removal of TCC.

In experiment IV, the performance and variability of two UF trains operated in parallel under consistent operating conditions and employing similar membrane modules (80 m²) fed by the same feed water quality, were tested at a flux of 40 LMH. Flow cytometry measurements were analyzed in the filtrates of both UF train 1 and 2 for 2 days. The arithmetic mean values of the parallel measured TCC values in the filtrate of UF train 1 and 2 were $7.68 \cdot 10^5$ per 100 mL and $6.78 \cdot 10^5$ per 100 mL, respectively. With a variability of about 0.11 log units in TCC values of both filtrate qualities, the study revealed no observed difference. Therefore, the two membrane filtration trains exhibited a very similar TCC removal efficiency.

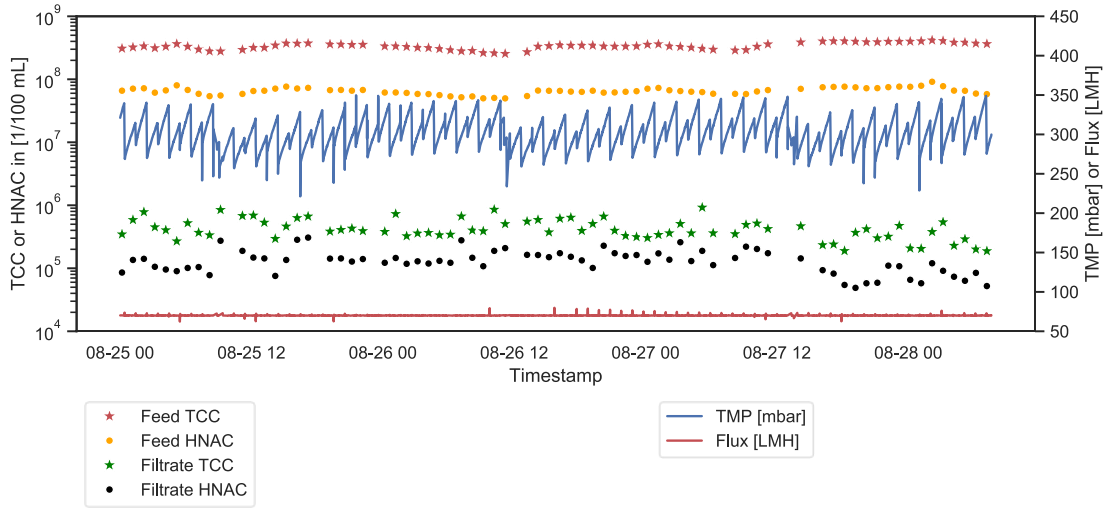

Figure 6-3: Long-term flow cytometry measurements in the tertiary effluent as feed and UF filtrate for 3 days during experiment III (the following operational parameters are illustrated: TCC and HNAC in feed and filtrate, flux and TMP).

6.4.2 Role of the fouling layer for additional AMR removal

In experiment V, the role of a growing fouling layer with progressive filtration time was investigated by performing sampling after 5 and 55 minutes during standard filtration mode. While the UF filtrate after 55 minutes of standard filtration mode exhibited slightly lower TCC values as well as *sul1*, *ermB* and *vanA* genes abundances than the UF filtrate after 5 minutes of standard filtration mode, HNAC and *16S rRNA* genes exhibited no significant difference in UF filtrate quality (Figure 6-4). Based on a confidence interval of 95 %, only *vanA* gene exhibited a significant difference between 5 min and 55 min of filtration, while the other parameters did not reveal any significant differences (see results of the paired t-test, Table 11-24).

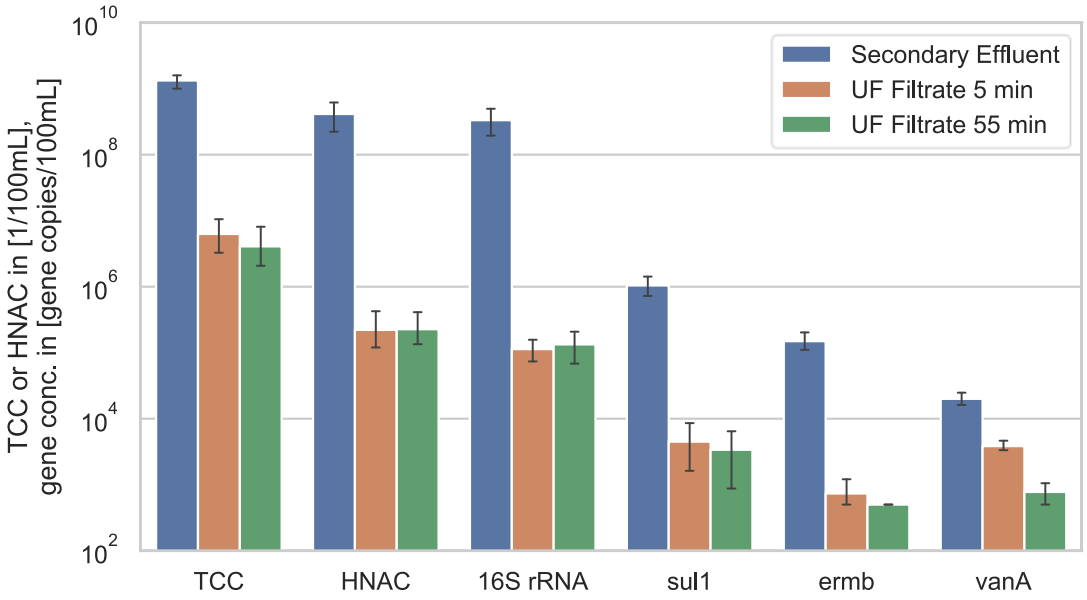

Figure 6-4: Arithmetic mean values of TCC, HNAC, 16S rRNA, ermB, sul1 and vanA genes analyzed in secondary effluent and corresponding filtrates after 5 minutes, 55 minutes and for the entire standard filtration cycle of UF operation. Error bars indicate the 95 % confidence interval. Number of samples and values below LOD are listed according to the samples secondary effluent, UF filtrate 5 min and UF filtrate 55 min. n_{TCC} = (12|3|3), LOD_{TCC} = (no values below LOD); n_{HNAC} = (9|3|3), LOD_{HNAC} = (no values below LOD); $n_{16SrRNA}$ = (12|7|7), $LOD_{16SrRNA}$ = (no values below LOD); n_{sul1} = (12|7|7), LOD_{sul1} = (0|3|4); n_{ermb} = (12|7|7), LOD_{ermB} = (0|6|7); n_{vanA} = (12|4|4), LOD_{vanA} = (0|0|4).

Considering the results of the treatment variability study (see section 6.4.1), it can be concluded that the observed removal of *16S rRNA* genes and HNAC value collected after 5 and 55 minutes are primarily a function of physical separation by pore size of the membrane module rather than driven by an additional fouling layer that is building up with progressive filtration time. Similarly, *ermB*, *sul1*, and TCC, showed only a marginal decrease between 5 and 55 min. In contrast, the *vanA* genes analyses revealed between 5 and 55 minutes of filtration a reduction by 87 % when the fouling layer was build-up (t-test, dF = 3; p = 0.004). This increasing fouling layer expressed in TMP increase is the

result of cake layer formation, pore constriction or partially clogged pores (Hallé 2010). However, *16S rRNA* genes and HNAC value analyzed within 5 and 55 minutes revealed no difference (t-test, *16S rRNA*: dF = 6; p = 0.548. HNAC: dF = 2; p = 0.629). It seemed that the fouled membrane module still had a high enough number of larger pores for cell breakthrough and the fouling layer did not result in any additional bacteria removal.

The fouling layer effect of an anaerobic membrane bioreactor process (MF, pore size 0.3 µm) concerning ARB removal was reported by Cheng and Hong (2017). The researchers analyzed bacteria and ARGs removal at different fouling layer conditions. Different ARGs to this AMR study were analyzed. Therefore, comparison of ARG removal efficiency is not possible. While the virgin membrane resulted in 5 log units of ARB removal, the subcritically fouled membrane exhibited lower log ARB removal due to an increase in filtration pressure. In contrast, the 5 log ARB removal was achieved by critically fouled membrane, again. The lower bacteria removal during subcritical fouled membrane (reversible fouling conditions), reported in Cheng and Hong (2017), cannot be confirmed in this fouling layer study. It seems that the smaller pore size of 20 nm of the UF in this study enabled an almost constant bacterial removal within 5 and 55 minutes of standard filtration mode. In contrast, the MF membrane had a lower bacteria removal due to higher filtration pressure. This probably bacteria deforming effect due to filtration pressure was already reported by Suchecka et al. (2003). Furthermore, the reported 5 log ARB removal was significant higher to this UF study (3.5 log units of *16S rRNA* gene). In the study of Cheng and Hong (2017), a different feed with significant higher colloid concentrations were applied. ARB and ARGs could additionally adsorb to wastewater colloids resulting in higher ARB and ARGs removal efficiency of the MF membrane. If the bacteria removal efficiency is compared between the MBR process and the UF process in this study, the AMR removal efficiency of the biological stage should be considered to the removal efficiency of the UF process. The pilot-scale study of Marti et al. (2011) also investigated bacteria and virus removal under different cake layer conditions during operation of a membrane bioreactor process in cross-flow mode (membrane area 8 m²; nominal pore size 0.4 µm). The MF operated 9 minutes in continuously cross flow mode with aeration (flux at 25 LMH) and after 1 minute in relaxation phase (filtration off). In this study, the bacteria removal was examined directly after relaxation phase within the first minute with a low fouling layer and within 9 minutes of continuously membrane filtration, whereas the membrane experienced the highest fouling condition. The study results demonstrated that bacteria removal had no correlation with TMP, which was the surrogate for fouling layer increase. *E. coli* could be efficiently reduced by 5.1 log units. This bacteria removal efficiency is in line with the bacteria removal of the MBR study of Cheng and Hong (2017).

In contrast, the growing fouling layer resulted in a significant *vanA* gene removal. The range of this removal is in the range that has been reported for the removal of viruses by a fouling layer Chaudhry et al. (2015). Like viruses, *vanA* genes may be comparatively frequent in the mobile DNA fraction. Che et al. (2019) investigated in a metagenomic sequencing study the occurrence of intra- and extrachromosomal ARGs in wastewater and confirmed that the antibiotic resistance genes of the aminoglycoside class of antibiotics (e.g., *vanA* genes) had higher extrachromosomal abundances (sum of plasmid as well as integrative and conjugative elements) than intrachromosomal abundances (chromosome) compared to resistance genes *ermB* and *sul1* gene of the macrolide (e.g. erythromycin) and sulfonamide class (e.g. sulfamethoxazole). Hence, the observed *vanA* gene removal by the fouling layer may be the result of electrostatic charge effects of the fouling layer that lead to a reduced passage of mobile DNA. Wang et al. (2021) investigated the removal of plasmid with artificial marker genes as a surrogate for extracellular and extrachromosomal ARG using a lab-scale membrane bioreactor (flat-sheet membrane with 0.2 µm of pore size). The study results demonstrated that the plasmids were predominantly removed by adsorption onto sludge particles. An additional plasmid removal was the result of the fouling layer increase. Wang et al. (2021) hypothesized that the enhancement of plasmid removal with the increasing fouling layer was the result of narrow pores or of the enhanced interaction among foulants and plasmids. The foulants, especially extracellular polymeric substances (EPS) and soluble microbial products (SMP) have negatively charged functional groups and the DNA is negatively charged due to the phosphate groups. Extracellular ARGs can have a high tendency to interact with negatively charged EPS and SMP in the presence of divalent cations like Ca^{2+} und Mg^{2+}.

The MF and UF studies were executed with coagulant dosing at the feed side of the membrane module for fouling control. The continuous coagulant dosing of 2 mg/L with Al^{3+} cations can have an additional electrostatic charge effect according to extracellular ARGs removal. The study of Chen et al. (2020) is in line with electrostatic charge effects for ARGs removal. The author investigated intra- and extracellular ARGs removal in municipal wastewater effluent by electrocoagulation. It was reported that UV disinfection of wastewater effluent resulted in an extracellular ARGs increase and following electrocoagulation could significantly reduce extracellular ARGs.

This UF study is the first study in which the fouling layer of capillary membranes in dead-end operation was examined at pilot-scale with regard to ARG removal efficiency. Conversely, the build-up of a fouling layer under hydraulically and chemically reversible fouling conditions, did not result in any significant decrease for *sul1* and *ermB* genes. However, the fouling layer may facilitate a higher removal of free, mobile ARGs.

6.4.3 Role of feed water quality for UF filtrate water quality

It was hypothesized that AMR abundance in the feed water has a direct influence on AMR abundance in the UF filtrate (experiment VI). Two different wastewater qualities, namely secondary and tertiary effluents from the WWTP Steinhäule, were selected as feed waters. The qPCR and flow cytometry analyses exhibited that advanced treatment using powdered activated carbon followed by sand filtration (tertiary effluent) resulted in significant lower TCC, HNAC as well as *16S rRNA*, *ermB*, *sul1* and *vanA* genes abundances compared to the secondary effluent (Figure 6-5) (based on a t-test, Table 11-25). The study results of experiment VI revealed that *sul1*, *ermB* and *vanA* genes could be detected in both UF filtrates. The UF filtrate of the secondary effluent had significantly higher *sul1* genes abundances than the UF filtrate of the tertiary effluent. Since *ermB* genes were detected close to the detection limit, the ultrafiltered secondary and tertiary effluents showed a similar *ermB* gene abundance. No significant different vanA genes were measured in ultrafiltered secondary and tertiary effluents. While the TCC value was lower in the ultrafiltered tertiary effluent than in the ultrafiltered secondary effluent, HNAC value and *16S rRNA* gene showed no difference between the two filtrates. This effect of almost constant HNAC and *16S rRNA* gene abundances in UF filtrates was already confirmed in section 6.4.2.

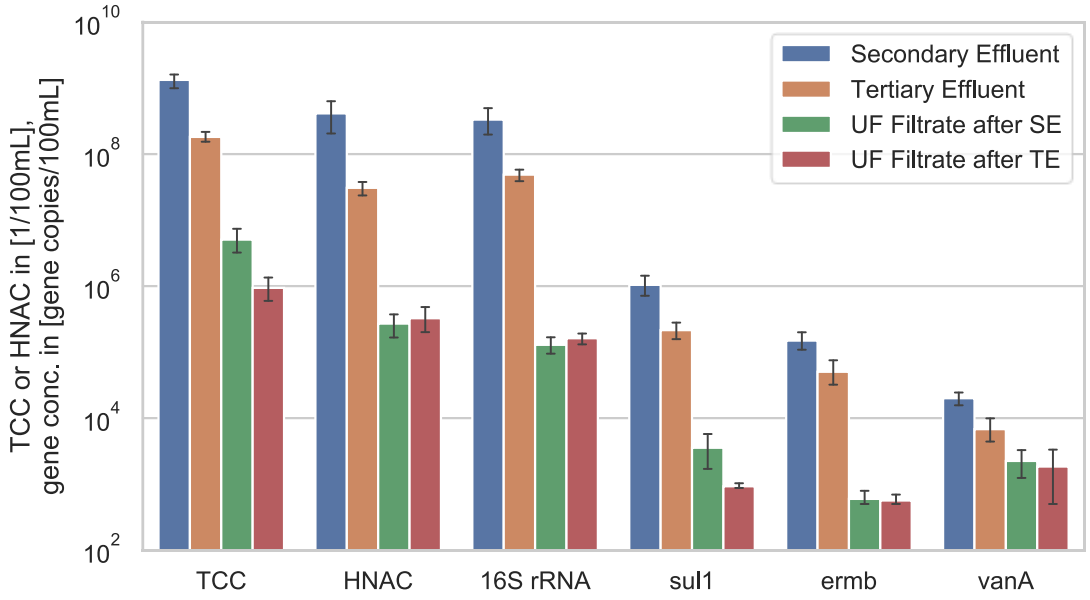

Figure 6-5: Arithmetic mean values of TCC, HNAC, 16S rRNA, sul1 ermB, and vanA genes analyzed in secondary effluent (SE), tertiary effluent (TE), and corresponding filtrates. Error bars indicate the 95 % confidence interval. Number of samples and values below LOD are listed according to the samples secondary effluent, tertiary effluent, UF filtrate after SE and UF filtrate after TE. n_{TCC} = (9|12|10|14), LOD_{TCC} = (no values below LOD); n_{HNAC} = (9|12|10|14), LOD_{HNAC} = (no values below LOD); $n_{16SrRNA}$ = (12|12|16|20), $LOD_{16SrRNA}$ = (no values below LOD); n_{sul1} = (12|12|16|20), LOD_{sul1} = (0|0|9|19); n_{ermb} = (12|12|16|20), LOD_{ermB} = (0|0|15|19); n_{vanA} = (12|10|10|11), LOD_{vanA} = (0|0|3|8).

The UF study of Du et al. (2015) is in accordance with the observations of this study. Du et al. (2015) studied ARG removal by a MBR (using a membrane with 0.1 µm to 0.4 µm mean pore size) analyzing ARGs in the influent and effluent of the MBR process as well as seasonal fluctuations of ARGs in wastewater. Seasonal fluctuations of the *sul1* gene resulted in higher *sul1* gene abundances in the feed and as a consequence in higher *sul1* gene abundance in the filtrate. To summarize, the results of *sul1* genes removal confirmed the hypothesis that higher AMR abundance in feed water results in higher AMR abundance in UF filtrate.

6.4.4 Comparison of MF and UF ARG removal efficiencies

To elucidate the effect of different pore sizes on the ARG removal efficiency, MF and UF with different pore sizes were employed in parallel operation in experiment VII. In this case the MF and UF modules were operated with secondary effluent as feed. The HNAC and *16S rRNA* gene showed a similar response to the MF and UF treatment with significantly higher removal rates with UF (3.2 log and 3.5 log removal, respectively) compared to MF (2.6 log and 2.8 log removal, respectively). The TCC, however, was not that strongly affected, pointing to a selective removal of the active cell fraction, represented by the HNAC (Lebaron et al. 2001), by the UF (Figure 6-6, see also Figure 11-17 and Figure 11-20). The UF had a significantly higher (T-test; dF = 6.8; p = 0.036) *sul1* gene removal by 2.9 log units compared to MF (2.1 log, respectively). The *ermB* gene was already approaching the lower limit of detection for both filtration units and were efficiently removed (Figure 6-6). In contrast, low *vanA* gene removal efficiencies were examined by both MF (1.1 log unit *vanA* gene) and UF (1.2 log units *vanA* gene) (Figure 11-17).

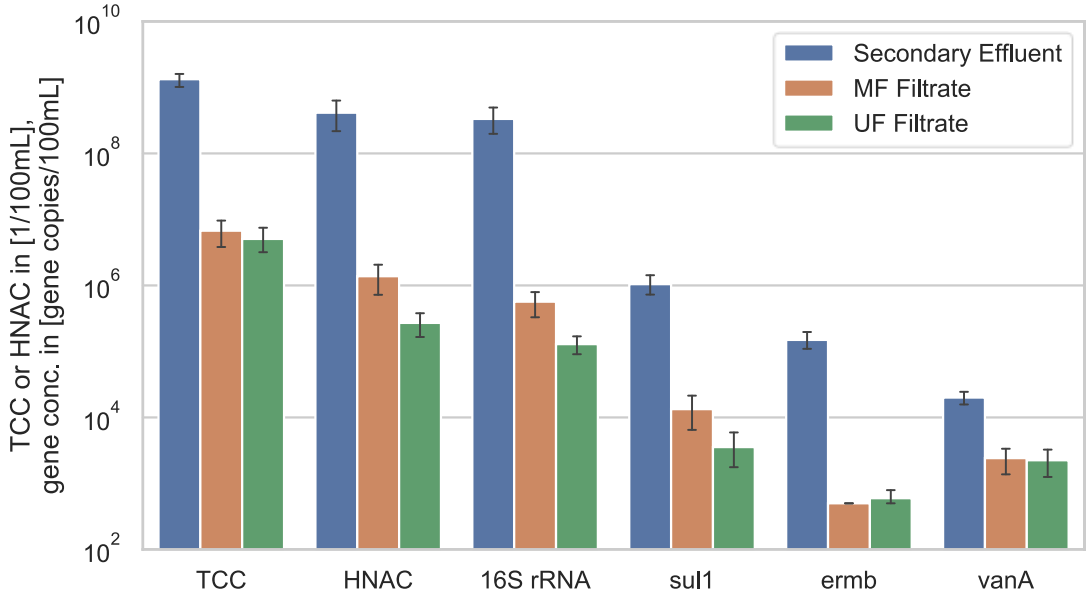

Figure 6-6: Arithmetic mean values of TCC, HNAC, 16S rRNA, ermB, sul1 and vanA genes from feed, MF and UF filtrate are presented. Error bars indicate the 95 % confidence interval. Number of samples and values below LOD are listed according to the samples secondary effluent, MF filtrate and UF filtrate. n_{TCC} = (9|7|10), LOD_{TCC} = (no values below LOD); n_{HNAC} = (9|7|10), LOD_{HNAC} = (no values below LOD); $n_{16SrRNA}$ = (16|7|16), $LOD_{16SrRNA}$ = (no values below LOD); n_{sul1} = (16|7|16), LOD_{sul1} = (0|0|8); n_{ermb} = (16|8|16), LOD_{ermB} = (0|8|15); n_{vanA} = (12|8|9), LOD_{vanA} = (0|2|3).

Previous membrane filtration studies comparing MF and UF reported similar ARG removal efficiencies. Similar to our results, a full-scale study of Munir et al. (2011), a bench-scale study of Kappell et al. (2018) and a pilot-scale study of Hembach et al. (2019) also reported detectable *ermB* and *sul1* genes in UF filtrate. Munir et al. (2011) examined the ARG removal of a full-scale MBR process (pore size of 40 nm) and observed *sul1* gene removal of about 3 log units. The lab-scale UF study (pore size of 17 nm) of Ren et al. (2018) also resulted in a 3 log *sul1* gene removal efficiency.

However, ARG removal by membrane filtration differs greatly between different types of ARGs. While UF samples had about 76 % lower *sul1* gene mean value than MF samples, almost the same *ermB* gene abundances were detected in MF and UF filtrate likely due to the fact that the *ermB* gene abundances were close to the detection limit. The low *vanA* gene removal efficiencies of MF as well as UF could be the result of higher mobile ARGs abundances in the feed water. Mobile or free DNA can easily penetrate through MF as well as UF pores. The breakthrough of extracellular ARGs through UF membrane pores was also reported elsewhere (Slipko et al. 2019; Krzeminski et al. 2020). ARGs removal efficiencies by MF and UF processes were already reported by Breazeal et al. (2013) where plasmid-associated ARGs in an artificial feed could be better removed with decreasing membrane pore size using laboratory-scale MF, UF and NF skids. While MF (pore size of 0.45 and 0.1 µm) resulted in less than 1 log unit removal of *blaTEM* and

vanA genes, UF (pore size of 100 kDa) could decrease *blaTEM* and *vanA* genes by 1.1-2.4 log units, NF (pore size of 10 kDa) reduced *blaTEM* and *vanA* genes by 4.2-5.8 log units. This UF study examined *vanA* gene removal (1.2 log units) using membrane with 20 nm pore size (about 1.200 kDa). The results are in line with the study of Breazeal et al. (2013).

This was the first study in which pilot-scale MF and UF plants were operated in parallel to investigate removal of ARGs under realistic operational conditions. UF capillary membranes with smaller pores could also increase the removal of ARGs, in our case *sul1* gene, potentially through the higher removal of active cells.

6.4.5 Distinguishing live and dead bacteria and intracellular ARG in UF filtrates

MF and UF membrane modules are specified by the manufacturer with nominal pore sizes of 450 and 20 nm, respectively, representing a pore size that should predominantly exclude passage of particles like bacteria. However, as described in the previous experiments above (e.g. Figure 6-6; see also Figure 11-18) we always measured a constant number of cells with flow cytometry (6 log units/ 100 mL in MF filtrate and 5 log units/ 100 mL in UF filtrate) and *16S rRNA* genes. Previous research mainly focused on the breakthrough of ARGs, however, bacteria breakthrough was not investigated in parallel. As microbial cells are the main ARG carriers, we distinguished dead and live bacteria in UF filtrate (experiment VIII). This was tested with the secondary and tertiary effluent to evaluate the effect of different feed water qualities. Arithmetic mean of HNAC in UF filtrate was 5.8 log units per 100 mL using tertiary effluent as feed and 6 log units per 100 mL using secondary effluent as feed (Figure 6-7). These detected HNAC values agreed well with the HNAC values analyzed by flow cytometry from Sigrist GmbH (see sections 6.4.2, 6.4.3, 6.4.4). Remarkably was the fact that 49-59 % of detected HNAC values in UF filtrate samples were live bacteria (Figure 6-7), confirming the results from above (Figure 6-7) that mostly active cells are removed by the filtration modules. The experiment analyzing dead and live bacteria in UF filtrate was executed using a virgin membrane module in the pilot plant and sterile syringe filters with the same pore size. The dead and live bacteria analyses in the filtrate of the sterile syringe filters resulted in arithmetic mean values of HNAC of 6 log units per 100 mL. The percentage of live bacteria was between 58 and 62 %. The study results of the virgin membrane modules and sterile syringe filters demonstrated similar HNAC values. Hence, bacterial contamination from the pilot plant using virgin membrane module can be excluded. Figures of live and dead bacteria analyses are illustrated in Figure 11-19.

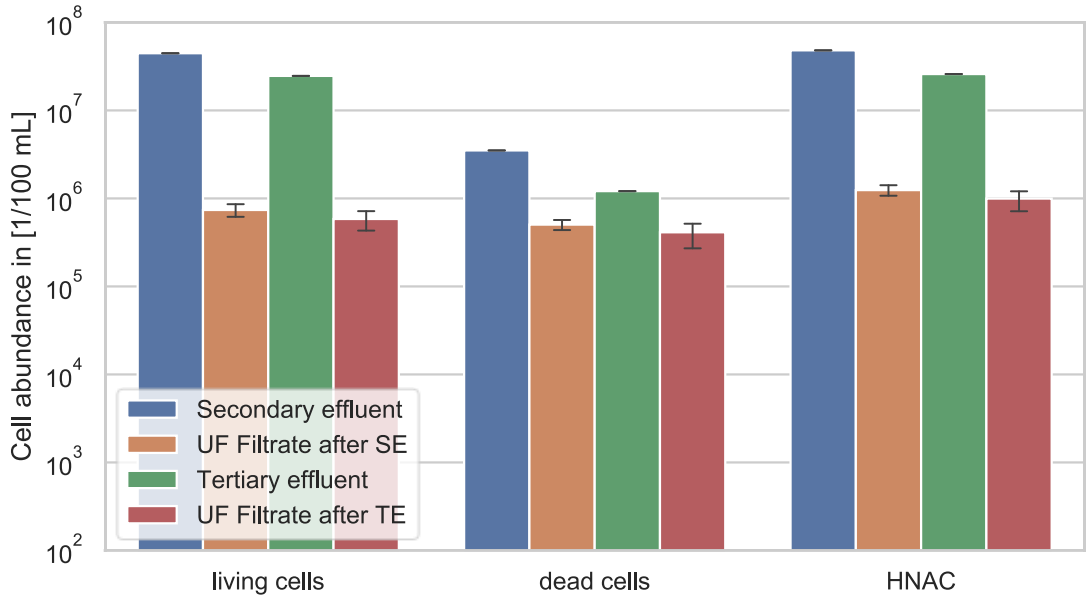

Figure 6-7: Arithmetic mean values of live and dead bacteria in secondary and tertiary effluent and corresponding UF filtrates. HNAC is the sum of live and dead cells. Error bars indicate standard deviation. $n_{\text{Secondary effluent}} = 2$, $n_{\text{UF Filtrate after SE}} = 5$, $n_{\text{Tertiary effluent}} = 2$, $n_{\text{UF Filtrate after TE}} = 5$.

The MF studies of Hahn (2004) and Liu et al. (2019) both confirm bacteria breakthrough using membranes with pore sizes between 0.2 µm and 0.1 µm. Hahn (2004) investigated in sterile 0.2 µm filters to quantify bacteria removal (size of isolated strains ranged from <1 to >10 µm in cell length) and concluded that two out of 19 bacterial strains were able to pass pores of 0.2 µm filter. The study of Liu et al. (2019) is in line with the MF study of Hahn (2004). Liu et al. (2019) examined the breakthrough of Hylemonella bacteria using 0.1 µm sterile filter. This filter also used in the study of Liu et al. (2019) had a nominal pore size of 100 nm. This range of pores were measured as largest pores (90 nm) in the UF study of ElHadidy et al. (2013b) using an UF membrane with a nominal pore size of 40 nm. According to this wide range of pore size distribution, it can be concluded that bacteria can pass larger pores of UF membranes. The UF study of Ren et al. (2018) confirmed that bacteria can breach UF membranes. Ren et al. (2018) reported an incomplete bacteria removal of 98.9 %, using an UF module with a pore size of 100 kDa.

Different mechanisms resulting in membrane breakthrough of bacteria, ARB and extracellular ARGs are summarized in the following section: There are different possibilities how pore sizes of membrane can be determined, but in all cases it needs to be considered that a nominal pore size always represents a pore size distribution. For example, the pore size or the molecular weight cutoff can be described as a molecule of a certain size that can be removed by 90 %. ElHadidy et al. (2013b) studied the pore size

distribution of ultrafiltration membranes with nominal pore size of 40 nm by atomic force microscopy and reported pores up to 90 nm. Therefore, a small number of larger molecules or particles could theoretically migrate through the membrane. Additional factors affecting ARB and ARGs breakthrough are membrane materials (Liu et al. 2019) or the increase of flux and TMP. Liu et al. (2019) reported rejection of bacteria by membranes of similar pore size (0.1 µm), but four different materials. While Hylemonella bacteria could pass the pores of polyvinylidene fluoride and polyethersulfone filters, no transmission was detected using polycarbonate and mixed cellulose esters filters. The increase of flux and TMP resulted in plasmids (Arkhangelsky et al. 2011), viruses (Arkhangelsky et al. 2011), and bacteria (Suchecka et al. 2003) breakthrough. The breakthrough effects caused by higher flux and TMP were the result of membrane pore enlargement (Arkhangelsky and Gitis 2008) and of bacterial cell deformation (Suchecka et al. 2003). The bacterial cell deformation seems to be strongly depended on the cell-wall structure of the bacteria. Lebleu et al. (2009) while investigating MF membranes concluded that bacteria removal depends on the kind of bacteria. While gram-positive bacteria have a thicker peptidoglycan layer and thus are less formable and better retainable by MF, gram-negative bacteria with their thin peptidoglycan layer enable their better deformation and transmission through MF pores. In addition, Slipko et al. (2019) investigated extracellular DNA breakthrough during membrane filtration. They concluded that both size exclusion and surface charge of the membrane were important for extracellular DNA retention. Hence, negatively charged membranes exhibited lower free DNA retention than neutral charged membranes. In addition, extracellular DNA like plasmids are ARG carriers and can pass membranes by elongation in converging and accelerating flow fields, which usually occurs above the immediate openings of the membrane pores (Arkhangelsky et al. 2011; Latulippe and Zydney 2011; Schwaller et al. 2022). The study of Arkhangelsky et al. (2011) focused on DNA transport of particles of 350 nm of diameter penetrating through UF membranes with pores as narrow as 10 nm. Arkhangelsky et al. (2011) reported of hydrodynamic strains that lead to 350 nm diameter particle breakthrough, due to elongation of those particles into long hair-shaped strands. The study of Latulippe and Zydney (2011) is in accordance with the study results of Arkhangelsky et al. (2011). In this study larger plasmids DNA from 3 to 17 kbp in size were able to filtrate through UF pores that were over an order of magnitude smaller than the plasmid DNA. High filtrate flux can cause elongation of plasmid DNA in the so-called converging flow field so that plasmid DNA breakthrough occurred (Schwaller et al. 2022).

To summarize, both dead and live bacteria concentrations were detected in high concentrations up to 6 log units/ 100 mL in UF filtrate. Bacteria, ARB and ARGs breaking through the UF membrane is likely the result of the pore size distribution of the membrane

module, membrane materials, membrane pore enlargement and bacterial cell deformation due to high TMP. Bacterial cell deformation and transmission tendency depends on cell-wall structure of the bacteria. Transfer of extracellular ARGs bonded on free DNA like plasmids depends on size exclusion and surface charging of the membrane as well as the elongation effects in the converging flow fields above the opening of the membrane pores. Therefore, detected ARG genes abundances in UF filtrate could be the result of both, breakthrough of cells and of extracellular DNA.

To illustrate the relation of bacterial genomes measured as *16S rRNA* gene (assuming a constant copy number of 16S) and ARGs, correlations of the values were evaluated in the Figure 6-8A and Figure 6-8B using feed and filtrate samples. While good correlations between *ermB, sul1* genes and *16S rRNA* gene existed in secondary and tertiary effluents, *vanA* gene showed no correlation with the *16S rRNA* gene in the secondary effluent (Figure 6-8A). The low correlation of *vanA* gene with *16S rRNA* genes suggests that *vanA* gene might be predominantly associated with either free extracellular or extrachromosomal DNA, like plasmids. This could explain the previously observed different ARG removal efficiencies by the fouling layer study (section 6.4.2) and the low *vanA* gene removal efficiencies of MF and UF membranes (section 6.4.4). The study results of detected *sul1* genes in UF filtrate of section 6.4.2, 6.4.3and 6.4.4 were confirmed by the evaluation of findings shown in Figure 6-8. The relation of intra- and extracellular ARGs in wastewater of a full-scale WWTP was analyzed by Liu et al. (2018), who showed that the lowest correlation of the *16S rRNA* gene abundance with 22 analyzed ARGs was the *vanA* gene, while the highest *16S rRNA* gene correlations were achieved with *sul1*, *sul2, tetM* and *ermB* genes. This is also in line with a study by Che et al. (2019) who investigated mobile and chromosomal antibiotic resistomes in WWTP influent, activated sludge, and WWTP effluent by metagenomic sequencing. The authors found that between 41 to 66 % of the ARGs detected in all wastewater compartments were associated with extrachromosomal mobile plasmids, integrative and conjugative elements (ICEs), whereas only 21 to 36 % of detected ARGs belonged to intrachromosomal group (Che et al. 2019).

To summarize, the study results of experiment IX showed that (living and dead) bacteria were capable of breaking through the pores of the UF membrane. Correlations of *sul1* gene and *16S rRNA* gene revealed that intracellular *sul1* gene likely penetrated through the pores of the UF membrane with the bacterial cell.

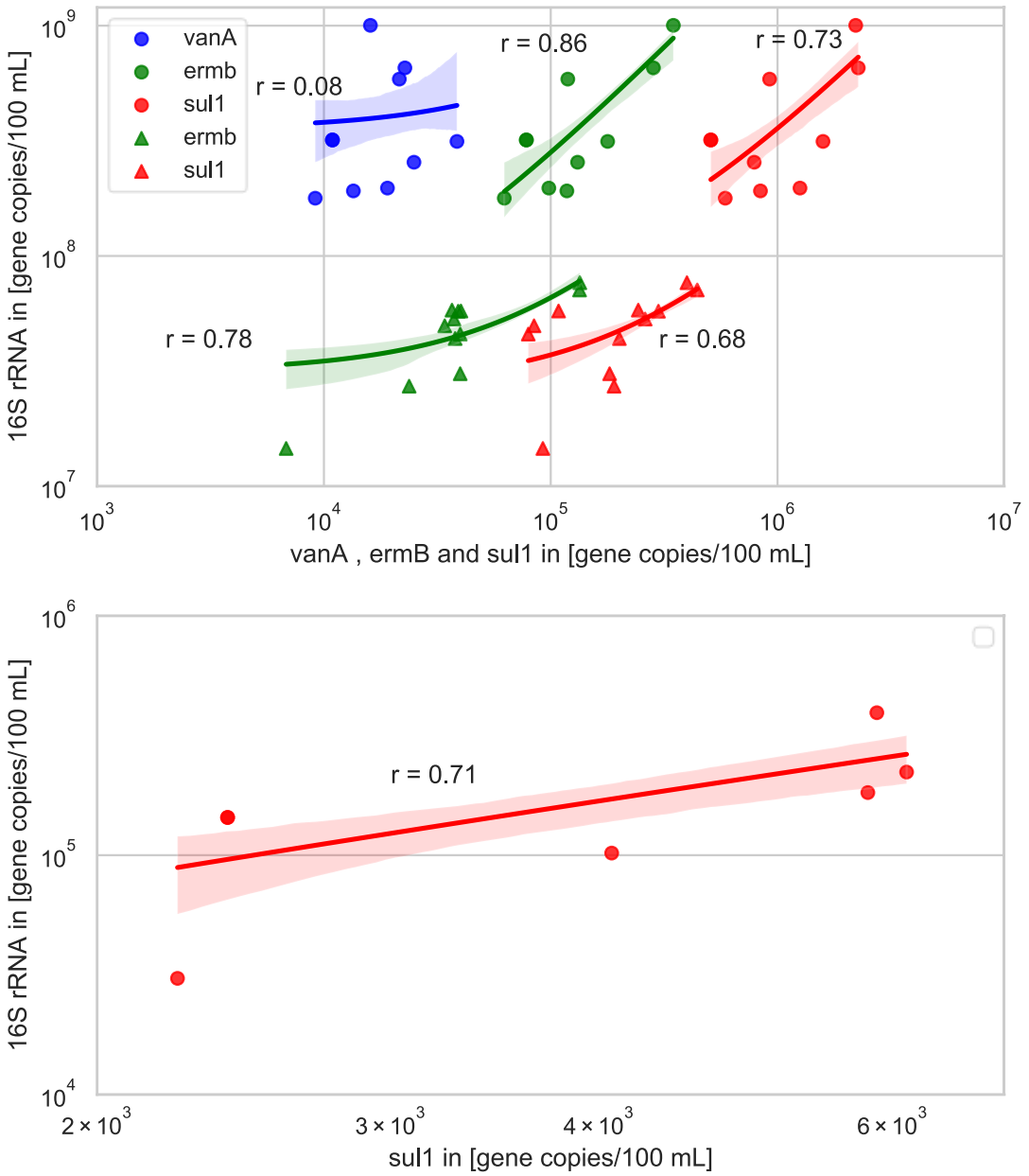

Figure 6-8: Pearson correlation of 16S rRNA gene with sul1, ermB and vanA genes analyzed in secondary effluent (circular markers) and tertiary effluent (triangular markers) (A). Pearson correlation of 16S rRNA and sul1 genes measured in UF filtrate samples using secondary effluent as feed (B). For both figures, the shaded area indicates the 95 % confidence interval.

6.5 Conclusions

Pilot scale membrane filtration studies using real wastewater of WWTPs should consider the following key operation parameter for AMR analyses: Dry weather flow of the WWTP should be applied for AMR analyses. Sampling is carried out at standard filtration mode (constant steady flux and constant filtrate quality). Fouling layer examinations for AMR analyses is executed at constant TMP increase. Membrane integrity is demonstrated before and after AMR examinations. Treatment variability of two trains of the pilot plant is checked before AMR studies.

The AMR examinations, using MF and UF, revealed a significant reduction of *ermB* genes (by 2.7 and 2.8 log units) and *sul1* genes (by 2.1 log units and 2.9 log units) using secondary effluent as feed. In contrast, with regard to *vanA* gene MF and UF achieved only a moderate reduction by 1.1 log units and 1.2 log units. These significant different degrees of removal of *ermB*, *sul1* and *vanA* genes by MF and UF were the result of different factors that were the focus of this study. Overall, the main factor for ARGs removal was the pore size of the applied membranes. While no significant additional AMR removal of intra- and extrachromosomal ARGs (e.g., *sul1* and *ermB* genes) was detected by the fouling layer, predominantly mobile ARGs (e.g., *vanA* gene) could be significantly decreased. The ARG abundance in the feed water is another factor influencing AMR removal. The higher the ARGs abundance in the feed water the higher was the ARGs abundance in the filtrate water. Beside of ARGs abundance in the feed water the AMR removal efficiency of the membrane filtration also depends on the relation of intra- and extracellular ARGs abundance. It was found that predominantly intra- and extrachromosomal ARGs (e.g., *sul1* and *ermB* gene) can result in higher ARGs removal efficiencies of the membrane filtration process while predominantly extracellular or extrachromosomal ARGs (e.g., *vanA* gene) can result in lower ARGs removal efficiencies. Lastly, dead and live bacteria as well as ARB can break through the membrane, which raises the question to what extent ARB-associated regrowth can occur on the filtrate side. This effect would reduce ARGs removal efficiency of MF and UF. Therefore, further investigations concerning ARB-associated regrowth at filtrate side are required.

6.6 Acknowledgement

The authors gratefully acknowledge partial support through a grant provided by the German Ministry of Education and Research (BMBF) as part of the research project ‘HyReKa’ (award number 02WRS137J). We also would like to thank Heidrun Mayrhofer for technical support.

7 INLINE DOSING OF POWDERED ACTIVATED CARBON AND COAGULANT PRIOR TO ULTRAFILTRATION AT PILOT-SCALE – EFFECTS ON TRACE ORGANIC CHEMICAL REMOVAL AND OPERATIONAL STABILITY

The following chapter presents investigations related to ***research hypothesis #4***: *Precoating the UF membrane with a cake layer using polyaluminium chloride (PACl) as coagulant with the continuous inline dosing of PAC prior to UF achieves a significant better TOrC removal efficiency as well as mitigated TMP built-up than an operational mode with simultaneous and continuous inline dosing of coagulant and PAC.*

This chapter has been published with some editorial changes as follows:

Schwaller, Christoph; Hoffmann, Grit; Hiller, Christian X.; Helmreich, Brigitte; Drewes, Jörg E. (2021): Inline dosing of powdered activated carbon and coagulant prior to ultrafiltration at pilot-scale – Effects on trace organic chemical removal and operational stability. In Chemical Engineering Journal 414, p. 128801. https://doi.org/10.1016/j.cej.2021.128801

Author contributions: Christoph Schwaller, Grit Hoffmann and Jörg E. Drewes developed the research objective. Christoph Schwaller conducted the experiments, analyzed the samples and data and wrote the manuscript. Christian X. Hiller reviewed the manuscript. Jörg E. Drewes and Brigitte Helmreich supervised the study and reviewed the manuscript. All authors approved the final version of the manuscript.

7.1 Abstract

Hybrid membrane processes such as inline dosing of powdered activated carbon (PAC) prior to ultrafiltration membranes (UF) have already shown promising potential for the abatement of trace organic chemicals (TOrCs). However, questions regarding the optimization of the operational stability by the employment of coagulation and its interferences with inline dosed PAC, have not yet been comprehensively investigated. Within the scope of this pilot-scale study, inline dosing of different sized PAC types at different dosages was combined with or without the addition of polyaluminium chloride (PACl) coagulant prior to UF. As expected, when PAC was not employed, negligible TOrC removal was observed, whereas all the operational modes with the application of PAC inline dosing showed significant TOrC removal. Coagulation with PACl clearly reduced the build-up of transmembrane pressure, especially owing to maintaining hydraulic backwash efficiency. The operational mode of precoating the UF with PACl combined with continuous inline dosing of PAC exhibited particularly good TOrC removal results along with optimized membrane fouling mitigation. In contrast, the simultaneous and continuous dosing of PAC and PACl is not recommended, in particular owing to detrimental effects of the coagulant on TOrC removal efficiency by PAC.

Keywords: Ultrafiltration; powdered activated carbon inline dosing; coagulant inline dosing; trace organic chemical removal; operational stability

7.2 Introduction

The pressure on our freshwater resources is increasing worldwide. In particular, the rapid growth of population, urbanization, industrialization, as well as agricultural activities are stressing global water resources (European Commission 2012; Holland et al. 2015c; Rosa et al. 2018; Greve et al. 2018). The World Resources Institute (WRI) estimates that a quarter of the world's population is already living in regions which can be characterized by acute water shortage (WRI 2019). This situation is even likely to worsen in the next few decades owing to the consequences of climate change (van Vliet et al. 2017; Greve et al. 2018). In order to alleviate water scarcity and conflicts due to competing needs between the drinking water, agricultural and energy sectors, water must be far more efficiently and sustainably managed (Drewes et al. 2012; Vollmer et al. 2018; Greve et al. 2018).

Water reclamation and reuse can efficiently and sustainably overcome water resource issues by creating new sources of high-quality local water supplies and therefore partially substituting already scarce freshwater resources (Miller 2006; Sanz and Gawlik 2014; 2020/741/EU). However, in order to comply with more stringent water quality requirements for certain reclaimed water applications, advanced treatment might be required, which effectively removes hygienic parameters such as pathogens but also trace organic chemicals (TOrCs). A broad range of TOrCs, including residuals or metabolites of pharmaceuticals and personal care products, occurs in wastewater treatment plant effluents (Ternes 2007a; Dong et al. 2015) and has already been widely detected in various environmental compartments such as soil, groundwater and surface water bodies (Nikolaou et al. 2007; Vieno et al. 2007; Wu et al. 2009; Li 2014b; Sui et al. 2015; Lin et al. 2015; Biel-Maeso et al. 2018). Therefore, these TOrCs and other contaminants, including inter alia antibiotic resistant bacteria or antibiotic resistance genes, have to be removed through advanced wastewater treatment for applications where stringent water qualities are required, such as groundwater recharge or agricultural irrigation of food crops eaten raw.

Ultrafiltration membranes (UF) are a highly reliable physical treatment process capable of efficiently removing pathogenic bacteria or even viruses (Di Zio et al. 2005; Iannelli et al. 2014; Ferrer et al. 2015; Cordier et al. 2020). Hybrid membrane processes (HMPs) like the hybridization of UF with processes such as oxidation via ozone or adsorption via powdered activated carbon (PAC), are likely to guarantee a safe water quality to enable water reuse via agricultural food crop irrigation or groundwater recharge. Several studies have investigated a combination of UF with PAC with respect to the abatement of TOrCs (Snoeyink et al. 2000; Snyder et al. 2007; Ivancev-Tumbas et al. 2008; Campinas and Rosa 2010; Ivancev-Tumbas and Hobby 2010; Stoquart et al.

2012; Margot et al. 2013; Löwenberg et al. 2014; Rodriguez et al. 2016; Ivancev-Tumbas et al. 2018). These studies differ clearly with respect to the PAC/UF process configurations and operating procedures, which in turn significantly affect not only the overall adsorptive removal efficiency of TOrCs but also operational conditions, such as reversible as well as irreversible membrane fouling (Stoquart et al. 2012). Three different configurations of PAC/UF HMPs can be distinguished (Stoquart et al. 2012): a) HMP with PAC pre-treatment; b) HMP with PAC post-treatment, and c) HMP with integrated PAC treatment. Furthermore, differences exist with respect to the pre-treatment of the influent water by coagulants or flocculants (Sheng et al. 2016), operational filtration mode such as dead end or cross-flow, in/out or out/in-filtration modes (Ivancev-Tumbas and Hobby 2010; Rodriguez et al. 2016; Ivancev-Tumbas et al. 2018), and PAC dosing procedure such as single pulse, multi pulse or continuous dosing (Campinas and Rosa 2010), among others. Owing to longer hydraulic retention times and the associated higher efficiency of natural organic matter (NOM) and TOrC adsorption as well as better membrane fouling mitigation, the option of HMP with PAC pre-treatment by employing a carbon contact reactor with or without coagulant addition is usually preferred (Ivancev-Tumbas et al. 2008; Margot et al. 2013; Löwenberg et al. 2014; Sheng et al. 2016). In a more compact process configuration, (Ivancev-Tumbas et al. 2008) and (Ivancev-Tumbas et al. 2018) tested inline dosing of PAC into the feed line prior to the UF membrane, thus avoiding the use of a (carbon) contact reactor. These studies focused on the TOrCs removal potential (p-Nitrophenol and Diclofenac) by the tested HMP (inline dosing of PAC prior to UF). Although they observed effective removal by the applied PAC/UF HMP, possible effects on the operational stability or the mitigation of membrane fouling via additional pre-treatment (e.g. by coagulation) were neglected. Other studies, in turn, concluded mitigated membrane fouling by PAC or coagulant employment but ignored effects on TOrCs removal or possible interferences between PAC and coagulant (Yu et al. 2014). Coagulation prior to UF has already been identified as an effective pre-treatment for reducing membrane fouling (Acero et al. 2012; Sun et al. 2013) and is commonly employed in full-scale UF water treatment (Gao et al. 2011). Although reduced TMP increases can be expected by employing coagulants prior to UF, previous studies did not account for possible interactions between PAC and coagulant (Konieczny et al. 2009; Bergamasco et al. 2011; Zheng et al. 2012; Yu et al. 2013; Yan et al. 2017; Yu et al. 2019). Based thereon, it can be stated that a research gap exists with regard to an improved operation of the PAC/UF HMP by the additional application of inline dosed coagulant prior to UF. So far, the effects of inline dosed coagulant on TOrC adsorption by PAC are unclear and to date no investigations have been conducted to elucidate a possible optimum operational mode for improved TOrCs removal with concomitantly maintaining operational stability.

We hypothesize that precoating the UF membrane with a cake layer using polyaluminium chloride (PACl) as coagulant with the continuous inline dosing of PAC prior to UF achieves a significant better TOrC removal efficiency with concomitantly maintaining operational stability than an operational mode with simultaneous and continuous inline dosing of coagulant and PAC. Within the scope of this study, inline dosing of PAC with or without the addition of coagulant prior to UF was investigated at pilot-scale. The obtained results are especially important for many full-scale PAC/UF HMP applications, where compact, easy adaptable and stable operating water reclamation technologies that enable the production of reclaimed water with high quality are desired, such as for agricultural irrigation. The removal of a broad range of TOrCs representing a wide adsorption spectrum (14 different TOrCs), and the influence of various operational modes on the process stability, expressed as TMP build-up, were analyzed – aspects regarding operational stability were usually not considered within the studies that investigated the TOrCs abatement potential of the PAC/UF HMP (Ivancev-Tumbas et al. 2008; Ivancev-Tumbas and Hobby 2010; Ivancev-Tumbas et al. 2018). Additionally, the effects of polyaluminium chloride (PACl) on the TOrC removal efficiency by the PAC/UF HMP (PACl and PAC both dosed inline prior to UF) as well as on TMP development were also investigated.

7.3 Material and methods

7.3.1 Experimental setup of the PAC/UF pilot unit

The schematic set-up of the employed pilot-scale membrane unit is illustrated in Figure 7-1. The pilot unit for partial flow treatment consisted of pressure driven UF membranes (type dizzer® XL 0.9 MB 80 WT) with a total active membrane area of 80 m^2 (Polyethersulfone PES; 0.9 mm capillary diameter; 7 capillaries per Multibore®-fiber; average pore size ≈0.02 µm), mounted in a T-Rack® 3.0 and provided by inge GmbH. The UF membrane was operated at an inside-out, dead-end filtration mode with filtration cycles lasting 60 min. Owing to the hydrophilic surface characteristics of the PES membrane, decreased adsorption of organic carbon and hence reduced fouling of the membrane were expected. The feed pipes (conveying the water from the filtration tank to the UF) were made of polyvinyl chloride with an inner diameter of about 60 mm.

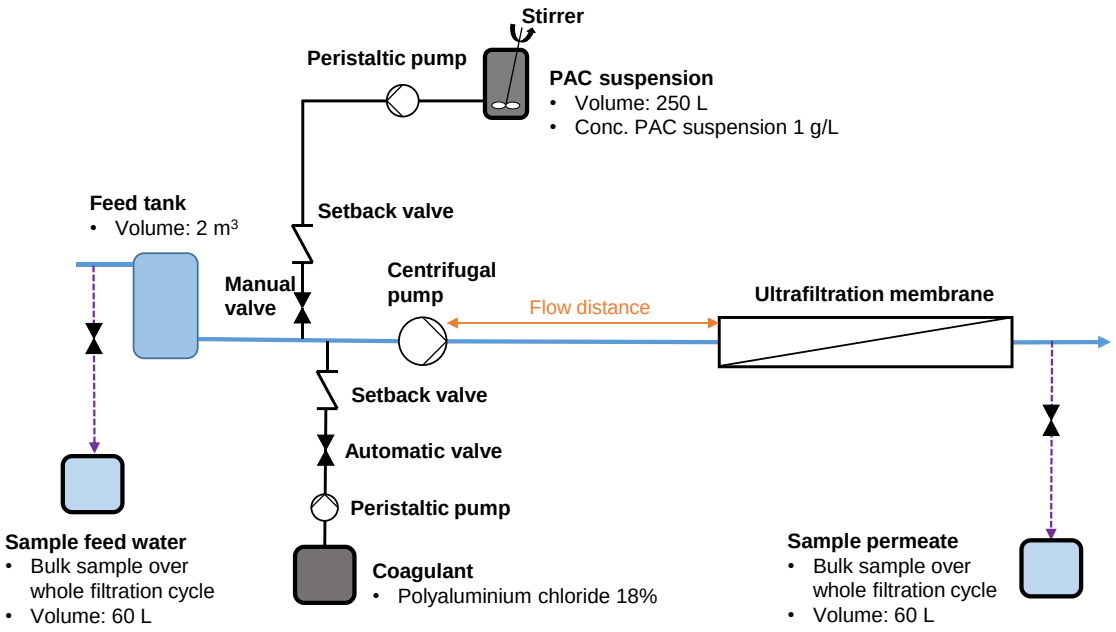

Figure 7-1: Experimental set-up of pilot-scale PAC/UF HMP. The operational modes tested with this experimental set-up are summarized in Table 7-1.

7.3.2 Process configuration and applied operational modes

Ten different process variations/operational modes were investigated (Table 7-1) with regard in both TOrC removal efficiency and process stability expressed as change (increase/decrease) of TMP at constant flux. For all operational modes, flux was kept constant at 30 L/(m^2·h) (LMH) yielding a flow of 2.4 m^3/h:

- In the mode of *'blank filtration'* the UF unit was operated without any dosing of PAC nor coagulant.
- In order to provide reference filtration cycles for comparison, filtration with continuous coagulation (*'filtration, cont. coag.*') was always performed prior to the quadruple repetition of the operational modes summarized in Table 7-1. In the mode of *'filtration, cont. coag.'* UF filtration was performed only with the continuous addition of PACl coagulant (18 % Al_2O_3) at coagulant dose of 3 mg_{Al}/L. Continuous dosing of PACl was performed throughout the whole filtration cycle which lasted for 60 min. The dosing nozzle for the addition of PACl was installed directly prior the centrifugal feed pump (Figure 7-1). Accounting for the pipe diameter of 60 mm, the applied flow of 2.4 m^3/h and the flow distance of 12 m, this resulted in a hydraulic residence time of approximately 51 seconds between the coagulant dosing location and the UF membrane.
- For the tested operational modes of *'coarse PAC 15 mg/L'*, *'coarse PAC 30 mg/L'*, *'fine PAC 15 mg/L'* and *'fine PAC 30 mg/L'*, UF filtration was conducted with continuous dosing of PAC (throughout the entire filtration cycle of 60 min), however, without any addition of coagulant. During these filtration modes either fine PAC (Chemviron PULSORB WP235 with mean particle size of 8 µm) or coarse PAC (Chemviron PULSORB WP260 with mean particle size 30 µm) was used in two different PAC doses, either 15 mg/L (*'coarse PAC 15 mg/L'*, *'fine PAC 15 mg/L'*) or 30 mg/L (*'coarse PAC 30 mg/L'*, *'fine PAC 30 mg/L'*). The dosing nozzle for the inline addition of PAC was installed directly prior to the dosing nozzle for the coagulant and thus, also directly prior to the centrifugal feed pump, with a hydraulic residence time of approximately 51 seconds.
- The filtration modes *'fine PAC 15 mg/L, cont. coag.'* as well as *'fine PAC 30 mg/L, cont. coag.'* were conducted with continuous dosing of both PAC (15 mg/L and 30 mg/L) as well as PACl as coagulant (3 mg_{Al}/L) during the entire filtration cycles.
- In contrast to that, during the filtration modes *'fine PAC 15 mg/L, precoat.'* as well as *'fine PAC 30 mg/L, precoat.'* PACl coagulant was only dosed for

the first ten minutes of the corresponding filtration cycle, while fine PAC was dosed continuously during the entire filtration cycle, at either 15 mg/L or 30 mg/L. This mode of only dosing PACl for the first ten minutes of each filtration cycle resulted in precoating of the UF membrane and in a reduction of the consumed PACl coagulant by a factor of six, thus yielding an overall PACl dose of 0.5 mg_{Al}/L instead of the 3 mg_{Al}/L.

All the operational modes listed in Table 7-1 were repeated quadruple. However, in order to provide a reference filtration, the operational mode *'filtration, cont. coag.'* (mode 2) was run ten times before each of the operational modes. By that also an efficient flushing and removal of any remaining PAC in the pipes could be ensured.

Table 7-1: Operational modes of the pilot-scale PAC/UF HMP, run with or without PACl coagulant prior to UF. CFP stands for centrifugal feed pump, FC stands for filtration cycle.

		PAC dosing procedure			**Coagulant dosing procedure**		
Mode #	**Referred to as**	**Point of PAC dosing**	**Dosing procedure PAC**	**PAC dose [mg_{PAC}/L]**	**Point of coagulant dosing**	**Dosing procedure coagulant**	**Coagulant dose [mg_{Al}/L]**
1	*blank filtration*	None	None	None	None		
2	*filtration, cont. coag.*				Directly prior CFP	Continuous, during whole FC	3
3	*coarse PAC 15 mg/L*	Directly prior CFP	Continuous, during whole FCs	15	None	None	None
4	*coarse PAC 30 mg/L*			30			
5	*fine PAC 15 mg/L*			15			
6	*fine PAC 15 mg/L, cont. coag.*				Directly prior CFP	Continuous, during whole FC	3
7	*fine PAC 15 mg/L, precoat.*					Continuous, only for first 10 min of FC → 'precoating'	0.5
8	*fine PAC 30 mg/L*			30	None	None	None
9	*fine PAC 30 mg/L, cont. coag*				Directly prior CFP	Continuous, during whole FC	3
10	*fine PAC 30 mg/L, precoat.*					Continuous, only for first 10 min of FC → 'precoating'	0.5

After each filtration cycle, hydraulic backwashing was performed by applying water from the backwash tank to the module at an outside-in mode. Backwash lasted for 45 seconds at a flux of 230 LMH. After 15 filtration cycles, chemical enhanced backwashing (CEB) was carried out by injecting and rinsing the UF for 90 seconds with alkaline NaOCl at an intake flux of 120 LMH. The UF module was then soaked for 15 min with the injected alkaline NaOCl and a final (hydraulic) backwash to rinse out the chemical at a flux of 230 LMH for 70 seconds was conducted. Immediately after the alkaline CEB, a short backwash at 70 LMH for 900 seconds with only filtrate was

conducted, and then the CEB procedure was repeated with sulphuric acid (H_2SO_4) (according to process and design guidelines of the inge® product series: dizzer® XL series modules for open platform and T-Rack® 3.0 Series).

7.3.3 Characteristics of the applied coagulant PACl solution and PAC

The obtained PACl solution (FDPAC 18, Feralco Deutschland GmbH) conformed to DIN EN 883. For the PACl solution with 18 % Al_2O_3 a density of 1.37 g/cm^3 at a temperature of 20 °C was reported and the free aluminium (Al^{3+}) mass concentration in the PACl solution was 9 %. According to (Konieczny et al. 2009) and (Yu et al. 2013), alum based coagulants show higher turbidity, total organic carbon (TOC), and UV_{254} absorbance removal efficiencies compared to iron-based coagulants. This in turn lowers the membrane fouling potential during UF treatment. To obtain a final coagulant dose of 3 mg_{Al}/L, a peristaltic pump PACl solution dosing rate of ≈60 mL/h was calculated using equation (7-1).

$$Dosing\ rate\ \left[\frac{L}{h}\right] = \frac{dose * flow}{\rho_{Solution} * C * 10^6 \frac{mg}{kg}} \quad (7\text{-}1)$$

Where:

dose	= required PACl (3 mg/L) or PAC dose (either 15 mg/L or 30 mg/L)
flow	= applied flow of filtration (2,400 L/h)
$\rho_{Solution}$	= density of PACl (1.37 kg/L) or PAC stock solution (≈1.0 kg/L)
C	= free aluminium mass concentration in the PACl solution (9 %) or mass
	= concentration of PAC in PAC stock solution (1 g/L = 0.1 %)

Two different sized PACs (Chemviron) were used in the pilot-scale study to investigate size dependent TOrC removal efficiencies and effects on process stability:

- PULSORB WP235 with a minimum iodine number of 850 mg/g, a median particle size d_{50} of 20 µm, and a mean particle diameter of 30 µm (referred to as coarse PAC).
- PULSORB WP260 with a minimum iodine number of 1,000 mg/g, a median particle size d_{50} of 6 µm, and a mean particle diameter of 8 µm (referred to as fine PAC).

More detailed characteristics of the two PACs employed for the experiments are summarized in Table 11-27. The 1 g_{PAC}/L PAC stock suspension was continuously stirred in a 250 L container and was dosed by a peristaltic pump (Figure 7-1). The dosing rates

required for achieving PAC doses of either 15 mg/L (36 L/h) or 30 mg/L (72 L/h) were determined using equation (7-1). These PAC doses were similar to those employed e.g. by Ivancev-Tumbas et al. (2018) or Acero et al. (2016) and constitute commonly applied PAC doses in full-scale advanced treatment processes of municipal wastewater by PAC adsorption (Margot et al. 2013).

7.3.4 Feed water characteristics and analytical methods

The feed water for the PAC/UF HMP was drawn from the secondary clarifier of the municipal wastewater treatment plant (WWTP) Zweckverband Klärwerk Steinhäule in Neu-Ulm, Germany. The WWTP has a total population equivalent of 440,000, treating about 40 million m^3/year of wastewater before discharging into the Danube river.

Bulk water samples from the feed water (secondary effluent) as well as the filtrate for each of the investigated filtration cycles (Table 7-1) were collected by equal and constant flow into 60 L containers (Figure 7-1). These bulk sample containers were rinsed several times with deionized water (Milli-Q®) prior to each experimental run. From these bulk samples, 500 mL grab samples were collected for the following analyses: chemical oxygen demand (COD), TOC, DOC, nitrate-nitrogen (NO_3^--N) as well as ortho-phosphate-phosphorus (PO_4^{3-}-P). Samples for TOrC analysis were collected in 20 mL amber glass bottles. Laboratory analyses for water quality parameters were carried out according to standard or established methods summarized in Table 11-28. TOrCs were measured using liquid chromatography coupled with tandem mass spectrometry (LC-MS/MS) according to Müller et al. (2017) (for a detailed description of the analytical method with corresponding limits of quantification refer to Table 11-28).

During the experimental period, the following feed water parameters were measured online on an hourly basis: pH value 7.3 ± 0.1, electrical conductivity 621 ± 147 µS/cm, temperature 19.1 ± 0.4 °C, and ultraviolet absorbance at 254 nm (UV_{254}) 8.6 ± 0.9 1/m (number of measured values for each parameter n = 120). Furthermore, based on laboratory analyses the feed water was characterized by the following quality: COD 13.4 ± 2.0 mg/L, TOC 4.8 ± 0.7 mg/L, DOC 4.0 ± 0.4 mg/L, NO_3-N 3.2 ± 1.0 mg/L as well as PO_4^{3}-P 0.5 ± 0.1 mg/L, with n = 56 each. A detailed summary of feed water quality parameters for each filtration mode (Table 7-1) can be found in Table 11-29.

7.3.5 Data analysis and visualization

The relative removal (efficiency) was calculated according to equation (7-2) (Yoon et al. 2006; Acero et al. 2012):

$$Rel.removal\ [\%] = \frac{C_f - C_P}{C_f} * 100 \qquad (7\text{-}2)$$

Where:

C_f = feed concentration (ng/L)
C_P = permeate concentration (ng/L)

To graphically illustrate the acquired data, Seaborn, a Python data visualization library based on Matplotlib was utilized. To visualize TOrC removal efficiencies, the investigated TOrCs were grouped according to their adsorbability based on the averaged removal efficiencies by the process configurations in which only PAC dosing was applied (Table 7-1, modes #3, #4, #5, #8). TOrCs with relative removals of >80 %, 50–80 % and <50 % were classified as well adsorbable, medium adsorbable and poorly adsorbable (Table 7-2) and confirmed findings of previous studies (Snyder et al. 2007; Acero et al. 2012; Margot et al. 2013; Altmann et al. 2014; 2016; Jekel et al. 2015; Ziska et al. 2016; Jeirani et al. 2017). TOrCs with measured concentrations below the limit of quantification were excluded from further considerations.

Table 7-2: Adsorbability of investigated TOrCs on activated carbon according to their average removal efficiencies by PAC/UF HMP configurations, where only PAC dosing was applied, with a PAC contact time of ≈51 seconds (Table 7-1, modes #3, #4, #5, #8).

Name of TOrC	**Substance group**	**Classification of TOrCs by relative adsorbability**	**Average TOrC removal efficiencies achieved by dosing only PAC [%]**
Carbamazepine	Pharmaceutical residuals	Good (>80 % average removal by dosing only PAC)	86
Metoprolol			92
Tramadol			85
Trimethoprim			93
Venlafaxine			83
Benzotriazole	Corrosion inhibitor		84
4-Formylaminoantipyrine	Pharmaceutical residuals	Medium (50–80 % average removal by dosing only PAC)	65
Citalopram			79
Diclofenac			74
Iopromide			57
Primidone			66
Sulfamethoxazole			62
Valsartanic acid			52
Gabapentin	Pharmaceutical residuals	Poor (<50 % average removal by dosing only PAC)	19

Operational stability is usually described by a change of TMP at constant flux or a decrease/increase of the flux or permeability at constant TMP (Snoeyink et al. 2000; Stoquart et al. 2012). Within this study flux was kept constant, hence the built-up TMP served as measure for operational stability. The parameters for the trendlines of the TMP measurements (intercepts with y-axis and slopes) were determined by using the 'linregress-function' in Python. This function calculated the linear least-squares regression for two sets of measurements. To quantify the difference of the slope or intercept of the TMP trendline (with y-axis) of a tested operational mode in comparison to the corresponding reference filtration (cf. Table 7-1), equation (7-3) was applied:

$$Rel.difference\ [\%] = \frac{X_{tested} - X_{ref}}{X_{ref}} * 100\ [\%] \quad (7\text{-}3)$$

Where:

Xtested = slope or intercept of trendline of the tested operational mode
Xref = slope or intercept of the trendline of the reference filtration

7.4 Results and discussion

7.4.1 Removal efficiencies of TOrCs

This study investigated ten different operational modes of PAC/UF HMP to determine TOrC removal efficiencies. Removal results are presented in Figure 2 as box plots for the TOrCs grouped according to their adsorbability (Table 7-2).

During '*blank filtration*' as well as during '*filtration, cont. coag.*' only negligible effects on the retention of TOrCs (arithmetic mean of relative removal ≈0 %, cf. Figure 7-2) were observed. This was expected since during these two operational modes no PAC which would represent the adsorptive treatment process was applied and given the UFs' pore size of ≈0.02 µm, neither the UF nor UF in combination with coagulant dosing constituted efficient removal processes for TOrCs. This is in line with the results of Yoon et al. (2006; 2007), who also observed no significant abatement of carbamazepine, sulfamethoxazole, diclofenac or iopromide by UF membranes.

All the operational modes with PAC dosing showed significant but varied TOrC removal. When applying the same concentration of PAC, fine PAC performed much better than coarse PAC in regards to TOrC removal. This could be especially attributed to the faster adsorption kinetics using fine PAC (Worch 2012; Bonvin et al. 2016). Given the premise of same PAC grain size, dosing of higher concentrations of PAC (30 mg/L compared to 15 mg/L) resulted in a higher TOrC removal – this was also observed in previous studies (Ivancev-Tumbas et al. 2018).

It is worth noting that the coagulant dosing procedure (continuously during the entire filtration cycle vs. precoating) resulted in significant differences in TOrC removal by the PAC (Figure 7-2, Figure 11-21). The operational mode '*fine PAC 15 mg/L, cont. coag.*' (coagulant dosed during whole filtration cycle) performed significantly worse compared to the operational mode '*fine PAC 15 mg/L, precoat.*' (coagulant dosed only during the first 10 minutes of the filtration cycle to achieve precoating). The same can be stated for the corresponding operational modes but with a higher PAC concentration ('*fine PAC 30 mg/L, cont. coag.*' and '*fine PAC 30 mg/L, precoat.*'). This may be explained by the interactions between the PAC and the coagulant interfering with the adsorptive removal capacity of the PAC. Coagulant dosing might cause the PAC to be incorporated in the formed flocs (Altmann et al. 2015) resulting in larger carbon-coagulant agglomerates and consequently in a decreased specific surface area available for adsorption and a hindered mass transfer towards the PAC. Pan et al. (2016) came to a similar conclusion concerning the effect of agglomeration on the adsorptive removal potential by PAC, namely: the stronger the agglomeration phenomena of PAC, the lower the PAC adsorptive removal of 2-methylisoborneol was. Larger particles also tend to deposit after a longer flow distance from the membranes' capillary inlet than smaller particles. Therefore, particles with diameters larger than the so-called 'plug forming diameter' will be transported to the dead-end of the capillary (Panglisch and Gimbel 2004). Accordingly, this would prevent the PAC particles from forming a homogenous cake-layer on the capillary surface, which would otherwise present an additional layer for adsorption of TOrCs (Panglisch 2001; Lerch 2008; Ivancev-Tumbas and Hobby 2010). By reducing the coagulant dosing time, e.g. by only precoating the UF instead of continuously dosing the coagulant, this adverse effect might be attenuated.

Consequently, the best reduction of TOrCs could be achieved by precoating the UF membrane with PACl and continuously dosing PAC. For the operational mode '*fine PAC 15 mg/L, precoat.*' arithmetic mean removals were 11 %, 53 % or 77 % for poorly, medium or well adsorbable TOrCs, respectively. In contrast, by applying the operational mode '*fine PAC 30 mg/L, precoat.'* even higher TOrC removal rates could be achieved, namely 33 %, 84 % or 93 % for poorly, medium or well adsorbable TOrCs, respectively (Figure 7-2). In particular, the operational mode '*fine PAC 30 mg/L, precoat.'* was capable of reducing the TOrC concentrations to levels similar to or even lower than the typical TOrC concentrations in water resources that are commonly used for irrigation purposes (e.g. rivers). For instance, results reported by Fleig et al. (2015) and Schüßler (2017) revealed concentrations for various TOrCs being present in water from the river Main (Germany) in concentrations nearly consistently higher than those that were measured in the filtrate of the HMP process '*fine PAC 30 mg/L, precoat.'* (Table 7-3, for a comprehensive summary of the absolute concentrations of TOrCs in the feed and the

permeate water refer to Table 11-30). This comparison highlighted the promising potential of the PAC/UF HMP with coagulant-precoating prior to UF for the generation of a water quality that is better than some of the conventionally used water resources such as impaired river water. However, compounds with poor adsorbability such as gabapentin might require an additional treatment step to sufficiently reduce their concentrations. This compound showed only negligible attenuation for all operational modes (Figure 7-2 and Table 7-3).

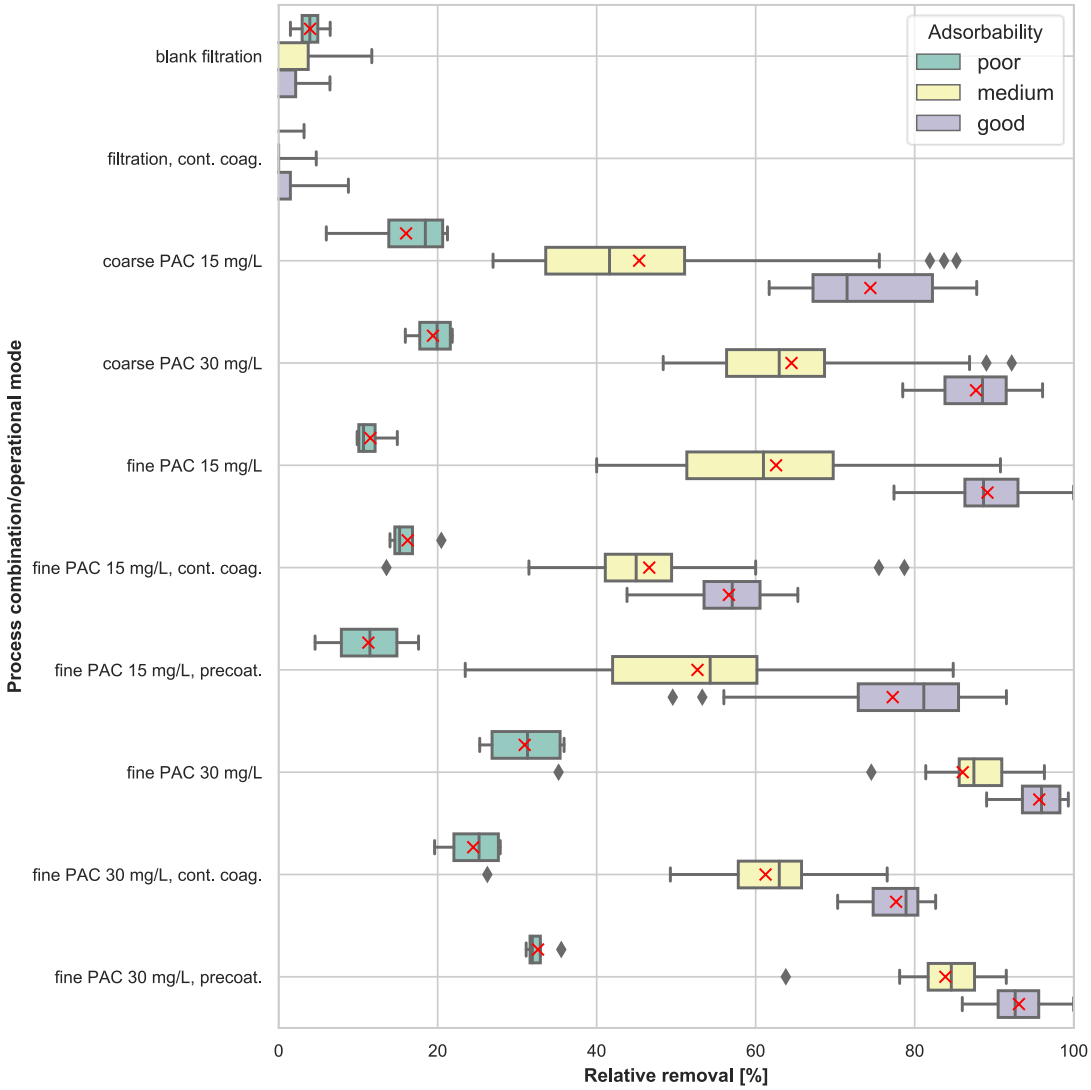

Figure 7-2: Box plots of relative removal efficiencies of TOrCs by operational modes (Table 7-1) of the PAC/UF HMP tested in pilot-scale. TOrCs that were removed by >80 %, 50–80 % and <50 % by the process configurations in which only PAC dosing was applied (Table 7-1, modes #3, #4, #5, #8) were classified as well adsorbable, medium adsorbable and poorly adsorbable (Table 7-2). Each box shows the 25 %- and 75 %-quantiles of the dataset, while the whiskers extend to show the rest of the distribution, except for points that are determined to be 'outliers' using the method that is a function of the 1.5 inter-quartile range. The median is indicated by the vertical line within the box and the arithmetic mean is represented by the red cross.

Table 7-3: Absolute arithmetic mean concentrations and corresponding standard deviations (Std) of TOrCs in feed water and permeate/filtrate water for the PAC/UF HMP operational mode '*fine PAC 30 mg/L, precoat.*' (number of analyzed samples n = 4) compared with arithmetic mean concentrations of corresponding TOrCs in water from Main river in Germany (Fleig et al. 2015; Schüßler 2017). Concentrations below the limit of quantification (LOQ) are preceded by '<'. The respective LOQs are given within Table 11-28.

Name of TOrC	Feed water [ng/L]		Permeate/filtrate water [ng/L]		Main River [ng/L]
	Mean	Std	Mean	Std	Mean
4-Formylaminoantipyrine	788	136	104	22	300
Benzotriazole	2,446	136	251	62	700
Carbamazepine	106	7	<5	<5	90
Citalopram	59	3	11	7	8
Diclofenac	423	32	63	14	52
Gabapentin	895	186	604	132	400
Iopromide	1,500	543	244	144	250
Metoprolol	98	18	6	<3	80
Primidone	66	9	<25	<25	20
Sulfamethoxazole	124	15	19	<5	45
Tramadol	61	5	<5	<5	70
Trimethoprim	48	2	<5	<5	-
Valsartan acid	381	19	73	12	83
Venlafaxine	111	7	11	3	36

7.4.2 Effects on operational stability

The influence of the tested operational modes (Table 7-1) on the process stability, measured by change of the TMP, are illustrated in Figure 7-3. According to the 1st panel in Figure 7-3, the operational mode '*blank filtration*' caused an offset of the TMP line (compared with TMP of the '*reference filtration*'). This could be attributed to a reduced hydraulic backwash efficiency for this specific operational mode compared to the reference filtration. This assumption was confirmed by a progressive increase of the respective starting points of the TMP for each of the four consecutive filtration runs that were performed for this specific operational mode (Figure 7-4). Obviously, the missing coagulation for the operational mode '*blank filtration*' deteriorated the hydraulic backwash efficiency by causing hydraulic irreversible fouling of the membrane (Nguyen et al. 2011). Amy and Cho (1999) and Yuan and Zydney (2000) already identified NOM, a complex mixture of particulate organic matter and dissolved organic matter, as a very high potential foulant. In order to attenuate the associated membrane fouling, other studies highlighted the importance of an improved NOM removal by coagulation (Carroll et al. 2000; Park et al. 2002; Kim et al. 2006; Long et al. 2021) . In contrast to the observed increase of the TMP at the starting point of the operational mode '*blank filtration*', the slope of the trendline of the TMP development was comparable to the slope of the corresponding reference filtration. The slopes of the trendlines represent the increase of

the cake layer resistance owing to its growing thickness, according to van den Berg and Smolders (1990). Hence, the increases of cake layer resistances during both operational modes ('*blank filtration*', '*reference filtration*') were comparable.

In the 2nd panel in Figure 7-3, the compared processes were completely the same – the four filtration cycles operated in *'filtration, cont. coag.'* were compared with the previous ten filtration cycles operated in the same mode. Based on the fact that the two curves were almost congruent, it could be deduced that these two operational modes showed neither significant differences with regard to the slope, nor with respect to the offset of the respective TMP regression lines. This in turn confirmed the validity of the approach of comparing any operational mode in a four-time repetition with the previous ten filtration modes operated as reference filtration in the mode *'filtration, cont. coag.'*. Since no increase of the starting points of the TMP could be observed for the four consecutive filtration cycles which were run in this operational mode (Figure 7-4), it was further inferred that the performance of the membrane could be efficiently recovered by hydraulic backwashing (which was carried out after each filtration cycle). This effect of an enhanced hydraulic backwash efficiency through the application of coagulation was already stated by Galjaard et al. (2001).

According to the panels 6, 7, 9 and 10 (Figure 7-3) the offset of the TMPs at the start of the corresponding filtration cycles with coagulation in combination with continuous PAC dosing were similar to that of the reference filtration. This was regardless of whether the coagulant was dosed continuously during the entire filtration cycle (panel 6: '*fine PAC 15 mg/L, cont. coag.*' and panel 9: '*fine PAC 30 mg/L, cont. coag.*') or the coagulant was dosed just within the first 10 min for precoating (panel 7: '*fine PAC 15 mg/L, precoat.*' and panel 10: '*fine PAC 30 mg/L, precoat.*'). This could again be attributed to more or less equal TMP starting points of each of the filtration cycles within the corresponding operational mode (Figure 7-4). In turn, the formation of micro-flocs and the associated overall reduced organic fouling induced by coagulation (Carroll et al. 2000; Kim et al. 2006; Howe and Clark 2006; Huang et al. 2011; Long et al. 2021) apparently guaranteed an efficient hydraulic backwash (Galjaard et al. 2001). Based on these observations, it can be concluded that by only precoating the UF with PACl ensured a comparable backwash efficiency to the continuous dosing of PACl, despite the fact that during the precoating mode only a sixth of the PACl coagulant dose was applied (PACl dose of 0.5 mg_{Al}/L instead of 3 mg_{Al}/L for continuous PACl dosing).

In contrast, for the operational modes with PAC but without coagulant addition (panels 3, 4, 5, 8, cf. Figure 7-3), clear offsets of the TMP were typical at the beginning of the corresponding filtration cycles, indicating organic fouling which could not be efficiently removed by the subsequent hydraulic backwashing (Figure 7-4).

The two different procedures of dosing the coagulant showed interesting effects with respect to the slope of the TMP regression lines (panels 6, 7 and 9 and 10 in Figure 7-3). As already mentioned, the slopes of the trendlines basically represent the increase of the cake layer resistance owing to its growing thickness according to van den Berg and Smolders (1990). The procedures of continuous coagulant dosing during the entire filtration cycles (panel 6, 9) resulted in a more or less unchanged (panel 6) or even slightly increased (panel 9) slope of the TMP. In contrast, the employment of precoating during the first 10 minutes (panel 7 and 10) resulted in the slight but significant reduction of the slope of the TMP (no overlapping of the respective confidence intervals of 95 %, cf. Figure 7-3). The TMPs of the individual consecutive filtration cycles of these two operational modes also exhibited stable, consistent and comparable trends (Figure 7-4, panel 7 and 10). The developments of the individual TMPs of the filtration cycles within one operational mode were nearly congruent and a reliable repeatability of the effect of this operational mode on the operational stability could be observed (Figure 7-4). By precoating, an incompressible, permeable and removable cake layer (by hydraulic and chemical backwashing) on the membrane surface was formed (Galjaard et al. 2001). Owing to the incompressibility of the formed cake layer, it was likely characterized by a lower resistance (Lee et al. 2000; Kennedy et al. 2003; Howe and Clark 2006; Huang et al. 2011). Dosing of PAC within the precoating operational modes (Figure 7-4, panel 7: '*fine PAC 15 mg/L, precoat.*' and panel 10: '*fine PAC 30 mg/L, precoat.*') might have led to a further reduced fouling and hydraulic cake layer resistance during each of the corresponding filtration cycles, which would explain the decreased overall development of the slope of the TMP (Figure 7-3, panel 7 and 10). In particular, the higher adsorptive removal potential of the PAC during the precoating process (cf. section 7.4.1) might have better attenuated membrane fouling than the process where PACl and PAC were continuously employed. Adsorption, especially of a DOC fraction with high fouling potential onto the PAC covering the precoated cake layer is an important mechanism in membrane fouling mitigation. Findings by Jucker and Clark (1994) and Yuan and Zydney (2000) already revealed that a specific DOC fraction, especially humic acids, is a major factor during fouling. According to Altmann et al. (2014) and Zietzschmann et al. (2014), PAC is capable of efficiently removing a broad range of these DOC fractions. Measurements of the removal of DOC and UV_{254} affirmed this assessment (Figure 7-5): the experiments where only PAC was dosed without coagulation (*'coarse PAC 15 mg/L', 'coarse PAC 30 mg/L', 'fine PAC 15 mg/L', 'fine PAC 30 mg/L'*), could be characterized by efficient removal of the aforementioned parameters (DOC and UV_{254}). In particular, smaller organic matter molecules which constitute crucial foulants adsorb quickly to PAC (Amy and Cho 1999; Yuan and Zydney 2000). Moreover, Sun et al. (2013) and Sun et al. (2017) reported mitigated flux declines by coating the membrane with hydrophilic substances such as PAC.

In summary, precoating of the membrane initially with coagulant and subsequently coating with PAC had an especially beneficial effect on membrane fouling, since in addition to forming an incompressible cake layer with an overall lower hydraulic resistance, the adsorption of organic matter molecules to the PAC further reduced the membrane fouling potential of the feed water.

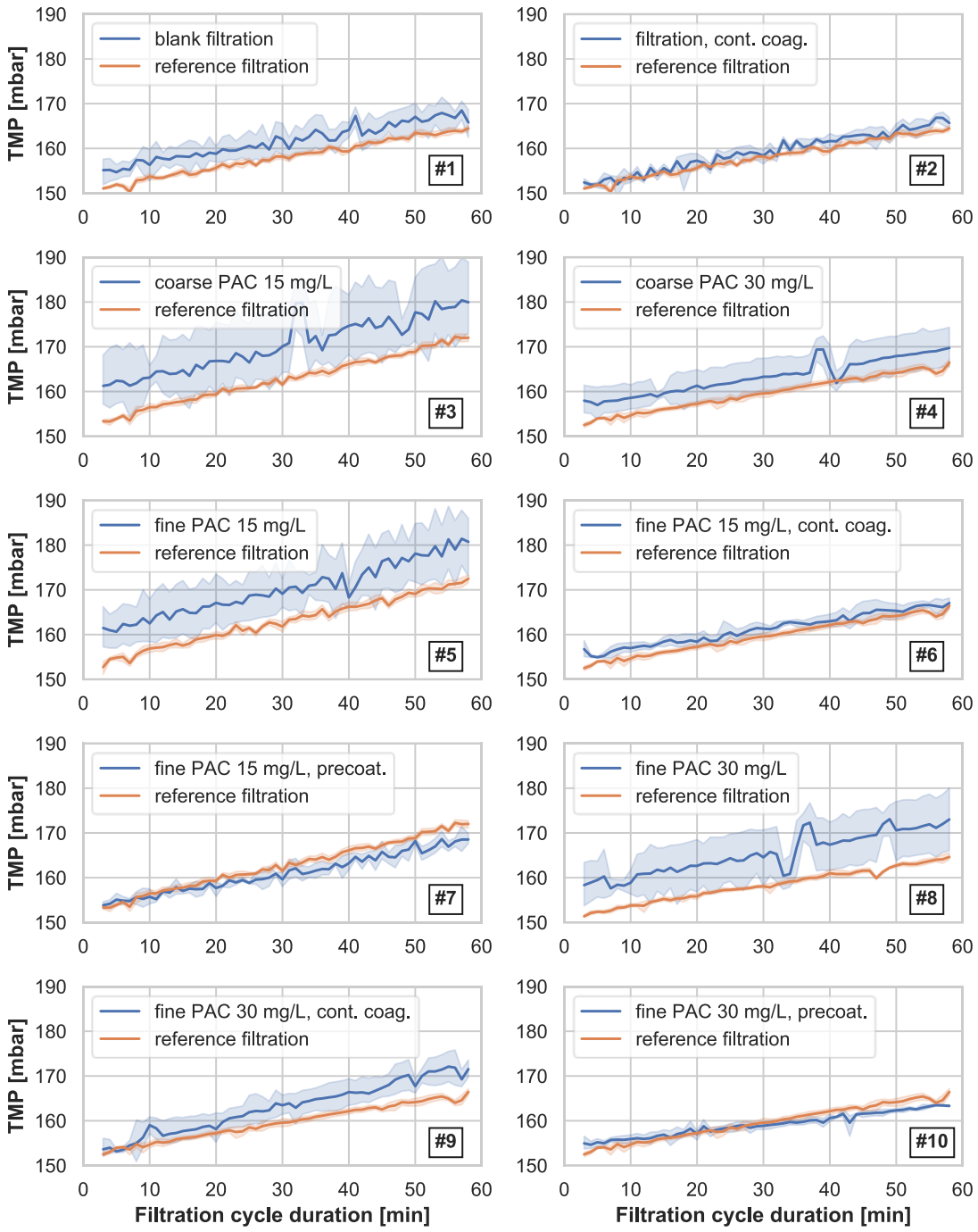

Figure 7-3: TMP developments during operational modes of PAC/UF HMPs tested in pilot-scale, compared with TMP developments of the corresponding reference filtrations. The confidence interval of 95 % is indicated by the pale-colored area along each line: Each filtration mode was repeated quadruple (n = 4), while the corresponding reference filtration process comprised 10 runs (n = 10).

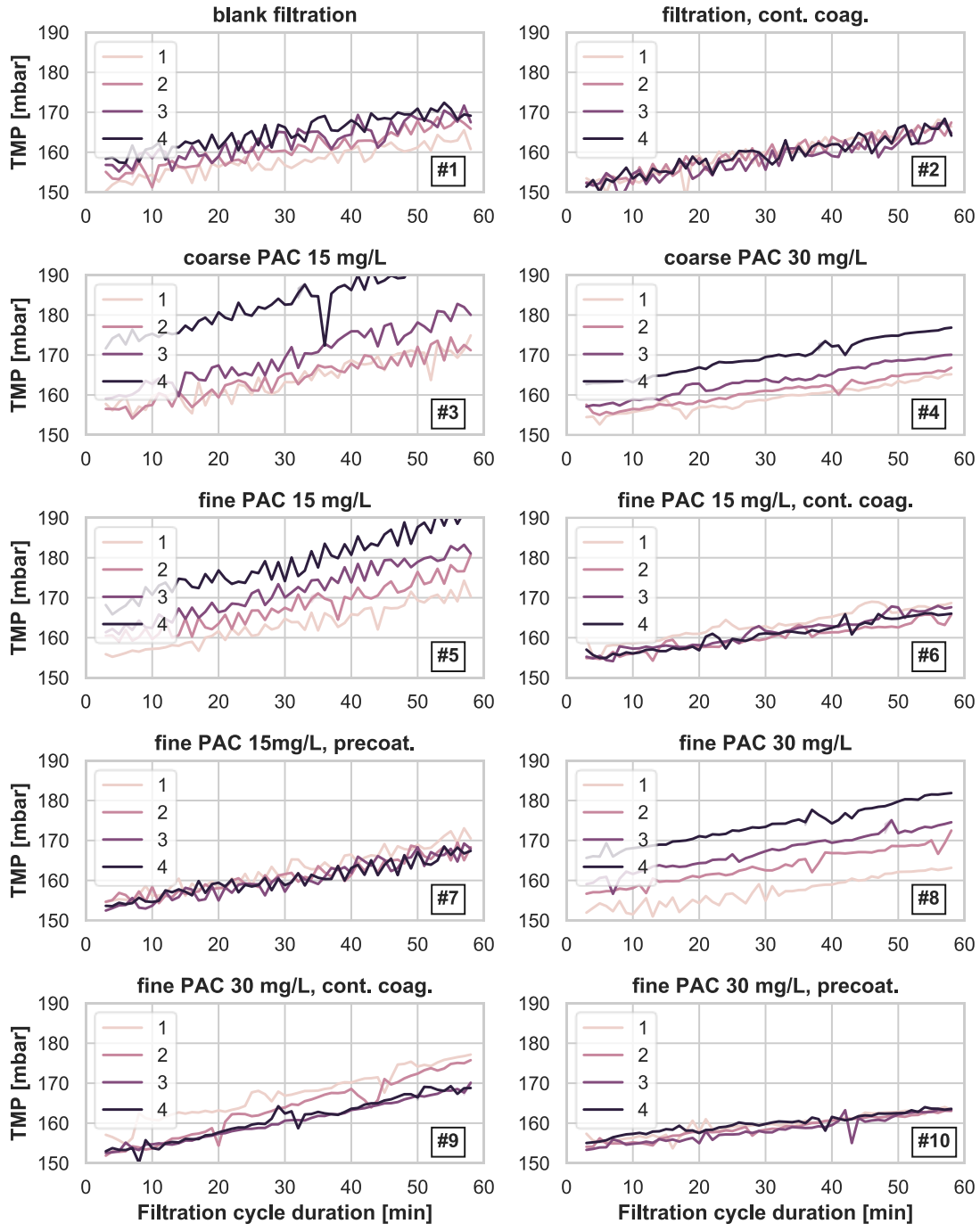

Figure 7-4: TMP developments for each filtration cycle of the respective operational modes of PAC/UF HMPs tested in pilot-scale. The numbers 1, 2, 3, 4 in the legend stand for the individual test runs/filtration cycle in chronological order (quadruple repetition of each tested operational mode, cf. section 7.3.1).

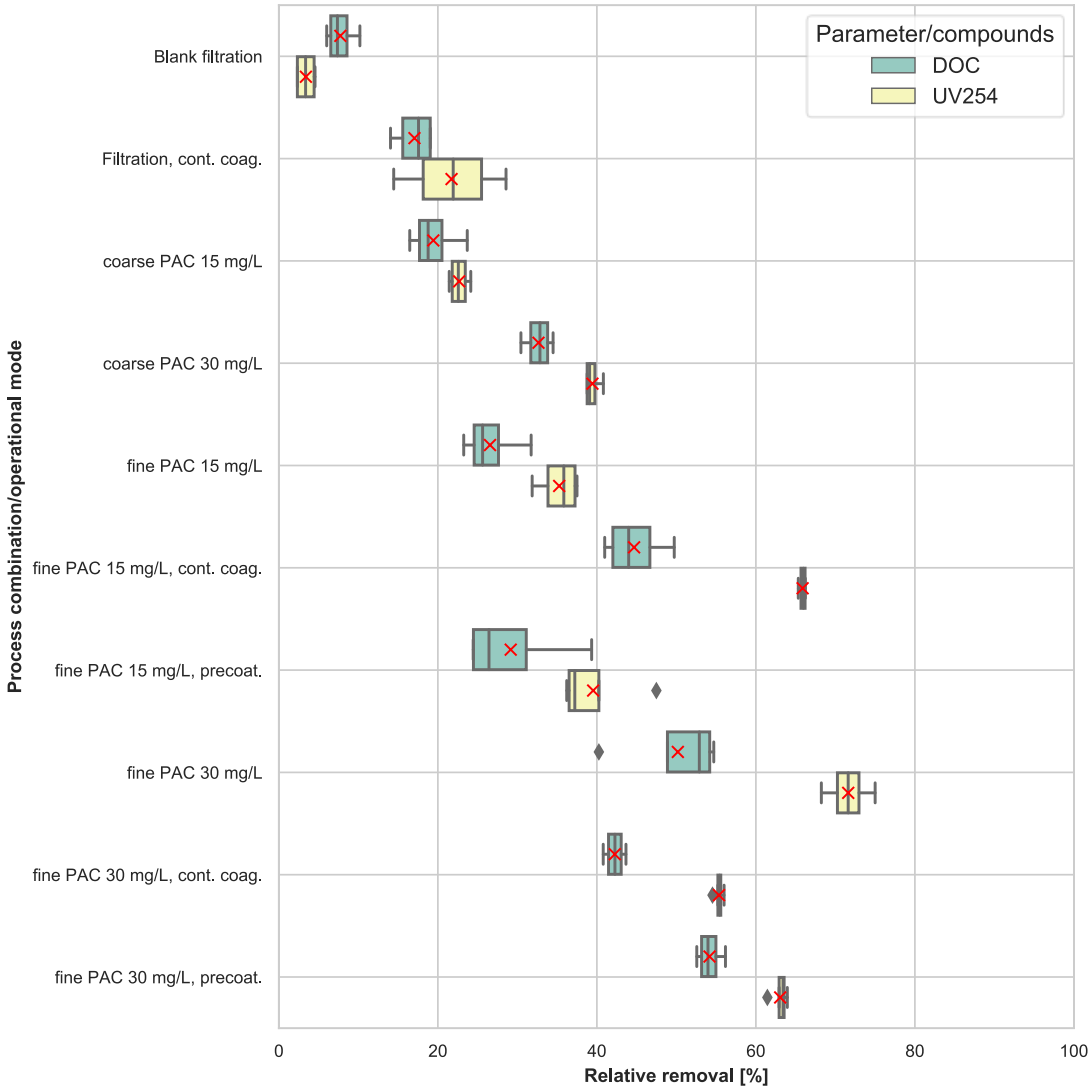

Figure 7-5: Relative removal efficiencies by applied operational modes of PAC/UF HMP (Table 7-1) for the parameters/compounds UV_{245} and DOC. Each box shows the 25 %- and 75 %-quantiles of the dataset while the whiskers extend to show the rest of the distribution, except for points that are determined to be 'outliers' using the method that is a function of the 1.5 inter-quartile range. The median is indicated by the vertical line within the box and the arithmetic mean is represented by the red cross.

7.4.3 Optimal operational mode with regard to TOrC removal and process stability

To identify a possible optimal configuration of the PAC/UF HMP with or without coagulation with respect to both, the maximum TOrC removal and the best membrane fouling mitigation, the acquired results were visualized in scatterplots with error bars (Figure 7-6). The following parameters were compared with each other: the relative removal efficiency of all analyzed TOrCs regardless of their respective adsorbability (Table 7-2); the relative difference between the intercepts (with y-axis) of the TMP trendlines of the tested operational modes and their corresponding reference filtrations; and the relative difference between the slopes of the trendlines of the tested operational modes and their corresponding reference filtrations.

The relative differences between the intercepts of the TMP trendlines of the tested operational modes and their corresponding reference filtrations represented the differences between the hydraulic backwash efficiencies. The lower this difference, the closer the hydraulic backwash efficiency of the tested operational mode was to the hydraulic backwash efficiency of the reference filtration. According to the results shown in Figure 7-3, it can be assumed that by the reference filtrations the optimal backwash efficiency could be guaranteed (TMP trendlines of reference filtrations consistently showed lowest starting points/intercepts with y-axis). Hence, the lower the relative difference between the intercepts of the tested/reference filtration, the better the hydraulic backwash efficiency for the respective operational mode was.

The relative differences between the slopes of the TMP trendlines of the tested operational modes and their corresponding reference filtrations constituted the differences between the cake layer resistances as well as membrane fouling during a filtration cycle (section 7.4.2). The lower the relative difference between the slopes of the tested/reference filtrations, the closer membrane fouling and/or the hydraulic resistance of the cake layer formed during the respective operational mode was to that of the reference filtration. From a negative relative difference between the slopes of the tested/reference filtrations, a reduced membrane fouling and/or cake layer resistance of the corresponding operational mode compared to the reference filtration could be inferred.

Based on the previous explanations, the operational modes where precoating of the membrane with coagulant combined with PAC dosing was applied (#7 = '*fine PAC 15 mg/L, precoat.*' and #10 = '*fine PAC 30 mg/L, precoat.*') represented the most promising option with regard to both optimized removal efficiency of TOrCs (Figure 7-6, panels 'a' and 'c') as well as the reduction of TMP owing to the lowest cake layer

resistance (expressed as relative difference between the slopes of the TMP trendlines, cf. Figure 7-6, panels ‘a’ and ‘b’) and maintaining the optimal hydraulic backwash efficiency after each filtration cycle (expressed as relative differences between the intercepts of the TMP trendlines, cf. Figure 7-6, panels ‘b’ and ‘c’).

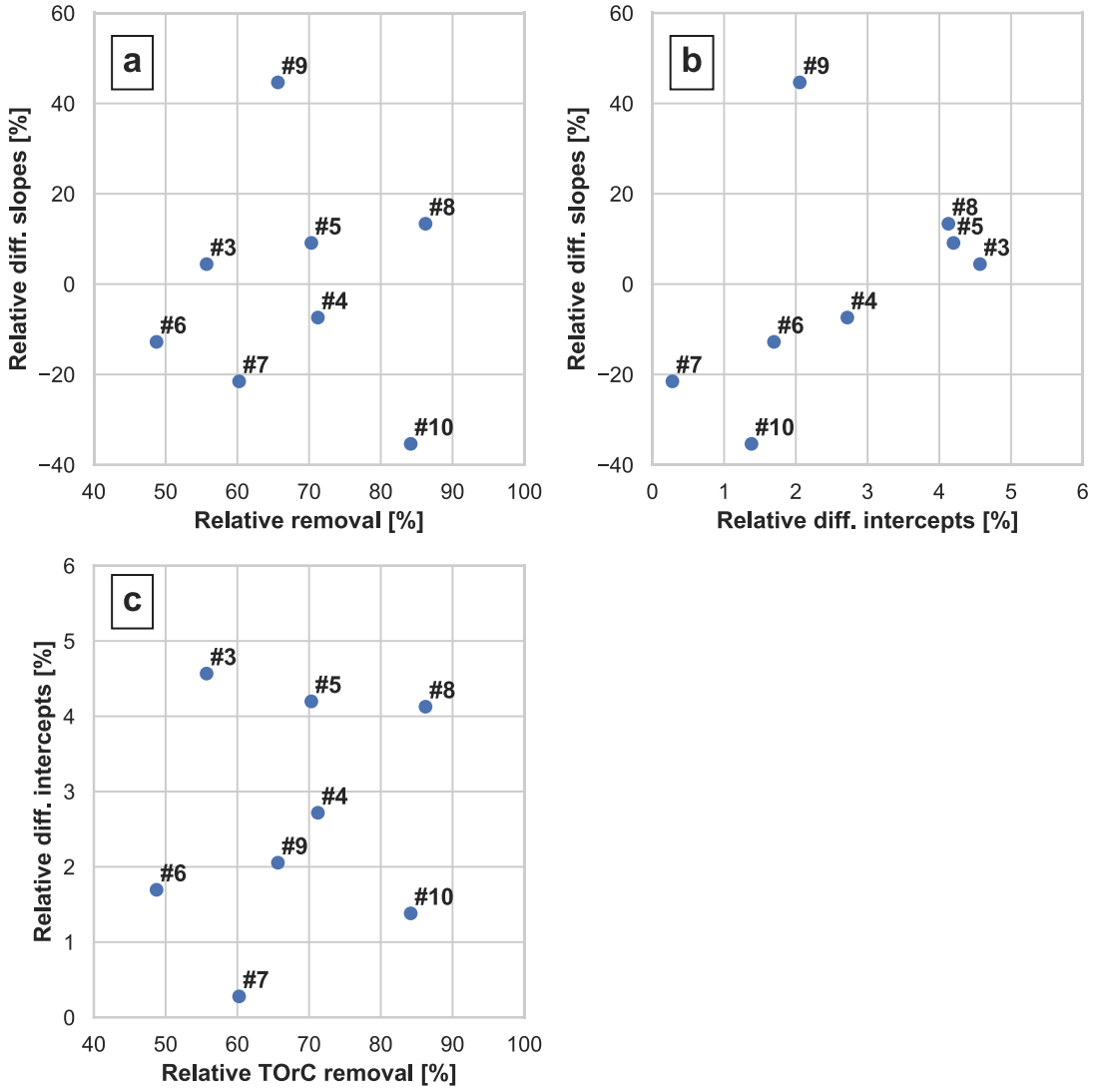

Figure 7-6: Scatter plots of relative removal efficiencies of all analyzed TOrCs (regardless of their respective adsorbability, cf. Table 7-2), relative differences between the slopes as well as the intercepts (with y-axis) of the TMP trendlines (n = 4) of the tested operational modes and their corresponding reference filtrations (n = 10). The numbers stand for the tested operational modes (cf. Table 7-1, Mode #): **#1** = *‘blank filtration’*, **#2** = *‘filtration, cont. coag.’*, **#3** = *‘coarse PAC 15 mg/L’*, **#4** = *‘coarse PAC 30 mg/L’*, **#5** = *‘fine PAC 15 mg/L’*, **#6** = *‘fine PAC 15 mg/L, cont. coag.’*, **#7** = *‘fine PAC 15 mg/L, precoat.’*, **#8** = *‘fine PAC 30 mg/L’*, **#9** = *‘fine PAC 30 mg/L, cont. coag.’*, **#10** = *‘fine PAC 30 mg/L, precoat.’*

7.5 Conclusion

Previous studies in the field of PAC/UF HMP research have not yet comprehensively addressed the possible interactions of inline dosed PAC and coagulant with respect to TOrC removal efficiency and operational stability. Hence, ten different operational modes, including: a) UF with or without addition of coagulant (PACl) prior to UF treatment, b) UF only with inline dosing of PAC prior to the membrane, c) UF with continuous inline PAC and coagulant dosing, and d) precoating of the UF with coagulant with continuous inline PAC dosing, were investigated at pilot-scale in order to cover these so far unaddressed aspects. In general, the results presented within this study highlighted the potential of one specific configuration of the compact PAC/UF HMP to efficiently remove a broad range of TOrCs while simultaneously maintaining operational stability. However, significant differences existed between each of the tested operational modes with regard to TOrC removal efficiency as well as effects on TMP built-up. The key findings and conclusions of this study are:

- When using similar PAC doses, fine PAC (≈8 µm) removed TOrCs significantly better than coarse PAC (≈30 µm), especially because of the associated faster adsorption kinetics.
- Given the premise that the same size PAC is dosed, PAC dosing of 30 mg_{PAC}/L resulted in significantly higher TOrC removal than PAC dosing of 15 mg_{PAC}/L.
- The simultaneous and continuous inline dosing of PACl coagulant and PAC prior to the UF is clearly not recommended because of its detrimental effects on TOrC removal efficiency. This was mainly attributed to the incorporation of the PAC in the formed flocs, resulting in lower adsorptive capacity of the PAC as well as to the transportation of the formed larger flocs to the dead-end of the UF capillaries.
- In contrast to the TOrC removal efficiency, operational stability was not negatively impacted by the combination of coagulation and PAC inline dosing. Apparently, the hydraulic backwash efficiency for all operational modes where PACl coagulant was dosed could be maintained regardless of how the PACl was applied (precoating or continuously) and regardless of whether PAC was employed or not. On the other hand, when no coagulation was applied, hydraulic backwash efficiency was adversely affected.
- As a consequence of the previous observation, namely that precoating showed comparable performance in maintaining the hydraulic backwash efficiency as the continuous PACl dosing procedure, it can be further

inferred that dosing time and thus overall PACl dose can be reduced without impairing the operational stability.

- Most importantly, the findings revealed that the operational modes where precoating with coagulant was carried out with continuous inline dosing of PAC prior to UF had particularly beneficial effects on the operational stability as well as the reduction of TOrCs. Besides guaranteeing a high hydraulic backwash efficiency, this specific operational mode slightly but significantly attenuated membrane fouling and the hydraulic resistance of the cake layer formed during the filtration cycles. Consequently, for this option, both reduced operational expenditures due to lower consumption of coagulant and also a higher operational stability and better water quality in terms of TOrCs can be expected. In general, this specific PAC/UF HMP might constitute a viable technology for the production of high-quality water sufficient for various water reuse practices, which is easy to adapt to various environmental conditions.

7.6 Acknowledgements

This work was funded by the Government of Lower Franconia (RUF), Germany, which we are particularly grateful for (grant number: AZ: 52-4429-10). Moreover, we acknowledge the permission to use the pressure driven UF membrane pilot unit provided by inge GmbH. Furthermore, we would like to express our gratitude to Chemviron Carbon for the donation of the powdered activated carbon (PULSORB WP235 and PULSORB WP260). Finally, we thank our colleague Veronika Zhiteneva for the extensive English proofreading of this manuscript.

8 CFD SIMULATIONS OF FLOW FIELDS DURING ULTRAFILTRATION: EFFECTS OF HYDRODYNAMIC STRAIN RATES WITH AND WITHOUT A PARTICLE CAKE LAYER ON THE PERMEATION OF MOBILE GENETIC ELEMENTS

The following chapter presents investigations related to ***research hypothesis #5***: *The formation of a PAC particle layer will act like a funnel, thereby increasing the distance over which flow accelerates prior to entering the UF pore and hence decreasing the fluid strain rate, which would result in less deformation of MGEs and therefore less permeation through the UF membrane.*

This chapter has been published with some editorial changes as follows:

Schwaller, Christoph; Fokkens, Kevin; Helmreich, Brigitte; Drewes, Jörg E. (2022): CFD simulations of flow fields during ultrafiltration: Effects of hydrodynamic strain rates with and without a particle cake layer on the permeation of mobile genetic elements. In Chemical Engineering Science 254, p. 117606. DOI: https://doi.org/10.1016/j.ces.2022.117606

Author contributions: Christoph Schwaller developed the research objective, acquired the required data for the CFD simulation and implemented a first version of the CFD simulation within COMSOL Multiphysics Version 5.4. Kevin Fokkens implemented the comprehensive CFD simulation. Kevin Fokkens and Christoph Schwaller analyzed the data and wrote the manuscript. Jörg E. Drewes and Brigitte Helmreich supervised the study and reviewed the manuscript. All authors approved the final version of the manuscript.

8.1 Abstract

Membrane ultrafiltration (UF) combined with inline dosing of powdered activated carbon (PAC) are popular hybrid processes for water reclamation. However, hydrodynamic forces can allow mobile genetic elements (MGEs) that are larger than the membrane pore size to penetrate through UF membranes. The flow fields in the feed channel of a dead-end UF membrane module were modelled using computational fluid dynamics (CFD) in order to analyze shear and elongational strain rates and associated potential hydrodynamic effects by a PAC particle layer on MGE retention. The most significant magnitudes of strain rates occurred within a distance of tens of nanometers from the membrane surface, meaning that this is where significant deformation of MGEs occurs. Since flow fields were not considerably altered at the membrane surface, the presence of the PAC particle layer was expected to have a negligible impact on the permeation of MGEs through UF membrane pores.

Keywords: Nanoscale CFD simulation; hydrodynamic strain rates; mobile genetic elements deformation; PAC particle cake layer

8.2 Introduction

Water reclamation and reuse for agricultural, industrial, or even potable use represent a promising approach to combat water scarcity (Water Reuse Europe 2018; Drewes and Khan 2011; National Research Council 2012). As reuse applications become more widespread, it is important to assess the risks associated with water reuse (Drewes and Khan 2011). One such risk which is often overlooked is the potential of spreading antimicrobial resistance (AMR) through antibiotic resistant bacteria (ARB) or antimicrobial resistance genes (ARGs) (Bürgmann et al. 2018). The World Health Organization has already identified the spreading of AMR as a growing public health concern (WHO 2014, 2015, 2020).

Wastewater treatment plant (WWTP) effluents have been recognized as significant sources of AMR with substantial dissemination of ARB as well as ARGs to the receiving aquatic environment (Kumar and Pal 2018). In the environment ARGs are present either as intracellular (iARG) or extracellular (eARG) fractions of DNA (Zarei-Baygi and Smith 2021). Due to frequencies of natural transformation of eARGs comparable to conjugation frequencies of iARGs, the high adsorption potential of eARGs to particulate matter and their associated higher persistence compared to iARGs, eARGs play a crucial role in the spread of AMR (Zarei-Baygi and Smith 2021). Both plasmids as well as phages represent relevant mobile genetic elements (MGEs) enabling the acquisition, maintenance, and spread of eARGs in the environment (Matsui et al. 2001; Matsui et al. 2003; Calero-Cáceres et al. 2019).

Since ARGs are not efficiently removed or inactivated through conventional biological wastewater treatment (Bürgmann et al. 2018; Hembach et al. 2019), UF can be applied downstream to provide a barrier against ARGs, which are removed by means of size exclusion and adsorption to the membrane surface (Hembach et al. 2019). Previous studies have also investigated the effect of membrane filtration on ARB/ARGs removal and separation. While some studies reported the efficient elimination of eARGs by UF (Böckelmann et al. 2009; Breazeal et al. 2013; Hembach et al. 2019), others highlighted the ability of extracellular plasmids to permeate through membrane pores with sizes much smaller than the radius of the corresponding plasmids (Arkhangelsky and Gitis 2008; Arkhangelsky et al. 2008; Arkhangelsky et al. 2011; Latulippe et al. 2007; Latulippe and Zydney 2009; Latulippe and Zydney 2011). Transmission of free DNA was even observed for solution-diffusion based ‘dense’ nanofiltration or reverse osmosis membranes (Slipko et al. 2019; Arkhangelsky et al. 2011). The underlying cause for this is assumed to be stretching of the flexible MGEs due to the highly converging and thus accelerating flow fields in the vicinity of the membrane pore openings (Larson et al. 2006; Arkhangelsky and Gitis 2008; Arkhangelsky et al. 2011; Latulippe et al. 2007; Latulippe

and Zydney 2009; Latulippe and Zydney 2011). Via a hybridization of UF with processes such as adsorption by inline dosing of powdered activated carbon (PAC) prior to the UF membrane, the removal of ARGs could possibly be improved, as has already been demonstrated with respect to trace organic chemicals (such as pharmaceuticals, industrial chemicals and residuals of personal care products) (Stoquart et al. 2012; Margot et al. 2013; Löwenberg et al. 2014; Ivancev-Tumbas et al. 2018; Schwaller et al. 2021).

Other studies have modelled flow fields inside membranes (Oxarango et al. 2004; Ghidossi et al. 2006a; Ghidossi et al. 2006b; Marcos et al. 2009; Keir and Jegatheesan 2014), though these studies did not model on small enough scales to observe flow effects around the membrane pores. Schmitz and Prat (1995) modelled the flow field around a pore during microfiltration with great detail, including the effects of different pore sizes and flow rates. This was expanded on by Frey and Schmitz (2000), where the movement of particles in the flow field adjacent to the micropores was studied. However, neither Schmitz and Prat (1995) nor Frey and Schmitz (2000) quantitively analyzed the flow fields with respect to fluid strain rates and deformation of suspended particles. Furthermore, current research into PAC-UF hybrid processes has not analyzed how the flow fields in UF processes are modified by the presence of PAC particles. Besides the adsorption or entrapment of AMR inside the PAC pores (Zhang et al. 2017; Ashbolt et al. 2018; Bürgmann et al. 2018; Rizzo et al. 2020; Calderón-Franco et al. 2020; Cookson and North 1967; Powell et al. 2000; Matsushita et al. 2013), it was expected that the hybridization of UF with PAC would improve the MGE removal efficiency in comparison to UF treatment alone due to the hydrodynamic effects of the formed PAC cake layer. Based thereon, it was hypothesized that the formation of a PAC particle layer would act like a funnel, increasing the distance over which flow accelerates prior to entering the pore and hence decreasing the fluid strain rate, which would result in less deformation of MGEs and therefore less permeation through the UF membrane.

With regard to these research questions, no specific studies have as of yet been carried out. Hence, within this study Computational Fluid Dynamics (CFD) simulations of the flow fields inside UF membranes were performed on scales where hydrodynamic effects which are relevant to MGEs could be observed. Baseline information on flow fields without any PAC cake layer was first obtained through modelling. The flow fields were then modelled with the presence of a cake layer in order to gain better understanding of the physical effects that would evolve from the particle cake layer specifically with regard to hydrodynamic effects. Using the applied modelling approach a more detailed and conclusive look at and understanding of the mechanisms (such as shear as well as elongational strain rates or relaxation times/MGE stiffness) which are responsible for MGE permeation in UF membranes could be provided. Based on our investigations it could be concluded that relevant strain rates occurred within a distance of tens of

nanometers from the membrane surface while the presence of the PAC particle cake layer only had negligible effects on the hydrodynamic strain rates relevant for MGE deformation.

8.3 Material and methods

8.3.1 General information regarding the CFD simulations

All simulations were performed using the commercial Finite Element Method based CFD software COMSOL Multiphysics Version 5.4, while postprocessing and creation of images were performed in the open-source program Paraview Version 5.6.2.

Since this study aimed to determine flow conditions which were accurate to real-world situations, manufacturer specifications of the commercially available Inopor® CA tubular membrane (19 channels, channel diameter 3.5 mm, membrane diameter 25 mm, membrane length 250 mm, total membrane area 0.05223 m^2) made of TiO_2 were used as model inputs. The membrane with a median pore size of 30 nm, a median cut-off of 100 kDa (cut-off measured with polyethylene glycol), and a median skin layer porosity of 45 % was assumed to be operated in dead-end mode at fluxes between 100 and 500 LMH. The membrane state at the startup when it is most susceptible to MGE permeation (Arkhangelsky et al. 2011) was considered and ultrapure water only spiked with MGEs was assumed as flow media for modelling, so neither concentration polarization nor fouling effects had to be considered. Additional assumptions included steady-state operation, incompressible flow, and isothermal conditions at a temperature of 20 °C.

8.3.2 Set-up of the physical domains and boundary conditions

8.3.2.1 General assumptions and initial flow boundary conditions

Continuity

Continuum mechanics were assumed to be applicable to flows at the nanopore scale. This was based on a Knudsen number, Kn, being much less than 1 for 30 nm pores. The Knudsen number is most simply described as the ratio of the mean free path length of fluid particles, λ (in nm), to the characteristic length scale of the fluid domain, l_c (in nm, equation (8-1), for details cf. section 11.7.1.3).

$$Kn = \frac{\lambda}{l_c} \tag{8-1}$$

Slip velocity

Rather than applying a no-slip condition at solids surfaces, where tangential velocity is zero, for Kn >0.001, the magnitude of the tangential velocity at solid surfaces is commonly modelled using the Navier-slip condition (Holland et al. 2015a; Holland et al. 2015b; Kobayashi 2020; Priezjev et al. 2005). This condition is given by equation (8-2), where the tangential velocity, u_R (in m/s), is equal to a slip length, ζ (in m), multiplied by the negative shear strain rate at the wall $\frac{du}{dr}$.

$$u_R = -\zeta \frac{du}{dr} \tag{8-2}$$

Slip length was approximated by the contact angle using equation (8-3) (Huang et al. 2008):

$$\zeta \propto \frac{1}{(1 + cos\theta_c)^2} \tag{8-3}$$

The effective slip length is calculated as a function of empirical relationships of velocities near the wall and is given in equation (8-4), where ζ_e is the effective slip length, θ_c is the contact angle in degrees, A_i is the interfacial area (defined as the pore cross section area within 0.7 nm of the wall), and A_t is the total pore cross section area (Holland et al. 2015b). For details the reader is referred to the section 11.7.1.4.

$$\zeta_e = \left[\frac{1}{(-0.018\theta_c + 3.25)\frac{A_i}{A_t} + \left(1 - \frac{A_i}{A_t}\right)} \right] \left(\frac{d}{8} + \zeta\right) + \zeta \tag{8-4}$$

Initial feed channel boundary conditions

An important step prior to the CFD simulations was to confirm the assumption of laminar flow in the feed channel. It was assumed that flow was equally distributed among the feed channels, and entrance effects were ignored. For the maximum flux of 500 LMH, the average flow velocity at the entrance to the feed channels was about 0.0397 m/s. This corresponded to a maximum Reynolds number, Re, of about 140, which is well within the laminar regime. Intermediate steps for this calculation can be found in section 11.7.4.2.

Initial flow boundary conditions (BC) inside the feed channel for the simulations at pore and particle scale were determined via an analytical approach by Oxarango et al. (2004), who derived a formula from Yuan and Finkelstein (1955) for a circular tube with constant flux at the walls. The wall Reynolds number, Re_w, was introduced according to equation (8-5), where *R* (in m), the tube radius, is used as the length scale and the filtration velocity, v (in m/s), is considered. The kinematic viscosity is represented by υ (in m^2/s).

Radial velocities near the wall were assumed being equal to the filtration velocity at the membrane surface. Axial flow velocities are calculated by equation (8-6). In these equations, *r* is the radius of interest inside the tube (in m) and u_{ave} (in m/s) is equal to the remaining flow at a given axial distance, *y*, divided by the feed channel cross sectional area (the average flow velocity at that axial distance, equation (8-7)).

$$Re_w = \frac{vR}{\upsilon} \tag{8-5}$$

$$u(y,r) = u_{ave}\left[2\left(1-\left(\frac{r}{R}\right)^2\right)+\frac{Re_w}{18}\left(2-9\left(\frac{r}{R}\right)^2+9\left(\frac{r}{R}\right)^4-2\left(\frac{r}{R}\right)^6\right)\right] \tag{8-6}$$

$$u_{ave} = (Q - 2\pi r v y) \tag{8-7}$$

8.3.2.2 Pore scale simulations

In order to test the theory that hydrodynamic forces outside the membrane pores are capable of deforming MGEs and thereby reducing their effective size, flow fields were simulated on the scale of the membrane nanopores, then the hydrodynamic effects relevant to small, flexible particles were examined. By establishing the magnitudes of strain rate experienced by MGEs at the pore entrance, a baseline scenario was established to later compare how modifications to the membrane surface by a particle layer might affect MGE permeation. The methods used to set up the CFD simulation were similar to those established by Schmitz and Prat (1995). The first step was to define new *Re*'s that were applicable to the new geometry. These Re's are given as the tangential Re_t, and normal Re_n, to the membrane surface in equations (8-8) and (8-9), respectively.

$$Re_t = \frac{u_t b}{\upsilon} \tag{8-8}$$

$$Re_n = \frac{vb}{\upsilon} \tag{8-9}$$

Where u_t is the tangential flow velocity (in m/s), b is the distance between pore centers (in m), υ is kinematic viscosity, and v is the superficial flow velocity at the membrane surface (in m/s). In scenarios where $Re \ll 1$, inertial fluid effects become negligible and the non-linear inertial term can be dropped from the Navier-Stokes conservation of momentum equation to produce Stokes equation. For steady, incompressible flow with no momentum sources, this greatly simplifies the momentum equation calculation down to equation (8-10), where P is pressure (in Pa), μ is dynamic viscosity (in Pas), and $\boldsymbol{u}$ is the velocity vector (in m/s). Due to the second order Laplacian operator for the velocity term (∇^2), Stokes flow is dominated by diffusion of momentum through viscosity, balanced only by pressure forces. For this reason, second-order

velocity discretization was used, as this would reduce errors due to numerical diffusion. Pressure discretization was kept as first order.

$$-\nabla P = \mu \nabla^2 \boldsymbol{u} \tag{8-10}$$

Physical domain

As was considered by Schmitz and Prat (1995), the scale of the feed channel was orders of magnitude larger than the scale of a single membrane pore, making it suitable to treat the membrane as a flat, evenly spaced square grid of cylindrical pores. This allowed for immense simplification of the model, as the repeating pattern allowed for a unit cell consisting of a single pore to be simulated. This unit cell is shown in Figure 8-1. The simplification of the pore shape to an ideal cylinder can be regarded as justified as it was found that the entrance shape of the pores would not dramatically effect DNA extension (Larson et al. 2006).

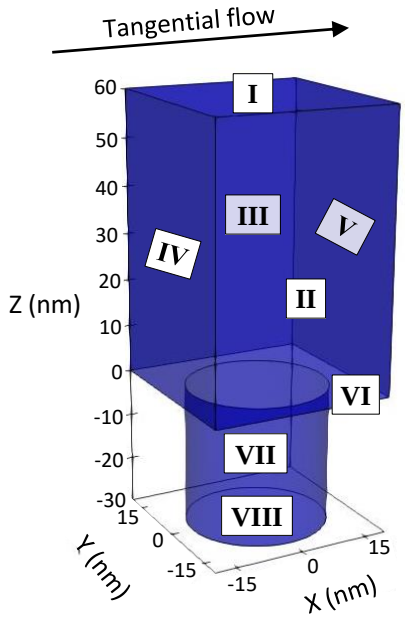

Figure 8-1: Pore scale simulation domain with BCs according to Table 8-1.

A pore diameter of 30 nm was used. The center-to-center distance between pores was used as the width and length (x and y dimensions) of the physical domain. This was calculated based on a surface porosity of 45 %, resulting in x and y dimensions of about 39.6 nm. The height of the domain above the pore was set to 60 nm which corresponded roughly to the recommended value by Schmitz and Prat (1995). The pore depth was set to 30 nm (1 pore diameter) which was more conservative than the suggestion by Schmitz and Prat (1995). This ensured the flow to become fully developed in the pore, making the flow outside the pore independent of the location of the bottom BC.

Boundary conditions

The BC used in the pore scale simulation are labelled in Figure 8-1 with descriptions of each BC provided in Table 8-1. Due to the tangential flow in the x direction, a periodic BC in x direction was appropriate so that flow out of the side of the domain would re-enter at the opposite side. The pressure gradient along the length of the feed channel in dead- end operation was considered to be negligible, so no pressure gradient was applied. Symmetry boundaries in the form of full-slip walls were applied on the y-normal faces. At the outlet of the pore, it was assumed that the pore structure widened and that flow would become less restricted, hence an open BC was used to simulate this.

Table 8-1: Descriptions of the BCs applied in the pore scale simulation.

BC No.	Description	BC type	Flow field values
I	Inlet region	Inlet	defined in Table 11-31
II & III	Axial tangential faces	Full-slip wall	$\frac{\partial \boldsymbol{u}}{\partial \boldsymbol{x}} = 0, \frac{\partial p}{\partial \boldsymbol{x}} = 0$
IV & V	Axial normal faces	Periodic	$\Delta P = 0$
VI	Membrane external surface	No-Slip	$u = 0, \frac{\partial p}{\partial \boldsymbol{x}} = 0$
VII	Membrane internal surface	No-Slip	$u = 0, \frac{\partial p}{\partial \boldsymbol{x}} = 0$
VIII	Inner membrane region	Open	P = 0

The inlet BC was varied over 5 simulations to mimic the conditions over a range of fluxes starting from 100 LMH to 500 LMH in increments of 100 LMH. Normal velocities were obtained based on the flux velocities corresponding to each flux rate, and they were defined as negative to indicate flow in the negative z direction. Equation (8-6) was used to determine the tangential flow velocity, u_x. No-slip condition was justifiably applied to the solid membrane surfaces. Details can be found in the section 11.7.2.1.

8.3.2.3 Particle scale simulations

The final stage of this study was to determine the effects that a layer of particles covering the UF membrane would have on flow fields. By running the simulations at the same fluxes as for the pore scale simulations (cf. section 8.3.2.2), changes to flow fields resulting from the presence of the particle layer could be examined. The particles for which their effect on the hydrodynamic flow field should be investigated were uniformly sized 8 µm diameter spheres in hexagonal closest packed configuration. Given that this introduced a new length scale, a new *Re* was obtained using the particle diameter, D_p, as the length scale and the filtration velocity, u, as the velocity. The new 'Particle Reynolds Number', Re_p, was calculated based on Equation (8-11). At the highest flux value of 500 LMH the flux velocity was 1.3889 x 10^{-4} m/s, resulting in an Re_p of about 1.1 x 10^{-3}. As this was much less than 1, Stokes flow according to equation (8-10) was

considered. Hence, the dominance of Stokes flow meant that the inertial term in the Navier-Stokes equations could be ignored. Since Stokes flow is largely characterized by the diffusion of momentum through viscosity, second-order velocity discretization was used. Pressure discretization remained as first order.

$$Re_p = \frac{uD_p}{\upsilon} \tag{8-11}$$

In order to examine the effects of the particle layer on flow fields at the membrane surface, the filtration velocity was used as a critical metric. The baseline was considered as the filtration velocity corresponding to the flux which was being simulated.

Physical domain

Symmetries in the hexagonal closest packed sphere configuration were taken advantage of to minimize the size of the simulation domain. The plan view of the section taken from the sphere pack is shown in Figure 8-2A, followed by the entire simulation domain in Figure 8-2B. The domain was half a particle diameter wide in the y direction. Periodic symmetry was required in the direction of flow tangential to the membrane, requiring the x dimension to extend from one particle centre to the centre of the next particle located at the same y coordinate (about 13.9 µm). It was suitable to consider the domain to be an infinite flat plate, since the curvature of the feed tube was on a length scale orders of magnitude larger than the domain width. The particle layer was considered to only be one particle thick because additional particles layers would not have been expected to make a difference to flow patterns near the membrane surface given the viscosity dominated nature of Stokes flow. The domain height was set to 20 µm, which was sufficient for the flow fields to be independent of the top BC location. The particles were reduced to 99 % of their original size, as recommended by Alkhalaf et al. (2018). This circumvented simulation issues due to very small relative cell dimensions (contact points where the spheres meet each other and the membrane) and high cell skewing in these regions.

The porous membrane material was modelled in COMSOL by designating the membrane region as porous. In COMSOL, Brinkman's equation is used to model flows where both free and porous domains are present. More details about the implications of this can be found in section 11.7.1.1. A membrane permeability of 4.69 x 10^{-17} m^2 was used for all simulations. For details on the determination of the membrane permeability the reader is referred to the section 11.7.2.2.

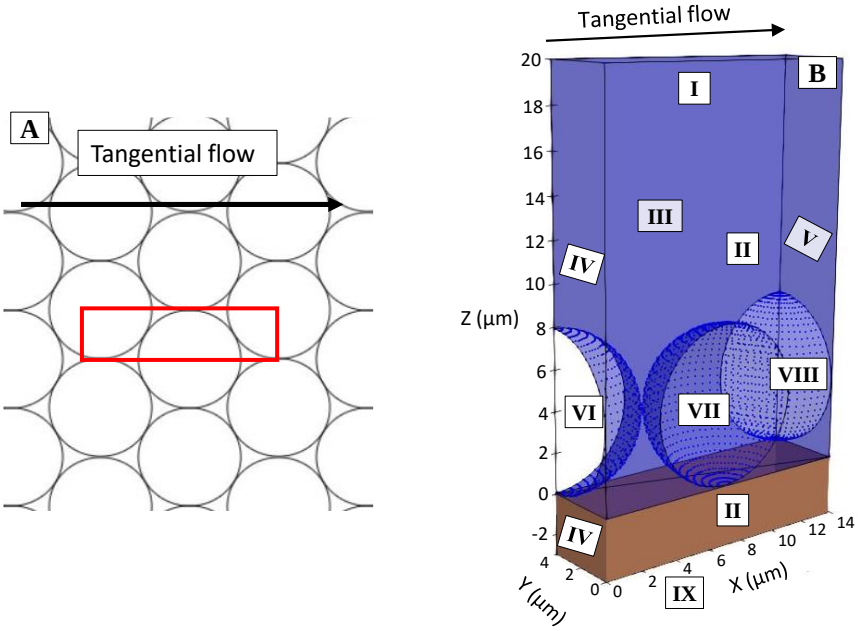

Figure 8-2: (A) Plan view of domain cut-out from sphere pattern and (B) Simulation domain used for particle scale simulations with BCs according to Table 8-2.

Boundary conditions

The BC for the particle scale simulation were very similar to those used in the pore scale simulation and are given in Table 8-2. As the y-normal faces were symmetric in the sphere pack, they were defined as full-slip walls. The x-normal faces were all defined as periodic, allowing tangential flows to enter and leave the domain through the side boundaries. As with the pore scale model, pressure gradients over the length of the domain due to tangential flow in the feed channel were considered to be negligible. The length scales for the particles at the membrane surface were larger than those where slip-velocities are relevant, so they were defined as no-slip. Finally, absolute pressures in this simulation were irrelevant, so the bottom face was set as a pressure outlet with a reference pressure of zero.

Table 8-2: Descriptions of BCs in particle scale simulations.

BC No.	Description	BC type	Flow field values
I	Inlet Region	Inlet	defined in Table 11-34
II & III	Axial Tangential Faces	Full-slip wall	$\frac{\partial \boldsymbol{u}}{\partial \boldsymbol{x}} = 0, \frac{\partial p}{\partial \boldsymbol{x}} = 0$
IV & V	Axial Normal Faces	Periodic	$\Delta P = 0$
VI, VII, VIII	Particle Surfaces	No-Slip	$u = 0, \frac{\partial p}{\partial \boldsymbol{x}} = 0$
IX	Inner Membrane region	Outlet	$P = 0$

The z velocities, u_z, at the inlet were assigned as the filtration velocities corresponding to the flux values that were used. The tangential velocities, u_x, were determined based on equation (8-6), noting that the feed channel diameter was reduced by one particle diameter to account for the extension of the boundary layer from the membrane surface. Details are provided in the section 11.7.2.2.

8.3.3 Theory on hydrodynamic strain rates and their deformational effects on MGEs

The elongational response of flexible polymers such as DNA to fluid strain rate is a well-studied problem (Latulippe and Zydney 2011; Dobson et al. 2017; Smith et al. 1999; Meacle et al. 2007; Afonso et al. 2009). In examining fluid strain rate, one differentiates between shear strain rate and elongational strain rate. Shear strain rate represents the transverse flow gradients to a given vector, while elongational strain rate is the flow gradient parallel to that vector. Given the strain rate tensor in equation (7-1), shear strain rate was calculated by the off-diagonal terms and elongational strain rate by the diagonal terms. Shear flows can cause extension of particles, as well as producing a weak rotational motion. In contrast, elongational flow causes a direct stretching of particles as if pulling on opposite ends.

$$\epsilon_{ij} = \begin{bmatrix} \frac{du_1}{dx_1} & \frac{1}{2}\left(\frac{du_1}{dx_2} + \frac{du_2}{dx_1}\right) & \frac{1}{2}\left(\frac{du_1}{dx_3} + \frac{du_3}{dx_1}\right) \\ \frac{1}{2}\left(\frac{du_2}{dx_1} + \frac{du_1}{dx_2}\right) & \frac{du_2}{dx_2} & \frac{1}{2}\left(\frac{du_2}{dx_3} + \frac{du_3}{dx_2}\right) \\ \frac{1}{2}\left(\frac{du_3}{dx_1} + \frac{du_1}{dx_3}\right) & \frac{1}{2}\left(\frac{du_3}{dx_2} + \frac{du_2}{dx_3}\right) & \frac{du_3}{dx_3} \end{bmatrix} \tag{8-12}$$

MGEs are considered to mechanically behave like polymer chains (Larson et al. 2006). Relating the computed strain rates to particle deformation was performed using the Weissenberg number, Wi, given in equation (8-13). This dimensionless number is the product of the fluid strain rate, $\dot{\gamma}$, and a characteristic time scale for the organic polymer, τ_r, known as the relaxation time (Smith et al. 1999).

$$Wi = \dot{\gamma}\tau_r \tag{8-13}$$

τ_r is inversely proportional to the particles stiffness and is specific to the organic polymer chain. Particles can behave differently under shear strain rate than they do under elongational strain rate (Meacle et al. 2007). Under elongational strain rate, the particle becomes considerably deformed as *Wi* approaches a value of 1 (Latulippe et al. 2007; Hsieh et al. 2007; Smith et al. 1999). However, Smith et al. (1999) found that considerable deformation was not observed under shear strain rate until a *Wi* of about 5. This indicates that polymers are much less sensitive to shear strain rate, which was also confirmed by Dobson et al. (2017).

8.3.4 Meshing and convergence studies

In each section, three different meshes were used for the convergence studies. The initial physics generated mesh was refined and/or coarsened using a scaling feature, which scaled the edge length between elements by a scaling factor, r. This resulted in a change in the number of elements by a factor of approximately r^N, where N is the number of physical dimensions being modelled. Scaling was performed over the entire flow domain to ensure similarity of the meshes. Separate simulations were performed for each grid using BCs corresponding to a flux of 500 LMH, which was the highest flux rate that was simulated. Finally, the results were postprocessed, and the errors between the finest two meshes were analyzed to ensure that the finest mesh, which was to be used for subsequent simulations, was able to sufficiently capture the flow features of interest. The detailed descriptions of the meshing studies for the pore scale as well as particle scale simulations are provided in the 11.7.3.

8.4 Results and discussion

8.4.1 Pore scale simulations

The behavior of the flow field in the region outside of the pore opening is visualized in Figure 8-3 using streamlines. As one would expect for Stokes flow, the streamlines appeared very orderly with no vortical structures or unexpected flow disturbances. The streamlines which came very close to the membrane surface were those which originated immediately next to the x and y boundaries. The chances of particles interacting with the membrane surface are much more likely for flow entering the domain at these locations, though this only accounted for a small portion of the incoming flow. The impacts of tangential flow only caused deflection of the streamlines in the x direction by about 1 nm over the 60 nm domain height, indicating that the magnitude of tangential flow which occurs in dead-end configuration had very little impact close to the membrane surface.

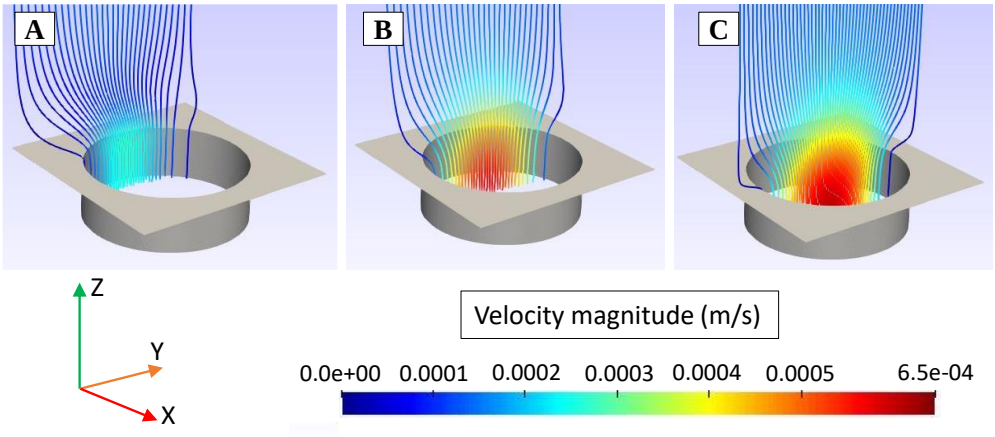

Figure 8-3: Streamlines of flow into the membrane pore, originating at (A) x=-19.5 nm (B) x =-9.9 nm and (C) x=0 nm (center axis of pore).

8.4.1.1 Elongational strain rate

Figure 8-4A shows that the greatest magnitude of elongational strain rate occurred along the centre axis of the pore (x = 0). The strain rate developed a somewhat parabolic profile across the pore, similar to the velocity. Extensional strain rate was present in regions directly above the pore from the centre of the pore to a radius of about 13 nm. At this point the strain rate became negative, likely due to the fact that flow outside of this radius was approaching the boundary layers at the solid membrane surfaces. This transition point is also seen in Figure 8-4B where the orientation of elongational stretching turned from vertical to horizontal. It was observed that particles approaching the pore from directly above would become elongated in the direction of the pore opening, making it easier for them to pass through. The regions located above the edges of the pore were more likely to elongate MGEs laterally, making them less likely to pass through.

However, since the regions where elongation occurred normal to the pore opening had higher strain rate magnitudes than those which elongated particles laterally, the effects pulling particles into the pores are expected to dominate.

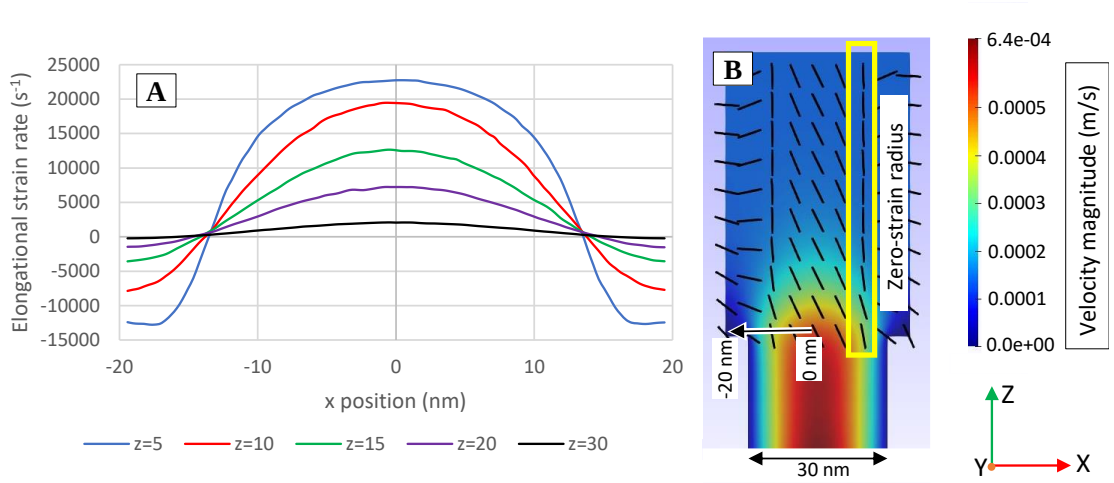

Figure 8-4: (A) Elongational strain rate magnitude throughout flow domain for flux of 500 LMH and (B) Orientation of elongation.

As seen in Figure 8-5A, elongational strain rates at distances farther than about 25 nm from the pore opening were much smaller than those observed closer to the pore opening. However, the strain rates increased rapidly between approximately 25 nm and 6 nm from the pore opening. The viscosity term in the Navier-Stokes equations is a second order differential term, which explains why the strain rate increases, because the influence of viscosity will decrease at an increasing rate with distance. The flow rate did not have an impact on this range because, with the flow being Stokes flow, the inertial forces were too small in comparison to have any effect. The elongational strain rate peaked at a distance of approximately 6 nm from the pore opening, then decreased sharply with decreasing distance from the pore opening. The elongational strain rate, $\acute{\varepsilon}$, could be approximated by a function of the distance, z, from the pore opening: $\acute{\varepsilon} \sim z^{-3}$. This observation corresponds to a mathematical derivation of the elongational shear strain rate by Nguyen and Neel (1983). Elongational strain rate was still considerable at the entrance of the pore, which would help to keep MGEs extended until they enter the membrane structure. Figure 8-5B provides further illustration of this, where a lower distance between velocity contours indicates a higher fluid strain rate. The gradual decline of the velocity gradient at a pore distance closer than 6 nm necessarily resulted in the decrease of the elongational strain rates. Dobson et al. (2017), Meacle et al. (2007), and Daoudi and Brochard (1978) also reported that significant strain rates occur at a distance from the pore which is in the order of magnitude of the pore length scale, indicating that peak hydrodynamic forces occur very close to the porous surface.

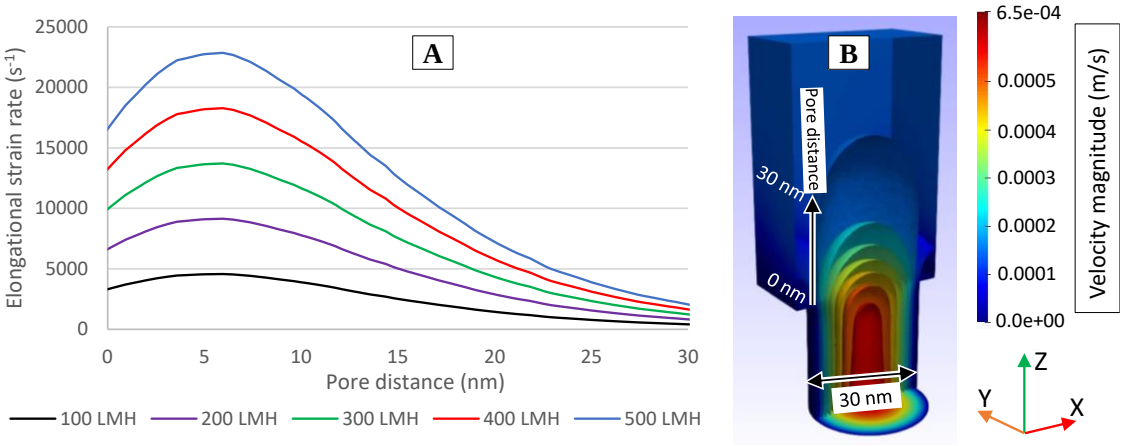

Figure 8-5: (A) Elongational strain rates along the z axis (pore distance) for various flux rates and (B) Velocity contours around the membrane pore.

As was also observed by Dobson et al. (2017), the distance which strain rates occurred over was not noticeably affected by the flux rate. This resulted in a highly linear correlation between the flux and the elongational strain rate. To elaborate on this further, the peak strain rate corresponding to a flux of 500 LMH (≈23,000 s^{-1}), was almost exactly five times that for a flux of 100 LMH (≈4,600 s^{-1}). This highly linear behavior allows for linear interpolation to be used to accurately estimate strain rates associated with intermediate fluxes.

Elongational strain rate is expected to be the dominant form of strain rate which affects the permeation of flexible particles such as MGEs into membranes (Smith et al. 1999). With detailed knowledge on the relaxation times of MGEs to be retained, the strain rate data from Figure 8-4 and Figure 8-5 could be used to estimate the fluxes and locations at which considerable deformation would occur. In absence of relaxation time data, the relaxation times of linear and supercoiled plasmids were estimated based on the maximum strain rates corresponding to critical flux velocities. Latulippe and Zydney (2011) reported critical flux velocities for linear and supercoiled plasmid DNA for a membrane with a similar size exclusion, which was assumed to produce similar magnitudes of strain rates. These critical flux velocities are provided in Table 8-3, along with the peak strain rates interpolated from Figure 8-5 for the corresponding fluxes. Relaxations times were determined by rearranging equation (8-13), assuming that critical flux corresponds to a peak *Wi* of 1 (cf. section 8.3.3).

Table 8-3: Determination of relaxation times for linear and supercoiled plasmids based on findings by (Latulippe and Zydney 2011)

		Linear plasmid		**Supercoiled plasmid**	
	Unit	**Low**	**High**	**Low**	**High**
Critical flux velocity	10^{-5} m/s	0.6	1.8	4.0	5.6
Corresponding flux	LMH	22	65	144	212
Peak strain rate	s^{-1}	987	2961	6581	9213
Relaxation time	µs	1013	338	152	109

The fluxes that were observed by Latulippe and Zydney (2011) associated with the permeation of linear plasmids through the membrane (22 or 65 LMH, cf. Table 8-3) were quite low in comparison to normal operating fluxes (≈120-200 LMH). Based thereon it can be stated that MGEs encoded in linear plasmids are highly likely to permeate through UF membranes at normal operational fluxes. In contrast, less flexible plasmids such as those in the supercoiled conformation are less prone to deformation and therefore less susceptible to transmission through UF pores. At a distance greater than 30 nm from the pore opening, only the most flexible linear plasmids will experience noticeable deformation, even at the highest flux observed (elongational strain rate ≈<2,000 s^{-1}).

Dobson et al. (2017) also assessed effects of extensional flow field on protein behavior. They quantified the strain rates that are generated due to a reduction in flow channel diameter resulting in an increase in linear velocity. Even though the geometry of their experimental device was different to that of a membrane, the underlying principles are the same. By a CFD simulation applying a finite element method they determined strain rates in the range of 10^3 to 10^4 s^{-1} which are comparable the strain rates obtained in our study. Furthermore, the comparison with relaxation times of confined DNA obtained by Hsieh et al. (2007) were on the order of 10^{-3} s at nanometer length scales, which is in agreement with the results found in this study. Lewis and Pecora (1986) determined the relaxation time of a DNA fragment to be 680 µs, which further indicates that the predicted relaxation times were at the correct order of magnitude and underlines the validity of the computed values in Table 8-3. The results for the elongational strain rates obtained via the CFD simulation can also be validated via an analytical approximation: According to Metzner and Metzner (1970), the elongational strain rate, $\acute{\varepsilon}$, can be calculated as follows:

$$\acute{\varepsilon} = \frac{Q}{\pi * r^3 * (1 - \cos\Theta)} \tag{8-14}$$

where r is the pore radius and Θ is the pore entrance angle. The flow Q through one pore was estimated by assuming that the total flow through the membrane would be distributed evenly over an estimated pore number of $3.3*10^{13}$ (membrane surface multiplied by porosity divided by pore area).

Table 8-4 shows that CFD predictions of the elongational strain rates matched closely its analytical approximations.

Table 8-4: Comparison of CFD simulation results and analytically determined results. Θ was assumed to be 75 ° (Meacle et al. 2007)

		Unit	CFD simulation	Analytical calculation
Flow, Q, through a single pore at	100 LMH	10^{-19} m^3/s	0.56	0.44
	500 LMH		2.8	2.2
Elongational strain rate, ε̇, at	100 LMH	s^{-1}	5000	5500
	500 LMH		23000	27800

8.4.1.2 Shear strain rate

Magnitudes of shear strain rate throughout the flow domain are shown in Figure 8-6A. Negative values were due to the strain rate vectors facing opposite directions, though the effects are identical to those of positive values. Figure 8-6B shows the orientation of particle deformation due to shear. The effect of shear at nearly all locations was rotation and deformation of the flow field in the direction of the pore opening, a result also observed by Frey and Schmitz (2000) when simulating particle movement in this region.

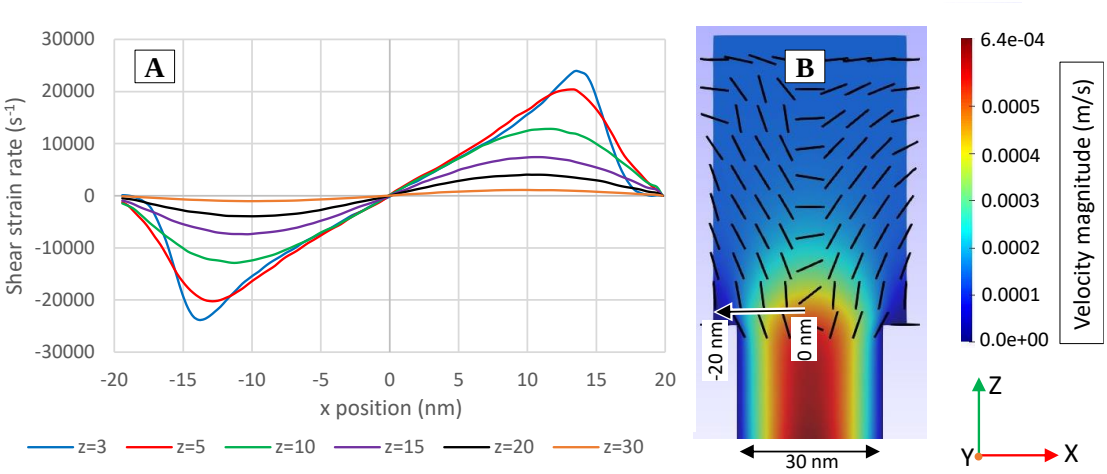

Figure 8-6: (A) Shear strain rate magnitude throughout the flow domain at y = 0 nm and (B) orientation of shear deformation.

The exception to this occurred directly above the pore centreline where the shear strain rate was zero. The shear strain rate orientations would cause rotation and elongation of MGEs in a direction such that passage through the pore opening would become more likely. The presence of shear strain rates very close to the outer membrane surface could also act to deform attached (MGE) particles in the direction of the pore, causing them to be pulled into the pore by elongational strain rates.

The shear strain rate along the z axis at various flux rates is shown in Figure 8-7. The values were observed at a radial distance of 13 nm (x=13 nm), as this is approximately

where the elongational strain rate became zero, and where maximum shear strain rate values were observed. Similar to elongational strain rates, shear strain rates were negligible until distances closer than about 25 nm from the pore opening, after which they increased with decreasing distance from the pore. Another similarity to elongational strain rates is that the shear strain rates reached a peak at a short distance before the pore opening. With shear strain rates, however, the distance of the peak from the pore opening was mildly influenced by the flux rate, making linear interpolation of results less accurate. It is noted that the peak occurred around the same location where the mesh results became uncertain (for detailed explanation refer to section 11.7.3.1), so the peak likely indicated a point where boundary layer effects at the membrane surface became prevalent. The shear strain rates had a similar magnitude as the elongational strain rates, though equivalent values did not occur until about half the distance from the pore opening as compared with elongational strain rates.

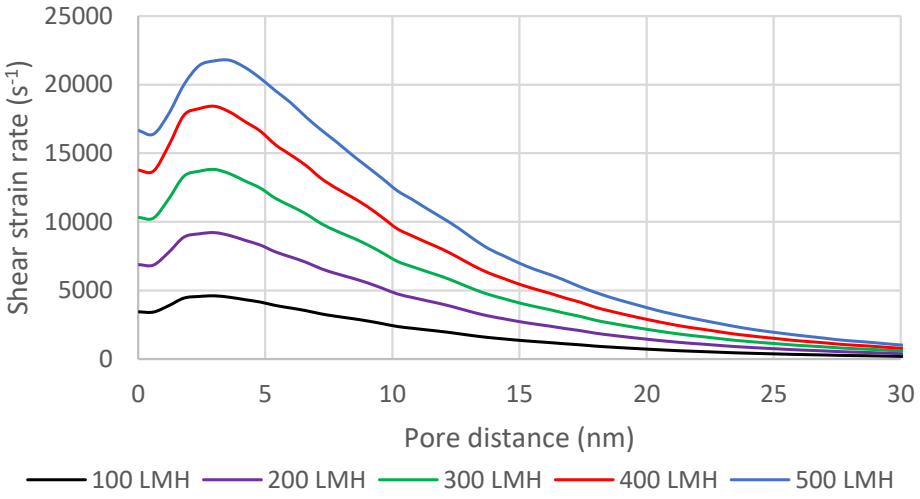

Figure 8-7: Shear strain rate along the z-axis at x=13 nm, y=0 nm.

Though the magnitudes of shear and elongational strain rate are similar, particles such as MGEs are likely much less sensitive to deformation by shear strain rate than they are to elongation strain rate (Dobson et al. 2017). Smith et al. (1999) found that a *Wi* of 5 was required for significant deformation due to shear strain rate. In other words, shear strain rate must have 5 times the magnitude of elongational strain rate to cause significant deformation of particles. Using the relaxation times obtained in Table 8-3, shear strain rates corresponding to a *Wi* of 5 are between about 5,000 and 15,000 s^{-1} for linear plasmids and 33,000 and 46,000 s^{-1} for supercoiled plasmids (cf. equation (8-13)). Comparing this to the values in Figure 8-7, significant deformation due to shear strain rate was likely for linear plasmids at fluxes between approximately 100 and 330 LMH and was unlikely to occur for supercoiled plasmids. When comparing this to the reported

critical fluxes in Table 8-3, it is evident that the primary cause for permeation of MGEs through UF membranes is elongational strain rate. Given that plasmids will only experience limited deformation due to shear strain rate, it is not surprising that they do not experience damage until shear strain rates are on the order of 10^6 s^{-1} (Meacle et al. 2007). However, Furiga et al. (2011) noted that MS2 phages may be much more sensitive to damage from shear at low flux rates than plasmids, with shear being the primary driver of degradation.

8.4.2 Particle scale simulations

8.4.2.1 Effect of tangential flow

Since tangential flow velocities were an order of magnitude greater than flow velocities normal to the membrane, it was important to determine the effects that the particle layer had on flow velocities tangential to the membrane surface. Figure 8-8 shows a comparison of streamlines for scenarios with and without tangential flow. There was an obvious difference in how flow approached the particle layer. Without tangential flow, the streamlines approached uniformly from the top of the domain, whereas with tangential flow they approached with a higher velocity and entirely from the side of the domain. However, once the flow began to enter into the particle layer, there was very little difference in the streamlines. In fact, if the streamlines are overlaid on top of each other, there is no perceivable difference within the particle layer.

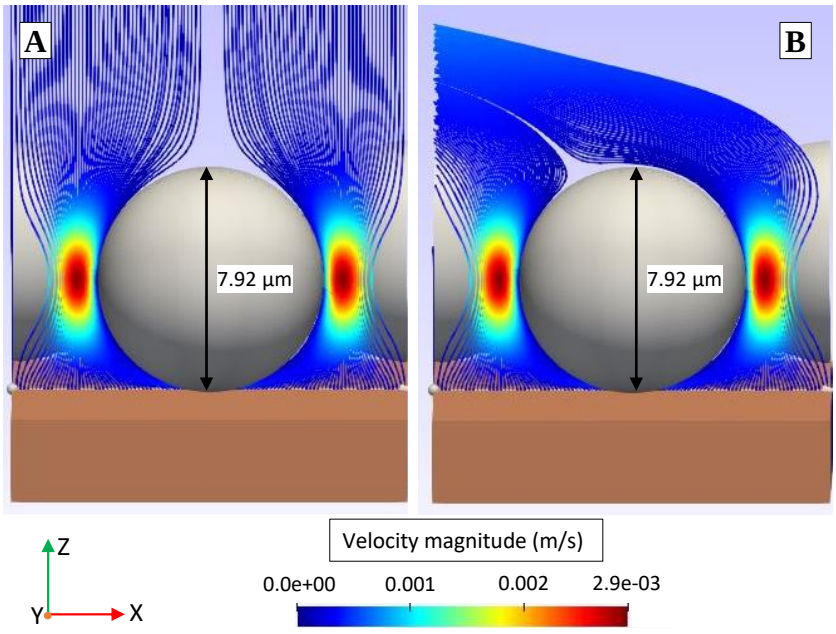

Figure 8-8: Streamlines around a particle for simulations (A) without and (B) with tangential flow.

Figure 8-9 provides a quantitative comparison of the tangential flow velocities along a vertical line which passes through the gap between the particles. As one would expect, the three scenarios without crossflow/tangential flow were indistinguishable, and the velocity in the x direction was zero for these cases. For the scenarios which consider tangential flow, the x velocity decreased linearly as the distance from particle layer (z position) decreased, with the slope depending on the input velocity or flux. As in Figure 8-8, the scenarios with and without tangential flow became difficult to distinguish at around z=6 µm, with values of approximately zero. This shows that the presence of the particle layer will largely negate tangential flow effects at the membrane surface. Since tangential flow was seen in section 8.4.1 to have negligible effect on the flow fields outside of the pore structures, this would not have any significant effect on strain rates at the membrane pore openings.

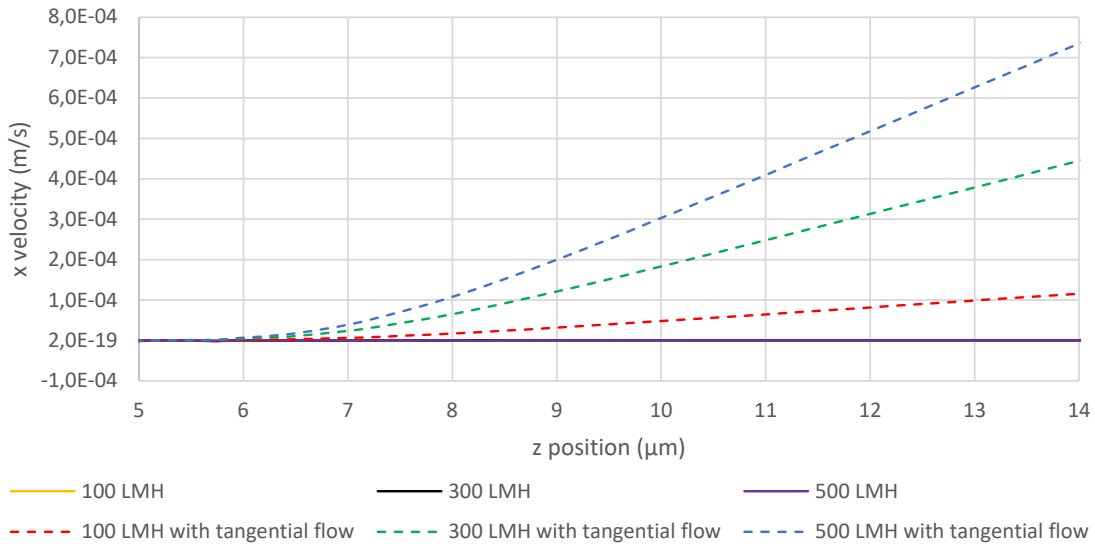

Figure 8-9: Tangential flow velocities at x=2.31 µm, y=0 µm for different flow scenarios.

8.4.2.2 Effects at membrane surface

In the previous section 8.4.1, it was found that strain rates with a magnitude capable of deforming MGEs occurred within about 30 nm (1 pore diameter) of the membrane surface. Since the scale of the particle layer was much larger than this, the only region of interest for changes to the flow field was directly next to the membrane surface. Bağcı et al. (2014) noted that for Darcy flow, the flow field will form to the porous geometry. This was previously observed in the streamlines in Figure 8-8, where the flow velocity rapidly decreased and the flow streamlines fanned out after the constriction between particles. For a complete view of the flow distribution at the membrane surface, filtration velocities

across a unit area of membrane surface are shown in Figure 8-10 relative to outlines indicating where particles were located.

If the gradients of filtration velocities across the membrane surface are small enough, then the inflow to a single pore will essentially be uniform and there will be no difference in the flow fields compared to the result in section 8.4.1. Analyzing filtration velocities at a flux of 500 LMH and a distance of 60 nm from the membrane surface (the upper edge of the flow domain in section 8.4.1), the highest gradient in the x or y directions was about 276 s^{-1}. Over a distance of 40 nm (the approximate flow domain extents for a single pore), this corresponds to a change in velocity of approximately 1.1 x 10^{-5} m/s, or about 8 % of the baseline velocity. Given that this is the maximum, and the filtration velocities in Figure 8-10 are nearly constant over the majority of the membrane surface, the presence of the particle layer will not cause significant funnelling of the flow field into the membrane pores, as was initially hypothesized.

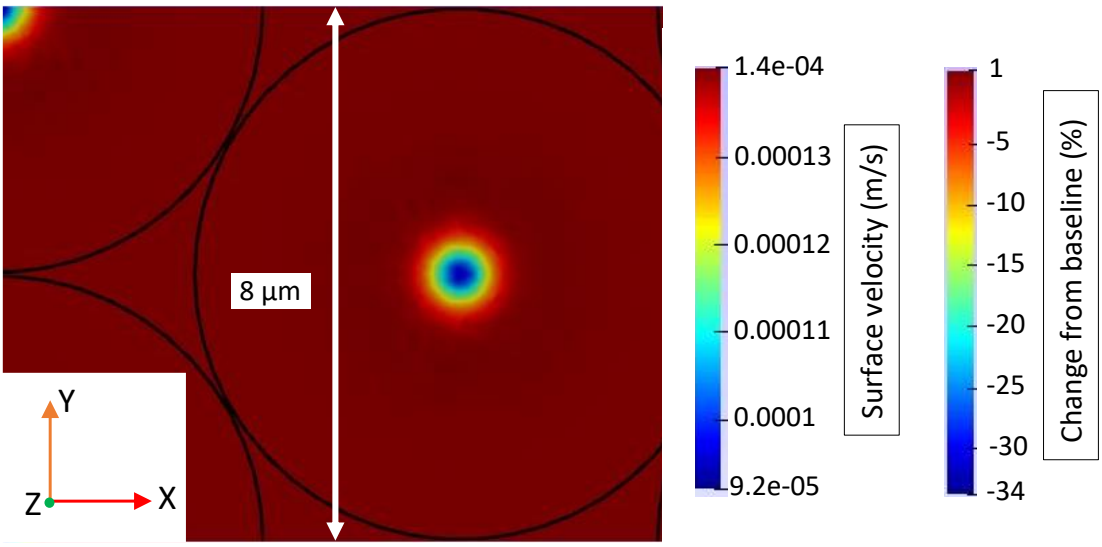

Figure 8-10: Filtration velocities at flux of 500 LMH in the presence of a particle layer. Particle outlines shown in black. Baseline or the reference are surface velocities at 500 LMH without a particle layer.

8.4.2.3 Effects on MGE permeation

It was expected that the increased confinement of flow between the particles and the membrane would redistribute flow to other areas of the membrane, increasing filtration velocities. However, the addition of a particle layer only increased filtration velocities by a maximum of about 1 % compared to baseline velocities (Figure 8-10). To provide insight into locations and magnitudes of filtration velocity effects resulting from the particle layer, Figure 8-10 displays a scale bar to show changes from the baseline velocity.

With the exception of regions directly underneath particles, the majority of the membrane area had a miniscule change in velocity. The minimum velocity directly underneath the particles was approximately 66 % of the baseline velocity. It is possible that this could cause a reduction in MGE permeation, as the regions of increased velocity saw only a slight increase, whereas in regions where velocity decreased, the decrease was substantial. However, the decrease in velocity also meant that flow decreased to these regions. With only about 6 % of the membrane experiencing decreased filtration velocities, and the consideration that these regions would account for less than 6 % of the flow into the membrane, the particle layer would likely cause rather insignificant reduction of MGE permeation.

In Figure 11-26, the elongational strain rate was analyzed as a quality control measure for the mesh study. However, this figure also provided useful information on strain rates which could potentially cause pre-stretching of MGEs. Comparing the magnitudes of strain rate in this region with the relaxation times obtained previously (cf. Table 8-3), the peak strain rate of about 1,100 s^{-1} would only produce a *Wi* greater than 1 for the most flexible of linear plasmids, and not for supercoiled plasmids. This means that only the most flexible of linear plasmids would be susceptible to deformation from hydrodynamic forces around the particles. The area under the particle constriction also had a negative elongational strain rate, so any deformation of MGEs in the particle layer would likely be counteracted before they reached the membrane surface. Given that the values shown in Figure 11-26 are for the highest flux value of 500 LMH, any lower flux values would have an even lesser effect on plasmid deformation, if any at all. This further supports the findings which have been prevalent up to this point, that the particle layer would not have any significant effect on the permeation of MGEs through UF membranes.

8.5 Conclusion

The potential effects of fluid strain rates in the vicinity of UF membrane surfaces on MGE's deformation have not yet been completely understood. Previous studies where modelling was applied for investigating the movement of particles in the flow field neglected the effects of associated fluid strain rates on the deformation of flexible particles while experimental studies did not quantify the strain rates. Moreover, the hydrodynamic consequences of a particle layer that forms during a hybrid PAC-UF process on top of the membrane surface on MGE's mechanics have so far not be addressed at all. Hence, within this study CFD simulations were conducted to elucidate these research gaps.

It was found that the most significant magnitudes of shear and elongational strain rates occurred within a distance of tens of nanometers away from the membrane surface.

In this region deformable MGEs such as plasmids would experience sufficient elongation, allowing them to more easily pass through the membrane. The magnitudes of elongational and shear strain rates outside of the pore opening were comparable. However, given that flexible particles are expected to be much more sensitive to elongational strain rates, shear strain rates are only expected to have a minor effect in comparison to elongational strain rates on the permeation of MGEs through UF membranes.

Contrary to what was initially hypothesized, the introduction of a particle layer on top of the membrane surface did not extend the distance over which flow field accelerations occurred. This was due to the very large scale of the particles compared to that of the affected flow region for a single pore. Flows were able to quickly reform around particles, resulting in a relatively uniform filtration velocity. Given that flow fields for individual pores remained largely unaffected, the presence of a PAC cake layer on the membrane surface in hybrid PAC-UF processes will not have any considerable impact on the permeation of MGEs due to hydrodynamic effects. Therefore, the potential adsorption onto PAC or entrapment of AMR inside the PAC pores in a hybrid PAC-UF process is expected to be the major abatement mechanism of AMR while hydrodynamic effects can be regarded as neglectable.

8.6 Acknowledgements

This work was funded by the Federal Ministry of Education and Research (BMBF), Germany which we especially acknowledge (grant 02WV1563A). We would like to express our gratitude to Rauschert Distribution GmbH, Business Unit Inopor for the donation of the ceramic UF membrane and the provision of necessary specifications on the UF membrane. Moreover, we acknowledge the support by our colleague Dr.-Ing. Thomas Lippert who provided an in-depth introduction to the COMSOL software.

9 OVERALL DISCUSSION AND FUTURE RESEARCH NEEDS

Key factors for the successful implementation of water reuse projects are a proper definition of projects objectives particularly by consulting stakeholder groups, participation of the public, considerations of relevant regulations/standards, a proper economic assessment of recycled water, choice of adequate technologies for water reclamation that match with the intended application, and as biggest challenge proper management of the associated chemical and microbiological risk of reclaimed water (Miller 2006).

As previously mentioned, the understanding of the quantitative irrigation water demand is required in order to choose and size an adequate water treatment technology for the production of reclaimed water matching site-specific demand. Furthermore, the technologies chosen for water reclamation have to be assessed thoroughly with regard to treatment efficiency. In this context, not only the potential of removing relevant contaminants that are of concern for human health should be accounted but also operational stability. This dissertation elaborated these aspects:

Research objective #1 aimed to estimate agricultural irrigation demand via modelling. Within **chapter 4** a modelling approach for the determination of site-specific agricultural demand was developed, validated and applied in order to estimate overall daily gross irrigation demand for an entire agricultural area cultivated with different crops on different soils.

Ultrafiltration combined with an adsorptive treatment step via powdered activated carbon was identified as promising treatment technology. Since UF is expected to be the main barrier and PAC is assumed to have rather negligible removal effects against microbiological contaminants such as bacteria, viruses or ARGs, factors that influence the corresponding removal efficiency only during membrane UF were investigated (**Research objective #2** in **chapter 5**, and **research objective #3** in **chapter 6**). The most important findings from these studies were:

- The physical separation of MS2 phages significantly increases with increasing flux and TMP during ceramic UF.
- The formation of the fouling layer that forms during UF resulted in a slightly increased removal of intra- and extrachromosomal ARG or partially had only negligible effects.
- Higher ARG abundance in the feed resulted in higher ARG abundance in the UF filtrate.

- Some intact bacteria were able to break through UF membranes.

Finally, the treatment efficiency of the hybrid membrane process PAC/UF (PAC dosed inline prior to start of a UF cycle) was assessed. Focus was laid on TOrC removal, operational stability measured as TMP built-up (**research objective #4** in **chapter 7**) and effects of the PAC cake layer on the hydrodynamic flow fields during UF (**research objective #5** in **chapter 8**). It was found that at a specific operation mode, the PAC/UF HMP could effectively remove TOrCs while maintaining operational stability. Moreover, it could be concluded that a PAC particle cake layer only will have negligible effects on the hydrodynamic strain rates relevant for mobile genetic elements deformation possibly leading to their transmission through the UF membrane.

The following sections intend to comprehensively discuss the results obtained in these studies presented in chapters 4 to 8. For that the methodological approaches that were applied in the studies undergo a critical assessment, alternatives or modifications are proposed, the relevance and transferability of the study results are evaluated and future research needs are elaborated. The feasibility of the PAC/UF treatment process is discussed and an alternative multi-barrier treatment system is presented. Finally, based on a literature review, the potential risk associated with accumulation of certain contaminants in the environment is discussed.

9.1 From a supply-focused water management to a demand-oriented water management

On a global scale, 70 % of our freshwater resources are ‘consumed’ by agriculture (UN 2021) and it is projected that by 2030 water demand will exceed supply by 40 % (UN Programme, International Resource Panel 2015). This upcoming water crisis highlights the importance of a water management that addresses both, water supply as well as water demand. Besides improving the efficiency of water supply, it is emphasized that policy measures should be taken to ‘*curb water demand and re-allocate water between sectors and users according to where water produces goods and services most beneficial to society, i.e. where it contributes to most economic output per drop*’ (UN Programme, International Resource Panel 2015). Improving water use efficiency via an adequate supply and demand management could substantially help to alleviate future water use conflicts between urban and agricultural areas (Flörke et al. 2018).

Even in a high-tech country like Germany we are often unaware of the exact water demand required for agricultural irrigation (Schwaller et al. 2020). Despite good practices of recording and reporting of agricultural water demand, corresponding field data are rare or insufficient in temporal or spatial resolution for enabling adequate water demand management (Schwaller et al. 2020). Particularly in agriculture focus is laid on optimized

supply management, thereby neglecting an adequate demand-management. This is why we considered it necessary to estimate site specific agricultural irrigation demand via modelling, as it was performed within the context of research objective #1 (chapter 4). It was hypothesized that *'the local overall daily peak gross irrigation requirement for an entire agricultural area cultivated with different crops on different soils can be estimated via a modelling approach implemented in Python based on the Penman-Monteith equation and a modified computational procedure of the CROPWAT 8.0 software* **(research hypothesis #1)**'. The comparison of the simulated results with corresponding literature data, field data of monthly and annual irrigation demand proofed the validity of the applied approach. The results obtained in this study did not only allow to **accept research hypothesis #1** but also constitute a viable as well as helpful basis not only for the agricultural management of individual local farmers but in particular an essential prerequisite for the planning of non-potable water reuse projects for agricultural purposes adapted to local conditions. However, it has to be noted that the modeling approach presented within this thesis requires detailed meteorological data that are also not always available. This represents a clear drawback of this approach.

Alternatively, an optimized irrigation management where supply matches demand could be realized via the approach conceptualized within a report by Schwaller et al. (2020). This approach is currently implemented within the project *'Nutzwasserbereitstellung und Planungsoptionen für die urbane und landwirtschaftliche Bewässerung'* (Link to project website). With the advances in digitalization and computing, the automated recording, archiving and determination of the local (agricultural) irrigation demand in real time becomes a realistic and feasible approach. Within the project an automated system for the determination of the local agricultural irrigation demand is developed. A cloud-based 'Internet of Things (IoT) system' was established in order to automatically determine and forecast the agricultural irrigation demand. For this purpose, real-time and weather forecast data, as well as field-specific data (soil moisture, crop data, etc.) for an agricultural irrigation test area are stored and processed in an irrigation app that is freely available to farmers. In addition, data from local groundwater monitoring wells and water meters are read out in real time. These data are transmitted via LoRaWAN to a central gateway and from there via LTE/UMTS to a cloud of the Leibniz computing center where the data are available for a demand-based reclaimed water management. Despite the fact that the determination of the irrigation demand via the automated and cloud-based 'IoT system' is more accurate, the estimation of irrigation demand via modelling, is the faster and more cost-effective approach.

The author sees great potential in combining both approaches (modeling and monitoring of field data) in order to gather comprehensive understanding of the dynamic irrigation demand in agriculture. The field data could serve for the validation and

calibration of a continuously improving model making it easier and faster transferable to other sites. Using such approaches for determining site specific (agricultural) irrigation demand would also help to build awareness of possible site-specific water supply/demand bottlenecks and therefore support farmers in their decision making. Questions such as

- A proper choice of crops adapted to future supply scenarios (i.e., crops with high water demand vs. drought and heat resistant crops),
- implementation of adequate irrigation systems (e.g., drop irrigation vs. sprinkler),
- planning of sufficient storage systems,
- plans on management of available conventional water resources (e.g., surface or ground water),
- conceptualization and design of alternative water supply systems, such as reclamation of municipal wastewater treatment effluents,
- proper pricing of agricultural products in order to account of costs that were so far externalized,

could be addressed more efficiently and effectively. Correspondingly, site specific and daily based irrigation demand data could be provided via open access tools as it is already the case e.g. for drought and soil moisture monitoring (Drought monitor Germany). For instance, ALB Bayern e. V. as a partner of the 'Nutzwasserprojekt' is developing a web-based app providing site- and crop-specific irrigation demand data to farmers.

In addition to savings in water amount, more efficient irrigation and water management practices adapted to local conditions could help to reduce risk in the context of reuse of reclaimed water. The demand-based supply, i.e. only using the amount of water that is actually really needed instead of irrigating based on a rule-of-thumb, would reduce the amount of excess water and therefore reduce surface runoff or infiltration to groundwater. This approach is also recommended within the 'Framework for the environmentally sound use of reclaimed wastewater for agricultural irrigation' (Seis et al. 2016). It is also emphasized elsewhere that by adequate, demand-based irrigation health risks associated with water reuse can be significantly reduced (Chiou 2008; Qin et al. 2015).

To sum up, a more demand-based water management will help improving irrigation efficiency and risk mitigation in the context of water reuse. The modeling approach of the irrigation demand presented this dissertation thesis could serve as a crucial component of such a demand-based water management.

9.2 Relevance of effects of flux/TMP conditions on UF removal efficiency investigated in lab-scale in real case applications

Membrane ultrafiltration is regarded a promising technology for advanced treatment trains designed for water reclamation (Falsanisi et al. 2010; Guo et al. 2014; Seis et al. 2016; Chew et al. 2018). However, mechanism and factors that influence removal efficiency during UF of microbiological contaminants such as bacteria, viruses or ARGs are often not well understood. A better understanding of removal mechanisms and influencing factors is important, especially in the context of the validation monitoring proposed by recent guideline on water quality requirements for water reuse adopted by the 2020/741/EU. Performance targets of ≥ 5.0 LRVs for *E. coli* and ≥ 6.0 LRVs for coliphages are required. To elucidate factors and mechanism affecting the separation of MS2 phages, ARGs or bacteria, two studies were performed.

Within the first study (chapter 5), effects of varying flux and transmembrane pressure (TMP) conditions during ceramic ultrafiltration on the infectivity and retention of MS2 phages was investigated. It was hypothesized that '*increasing fluxes/TMPs during ceramic membrane UF can lead to the damage or inactivation of MS2 phages due to elevated hydrodynamic strain rates*' (**research hypothesis #2.1**). Secondly, it was stated that '*increasing fluxes/TMPs during ceramic membrane UF will cause a decreasing retention of MS2 phages due to the elongation of the MS2 phages in the converging flow field or due to enlargement of the UF pores*' (**research hypothesis #2.2:**). Contrary, to what was initially hypothesized it was found that despite quite high fluxes and TMPs during ceramic membrane UF, the infectivity of MS2 phages was not impaired and that with increasing flux and TMP the physical separation of MS2 phages during ceramic UF was significantly enhanced. Hence, both **research hypotheses #2.1** and **#2.2** were **rejected**.

The second study (chapter 6) investigated key factors influencing removal efficiency of antimicrobial resistance (AMR) during membrane UF. Firstly, it was expected that '*higher ARG abundances in the feed water will result in higher ARGs abundances in the corresponding UF filtrates*' (**research hypothesis #3.1**). The second research hypothesis stated that '*The built-up of a fouling layer during UF will lead to a higher AMR removal efficiency*' (**research hypothesis #3.2**) and thirdly it was assumed that '*Despite nominal pore sizes of UF membranes being smaller than the diameter of bacteria, intact bacteria and AMR will break through UF membranes*' (**research hypothesis #3.3**). **Research hypotheses #3.1** and **#3.3** were **accepted** because we measured higher ARG abundance in the filtrate at higher ARG abundance in the feed and also observed intact bacteria breaking through the UF membrane. **Research hypothesis #3.2** was only **partially confirmed**, since the formation of the fouling layer during membrane UF resulted in a

slightly increased removal of intra- and extrachromosomal ARG or partially had only negligible effects.

The findings of these two independent studies triggered some quite interesting questions, especially since they were partially contradictive:

During ceramic UF at lab-scale, enhanced separation of MS2 phages at increasing fluxes was observed (chapter 5). Apparently, increasing fluxes resulted in higher MS2 phage concentrations in front of the UF membrane which in turn led to enhanced aggregation and size exclusion. At higher initial MS2 phage concentrations in the feed, LRVs even further increased which in turn supports the explanation that increased concentrations due to increased fluxes/TMPs enhance the physical separation of MS2 phages. The results from the pilot-scale study (chapter 6) contradicted the observation obtained during the lab-scale experiments (chapter 5): Higher ARG abundances in the feed water resulted in higher ARGs abundances in the corresponding UF filtrates. Obviously, higher ARG concentrations in the feed had not caused relevant aggregation that resulted in enhanced separation during UF.

First of all, it has to be noted that the experimental conditions between these two studies were substantially different. The study in chapter 5 was conducted at lab-scale while the study in chapter 6 was performed at pilot-scale. Moreover, for the lab-scale study Milli-Q water buffered with PBS and spiked with MS2 phages was used while for the pilot-scale study feed water was secondary treated effluent. This difference has most likely resulted in very different fouling conditions. The UF membrane in the pilot-scale study experienced substantial fouling while the UF membrane in the lab-scale study only showed negligible fouling. Furthermore, lab-scale effects are likely to be different from pilot-scale effects and also the materials of the employed UF membranes were different. A ceramic membrane was employed for the lab-scale study and for the pilot-scale study a polymeric membrane was used. Finally, the ARGs investigated in the pilot scale study basically represent a ‘sum parameter’. The origin and state of the analyzed ARGs was not specified in detail (bound to virus, bacteria, plasmid, integron, etc.) while in the lab-scale study solely MS2 phages as possible mobile genetic elements were analyzed.

The removal of particles during UF membrane filtration is governed mainly by three parameter groups: membrane properties, feed characteristics, and properties of the particles or solutes to be removed (Bellona et al. 2004). Hence, all the aforementioned differences between the studies from chapters 5 and 6, affect at the end the removal efficiency that can be achieved by membrane UF. It is quite complex to identify the main factor that led to the contradicting observations of the two studies but most likely the very different feed water characteristics do not really allow a direct comparison between the

two studies. The explanation of the aggregation effect that was regarded as driver for an enhanced retention of MS2 phages at increasing fluxes in the lab-scale study (chapter 5) is hardly applicable to the study at pilot-scale (chapter 6). While aggregation in the lab-scale experiment was assumed to improve the size exclusion, ARGs in the feed water of the pilot-scale study were anyway already mainly particle associated (Czekalski et al. 2014). Thus, the separation of ARGs at pilot scale, independent of its original origin (bound to viruses, bacteria, plasmids or integrons) is directly influenced by the particles that they associated with. The improvement of ARG removal due to higher feed water concentrations leading to aggregation, can therefore be regarded as negligible for UF applications with wastewater as feed water.

Another interesting and contradictive finding of the two different study was that in the lab-scale study (chapter 5) it was found that with increasing filtration time LRVs of MS2 phages tended to decrease while at pilot scale it was observed that with increasing filtration time the removal efficiency of ARGs slightly increased. Again, the quite different experimental conditions can be seen as the underlying reason for this difference. Within the lab-scale study no observable fouling of the membrane could be observed. This was reasonable since the feed water was low in DOC concentration. In contrast to that the pilot scale-study showed clear fouling of the polymeric UF membrane indicated by the built-up of TMP during the filtration. Membrane fouling which is a function of the feed water quality and membrane characteristics also affect removal efficiency during UF and in many cases it has a positive effect on the UF rejection efficiency due to clogging of pores and reducing their diameter as well as formation of a cake layer (Cheng and Hong 2017; ElHadidy et al. 2014). For instance, ElHadidy et al. (2014) reported that membrane fouling increased the LRV by a value up to 2.5. Apparently, the fouling layer that forms during UF when secondary effluent is used as feed water (chapter 6), counteracts the mechanism that resulted in increasing transmission of MS2 phages in the lab-scale study (chapter 5). Thus, it may be inferred that the formation of a fouling layer is likely to outweigh enhanced diffusion due to an increasing concentration gradient. Despite the ‘contradictive’ observations in these two studies, most importantly it can be concluded that, for validation monitoring for water reuse as recommended within 2020/741/EU, well-defined operating conditions and their influence on the removal performance of viruses, bacteria or antibiotic resistance genes should be taken into account.

In order to confirm or falsify the provided assumptions/explanations it is recommended to repeat the pilot-scale study, however, instead of using a polymeric membrane it is strongly recommended to employ a ceramic UF membrane. By that the comparability with the lab-scale experiments would be more reliable. The experiments can directly be performed with the multi-barrier pilot-scale treatment system consisting

of a ceramic UF as physical barrier as implemented in Schweinfurt for the 'Nutzwasserprojekt'.

9.3 PAC/UF hybrid membrane process – a feasible approach?

Since UF alone does not represent a reliable barrier against TOrCs it has to be combined with an adsorptive or oxidative process. Membrane ultrafiltration (UF) combined with inline dosing of powdered activated carbon (PAC) was identified as a promising hybrid membrane process (HMP) for the production of reclaimed water with adequate quality. Besides an efficient abatement of TOrCs, the PAC/UF HMP had to be optimized with regard to its operation.

This justifies the study presented in chapter 7 in which pilot-scale UF membrane process was combined with inline dosed powdered activated carbon and both, its TOrC removal efficiency and operational stability measured as TMP built-up was investigated in order to identify a possible optimal operational mode. It was hypothesized that '*precoating the UF membrane with a cake layer using polyaluminium chloride (PACl) as coagulant with the continuous inline dosing of PAC prior to UF achieves a significant better TOrC removal efficiency as well as mitigated TMP built-up than an operational mode with simultaneous and continuous inline dosing of coagulant and PAC*' (**research hypothesis #4**). We concluded that the simultaneous and continuous inline dosing of PACl coagulant and PAC prior to the UF had detrimental effects on TOrC removal efficiency. However, precoating with coagulant with continuous inline dosing of PAC prior to UF showed particularly beneficial effects on the reduction of TOrCs and the operational stability. Besides guaranteeing a high hydraulic backwash efficiency, this specific operational mode slightly but significantly attenuated membrane fouling and the hydraulic resistance of the cake layer formed during the filtration cycles. Hence, **research hypothesis #4** can be **accepted**.

Furthermore, it was investigated if the PAC particle layer modified the hydrodynamic flow fields to an extent at which ARG transmission through the UF pores is affected (chapter 8). For this purpose, the **research hypothesis #5** was stated: '*The formation of a PAC particle layer will act like a funnel, thereby increasing the distance over which flow accelerates prior to entering the UF pore and hence decreasing the fluid strain rate, which would result in less deformation of MGEs and therefore less permeation through the UF membrane.*' Based on our investigations it could be concluded that the presence of the PAC particle cake layer only had negligible effects on the hydrodynamic strain rates relevant for MGE deformation. Therefore, the potential adsorption onto PAC or entrapment of AMR inside the PAC pores in a hybrid PAC-UF process is expected to be

the major abatement mechanism of AMR while hydrodynamic effects can be neglected. Based thereon, **research hypothesis #5** was **rejected**.

Despite the efficient TOrC removal and the fact that by coagulant precoating stable operation could be maintained during the PAC/UF HMP, some critical aspects have to mentioned.

The PAC/UF HMP showed efficient removal of TOrCs when 'super fine' PAC ($d_{50} \approx 6$ µm) was employed. When 'coarse' PAC ($d_{50} \approx 20$ µm) was used, a significantly lower TOrC removal could be achieved. The issue is that only the 'coarse' PAC is commercially available while the 'super fine' PAC has to be ground smaller. The associated costs are therefore much higher which limits an economical scalability of this technology. In addition, the PAC had only a rather short contact time (duration of one filtration cycle which was ≈60 min). Hence, the adsorption capacity of the PAC is far from being exhausted after one filtration cycle when it is flushed out of the UF membrane capillaries during hydraulic backwash. A lot of sludge, rich in PAC with high residual adsorption capacity is generated. Within the context of a life-cycle assessment this would certainly have a particularly negative impact since PAC is commonly generated from non-renewable coal and requires energy-intensive thermal activation to develop its adsorption properties (Thompson et al. 2016). Another potential drawback is the handling of PAC. Despite the quite compact implementation of a PAC/UF HMP, the handling of PAC will require special safety measures, in particular with regard to explosion protection (Strudgeon et al. 1980).

Even though some degree of removal of ARGs, viruses, or bacteria may be achieved via PAC due to possible adsorption or entrapment of ARB/ARGs inside the PAC pores (Zhang et al. 2017; Ashbolt et al. 2018; Rizzo et al. 2020; Calderón-Franco et al. 2020), PAC does not represent a disinfection process. Moreover, as observed in the studies contained in this thesis (chapter 5 and 6) or elsewhere (Chhipi-Shrestha et al. 2017; Crittenden and Harza 2005), UF alone is capable of only a limited removal of bacteria, viruses, or ARGs. Hence, the PAC/UF HMP will require an additional disinfection step, such as UV irradiation or chlorination. Some TOrCs that are only poorly adsorbable (such as gabapentin) will also require additional treatment for the production of a chemically as well as microbiological safe water quality.

Based on this discussion it is worth to consider an alternative treatment train. There exist numerous options for advanced water treatment that might be promising for the production of reclaimed water with adequate quality (Table 9-1). Microbial or TOrC removal efficiencies that can be expected during some of the listed advanced water treatment technologies are summarized in Table 9-2 and Table 9-3.

Table 9-1: Overview of different advanced treatment methods.

Advanced treatment process	**Target contaminants**	**Reference**
Ultrafiltration (UF)	Capable to remove bacteria (also ARB), viruses, colloids, partly dissolved organics; Salts can pass; DNA (ARGs) may pass as well but ARGs were also reported to be efficiently removed;	(González et al. 2015; Rizzo et al. 2020; Hiller et al. 2019)
Nanofiltration (NF)	Retention of (in-)organic CECs, especially when hydrophobic; Lowers concentration of total dissolved solids (TDS) and salinity to a certain degree; Membrane dependent retention;	(González et al. 2015; Rizzo et al. 2020)
Reverse Osmosis (RO)	Rejects compounds down to a certain molecular weight, including most salts and dissolved organics;	(González et al. 2015)
Ultraviolet irradiation (UV)	Bacteria, viruses, microorganisms retained in general; Abatement of selected CECs at high dosage; Inactivation of ARB, also verified for ARGs, dose-dependent;	(Rizzo et al. 2020)
Ozonation (O_3)	Degradation of CECs; General disinfection, inactivation of ARB, of ARGs to some extend; Application of biological post-treatment to remove formed disinfection by-products (DBPs), consider related microbial/ARB re-growth;	(Rizzo et al. 2020)
Activated carbon adsorption (AC)	Trapping of ARB and ARGs in pores of carbon expected; Effective removal of well-adsorbable CECs;	(Rizzo et al. 2020)
Biologically active carbon adsorber (BAC)	= Granular activated carbon (GAC) filter, utilized for a longer time period, a biofilm is formed on the surface; Biological degradation and adsorption of compounds, e.g. transformation products (TPs) from O_3;	(Velten 2008)
Advanced oxidation processes (AOPs)	= combination of two or more oxidants (homogeneous processes e.g. UV/ hydrogen peroxide (H_2O_2), O_3/H_2O_2 or a solid semiconductor with a light source = heterogeneous processes e.g. UV/titanium dioxide (TiO_2)) CECs well degraded, target compounds depend on actual applied AOP; Effective inactivation of ARB, ARG often not sufficiently inactivated;	(Rizzo et al. 2020)

Table 9-2: LRVs expected during various conventional and advanced water treatment technologies.

Rejected pathogen	**Treatment method**	**LRV**	**Reference**
Protozoa	Primary sedimentation	0–1	(Chhipi-Shrestha et al. 2017)
	Biological nutrient removal (BNR) (e.g. CAS)	0–1	(Chhipi-Shrestha et al. 2017)
	MF	6–8	(Chhipi-Shrestha et al. 2017)
	MF, UF	>7[a]	(Crittenden et al. 2012, p. 849)
	UV	3–4	(Chhipi-Shrestha et al. 2017)
Bacteria	Primary sedimentation	0–1	(Chhipi-Shrestha et al. 2017)
	BNR	1–2	(Chhipi-Shrestha et al. 2017)
	MF	4–6	(Chhipi-Shrestha et al. 2017)
	MF	>8[a]	(Crittenden et al. 2012, p. 849)
	UF	∞[b]	(Crittenden et al. 2012, p. 849)
	UV	2–4	(Chhipi-Shrestha et al. 2017)
Viruses	Primary sedimentation	0–1	(Chhipi-Shrestha et al. 2017)
	BNR	0–2	(Chhipi-Shrestha et al. 2017)
	MF	2.5–6	(Chhipi-Shrestha et al. 2017)
	UF with low molecular weight cut-off rating	>7.2[a,c]	(Crittenden et al. 2012, p. 850)
	UV	0.25–4	(Chhipi-Shrestha et al. 2017)

[a] maximum value, can be lower at unfavorable conditions

[b] complete rejection expected

[c] LRV achieved for model virus of 25 nm in size and UF membrane with molecular weight cut-off (MWCO) of 100,000 Da

Table 9-3: TOrCs removal efficiencies during conventional and widely applied advanced water treatments.

TOrC	Treatment method	Removal in %, arithmetic mean in []	Reference
Diclofenac	Secondary treatment	0–68 [10]	(Biel-Maeso et al. 2018)
	CAS	<0–81	(Krzeminski et al. 2019)
	PAC; GAC	[69]; [72]	(Rizzo et al. 2019)
	O_3	98–100	(Rizzo et al. 2019)
	UV-C/H_2O_2	99–100	(Rizzo et al. 2019)
Carbamazepine	Secondary treatment	2–37 [18]	(Biel-Maeso et al. 2018)
	CAS	(-90) – (-3)	(Krzeminski et al. 2019)
	PAC; GAC	90–92; [72]	(Rizzo et al. 2019)
	O_3	97–100	(Rizzo et al. 2019)
	UV-C/H_2O_2	82–99	(Rizzo et al. 2019)
Clarithromycin	Secondary treatment	18–99 [80]	(Biel-Maeso et al. 2018)
	CAS	[37]	(Krzeminski et al. 2019)
	PAC; GAC	88–95; [54]	(Rizzo et al. 2019)
	O_3	99–100	(Rizzo et al. 2019)
	UV-C/H_2O_2	81–89	(Rizzo et al. 2019)
Sulfamethoxazole	Secondary treatment	19–79 [49]	(Biel-Maeso et al. 2018)
	CAS	35–84	(Krzeminski et al. 2019)
	PAC; GAC	58–64; [59]	(Rizzo et al. 2019)
	O_3	94–97	(Rizzo et al. 2019)
	UV-C/H_2O_2	38–99	(Rizzo et al. 2019)

Operational conditions for the listed studies:

- Biel-Maeso et al. (2018): Municipal wastewater treatment plant consisting of secondary biological treatment, comprising nitrification, denitrification and UV disinfection, treatment capacity ~100.000 m^3/day
- Krzeminski et al. (2019): reviewed the removal TOrC efficiencies of several studies (>20) without specifying operational conditions
- Rizzo et al. (2019): DOC 5-10 mg/L, PAC contact time 20-60 min, PAC dose 5-20 mg/L, GAC empty bed contact time ~15 min, 7000-25000 bed volumes during GAC treatment, specific O_3 doses 0.6 O_3/g DOC, UV-C/H_2O_2 20–50 mg H_2O_2/L with low pressure mercury lamps (254 nm) at 70 W/m^2

Based on the consideration of the previously summarized treatment performances of selected advanced treatment technologies (Table 9-1, Table 9-2, Table 9-3), a viable and particularly promising treatment option could be the combination of ceramic UF, followed by ozonation (O_3), biological activated carbon (BAC) filters, and a final UV disinfection. This multi-barrier treatment system was designed and implemented by a big team consisting of engineers, locksmiths, electricians and construction workers (from Xylem, Nanostone, "Stadtentwässerung Schweinfurt", De.EnCon, and TUM including the author himself) for the so called '[Nutzwasserprojekt](#)' located in Schweinfurt. This treatment combination is not only likely to be less cost intensive, but also will produce a better water quality than the PAC/UF HMP (Schwaller et al. 2020). The treatment efficiencies that can be expected by applying either the PAC/UF or the UF/O_3/BAC/UV HMP are compared in Figure 9-1 and Figure 9-2. The UF/O_3/BAC/UV hybrid membrane process is expected to outperform the PAC/UF/UV hybrid membrane process with regard to the reduction of microbiological parameters as well as TOrCs. The underlying modeling approach was described by Schwaller et al. (2020). The higher removal

performance by the HMP UF/O_3/BAC/UV in comparison to the HMP PAC/UF is also in accordance with the removal efficiencies provided in Table 9-2 and Table 9-3.

In order to confirm or reject the assumptions with regard to the benefit of the UF/O_3/BAC/UV HMP, it is recommended to accompany the 'Nutzwasserprojekt' with research focusing on treatment efficiency and life-cycle assessment as suggested by Miller (2006).

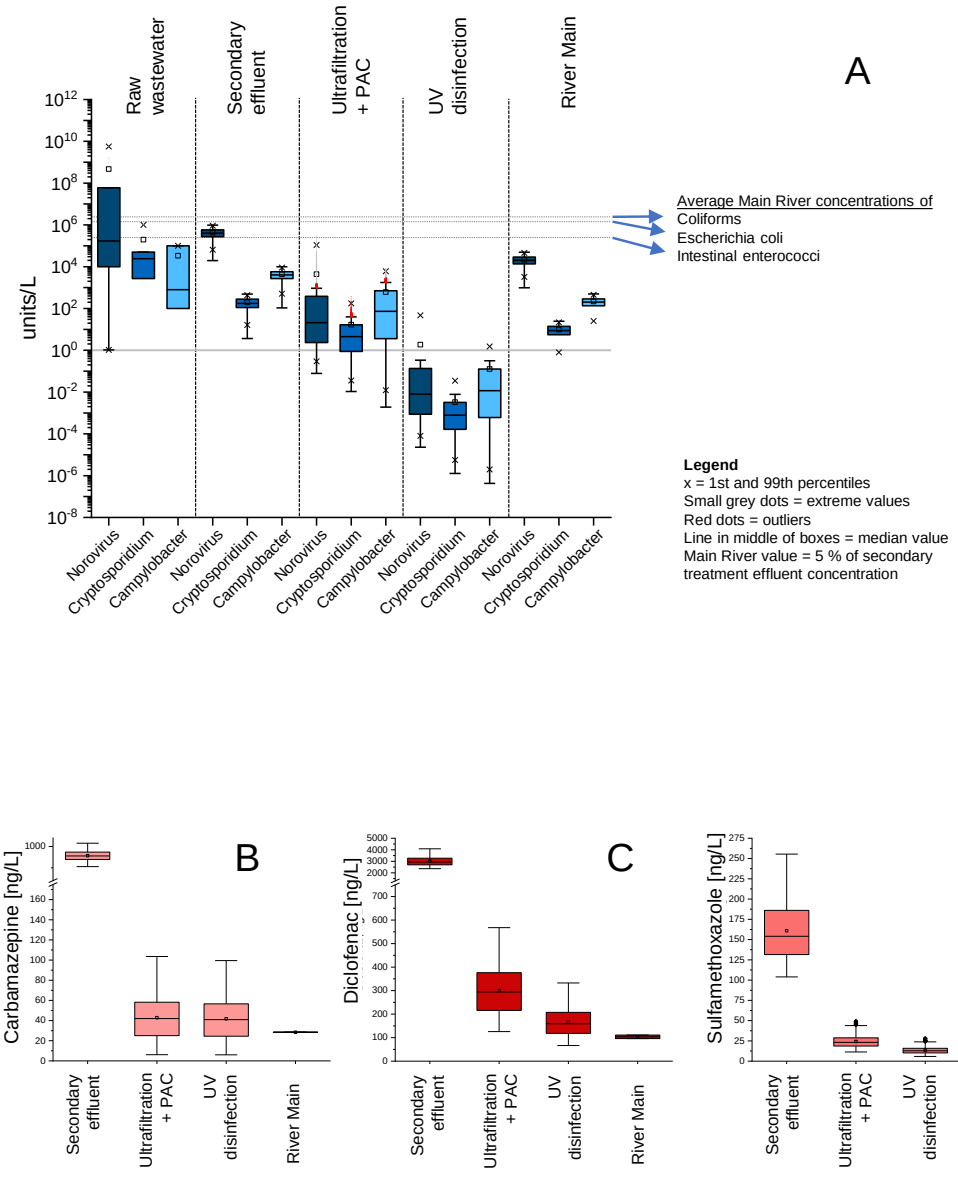

Figure 9-1: Modeled concentrations of typical pathogens and TOrCs during the advanced treatment of wastewater via PAC/UF/UV HMP; the box includes the values between the 25 % and 75 % quantile, the horizontal line within the box represents the median, the point represents the arithmetic mean and the ends of the "whiskers" of the box plots mark the 1.5 times the interquartile range. The underlying modeling approach is described by Schwaller et al. (2020).

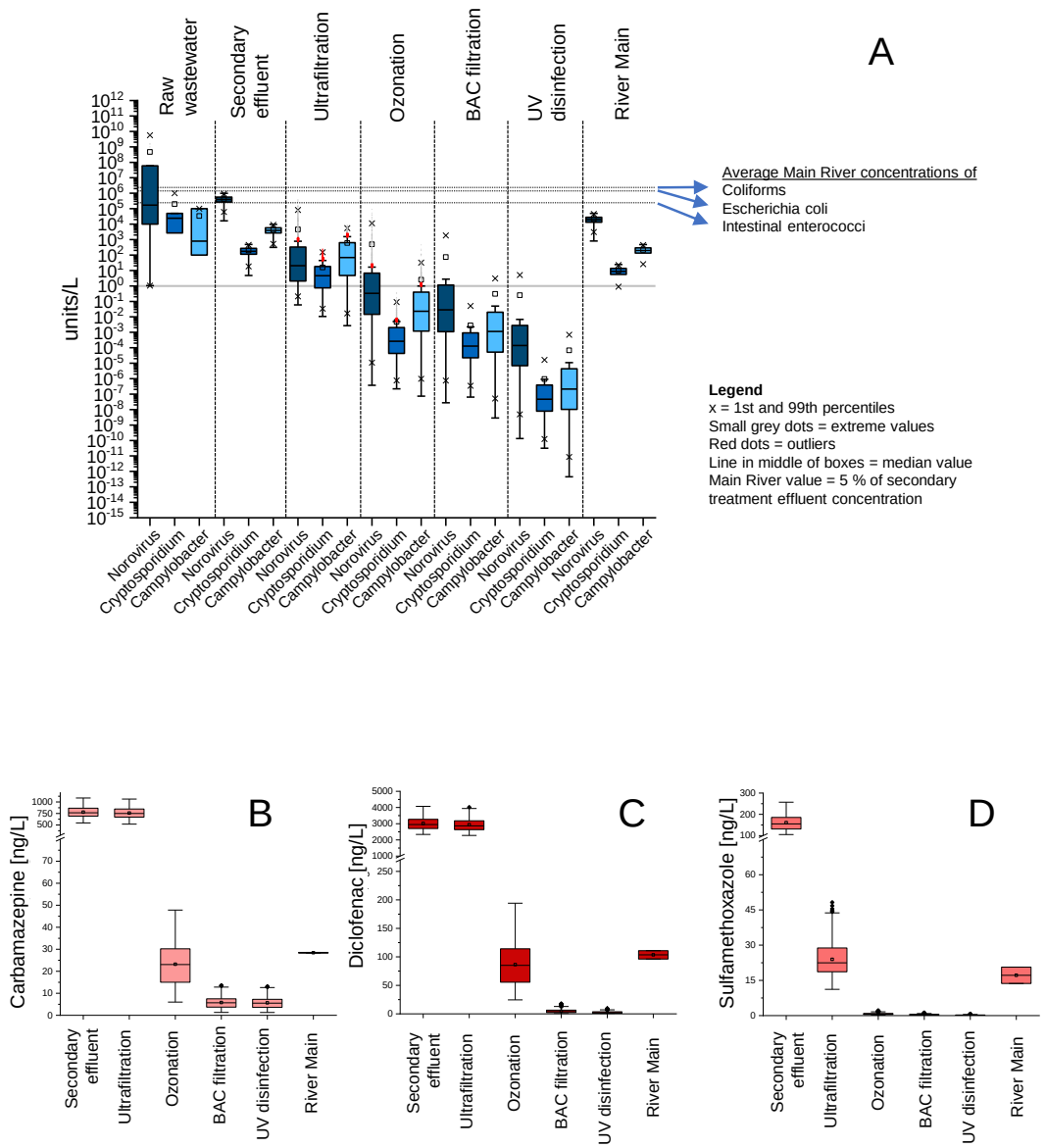

Figure 9-2: Modeled concentrations of typical pathogens and TOrCs during the advanced treatment of wastewater via UF/O_3//BAC/UV HMP; the box includes the values between the 25 % and 75 % quantile, the horizontal line within the box represents the median, the point represents the arithmetic mean and the ends of the "whiskers" of the box plots mark the 1.5 times the interquartile range. The underlying modeling approach is described by Schwaller et al. (2020).

9.4 Accumulation potential of pollutants in the soil, groundwater or on/in irrigated crops in the context of water reuse

If insufficient water treatment is applied or management is not properly performed, reclaimed water may still contain contaminants of concern, such as TOrCs, ARGs, viruses, bacteria, or heavy metals in relevant concentrations. These contaminants can accumulate in the environment and pose a risk for human or environmental health. Within this section, a brief summary of findings from literature are provided to gain a better understanding of risks potentially associated with water reuse for agricultural irrigation.

Various studies have already shown the accumulation potential of different pollutants in the soil, in groundwater or on irrigated crops during the reuse of reclaimed water for agricultural irrigation (Chen et al. 2013a; Chen et al. 2013b; Chiou 2008; Gallegos et al. 1999; Mahjoub et al. 2011; Qin et al. 2015; Wang et al. 2003; Xu et al. 2010; Zemann et al. 2016; Pedrero et al. 2010). However, these studies were focusing only on the effects of reusing secondary wastewater treatment plant effluent (wastewater after conventional treatment, i.e. mechanical and biological) or even raw sewage (Gallegos et al. 1999). They did not investigate the impacts of reclaimed water after advanced treatment.

Chen et al. (2013a) and Wang et al. (2017) concluded that the reuse of reclaimed water is beneficial both for plant growth and for the soil itself due to nutrients it contains (mainly nitrogen) and the associated fertilizing effect. As a consequence, economic benefits for agriculture are expected (Chen et al. 2013a). The risk that the soil or groundwater are contaminated by heavy metals or TOrCs present in reclaimed water was found to be very low, especially when appropriate and irrigation based on agronomic rates is employed. The accumulation of various TOrCs (e.g., clofibric acid, ibuprofen, 4-tert-octylphenol, 4-n-nonylphenol, naproxen, triclosan, diclofenac, bisphenol A and estrone) in sandy-loamy and loamy-sandy soils was investigated and it was found that even after a long irrigation period of 10 years only very low concentrations of <1 ng/g–140 ng/g were detectable in the topsoil within the upper 20 cm (Chen et al. 2013b). Through adsorption and microbial degradation, most of the TOrCs were already completely retained in the first 40 cm of the soil. Leaching and volatilization of TOrCs from the soil was regarded as unlikely (Chen et al. 2013b). This in turn means that the risk of groundwater contamination with the corresponding TOrCs would be classified as rather low. Hence the ecological risk from an accumulation of TOrCs in the soil for soil biota due to irrigation with reclaimed water was considered as rather low (Chen et al. 2013b). It is expected that also the human health risk can be reduced to a safe level by adequate irrigation based on agronomic rates (Chiou 2008). Despite comparatively adverse conditions (extremely sandy soils with low adsorptive capacity), very low or not even measurable concentrations of endocrine disruptors in soils irrigated with reclaimed water

were observed (Mahjoub et al. 2011). Another study reviewed the literature addressing the behavior of TOrCs in agricultural soils irrigated with reclaimed water and the adverse effects on soil organisms (including microorganisms and fauna), crops and humans (via food intake) (Qin et al. 2015). In addition to strategies and potential technologies to degrade or remove these TOrCs from soil, irrigation strategies and agricultural practices to minimize the transfer of TOrCs to crops and to groundwater were investigated. Based thereon, it was concluded that the agricultural risks originating from TOrCs possibly present in reclaimed water could be minimized under certain agroecological conditions. In particular, conservative practices (irrigation water of good quality, demand-based irrigation, management of crops while ensuring a low intake of pollutants, etc.) are urgently needed to minimize potential ecological hazards from TOrCs. The development of regulations specifically for irrigation with treated water, with adequate limits for different organic trace substances, was strongly recommended for safe irrigation use (Qin et al. 2015).

Elsewhere also the positive effect of irrigation with reclaimed water on the chemical and physical properties of the soil (supply of nutrients and organic matter) and the resulting higher yield and improved soil fertility were shown (Xu et al. 2010). However, it was also emphasized that there is an increased risk of heavy metals being washed out and seeping into the groundwater, particularly in regions with ‘light’ soils (sandy texture and poor in organic material). Another study highlighted the risk that TOrCs accumulated in the soil could be remobilized and leaching then into the groundwater (Zemann et al. 2016). In particular, chemicals with a high persistence against microbiological degradation (e.g., carbamazepine, artificial sweeteners or iodinated X-ray contrast media) are more likely to be transported into the groundwater by percolation. However, it should be noted that this study was conducted under arid climatic conditions and on sandy soils with poor or strongly inhibited microbiological activity.

Summarizing, besides a proper irrigation management, an advanced water treatment further mitigates the risk originating from the application of reclaimed water.

10 OVERALL CONCLUSION AND OUTLOOK

This thesis is addressing two main aspects that are important in the context of planning and implementation of a water reuse project for agricultural irrigation purposes.

Firstly, gaining an understanding of the agricultural irrigation demand. For the water treatment and storage systems for water reuse, in particular covering daily peak irrigation demand is important. Since respective field data are usually low in quality or even not available at all, we developed a modelling approach for the estimation of the site-specific irrigation demand. The modeled data could be validated by corresponding field data and by the application of this modelling approach it was possible to estimate overall daily gross irrigation demand for an entire agricultural area cultivated with different crops on different soils (**chapter 4**). The modeling approach represents a solid basis for future water reuse projects in the agricultural sector. Moreover, the simulation of the crop-specific, site-specific or overall daily, monthly, or annual irrigation demand will be very helpful for a more sustainable, demand-oriented water management which can be properly adapted to local conditions (climate, soil, water availability, crop, etc.).

Secondly, ultrafiltration (UF) combined with powdered activated carbon (PAC) was assessed with respect to its removal efficiency and operational stability measured via the built-up of transmembrane pressure. Initially, ceramic and polymeric UF without PAC was investigated focusing on its abatement potential of mobile genetic elements such as MS2 phages, ARGs and bacteria in general (**chapter 5** and **6**). During lab-scale experiments in **chapter 5** which was performed at very controlled experimental conditions (e.g., Milli-Q with spiked MS2 phages), it was observed that the removal efficiency during ceramic UF depends on the applied flux or transmembrane pressure (TMP) conditions. With increasing flux, an enhanced removal of MS2 phages could be observed. Within the pilot-scale study in **chapter 6**, most important findings were: The formation of the fouling layer during membrane UF resulted in a slightly increased removal of intra- and extrachromosomal ARG or partially had only negligible effects. Furthermore, higher ARG abundance in the feed resulted in higher ARG abundance in the filtrate and finally, some intact bacteria were able to break through the UF membrane. The results obtained within these two chapters were partially contradictive. The very different experimental conditions were identified as reason for the deviating results. Nevertheless, the main conclusion of these two studies is that operational conditions such as flux, TMP, membrane fouling and feed water characteristic are relevant factors influencing the overall treatment efficiency of membrane UF. This is of high relevance in the context of the guideline with respect to quality requirements for water reuse adopted by the 2020/741/EU. When it comes to the required validation monitoring, it is strongly

recommended to investigate removal efficiency at well-defined operational conditions in order to properly account for its effects on the overall removal efficiency of the specified microorganisms. After this initial assessment of the UF technology alone, the hybrid membrane process UF combined with inline dosed PAC was investigated in detail (**chapter 7** and **8**). It was found that precoating with coagulant with continuous inline dosing of PAC prior to UF had particularly beneficial effects on the operational stability as well as the reduction of TOrCs (**chapter 7**). Hydrodynamic effects of the PAC particle cake layer on the deformation of mobile genetic elements such as plasmids were negligible (**chapter 8**).

With regard to the assessment of the hybrid membrane process PAC/UF it can be concluded that due to its compactness and its promising results with regard to TOrCs removal while maintaining operational stability it constitutes a promising treatment system for some cases. For example, where crops that are not intended for raw consumption, need to be irrigated at short notice and for a short time period due to an emergency situation (e.g. heavy drought). However, for long-term applications with very high microbiological and chemical water quality requirements (e.g. crops eaten raw) alternative options should be preferred such as the hybrid membrane process UF combined with a downstream ozonation, biological activated carbon filter and a final UV disinfection (**chapter 9**).

11 APPENDIX

11.1 List of publications

Research articles (peer-reviewed)

1. *Schwaller, Christoph; Keller, Yvonne; Helmreich, Brigitte; Drewes, Jörg E. (2021): Estimating the agricultural irrigation demand for planning of non-potable water reuse projects. In Agricultural Water Management 244, p. 106529. DOI: https://doi.org/10.1016/j.agwat.2020.106529*

   This publication is included in Chapter 4.

2. *Schwaller, Christoph; Knabl, Magdalena; Helmreich, Brigitte; Drewes, Jörg E. (2022): Effects of varying flux and transmembrane pressure conditions during ceramic ultrafiltration on the infectivity and retention of MS2 bacteriophages. In Separation and Purification Technology 299, p. 121709. DOI: https://doi.org/10.1016/j.seppur.2022.121709*

   This publication is included in Chapter 5.

3. *Hiller, Christian X.; Schwaller, Christoph; Wurzbacher, Christian; Drewes, Jörg E. (2022): Removal of antibiotic microbial resistance by micro-and ultrafiltration of secondary wastewater effluents at pilot scale. In Science of The Total Environment, p. 156052. DOI: https://doi.org/10.1016/j.scitotenv.2022.156052*

   This publication is included in Chapter 6.

4. *Schwaller, Christoph; Hoffmann, Grit; Hiller, Christian X.; Helmreich, Brigitte; Drewes, Jörg E. (2021): Inline dosing of powdered activated carbon and coagulant prior to ultrafiltration at pilot-scale – Effects on trace organic chemical removal and operational stability. In Chemical Engineering Journal 414, p. 128801. https://doi.org/10.1016/j.cej.2021.128801*

   This publication is included in Chapter 7.

5. *Schwaller, Christoph; Fokkens, Kevin; Helmreich, Brigitte; Drewes, Jörg E. (2022): CFD simulations of flow fields during ultrafiltration: Effects of hydrodynamic strain rates with and without a particle cake layer on the permeation of mobile genetic elements. In Chemical Engineering Science 254, p. 117606. DOI: https://doi.org/10.1016/j.ces.2022.117606*

   This publication is included in Chapter 8.

Additional research articles (peer-reviewed) in other research areas

1. *Al-Azzawi, Mohammed S. M.; Kefer, Simone; Weißer, Jana; Reichel, Julia; Schwaller, Christoph; Glas, Karl et al. (2020): Validation of Sample Preparation Methods for Microplastic Analysis in Wastewater Matrices – Reproducibility and Standardization. In Water 12 (9), p. 2445. DOI: https://doi.org/10.3390/w12092445*

Research articles (non-peer-reviewed)

1. *Drewes, Jörg E.; Zhiteneva, Veronika; Karakurt, Sema; Schwaller, Christoph: Risk management in water reuse – International perspective and approaches for Germany (2019): https://www.wasser.tum.de/fileadmin/w00bup/trinkwave/zbl_I_grundwasser_0059_0066_drewes_et_al_online_wm.pdf*

Research reports

1. *Schwaller, Christoph; Helmreich, Brigitte; Gerdes, H.; Drewes, Jörg E. (2020): „Abschlussbericht zum Forschungsvorhaben Nutzwasser – Gewinnung und Einsatzmöglichkeiten am Beispiel der Schweinfurter Trockenplatte (AZ: 52-4429-10)': https://www.wwa-kg.bayern.de/abwasser/nutzwasser/doc/projekt_nutzwasser_abschlussbericht_barrierefrei.pdf*

Conference talks

1. *Schwaller, Christoph; Helmreich, Brigitte; Drewes, Jörg E. (2019): 'Feasibility of water reclamation for agricultural and urban reuse in Northern Franconia, Germany' at 12th IWA International Conference on Water Reclamation and Reuse in Berlin, Germany, 18.06.2019*

2. *Schwaller, Christoph; Helmreich, Brigitte; Scheyer, Nadine; Ahmadi, Javad; Heller, Helmut; Gerdes, Heiko; Gebhardt, Jens; Kirchner, Stefan; Baumann, Louis; Zumkeller, Frederik; Kebinger, Bastjan; Drewes, Jörg E. (2021): 'Nutzwasser - Water reclamation for agricultural and urban reuse' at BLUE PLANET Berlin Water Dialogues, virtual conference, 25.11.2021*

3. *Schwaller, Christoph; Helmreich, Brigitte; Drewes, Jörg E. (2022): Membrane UF combined with inline dosed PAC: 'A promising process for advanced wastewater treatment?' at 17th IWA Leading Edge Conference on Water and Wastewater Technologies in Reno, Nevada (USA), 30.03.2022*

Conference posters

1. *Schwaller, Christoph; Helmreich, Brigitte; Gerdes, H.; Drewes, Jörg E. (2020): „Nutzwasser – Gewinnung und Einsatzmöglichkeiten am Beispiel der Schweinfurter Trockenplatte" at IESP ad hoc Workshop „Bewässerung in ländlichen und urbanen Räumen" in Garching, Germany, 02.07.2019*

11.2 List of supervised student theses

Master theses

1. *Keller, Yvonne: 'Abschätzung des landwirtschaftlichen Bewässerungsbedarfs im Raum Schweinfurt mit Hilfe des CROPWAT-Modells', submitted 04.11.2019*

2. *Akhimova, Elizaveta: 'Recycling of laundry wastewater with the application of ceramic nanofiltration', submitted 14.12.2021*

3. *Knabl, Magdalena: 'Effects of varying flux and transmembrane pressure on the retention and integrity of MS2 bacteriophage during ceramic ultrafiltration', submitted 10.03.2022*

4. *Bergmann, Felix: 'Untersuchungen zur Brauchwassernutzung im Bereich des Vilstalsees bei Marklkofen', ongoing*

Study projects

1. *Stauner, Manoel: 'Strategien zur Wasserwiederverwendung in der Schweinfurter Trockenebene: Regenwasserwiederverwendung zur Bedarfskompensierung in der Landwirtschaft in den Regionen Gochsheim und Schwebheim', submitted 14.05.2019*

2. *Ahmadi, Javad: 'Investigation of artifact formation and changes of relevant characteristics of polystyrene microparticles by various sample preparation and isolation methods', submitted 20.10.2019*

3. *Akhimova, Elizaveta: 'A review on the hybrid systems of UF, MF combined with O3 and PAC, with the focus on removal efficiencies of micropollutants including pharmaceuticals and antibiotic resistant bacteria', submitted 02.11.2020*

4. *Fokkens, Kevin: 'Meso to Nanoscale CFD Simulations of Tubular Ultrafiltration Membranes: Effects of Particle Cake Layer on the Permeation of Mobile Genetic Elements', submitted 08.04.2021*

5. *Knabl, Magdalena: 'Possible impacts of urban and agricultural irrigation with reclaimed water on the related ecological system - A holistic literature review', submitted 08.04.2021*

6. *Bertram, Poojesh: 'Pre- and post-ozonation combined with ceramic UF and its effects on MS2 removal', ongoing*

7. *Al-Areqi, Ayaa: 'Investigation of coagulation and its effects on particle zeta potential, DOC removal, and UV_{254} reduction', ongoing*

Bachelor theses

1. *Lange, Kim: 'Quantitative und Qualitative Betrachtung von Niederschlag in Unterfranken zur landwirtschaftlichen Bewässerung', submitted 20.03.2020*

2. *Lehrer, Clara: 'Qualitative Bewertung von auf Dachflächen gesammeltem Niederschlags-wasser für landwirtschaftliche Bewässerungszwecke', submitted 09.10.2020*

3. *Heymes, Natasha: 'Die Wasserversorgung der Marktgemeinde Peißenberg', submitted 17.02.2022*

11.3 Supplementary information for Chapter 4

11.3.1 Figures

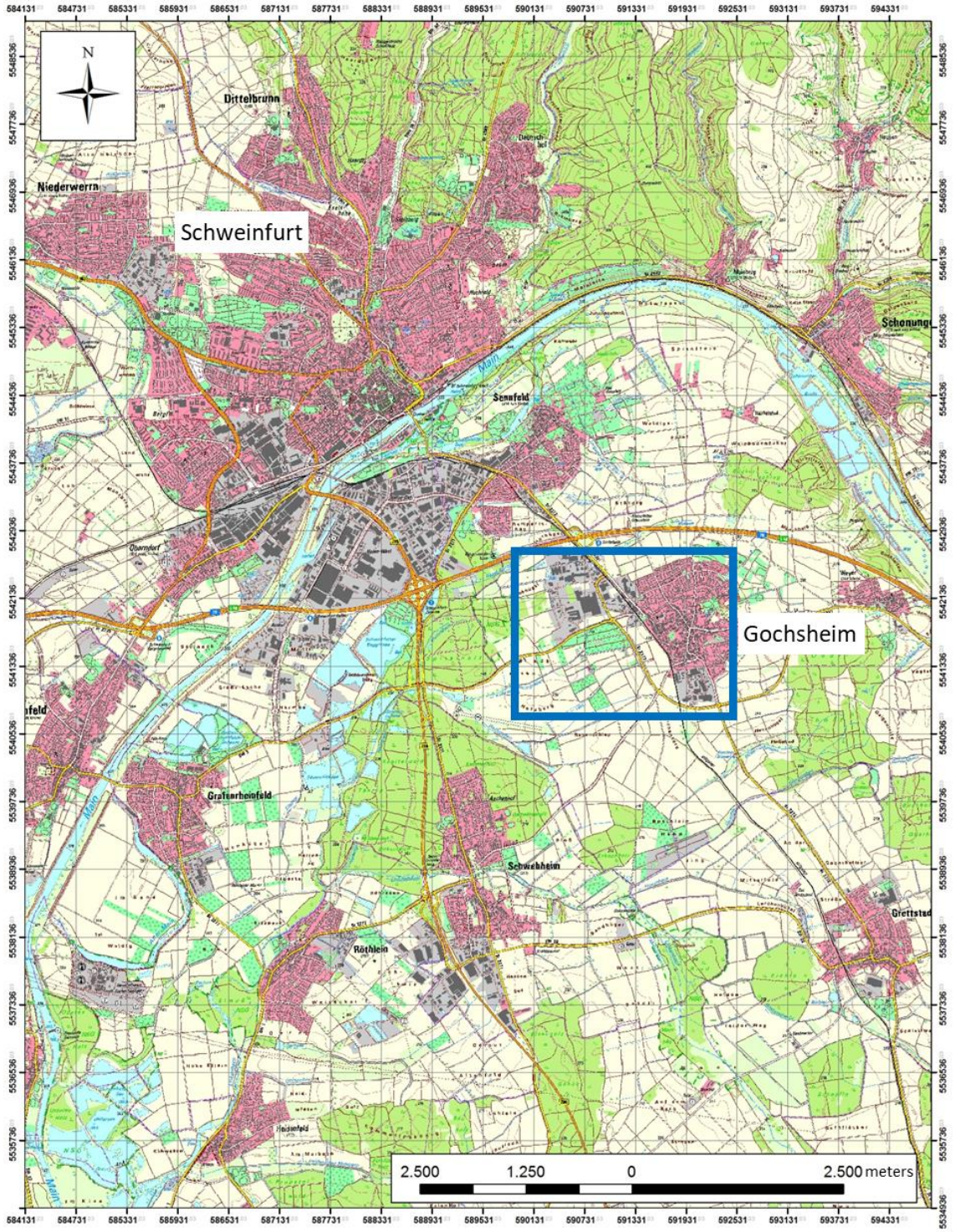

Figure 11-1: Planning region – case study area Gochsheim is framed in blue color (map source: WWA Bad Kissingen).

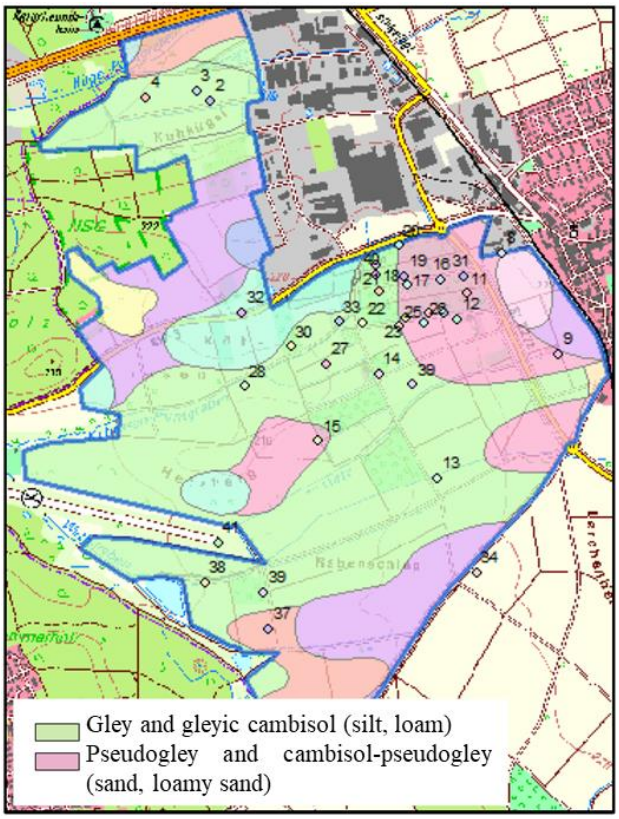

Figure 11-2: Soil types – agricultural area Gochsheim (BGR - Geoviewer 2020).

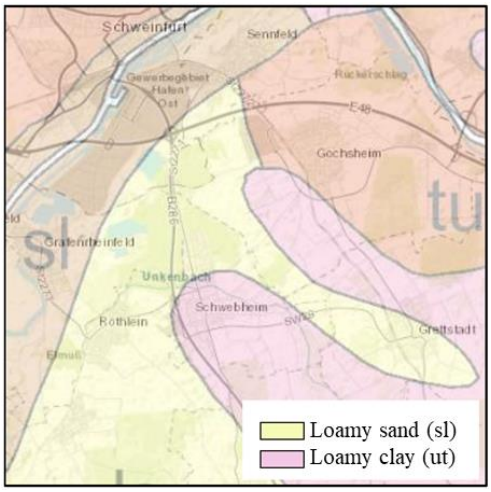

Figure 11-3: Soil type groups of topsoil in planning area (BGR - Geoviewer 2020).

Figure 11-4: Plant-available water [mm] in effective rooting zone (left panel) and depth [dm] of effective rooting zone (right panel) in planning area (BGR - Geoviewer 2020).

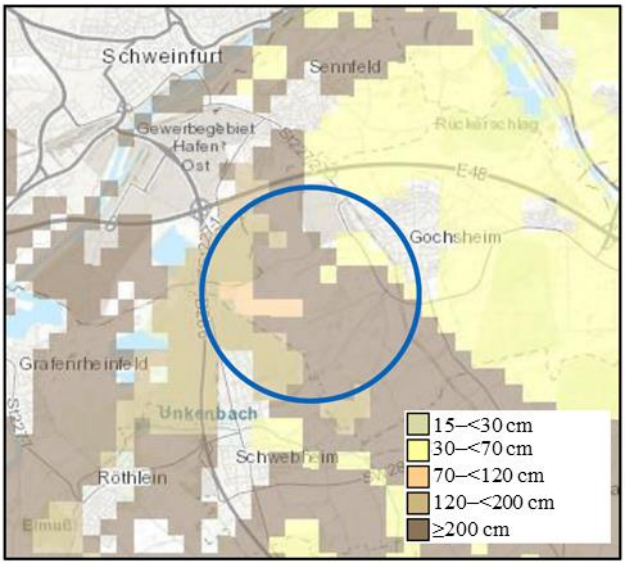

Figure 11-5: Maximum rooting depth of soil in planning area Gochsheim (BGR - Geoviewer 2020).

Figure 11-6: Groundwater table in Gochsheim for the year 2015 adapted from BGS Umwelt.

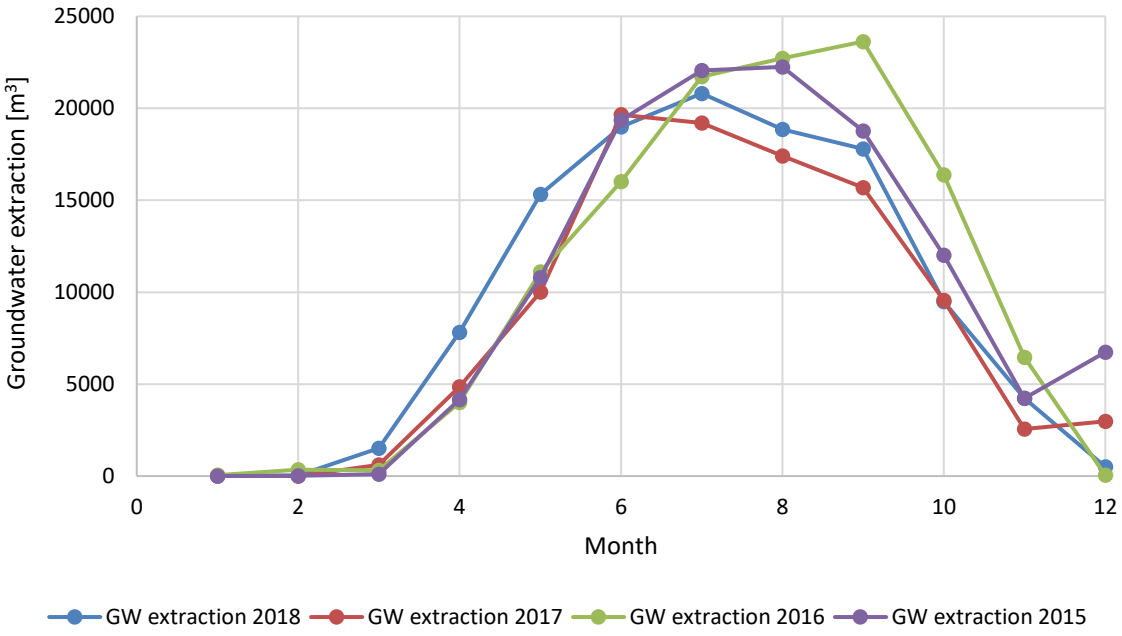

Figure 11-7: Monthly groundwater (GW) extraction rates in Gochsheim for agricultural irrigation purposes.

11.3.2 Tables with comments

Table 11-1: Data basis for modelling agricultural irrigation demand with CROPWAT 8.0.

Category	Parameter	Source/reference
Geographical data	Altitude, latitude, longitude	GPS data
Climate data	Precipitation, minimum/maximum air temperature, humidity, wind speed, sunshine duration	DWD (DWD 2018b), climate station Bad Kissingen
Crop data	Seeded crops, rooting depth, Seeding/planting period, growth stages, length of stage, K_c-values (crop coefficients), critical depletion, yield response	Table 11-3 and: Integrated Administration and Control System (IACS) data obtained from Bavarian State Research Center for Agriculture (LfL), Amt für Ernährung, Landwirtschaft und Forsten Kitzingen (AELF), Hochschule Geisenheim (2019), Savva et al. (2002), Allen et al. (1998), DWD (2018a), Wachendorf et al. (2018), Smith (1992), FAO-CROPWAT-Software 8.0: Help, FAO-CROPWAT-Software 8.0: Default values, BLZ (2017), Wirtschaftliche Vereinigung Zucker e.V. (2020), Mastel (2002), BZfE (2016), BZfE (2019), LfL (2006)
Soil data	Soil types	BGR-Geoviewer (2020), Wasserwirtschaftsamt Bad Kissingen, interviews with local farmers
	Mean effective rooting zone (RZ_e), plant-available water (PAW), plant available water in the effective rooting zone ($PAW*RZ_e$)	Amelung et al. (2018), BGR-Geoviewer (2020), Ad-hoc-AG Boden (2005)
	Maximum rooting depth	Amelung et al. (2018), BGR-Geoviewer (2020), Savva et al. (2002),
Irrigation efficiency	Assumption of 80 %	Savva et al. (2002), LfL (2008), local farmers
Recorded data regarding local irrigation requirements	Groundwater pumping rates for the years 2014–2018	Local irrigation association of Gochsheim, local farmers Gochsheim, Wasserwirtschaftsamt Bad Kissingen

Table 11-2: Cultivated crops and the respective shares of the fields cultivated with the corresponding crops in the total agricultural area in Gochsheim, derived from IACS.

Cate-gory	Crop name	before 2005	2005	2006	2007	2008	2009	2010	2011	2012	2013	2014	2015	2016	2017	2018	2019
Vegetables and other crops	Marrow	0 %	0 %	0 %	0 %	0 %	0 %	0 %	0 %	0 %	0 %	0 %	0 %	16 %	0 %	0 %	0 %
	Cabbage	0 %	0 %	0 %	0 %	0 %	0 %	0 %	0 %	0 %	0 %	0 %	0 %	16 %	18 %	28 %	28 %
	Lettuce	0 %	0 %	0 %	0 %	0 %	0 %	0 %	0 %	0 %	0 %	0 %	0 %	18 %	17 %	20 %	20 %
	Lavender	0 %	0 %	0 %	0 %	0 %	0 %	0 %	0 %	0 %	0 %	0 %	0 %	0 %	0 %	0 %	0 %
	Celery	0 %	0 %	0 %	0 %	0 %	0 %	0 %	0 %	0 %	0 %	0 %	0 %	0 %	6 %	0 %	0 %
	Onion	0 %	0 %	0 %	0 %	0 %	0 %	0 %	0 %	0 %	0 %	0 %	0 %	5 %		10 %	10 %
	Aromatic, medicinal and culinary plants	11 %	6 %	11 %	11 %	12 %	12 %	11 %	12 %	0 %	0 %	0 %	0 %	0 %	0 %	0 %	0 %
	Vegetables general	24 %	18 %	13 %	17 %	27 %	32 %	28 %	36 %	56 %	26 %	51 %	62 %	0 %	0 %	0 %	0 %
Root crops	Potatoes	7 %	8 %	6 %	0 %	0 %	11 %	4 %	7 %	4 %	0 %	6 %	11 %	5 %	0 %	10 %	10 %
	Sugar beet	42 %	55 %	27 %	59 %	47 %	28 %	46 %	32 %	26 %	50 %	29 %	13 %	29 %	20 %	18 %	18 %
Ornamental plants		15 %	11 %	38 %	10 %	10 %	15 %	11 %	13 %	14 %	18 %	11 %	10 %	8 %	24 %	9 %	0 %
Crops with share <5 %		2 %	2 %	3 %	3 %	4 %	2 %	0 %	0 %	0 %	5 %	3 %	4 %	3 %	13 %	4 %	0 %
Total area [ha]		50	44	35	51	42	27	37	29	27	45	33	36	47	59	55	56

Table 11-3: Development stages of crops in Gochsheim and the development of crop specific parameters.

Crop	**Initial**	**Develop**	**Mid**	**Late**	**Total days or mean of Yield response factor**
Cabbage (mean of broccoli, cauliflower, chinese cabbage, kale, cabbage, brussels sprouts)					
Length of stage [days] [1]	20	30	20	10	80
K_c [-] [2]	0.5		1.23	1.23	
Rooting depth [m] [5, 3]	0.25		0.4		
Critical depletion [-] [1, 7]	0.45		0.45	0.45	
Yield response factor [-] [1]	0.4	1.1	0.8	0.4	1.05
Planting period [1, 4]	Beginning of April–End of October				
Lettuce (mean of lettuce, ice lettuce)					
Length of stage [days] [1]	20	30	15	10	75
K_c [-] [2]	0.5		1.2	1.2	
Rooting depth [m] [5, 3]	0.25		0.3		
Critical depletion [-] [1, 7]	0.3		0.3	0.3	
Yield response factor [-] [6]	0.8	0.4	1.2	1	1
Planting period [1, 4]	Beginning of April–Mid of October				
Sugar beet					
Length of stage [days] [1]	50	40	50	40	180
K_c [-] [2]	0.2		0.8	0.8	
Rooting depth [m] [3]	0.25		0.7		
Critical depletion [-] [6]	0.5		0.6	0.6	
Yield response factor [-] [1]	0.5	0.8	1.2	1	1.1
Planting period [1, 8]	Beginning of April–End of November/December				
Potato					
Length of stage [days] [1]	30	35	50	30	145
K_c [-] [2]	0.4		0.8	0	
Rooting depth [m] [5, 3]	0.25		0.6		
Critical depletion [-] [1]	0.4		0.5	0.5	
Yield response factor [-] [1]	0.4	1.1	0.8	0.4	1.05
Planting period [1, 9]	Beginning of April–End of September				
Onion (mean of spring onion, onion)					
Length of stage [days] [1]	23	33	28	28	112
K_c [-] [2]	0.7		1.03	0.88	
Rooting depth [m] [5, 3]	0.25		0.4		
Critical depletion [-] [1, 7]	0.3		0.3	0.3	
Yield response factor [-] [1]	0.4	1.1	0.8	0.4	1.05
Planting period [1, 4]	Beginning of April–End of August				
Group ‘ornamental plants (Sunflower)’					
Length of stage [days] [1]	25	35	45	25	130
K_c [-] [1]	0.35		1.15	0.4	
Rooting depth [m] [1]	0.25		0.8		
Critical depletion [-] [1]	0.45		0.5	0.8	
Yield response factor [-] [1]	0.4	0.6	0.8	0.8	0.95
Planting period [1]	Beginning of April–End of September				

Table 11-3 continued

Crop	Initial	Develop	Mid	Late	Total days or mean of Yield response factor
Celery					
Length of stage [days] [1]	25	40	45	15	125
K_c [-] [2]	0.5		1.4	1.4	
Rooting depth [m] [5, 3]	0.25		0.5		
Critical depletion [-] [1, 7]	0.2		0.2	0.2	
Yield response factor [-] [6]	0.8	0.4	1.2	1	1
Planting period [1, 4]	Beginning of April–End of October				
Marrow (mean pumpkin/marrow and zucchini)					
Length of stage [days] [1]	23	33	30	20	106
K_c [-] [2]	0.5		1.2	1.2	
Rooting depth [m] [5, 3]	0.25		0.4		
Critical depletion [-] [1]	0.43		0.43	0.43	
Yield response factor [-] [6]	0.8	0.4	1.2	1	1
Planting period [1, 4]	Beginning of May–End of October				
Group 'small vegetable' (mean of vegetables cabbage, lettuce, carrot, celery, onion, spinach, radishes)					
Length of stage [days] [1]	20	29	28	13	91
K_c [-] [1]	0.56		1.08	1.04	
Rooting depth [m] [1]	0.25		0.37		
Critical depletion [-] [1]	0.31		0.31	0.31	
Yield response factor [-] [1]	0.69	0.6	1.09	0.83	1.01
Planting period [1]	Beginning of April–End of October				
Group 'herbs'					
Length of stage [days] [1]	20	30	15	10	75
K_c [-] [1, 2]	0.3		0.8	1	
Rooting depth [m] [5, 1]	0.25		0.4		
Critical depletion [-] [1]	0.4		0.4	0.4	
Yield response factor [-] [1]	0.8	0.4	1.2	1	1
Planting period [11]	Beginning of April–End of September				

[1] Savva et al. (2002)
[2] Hochschule Geisenheim (2019)
[3] DWD (2018a)
[4] Wachendorf et al. (2018)
[5] Smith (1992), FAO-CROPWAT-Software 8.0: Help
[6] Smith (1992), FAO-CROPWAT-Software 8.0: Default values
[7] BLZ (2017)
[8] Wirtschaftliche Vereinigung Zucker e.V. (2020)
[9] BZfE (2016)
[10] LfL (2006)
[11] BZfE (2019)

The critical depletion $\rho_{critical}$ represents the content of water that can be depleted before the plant starts suffering and therefore would result in crop losses. The fraction of TAW that a crop can extract from the root zone without suffering water stress is called the readily available soil water (Allen et al. 1998). The values for $\rho_{critical}$ required for modelling were obtained from Savva et al. (2002) and BLZ (2017). Since the $\rho_{critical}$-values provided by Allen et al. (1998) are valid for a crop specific evapotranspiration of ~5 mm/day these had to be adapted according to the following formula:

$$\rho = \rho_{ET=5mm/day} + 0.04 * (5 - ET_c) \quad (11\text{-}1)$$

Where:

$\rho_{ET=5mm/day}$ = critical depletion for evapotranspiration of ~5 mm/day
ET_c = crop specific evapotranspiration [mm/day]

In addition to the evapotranspiration rate, the critical depletion also depends on the soil type. Accordingly, the critical depletion values were reduced by 5–10 % for fine textured soils such as clay/loam, while for more coarse textured soils such as sand they were increased by 5–10 %. Often a constant value for $\rho_{critical}$ is used for a certain growth period instead of varying the value every day (Allen et al. 1998). Therefore, constant values were assumed in the further considerations (Table 11-3).

11.3.3 Details on computational approach for estimation of the crop specific irrigation requirements

The crop water requirement is mainly determined by the crop evapotranspiration ET_c (Allen et al. 1998) and ET_c was calculated in the model as follows (Savva et al. 2002):

$$ET_c = ET_0 * K_c \quad (11\text{-}2)$$

Where:

ET_c = crop evapotranspiration [mm/day]
ET_0 = reference evapotranspiration [mm/day]
K_c = crop coefficient

Crop evapotranspiration ET_c applies under standard conditions, which is equivalent to no water stress for the plant. In order to account for a water stress situation, the crop evapotranspiration was calculated for non-standard conditions ET_a according to the following formula using the water stress coefficient k_s (Allen et al. 1998):

$$ET_a = ET_c * k_s \quad (11\text{-}3)$$

Where:

ET_a = crop evapotranspiration under non-standard conditions [mm/day]
ET_c = crop evapotranspiration [mm/day]
k_s = water stress coefficient = 1

The net irrigation requirement was derived from the field balance equation according to Savva et al. (2002):

$$IR_n = ET_c - \left(P_{eff} + G_e + W_b\right) + LR_{mm} \quad (11\text{-}4)$$

Where:

IR_n = net irrigation requirement [mm]
ET_c = crop evapotranspiration [mm/day] = ET_a, since $k_s = 1$
P_{eff} = effective dependable rainfall [mm]
G_e = groundwater contribution from water table [mm]
W_b = water stored in the soil at the beginning of each period [mm]
LR_{mm} = leaching requirement [mm]

Since during irrigation usually water losses occur due to e.g. leaking pipes, the efficiency of the irrigation system also had to be accounted for when determining the gross irrigation requirements. Consequently, the gross irrigation requirement IR_g was determined according to Savva et al. (2002):

$$IR_g = \frac{IR_n}{E} \quad (11\text{-}5)$$

Where:

IR_g = gross irrigation requirements [mm]
IR_n = net irrigation requirements [mm]
E = overall irrigation project efficiency

11.4 Supplementary information for Chapter 5

11.4.1 Nucleotide sequence of MS2 phage RNA and utilized dPCR primers

The following paragraph gives the nucleotide sequence of the single stranded RNA of MS2 phages, as to be found in the genome database of the National Center for biotechnology Information (NCBI 2021). The nucleobases are abbreviated as follows: A = adenine, C = cytosine, G = guanine and T = thymine. The genome was given with thymine, despite the fact that it is replaced by uracil in the case of RNA. Additionally, the sequences targeted by the different primers and the probe during the dPCR analysis are color marked according to the following system: MS2 forward primer, MS2 probe, MS2 reverse primer. While the forward primer and probe can be directly read out with their sequence provided by the manufacturer, the sequence of the reverse primer as given by the manufacturer had to be translated to the complementary sequence.

GGGTGGGACCCCTTTCGGGGTCCTGCTCAACTTCCTGTCGAGCTAATGCCATTTTTAATGTCTTTAGCGAGACGCTACCATGGCT
ATCGCTGTAGGTAGCCGGAATTCCATTCCTAGGAGGTTTGACCTGTGCGAGCTTTTAGTACCCTTGATAGGGAGAACGAGACCTTCGTC
CCCTCCGTTCGCGTTTACGCGGACGGTGAGACTGAAGATAACTCATTCTCTTTAAAATATCGTTCGAACTGGACTCCCGGTCGTTTTAAC
TCGACTGGGGCCAAAACGAAACAGTGGCACTACCCCTCTCCGTATTCACGGGGGGCGTTAAGTGTCACATCGATAGATCAAGGTGCCT
ACAAGCGAAGTGGGTCATCGTGGGGTCGCCCGTACGAGGAGAAAGCCGGTTTCGGCTTCTCCCTCGACGCACGCTCCTGCTACAGCCT
CTTCCCTGTAAGCCAAAACTTGACTTACATCGAAGTGCCGCAGAACGTTGCGAACCGGGCGTCGACCGAAGTCCTGCAAAAGGTCACC
CAGGGTAATTTTAACCTTGGTGTTGCTTTAGCAGAGGCCAGGTCGACAGCCTCACAACTCGCGACGCAAACCATTGCGCTCGTGAAGGC
GTACACTGCCGCTCGTCGCGGTAATTGGCGCCAGGCGCTCCGCTACCTTGCCCTAAACGAAGATCGAAAGTTTCGATCAAAACACGTG
GCCGGCAGGTGGTTGGAGTTGCAGTTCGGTTGGTTACCACTAATGAGTGATATCCAGGGTGCATATGAGATGCTTACGAAGGTTCACCT
TCAAGAGTTTCTTCCTATGAGAGCCGTACGTCAGGTCGGTACTAACATCAAGTTAGATGGCCGTCTGTCGTATCCAGCTGCAAACTTCC
AGACAACGTGCAACATATCGCGACGTATCGTGATATGGTTTTACATAAACGATGCACGTTTGGCATGGTTGTCGTCTCTAGGTATCTTG
AACCCACTAGGTATAGTGTGGGAAAAGGTGCCTTTCTCATTCGTTGTCGACTGGCTCCTACCTGTAGGTAACATGCTCGAGGGCCTTAC
GGCCCCCGTGGGATGCTCCTACATGTCAGGAACAGTTACTGACGTAATAACGGGTGAGTCCATCATAAGCGTTGACGCTCCCTACGGGT
GGACTGTGGAGAGACAGGGCACTGCTAAGGCCCAAATCTCAGCCATGCATCGAGGGGTACAATCCGTATGGCCAACAACTGGCGCGTA
CGTAAAGTCTCCTTTCTCGATGGTCCATACCTTAGATGCGTTAGCATTAATCAGGCAACGGCTCTCTAGATAGAGCCCTCAACCGGAGT
TTGAAGCATGGCTTCTAACTTTACTCAGTTCGTTCTCGTCGACAATGGCGGAACTGGCGACGTGACTGTCGCCCCAAGCAACTTCGCTA
ACGGGGTCGCTGAATGGATCAGCTCTAACTCGCGTTCACAGGCTTACAAAGTAACCTGTAGCGTTCGTCAGAGCTCTGCGCAGAATCGC
AAATACACCATCAAAGTCGAGGTGCCTAAAGTGGCAACCCAGACTGTTGGTGGTGTAGAGCTTCCTGTAGCCGCATGGCGTTCGTACTT
AAATATGGAACTAACCATTCCAATTTTCGCTACGAATTCCGACTGCGAGCTTATTGTTAAGGCAATGCAAGGTCTCCTAAAAGATGGAA
ACCCGATTCCCTCAGCAATCGCAGCAAACTCCGGCATCTACTAATAGACGCCGGCCATTCAAACATGAGGATTACCCATGTCGAAGAC
AACAAAGAAGTTCAACTCTTTATGTATTGATCTTCCTCGCGATCTTTCTCTCGAAATTTACCAATCAATTGCTTCTGTCGCTACTGGAAG
CGGTGATCCGCACAGTGACGACTTTACAGCAATTGCTTACTTAAGGGACGAATTGCTCACAAAGCATCCGACCTTAGGTTCTGGTAATG
ACGAGGCGACCCGTCGTACCTTAGCTATCGCTAAGCTACGGGAGGCGAATGGTGATCGCGGTCAGATAAATAGAGAAGGTTTCTTACA
TGACAAATCCTTGTCATGGGATCCGGATGTTTTACAAACCAGCATCCGTAGCCTTATTGGCAACCTCCTCTCTGGCTACCGATCGTCGTT
GTTTGGGCAATGCACGTTCTCCAACGGTGCTCCTATGGGGCACAAGTTGCAGGATGCAGCGCCTTACAAGAAGTTCGCTGAACAAGCA
ACCGTTACCCCCCGCGCTCTGAGAGCGGCTCTATTGGTCCGAGACCAATGTGCGCCGTGGATCAGACACGCGGTCCGCTATAACGAGTC
ATATGAATTTAGGCTCGTTGTAGGGAACGGAGTGTTTACAGTTCCGAAGAATAATAAAATAGATCGGGCTGCCTGTAAGGAGCCTGAT
ATGAATATGTACCTCCAGAAAGGGGTCGGTGCTTTCATCAGACGCCGGCTCAAATCCGTTGGTATAGACCTGAATGATCAATCGATCAA
CCAGCGTCTGGCTCAGCAGGGCAGCGTAGATGGTTCGCTTGCGACGATAGACTTATCGTCTGCATCCGATTCCATCTCCGATCGCCTGG
TGTGGAGTTGGCTTCTCCCACCAGAGCTATATTCATATCTCGATCGTATCCGCTCACACTACGGAATCGTAGATGGCGAGACGATACGA
TGGGAACTATTTTCCACAATGGGAAATGGGTTCACATTTGAGCTAGAGTCCATGATATTCTGGGCAATAGTCAAAGCGACCCAAATCCA
TTTTGGTAACGCCGGAACCATAGGCATCTACGGGGACGATATTATATGTCCCAGTGAGATTGCACCCCGTGTGCTAGAGGCACTTGCCT
ACTACGGTTTTAAACCGAATCTTCGTAAAACGTTCGTGTCCGGGCTCTTTCGCGAGAGCTGCGGCGCGCACTTTTACCGTGGTGTCGAT
GTCAAACCGTTTTACATCAAGAAACCTGTTGACAATCTCTTCGCCCTGATGCTGATATTAAATCGGCTACGGGGTTGGGGAGTTGTCGG
AGGTATGTCAGATCCACGCCTCTATAAGGTGTGGGTACGGCTCTCCTCCCAGGTGCCTTCGATGTTCTTCGGTGGGACGGACCTCGCTG
CCGACTACTACGTAGTCAGCCCGCCTACGGCAGTCTCGGTATACACCAAGACTCCGTACGGGCGGCTGCTCGCGGATACCCGTACCTCG
GGTTTCCGTCTTGCTCGTATCGCTCGAGAACGCAAGTTCTTCAGCGAAAAGCACGACAGTGGTCGCTACATAGCGTGGTTCCATACTGG
AGGTGAAATCACCGACAGCATGAAGTCCGCCGGCGTGCGCGTTATACGCACTTCGGAGTGGCTAACGCCGGTTCCCACATTCCCTCAG
GAGTGTGGGCCAGCGAGCTCTCCTCGGTAGCTGACCGAGGGACCCCCGTAAACGGGGTGGGTGTGCTCGAAAGAGCACGGGTGCGAA
AGCGGTCCGGCTCCACCGAAAGGTGGGCGGGCTTCGGCCCAGGGACCTCCCCCTAAAGAGAGGACCCGGGATTCTCCCGATTTGGTAA
CTAGCTGCTTGGCTAGTTACCACCCA

11.4.2 Chemicals, equipment specifications and lab-scale UF system

Table 11-4: Utilized chemicals and their specifications

Substance name	Specification	Manufacturer
Agar	Bacteriological grade	VWR
CASO-Bouillon	Typical composition in g/L: Peptone from casein: 17.0; Peptone from soymeal: 3.0; D(+)Glucose: 2.5; Sodium chloride: 5.0; di-Potassium hydrogen phosphate: 2.5; pH = 7.3 ± 0.2 at 25°C;	Merck KGaA
Di-sodium hydrogen phosphate dihydrate (Na2HPO4·2 H2O)	Purity = ≥99.5 % (acidimetric), M = 177.99 g/mol;	Merck KGaA
Ethanol	80 v %;	Produced in the laboratory;
Hydrochloric acid (HCl)	Purity = 37 %, M = 36.46 g/mol, ρ = 1.19 kg/L; 0.1, 1 and 10 N, for pH adjustment;	Merck KGaA Produced in the laboratory;
Nitric acid (HNO3)	Purity = 65 %, M = 63.01 g/mol, ρ = 1.4 kg/L;	Merck KGaA
Potassium chloride (KCl)	Purity = ≥99.5 % (argentometric); *M* = 74.55 g/mol;	Merck KGaA
Potassium dihydrogen phosphate (KH_2PO_4)	Purity = ≥99.5 %[a]; *M* = 136.09 g/mol;	Merck KGaA
Sodium chloride (NaCl)	Purity = >99.8 %; *M* = 58.44 g/mol, ρ = 2.17 kg/L at 25°C;	Carl Roth GmbH
Sodium hydroxide (NaOH)	Purity = 32 %, *M* = 39.997 g/mol, ρ = 1.35 kg/L; 0.1, 1 and 10 N, for pH adjustment;	Merck KGaA Produced in the laboratory;
Soy peptone	Bacteriological grade	VWR
Tryptic Soy agar	Typical composition in g/L: Pancreatic digest of casein: 15.0; Papaic digest of soya bean 5.0; Sodium chloride: 5.0; Agar: 15.0; pH = 7.3 ± 0.2 at 25°C;	Merck KGaA
Tryptone/peptone	From casein, granulated, pancreatic digested, for microbiology;	Carl Roth GmbH
Additional equipment:		
Bacillol®AF	Disinfectant for washable surfaces;	BODE SCIENCE CENTER
Sterilium®	Hand sanitizer;	BODE SCIENCE CENTER

Table 11-5: Microorganisms for the PFU analysis

Substance name	Specification	Manufacturer
Escherichia coli stock	DSM number 5695, K12 HFR strain;	Leibniz Institute DSMZ-German Collection of Microorganisms and Cell Cultures GmbH
MS2 phages stock	-	Produced in the laboratory according to ISO 10705-1:2001;

Table 11-6: Substances for dPCR test - QIAcuity® One-Step Viral RT-PCR Kit

Substance name	Specification	Manufacturer
MS2 forward primer	5'-TCC TAA AAG ATG GAA ACC CGA TT-3'	Microsynth
MS2 reverse primer	5'-GGC CGG CGT CTA TTA GTA GAT G-3'	Microsynth
MS2 probe	5'-CAG CAA TCG CAG CAA ACT CCG-3'	Microsynth
Multiplex Reverse Transcription (Transcriptase) Mix	-	QIAGEN®
Nuclease-free water	-	QIAGEN®
One-Step Viral RT-PCR Master Mix	-	QIAGEN®
RNase-away spray	For RNase and DNA contamination removal;	M*β*P® -Molecular BioProducts

Table 11-7: Required equipment for experimental procedure

Equipment	Specification	Brand
Autoclave	Vertical lab sterilizer Fedegari FVA3 - A1	IBS Integra Biosciences
Beakers	Different sizes	Schott Duran®, VWR
Bunsen burner	Blowlamp Soudogaz X2000 PZ	Campingaz®
	Safety Bunsen Burner FIREBOY plus	IBS Intergra Biosciences
Cell density meter	Biowave CO8000	WPA
Colony counter	BZG 30	WTW
Conductivity meter	Multi 3410	WTW
Culture flasks	500 mL, Erlenmeyer shape, straight neck with metal caps	Schott Duran®
dPCR device	QIAcuity One	QIAGEN®
Freezer	-80°C	-
Fridge	5 ± 1°C	-
Graduated cylinders	250 mL ± 1 mL, 100 mL ± 0.05 mL	VWR
Heating cabinet	55 °C	Memmert
Laboratory balance	BP 1200, max 1200 g, 0.01 g precision;	Sartorius
Laboratory bottles	2 L, 1 L, 250 mL, with screw cap	Schott Duran®, Sigma-Aldrich®, VWR
Magnetic stirrer with agitators	IKAMAG® RCT (with heating function)	IKA™
	Heidolph MR 2000	Heidolph
Micro tubes	SafeSeal, 2 mL and 1.5 mL, material: PP	Sarstedt
Nanoplate for dPCR	QIAcuity™ nanoplate 26k (24-well) for dPCR analysis, dark blue, with adhesive, self-sealing blue sealing foil;	QIAGEN®
Petri dishes	PS, 92x16 mm with cams, sterile delivery	Sarstedt
pH meter	inoLab pH Level 1	WTW
	pH 1970i	WTW
Pipettes with pipette tips	5000 mL, 1000 mL, 200 mL, 20 mL (maximum volumes), 0.5–10 µL (range);	Sartorius
Pipette filler	Pipetus®-akku	Hirschmann®
PCR pre-plate	Standard PCR pre-plate, PP, white, for sample preparation, with adhesive sealing foil;	Sarstedt
Shaking incubator	Shaking incubator 3032	GFL®
Sterile pipettes	Serological pipettes, 10 mL	Sarstedt
Sterile workbench	Thermo Scientific™ Herasafe™ KS, Class II Biological Safety Cabinet	Thermo Scientific™
Test tubes	15 mL, glass, rimless, with metal caps;	Schott Duran®
	PP, 15 mL, 120x17 mm, with screw cap;	Sarstedt
Thermocycler	Biometra TONE Thermocycler for PCR, 96 well block;	Analytik Jena
Ultrapure water (MilliQ water) production device	PURELAB classic, water electrical conductivity = 18.2 MΩcm at 25°C	Elga
Volumetric flasks with PE or PP stoppers	5 L ± 1.2 mL	Hirschmann®, BRAND®
	2 L ± 0.6 mL	BRAND®
	1 L ± 0.4 mL	BRAND®
	500 mL ± 0.38 mL	BRAND®
	200 mL ± 0.15 mL	BRAND®
	100 mL ± 0.1 mL	VWR
	50 mL ± 0.06 mL	VWR
Vortex mixer	Vortex-Genie 2	Scientific Industries, Inc.
Waste canisters	For acidic and basic waste, 5 L, IKG;	IKG
Water bath	SUB Aqua Pro unstirred water bath	Grant
Working station	Tamer Template Quantum®	Appligene
Additional equipment: Autoclave tape, disposable pipette funnels, freezing box, insulated box and bowl for crushed ice, micro tube holders, rubber roller, squeegee, standards for pH meter calibration, weighing boats + spatulas;		

Table 11-8: Composition of PBS stock (NSF/ANSI 55 2019)

Ingredient	**Molecular formula**	***m* for 1 L stock solution**
Sodium chloride	NaCl	80 g
Potassium diydrogen phosphate	KH_2PO_4	2 g
Di-sodium hydrogen phosphat dihydrate	$Na_2HPO_4 \cdot 2\ H_2O$	14.42 g
Potassium chloride	KCl	2 g

Figure 11-8: Photo of lab-scale UF membrane system

11.4.3 PFU protocol details adapted from to NSF/ANSI 55 (2019)

- Label bottom agar plates
- Prepare micro tubes for dilution series by pipetting always 1.8 mL (=2x900 µL) autoclaved PBS into them, label appropriately
- Generate dilution series: Vortex sample, pipette 200 µL in prepared micro tube, vortex, pipette 200 µL of it for next dilution step and repeat procedure
  → Dilute feed tank samples, blank, backwash sample until 10^{-6}
  → Dilute tested flow samples until 10^{-4}

- Transfer incubated *E. coli* on crushed ice to sterile working bench
- Process every taken sample following the subsequent procedure:
  - Take glass test tube with top agar from water bath
  - Vortex, open cap, flame tube neck
  - Vortex sample, pipette 1 mL sample to top agar
  - Vortex
  - Flame tube neck, give to second person
  - Shake incubated *E. coli*, pipette 0.1 mL to top agar-sample-mix
  - Swivel the glass test tube and pour content on bottom agar plate
  - Move plate gently to spread top agar evenly
  - Set plates aside until top agar solidified
  - Then incubate at plates upside down and covered with aluminium foil at 35 ± 1°C for 18 ± 2 h
- Measure the cell density of the remaining *E. coli* solution indirectly via determining the optical density:
  - Measure TSB without *E. coli* as reference
  - Then measure the incubated TSB with *E. coli* subsequently

  → higher value indicates higher cell density

Table 11-9: Composition of TSA bottom agar (1.5 %TSA) and top agar (1.0 %TSA) following NSF/ANSI 55 (2019)

Ingredient	**For 500 mL**	
	1.5 % TSA (bottom agar)	**1.0 % TSA (top agar)**
Bacto-agar	7.5 g	5.0 g
Sodium chloride	2.5 g	2.5 g
Soytone (=Soy peptone)	2.5 g	2.5 g
Tryptone	7.5 g	7.5 g

Table 11-10: TSB composition following NSF/ANSI 55 (2019)

Ingredient	**For 100 mL**
Dextrose	0.25 g
Dipotassium phosphate	0.25 g
Sodium chloride	0.5 g
Soytone (=Soy peptone)	0.3 g
Tryptone	1.7 g

11.4.4 dPCR protocol

This chapter elaborates how the dPCR was performed, based on a protocol developed by the laboratory staff in accordance to the information provided by QIAGEN (2021). The detailed steps were the following:

1. Weighing room: switch on dPCR-device and computer
2. Define sample location on PCR plate, scheme in Table 11-11; Slot A1 is always reserved for the negative control sample (NC) and A2 for the positive control sample (PC)

Table 11-11: Slot scheme of PCR plate

	1	**2**	**3**
A	NC	PC	
B			
C			
D			
E			
F			
G			
H			

3. Thaw samples to be tested
4. Clean inside of working station with RNase-away spray → inside of working station is not sterile but provides a confined space to be managed cleanly
5. Prepare bowl of crushed ice
6. Prepare reagents:
    a. Store Multiplex Reverse Transkriptase and One-Step Viral on crushed ice
    b. Thaw nuclease-free water and Primer mix
    c. If Primer mix needs to be produced: The base composition for 100 µL is shown in Table 11-12. Produce Primer mix in bigger amount, for example 500 µL, and freeze in aliquots since frequent thawing and re-freezing of the mix is not desirable.
    d. Wrap Primer mix tube in aluminium foil, to protect it from light;

Table 11-12: Composition of Primer mix (QIAGEN; QIAGEN 2021)

Primer	**Amount**	**Comment**
MS2 Forward primer	8 µL	-
MS2 Reverse primer	8 µL	-
MS2 Probe	4 µL	Sensitive to light, wrap tube in aluminium foil;
Nuclease-free water	80 µL	-

7. Prepare reaction mix:
    a. Take 1.5 mL micro tube and label it;
    b. Pipette the reagents in the tube, following the composition and instructions given in Table 11-13; The reaction mix for the whole PCR plate (24 slots in total), the volumes given in Table 11-13 for 1 sample well were multiplied by the factor 26, to account also for pipetting losses;

c. After adding the One-Step Viral mix the reaction mix with the same tip via drawing the mixture in and out (8 to 10 times);
d. Store on crushed ice, wrapping the micro tube with aluminium not necessary because fast usage of the mixture;
e. Freeze Primer mix, Multiplex Reverse Transkriptase and One-Step Viral

Table 11-13: Composition of reaction mix (QIAGEN; QIAGEN 2021)

Ingredient	***V* per sample**	***V* for 26 samples**	**Comment/instructions**
Nuclease-free water	23.6 µL	613.6 µL	-
Primer mix	2 µL	52 µL	Vortex prior to pipetting;
Multiplex Reverse Transkriptase	0.4 µL	10.4 µL	Do not vortex, mix gently by drawing it in and out the pipette (8 to 10 times);
One-Step Viral	10 µL	260 µL	Mix also via drawing volume in and out (8 to 10 times) with pipette;

8. Sample transfer
    a. Place white PCR pre-plate on crushed ice
    b. Vortex all samples
    c. Transfer always 4 µL sample to pre-plate, starting from A2 (PC) (go with pipette tip to plate bottom and empty there
    d. Cover pre-plate with non-adhesive foil: Remove white protective foil layer, place foil on pre-plate and smooth out with squeegee, ensure that edges are covered well
9. Sample heating
    a. Switch on thermocycler, log in, choose and start program for RNA disintegration
    b. When block temperature of 95 °C is reached, insert covered pre-plate and close lid (gets heated for 5 min)
    c. Remove pre-plate from thermocycler when program is done after the 5 min
    d. Return pre-plate to working station and store on crushed ice to cool it to room temperature (to avoid evaporation losses when opening the foil)
    e. When room temperature reached: remove foil from pre-plate
10. Sample preparation
    a. Pipette 4 µL nuclease-free water to A1 as NC
    b. Then add 36 µL of reaction mix to each slot, place pipette tip (new one for each sample) for this on side wall of slot/ well and let run down
    c. Cover pre-plate again with transparent foil (step 8.d)
    d. Vortex pre-plate
    e. Centrifuge pre-plate in microscope room
    f. Return pre-plate on crushed ice in working station
11. Sample transfer to dPCR nanoplate
    a. Prepare dPCR nanoplate (dark blue), to protect sensitive bottom place an already used dPCR nanoplate as carrier below
    b. Remove foil from pre-plate

c. Pipette the total sample + reaction mix volume of 40 µL from pre-plate to respective slot at dPCR nanoplate via placing the pipette tip on slot wall and let liquid run in smoothly (avoid extensive bubble formation)
d. Cover the dPCR nanoplate with a blue, adhesive sealing foil: remove white protection foil, then place blue foil on nanoplate so that plate openings are well covered; Smooth foil down with rubber roller, roll edges thereby separately; then remove transparent protection foil and smooth blue foil again with rubber roller; Protruding foil areas are folded and smoothed over the edge;

12. dPCR analysis
    a. Log in to computer and the dPCR device
    b. In computer software: add a new plate → import template 'MS2' → parameters for dPCR analysis get loaded (cf. Table 11-14 for details) → label plate → confirm with 'Done', new plate is defined;
    c. Open plate try at dPCR device → place dPCR nanoplate parallel and with barcode to the front in tray → close tray → assign barcode to in software defined plate
    d. Start analysis with 'Run', takes approximately 3 h

Table 11-14: Parameters of MS2 dPCR - adapted Single-Nanoplate protocol for QIAcuity One (QIAGEN; QIAGEN 2021)

Step	Time	Temperature	Comment
Reverse Transcription	40 min	50 °C	
PCR initial heat activation	2 min	95 °C	
Denaturation	5 s	95 °C	2-step cycling → 40 cycles conducted
Combined annealing/extension	60 s	61.5 °C	

13. Clean up:
    a. Freeze nuclease-free water
    b. Freeze samples again at -80 °C
    c. Collected waste from working station to autoclave waste when full
    d. Clean working station, wipe inner surfaces with RNase-away spray, close station and start UV disinfection
    e. White pre-plate reusable, store in fridge in the meantime
14. Results evaluation in software:
    a. When run completed → choose plate, access results via 'Analysis' → choose wells, then 'Show results'
    b. 'Signalmap': See how samples were spread in wells, 1/3 of area is maximum acceptable sample-uncovered area
    c. 'Concentration diagram' – histogram: overview of all detected concentrations
    d. '1D-Scatterplot': Evaluation of thresholds = red line required → relocate so that broad scattering ('rain') is excluded via choosing slot, click on line, relocate and confirm via 'Recalculate'
    e. Safe data as .csv file
    f. Remove dPCR nanoplate from tray

11.4.5 Chemical cleaning protocol for UF membrane system

Chemical cleaning was always performed one day prior to conducting the experiment: Firstly, the system including the membrane was flushed with MilliQ water in order to remove all kind of easily soluble and movable matter still present in the system. According to inopor®, the ceramic membrane utilized during the experiments is stable towards bases up to a pH of 14 and NaOH concentrations of 1 mol/L. It can also resist towards acids, whereby a pH of 0.5 was given as lower limit value, which corresponds approximately to a concentration of 0.3 mol/L. Only towards HCl the material resistivity is limited. To minimize the material stress due to chemicals, the membrane was removed from the experimental system after the flush with MilliQ water, even though the subsequently applied NaOH concentration did not exceed the given limit molarity of 1 mol/L. The membrane was stored for sterilization in 80 v% ethanol overnight. The system without membrane was first flushed with 5 L 1 v% NaOH and then with HCl, whereby after each application of a chemical solution the system was neutralized with MilliQ water and PBS. The choice of cleaning chemicals was based on the fact that acids are capable of removing inorganic deposits inside the experimental system, while alkaline agents address organics (Al-Amoudi et al. 2007). The volumes of NaOH, HCl and HNO_3 that were applied for flushing the system were determined based on the dead-volume of the system. The dead-volume of the system was estimated to be 0.5 L for both the forward flush (FF) and backwash (BW) mode.

The CIP could be performed only for the FF mode or for both the FF and BW mode of the system. The latter option is given in italic in the subsequent list.

1. With membrane inserted in system: 1 h flushing with MilliQ in FF mode/*30 min flushing with MilliQ water in BW mode, then 30 min in FF mode*
2. Remove membrane in system ad store overnight in 80 v% ethanol (upright in graduated cylinder)
3. Flush system in FF mode with 5 L 1 v% NaOH, let soak for 5 min (pump switched off)/*flush system in BW mode discard first 500 mL, then collect effluent in feed tank, let soak for 5 min in between, then perform flush in FF mode* → discard base in appropriate container
4. Perform FF with approximately 2 L MilliQ water/*perform BW and then FF with approximately 2 L MilliQ water each* → to dilute base in system
5. Perform FF with approximately 2 to 3 L PBS (not autoclaved)/*perform BW and then FF with approximately 2 to 3 L PBS (not autoclaved) each* → to neutralize system, target pH = 7 ± 0.5;
6. Flush system in FF mode with 5 L 1 v% HCl, let soak for 5 min (pump switched off)/*flush system in BW mode discard first 500 mL, then collect effluent in feed tank, let soak for 5 min in between, then perform flush in FF mode* → discard acid in appropriate container
7. Perform FF with approximately 2 L MilliQ water/*perform BW and then FF with approximately 2 L MilliQ water each* → to dilute acid in system
8. Perform FF with approximately 2 to 3 L PBS (not autoclaved)/*perform BW and then FF with approximately 2 to 3 L PBS (not autoclaved) each* → to neutralize system, target pH = 7 ± 0.5;
9. Fill system with MilliQ water in FF mode/*FF and BW mode* → to leave over night

11.4.6 Detailed protocol for the experimental procedure

Experiments were conducted in forward flush mode only. The following protocol was followed:

- Prepare MilliQ water for rinsing, insulated box with crushed ice for sample storage and freezing box for bulk sample storage
- Remove membrane from ethanol, rinse with MilliQ and insert into system
- Flush system for 30 min in FF mode with MilliQ water, measure the membrane permeability thereby
- Flush system in FF mode with 5 L 1 v % HNO_3, let soak for 5 min (pump switched off)
- Perform FF with approximately 2 L MilliQ water → to dilute base in system
- Take 2 samples from autoclaved PBS from bottle (General sampling procedure: pipette 1 mL into micro tube for dPCR backup sample set, 2 mL for PFU analysis, store on crushed ice); [sample name = PBS-Fl.]
- Perform FF with approximately 2 to 3 L PBS (not autoclaved) → to neutralize system, target pH = 7 ± 0.5; collect thereby 500 mL effluent as bulk sample from FF [PBS-FF] and take 2 samples each;
- Dry out and flame out feed tank + the end of the FF mode hose end
- Fill PBS spiked with phages into feed tank → Take 2 samples [FT1]
- Start experiment: discard first 500 mL, then repeat for every teste flow rate:
    - System set to FF mode, adjust feed pump to targeted flow rate (maximum pressure 7.5-8.0 bar)
    - Discard 1 L, measure pH, EC and temperature
    - Switch off the pump, keep adjusted settings of pump
    - Collect 500 mL bulk sample in autoclaved bottle, take 2 samples + store them on ice, store bottle with bulk sample in freezing box; Overview of taken samples in Table 11-15;

  → repeat procedure for all tested flows
- For blank: Flame membrane casing, remove membrane from system, close casing gain, perform same procedure as for all previously tested flows, utilize a flow of 30 L/h or the maximal tested flow at 7.5 bar;

Table 11-15: Overview of the tested flows/fluxes and respective sample names

Repetition 1	Repetition 2	Repetition 3	Blank
0.5 L/min = 30 L/h [1S30]	0.08 L/min = 4.8 L/h [2S4,8]	0.4 L/min = 24 L/h [3S24]	Blank [B-0]
0.08 L/min = 4.8 L/h [1S4,8]	0.4 L/min = 24 L/h [2S24]	0.21 L/min = 12.6 L/h [3S12,6]	
0.4 L/min = 24 L/h [1S24]	0.21 L/min = 12.6 L/h [2S12,6]	0.5 L/min = 30 L/h [3S30]	
0.21 L/min = 12.6 L/h [1S12,6]	0.5 L/min [2S30]	0.08 L/min = 4.8 L/h [3S4,8]	

- Take 2 samples from feed tank in the experiment end [FT2]
- Insert membrane in experimental system
- Flush system in FF mode with MilliQ water and measure the permeability;
- Remove membrane from system and store dry

11.4.7 Scanning electron microscope images of the ceramic UF membrane

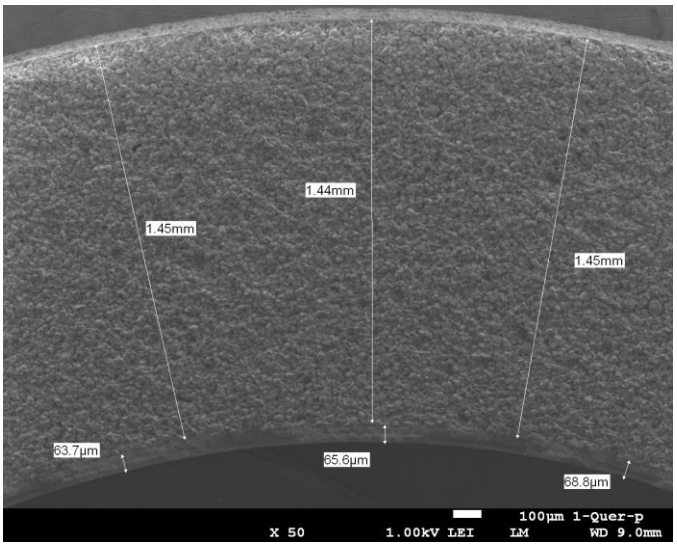

Figure 11-9: SEM image (50 x magnification) of the cross section of the ceramic UF membrane (type CA0250-A3T30G), support layer: α-Al_2O_3, about 1.45 mm; active filtration layer: TiO_2, about 65 µm.

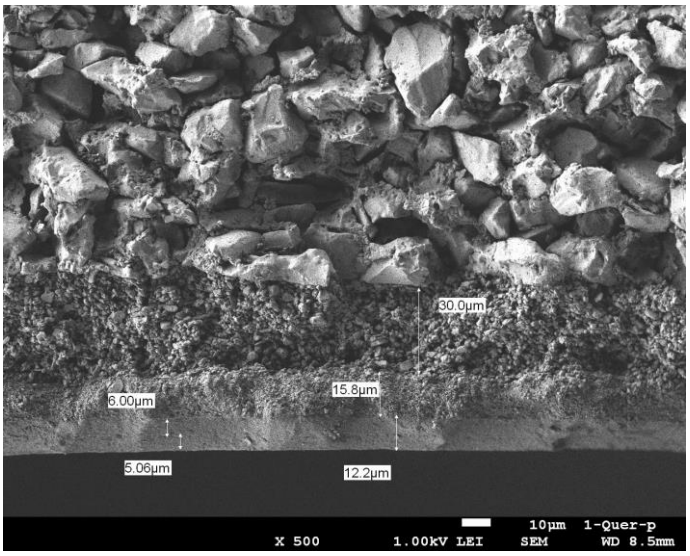

Figure 11-10: SEM image (500 x magnification) of the cross section of the ceramic UF membrane (type CA0250-A3T30G), support layer: α-Al_2O_3, about 1.45 mm; active filtration layer: TiO_2, about 65 µm

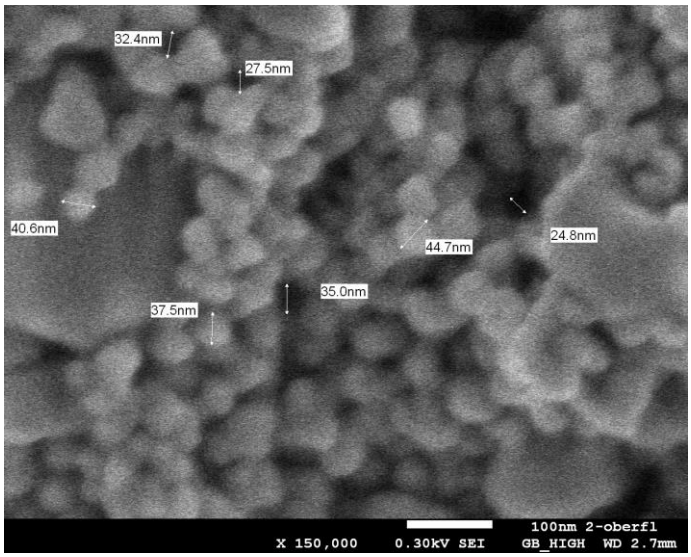

Figure 11-11: SEM image (150000 x magnification) of the surface of the ceramic UF membrane (type CA0250-A3T30G), active filtration layer: TiO_2, about 65 µm

11.4.8 Permeability tests

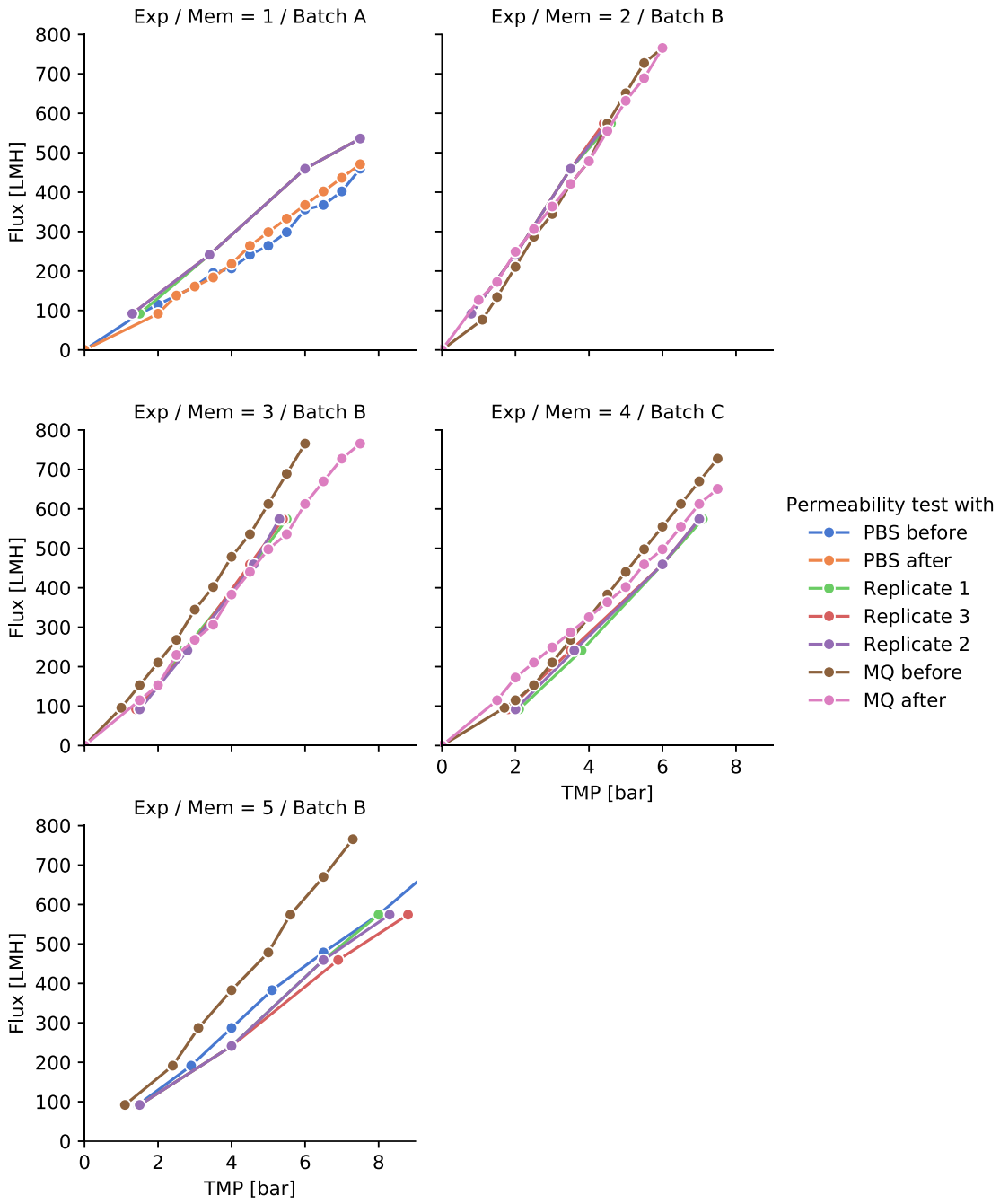

Figure 11-12: Permeability data of utilized ceramic UF membranes. Permeability was tested with different water qualities and at different stages of the respective experiment: PBS (phosphate buffered saline solution) before and after the experiments (PBS before and after), with PBS spiked with MS2 phages (replicate 1, 2, 3), MilliQ water before and after the experiment (MQ before and after).

Table 11-16: Permeability behavior before, during and after the individual experiments

Experiment (Membrane)	**Measurement**	**Permeability in LMH/bar***	**Pearson correlation coefficient *r***
2 (19A19563-3)	PBS permeability – before experiment	76.3	0.998
	Replicate 1	75.1	1.000
3 (19A19563-3)	MilliQ water permeability – before experiment	70.6	0.997
	PBS permeability – before experiment	60.6	0.997
	Replicate 1	60.6	0.998
	Replicate 2	58.1	1.000
	MilliQ water permeability – after experiment	56.4	0.994
	MilliQ water permeability – after hydraulic BW	80.2	0.999
4 (19A19563-3)	PBS permeability – before experiment	56.8	0.994
	Replicate 1	72.9	0.997
	Replicate 2	73.1	0.997
	Replicate 3	73.1	0.997
	PBS permeability – after experiment	60.2	0.997
5 (19A19563-2)	MilliQ water permeability – before experiment	124.8	0.996
	Replicate 1	126.3	0.998
	Replicate 2	127.8	0.999
	Replicate 3	129.4	1.000
	MilliQ water permeability – after experiment	124.3	0.999
6 (19A19563-2)	MilliQ water permeability – before experiment	121.0	0.998
	Replicate 1	99.4	1.000
	Replicate 2	100.6	0.998
	Replicate 3	100.8	0.999
	MilliQ water permeability – after experiment	99.6	0.997
7 (19A19563-#)	MilliQ water permeability – before experiment	89.7	0.993
	Replicate 1	75.5	0.999
	Replicate 2	76.8	0.999
	Replicate 3	77.5	0.999
	MilliQ water permeability – after experiment	84.3	0.998

Table 11-17: Temperature, electrical conductivity, pH, applied flux and TMP during the various experiments

Experiment	Membrane	Sample Name	Sample Type	Flux [LMH]	TMP [bar]	Permeability [LMH/bar]	Temperature [°C]	pH [-]	Electrical conductivity [mS/cm]
One	Batch A	PBS-Fl	PBS				20.9	7.1	13.0
One	Batch A	PBS-FF	PBS				20.4	7.1	13.0
One	Batch A	FT1	FT				20.5	7.0	13.0
One	Batch A	1S28	S	536	7.5	71.5	20.3	7.1	13.1
One	Batch A	1S4.8	S	92	1.5	61.2	20.4	7.1	13.0
One	Batch A	1S24	S	459	6	76.6	20.6	7.1	13.0
One	Batch A	1S12.6	S	241	3.4	70.9	20.5	7.1	13.0
One	Batch A	2S4.8	S	92	1.3	70.7	20.7	7.1	13.0
One	Batch A	2S24	S	459	6	76.6	20.9	7.1	13.0
One	Batch A	2S12.6	S	241	3.4	70.9	20.8	7.1	13.0
One	Batch A	2S28	S	536	7.5	71.5	20.8	7.1	13.0
One	Batch A	3S24	S	459	6	76.6	20.9	7.1	13.0
One	Batch A	3S12.6	S	241	3.4	70.9	20.9	7.1	13.0
One	Batch A	3S28	S	536	7.5	71.5	21.0	7.1	13.0
One	Batch A	3S4.8	S	92	1.3	70.7	21.2	7.1	13.0
One	Batch A	B	B	536	0		21.7	7.1	13.0
One	Batch A	FT2	FT				20.8	7.1	13.0
Two	Batch B	PBS-Fl.	PBS				20.2	7.0	13.1
Two	Batch B	FT1	FT				20.3	7.0	13.2
Two	Batch B	1S30	S	574	4.6	124.8	20.2	7.0	13.1
Two	Batch B	1S4.8	S	92	0.8	114.8	20.3	6.9	13.1
Two	Batch B	1S24	S	459	3.5	131.2	20.7	7.0	13.1
Two	Batch B	1S12.6	S	241	2	120.6	20.5	7.0	13.1
Two	Batch B	2S4.8	S	92	0.8	114.8	20.6	7.0	13.2
Two	Batch B	2S24	S	459	3.5	131.2	20.8	7.0	13.2
Two	Batch B	2S12.6	S	241	2	120.6	20.7	7.0	13.1
Two	Batch B	2S30	S	574	4.5	127.6	20.8	7.0	13.1
Two	Batch B	3S24	S	459	3.5	131.2	20.7	7.0	13.1
Two	Batch B	3S12.6	S	241	2	120.6	20.8	7.0	13.1
Two	Batch B	3S30	S	574	4.4	130.5	20.9	7.0	13.1
Two	Batch B	3S4.8	S	92	0.8	114.8	21.0	7.0	13.2
Two	Batch B	B	B	574	0		21.6	7.0	13.2
Two	Batch B	FT2	FT				21.0	6.9	13.1
Three	Batch B	PBS-Fl.	PBS				22.1	7.1	13.0
Three	Batch B	PBS-FF	PBS				21.7	7.0	13.0
Three	Batch B	FT1	FT				21.8	7.1	13.0
Three	Batch B	1S30	S	574	5.5	104.4	21.0	7.0	13.1
Three	Batch B	1S4.8	S	92	1.5	61.2	21.5	7.1	13.0
Three	Batch B	1S24	S	459	4.6	99.9	21.7	7.1	13.0
Three	Batch B	1S12.6	S	241	2.7	89.3	22.5	7.1	13.0
Three	Batch B	2S4.8	S	92	1.5	61.2	21.9	7.1	13.0
Three	Batch B	2S24	S	459	4.6	99.9	21.8	7.1	13.0
Three	Batch B	2S12.6	S	241	2.8	86.1	22.3	7.1	13.0
Three	Batch B	2S30	S	574	5.3	108.3	22.1	7.1	13.0
Three	Batch B	3S24	S	459	4.5	102.1	22.3	7.1	13.0
Three	Batch B	3S12.6	S	241	2.8	86.1	22.4	7.1	13.0
Three	Batch B	3S30	S	574	5.4	106.3	22.3	7.1	13.0
Three	Batch B	3S4.8	S	92	1.4	65.6	21.7	7.1	13.0
Three	Batch B	B	B	574	0		20.5	7.1	13.0
Three	Batch B	FT2	FT				20.3	7.1	13.0
Four	Batch C	PBS-Fl.	PBS				20.0	7.0	13.6
Four	Batch C	PBS-FF.	PBS				20.2	7.0	13.7
Four	Batch C	FT1	FT				21.2	7.1	13.6
Four	Batch C	1S30	S	574	7.1	80.9	19.2	7.0	13.6
Four	Batch C	1S4.8	S	92	2.1	43.8	21.0	7.0	13.6
Four	Batch C	1S24	S	459	6	76.5	21.3	7.0	13.6
Four	Batch C	1S12.6	S	241	3.8	63.4	21.6	7.1	13.6
Four	Batch C	2S4.8	S	92	2	46.0	21.2	7.0	13.7
Four	Batch C	2S24	S	459	6	76.5	21.4	7.0	13.7
Four	Batch C	2S12.6	S	241	3.6	66.9	21.8	7.1	13.6

Table 11-17 continued

Experiment	Membrane	Sample Name	Sample Type	Flux [LMH]	TMP [bar]	Permeability [LMH/bar]	Temperature [°C]	pH [-]	Electrical conductivity [mS/cm]
Four	Batch C	2S30	S	574	7	82.0	21.8	7.1	13.7
Four	Batch C	3S24	S	459	6	76.5	21.9	7.1	13.7
Four	Batch C	3S12.6	S	241	3.5	68.9	21.8	7.1	13.7
Four	Batch C	3S30	S	574	7	82.0	21.6	7.0	13.7
Four	Batch C	3S4.8	S	92	1.8	51.1	21.7	7.1	13.7
Four	Batch C	B	B	574	0		21.4	7.1	13.7
Four	Batch C	FT2	FT				21.2	7.1	13.6
Five	Batch B	PBS-Fl.	PBS				18.4	7.4	13.3
Five	Batch B	PBS-FF.	PBS				18.4	7.4	13.3
Five	Batch B	FT1	FT				18.4	7.4	13.4
Five	Batch B	1S30	S	574	8	71.8	18.4	7.4	13.4
Five	Batch B	1S4.8	S	92	1.5	61.3	18.4	7.4	13.4
Five	Batch B	1S24	S	459	6.5	70.6	18.4	7.4	13.3
Five	Batch B	1S12.6	S	241	4	60.3	18.4	7.4	13.4
Five	Batch B	2S4.8	S	92	1.5	61.3	18.4	7.4	13.4
Five	Batch B	2S24	S	459	6.5	70.6	18.4	7.4	13.3
Five	Batch B	2S12.6	S	241	4	60.3	18.4	7.4	13.3
Five	Batch B	2S30	S	574	8.3	69.2	18.4	7.4	13.3
Five	Batch B	3S24	S	459	6.9	66.5	18.4	7.4	13.4
Five	Batch B	3S12.6	S	241	4	60.3	18.4	7.4	13.4
Five	Batch B	3S30	S	574	8.8	65.2	18.4	7.4	13.4
Five	Batch B	3S4.8	S	92	1.5	61.3	18.4	7.4	13.4
Five	Batch B	B	B	574	0		18.4	7.4	13.4
Five	Batch B	FT2	FT				18.4	7.4	13.4

11.4.9 Box plots of LRV of PFU and dPCR of MS2 phages

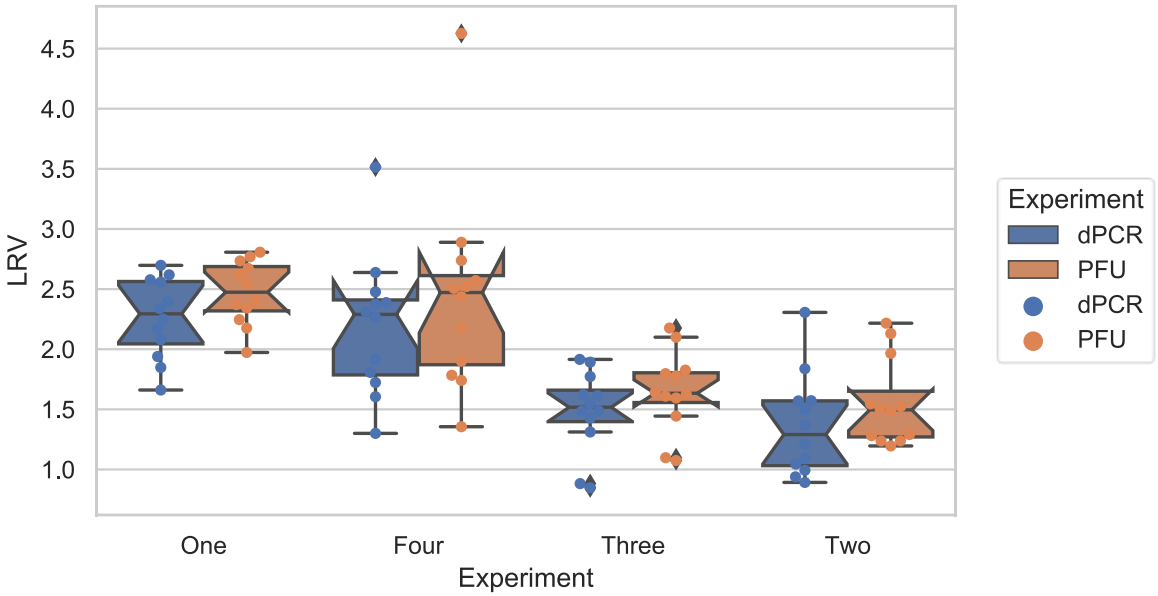

Figure 11-13: Boxplots of LRVs of experiments one to four for MS2 phages measured either by PFU (upper panels) or by dPCR (bottom panels). The notches of the box plots indicate the 95 % confidence interval of the corresponding data sets. Each box shows the 25 %- and 75 %-quantiles of the dataset, while the whiskers extend to show the rest of the distribution, except for points that are determined to be 'outliers' using the method that is a function of the 1.5 inter-quartile range. The median is indicated by the horizontal line within the box. Since the data were roughly normally distributed the arithmetic mean was close to the median.

11.4.10 Cook's distance analysis of linear regression models

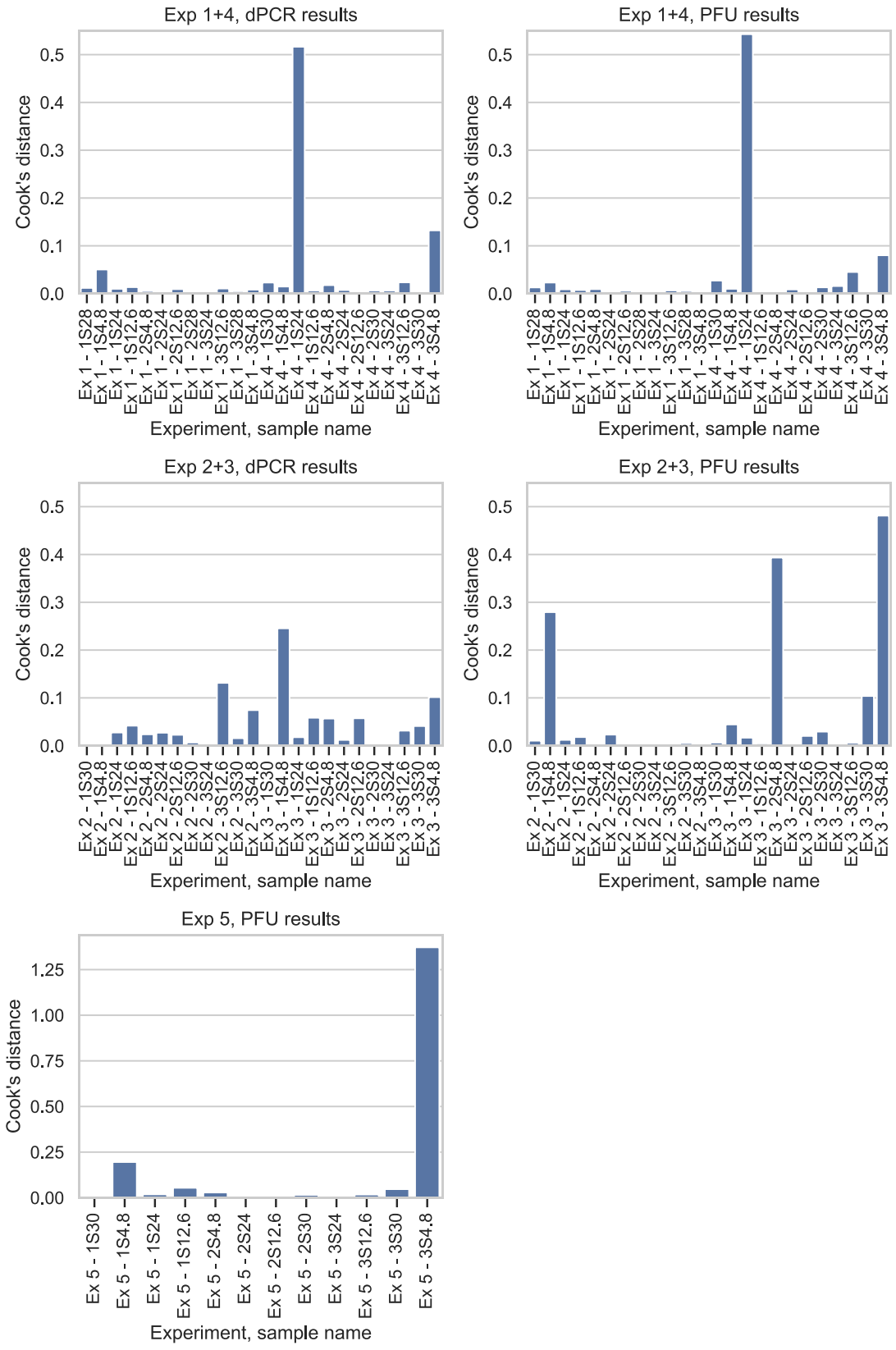

Figure 11-14: Cook's distances determined for the regression model analysis (cf. Figure 11-15)

11.4.11 Results student t-tests

Table 11-18: Two-sample t-test with dependent samples: Comparison of LRVs of experiment 2 with LRVs of experiment 5

	LRV Experiment 2	LRV Experiment 5
Arithmetic mean	1.55	2.99
Variance	0.13	0.18
Number of samples	12	12
Pearson correlation	0.36	
Hypothetic differenz between the arithmetic mean values	0.00	
degrees of freedom (df)	11	
t-statistic	-11.24	
P(T<=t) one sided	1.14E-07	
Critical t-value for one sided t-test	1.80	
P(T<=t) paired (two sided)	2.28E-07	
Critical t-value for paired (two sided) t-test	2.20	

Table 11-19: Two-sample t-test with dependent samples: Comparison of LRVs of experiment 3 with LRVs of experiment 5

	LRV Experiment 3	LRV Experiment 5
Arithmetic mean	1.65	2.99
Variance	0.11	0.18
Number of samples	12	12
Pearson correlation	0.78	
Hypothetic differenz between the arithmetic mean values	0.00	
degrees of freedom (df)	11	
t-statistic	-17.49	
P(T<=t) one sided	1.12E-09	
Critical t-value for one sided t-test	1.80	
P(T<=t) paired (two sided)	2.24E-09	
Critical t-value for paired (two sided) t-test	2.20	

Table 11-20: Two-sample t-test with dependent samples: Comparison of LRVs of experiment 1 with LRVs of experiment 5

	LRV Experiment 1	LRV Experiment 5
Arithmetic mean	2.51	2.99
Variance	0.07	0.18
Number of samples	12	12
Pearson correlation	0.40	
Hypothetic differenz between the arithmetic mean values	0.00	
degrees of freedom (df)	11	
t-statistic	4.58	
P(T<=t) one sided	3.94E-04	
Critical t-value for one sided t-test	1.80	
P(T<=t) paired (two sided)	7.88E-04	
Critical t-value for paired (two sided) t-test	2.20	

Table 11-21: Two-sample t-test with dependent samples: Comparison of LRVs of experiment 4 with LRVs of experiment 5

	LRV Experiment 4	LRV Experiment 5
Arithmetic mean	3.04	2.99
Variance	0.18	0.18
Number of samples	12	12
Pearson correlation	0.45	
Hypothetic differenz between the arithmetic mean values	0.00	
degrees of freedom (df)	11	
t-statistic	3.40	
P(T<=t) one sided	2.97E-03	
Critical t-value for one sided t-test	1.80	
P(T<=t) paired (two sided)	5.94E-03	
Critical t-value for paired (two sided) t-test	2.20	

11.4.12 Trends of absolute dPCR and PFU counts of MS2 phages in permeate

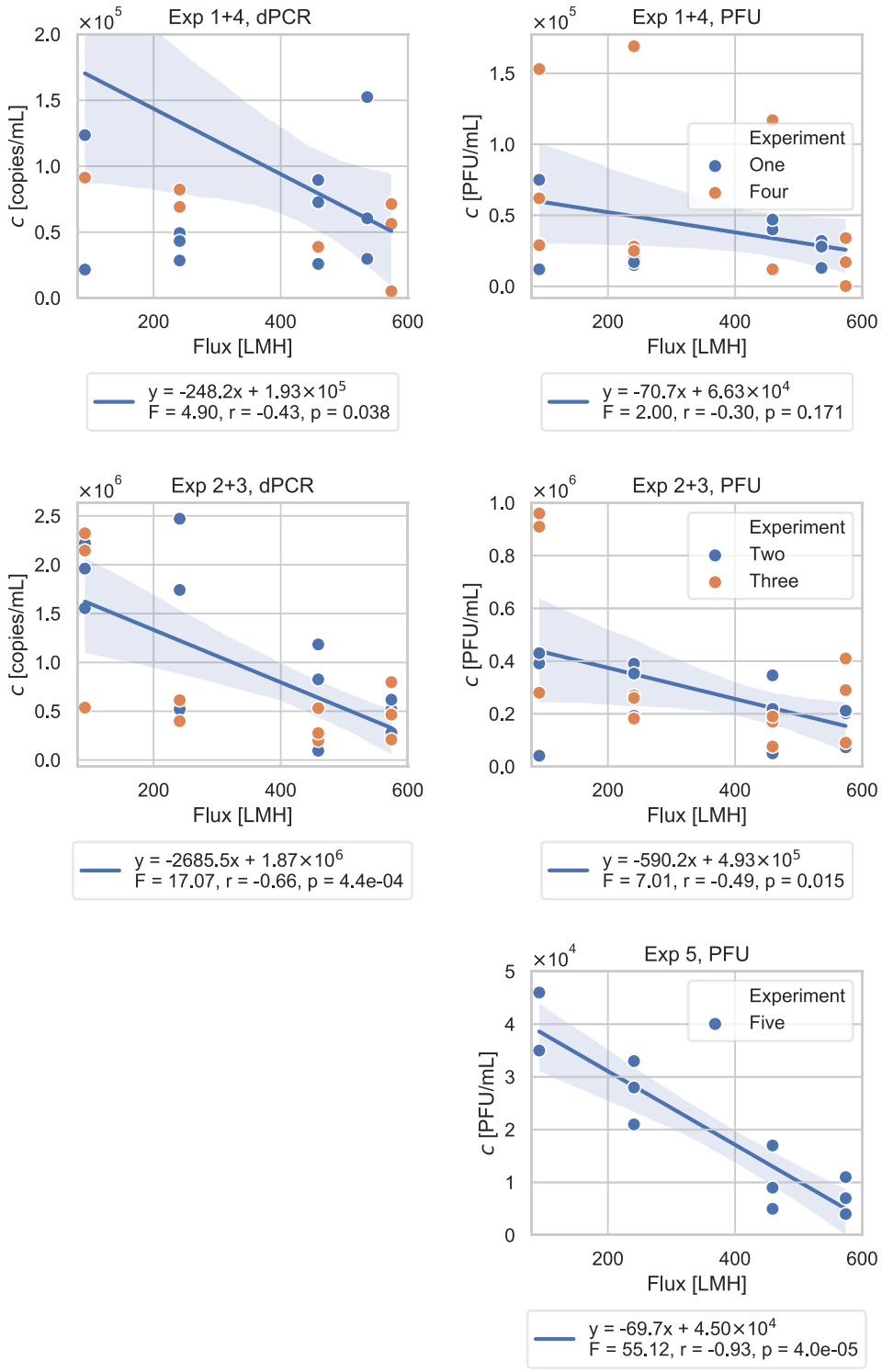

Figure 11-15: Linear regression models fitting the decreasing values of the absolute concentration of the MS2 phages with increasing flux or TMP measured by dPCR as well as PFU. The shaded areas around the fitted lines indicate the 95 % confidence interval of the regression lines. y describes the equation of the trend line equation. r represents the Pearson correlation coefficient. For $p < \alpha = 0.05$ the corresponding observed trend can be regarded as statistically significant. The LRV that were based on these absolute values are visualized in Figure 5-5.

11.4.13 Trends of LRVs measured by PFU and dPCR for all individual experiments

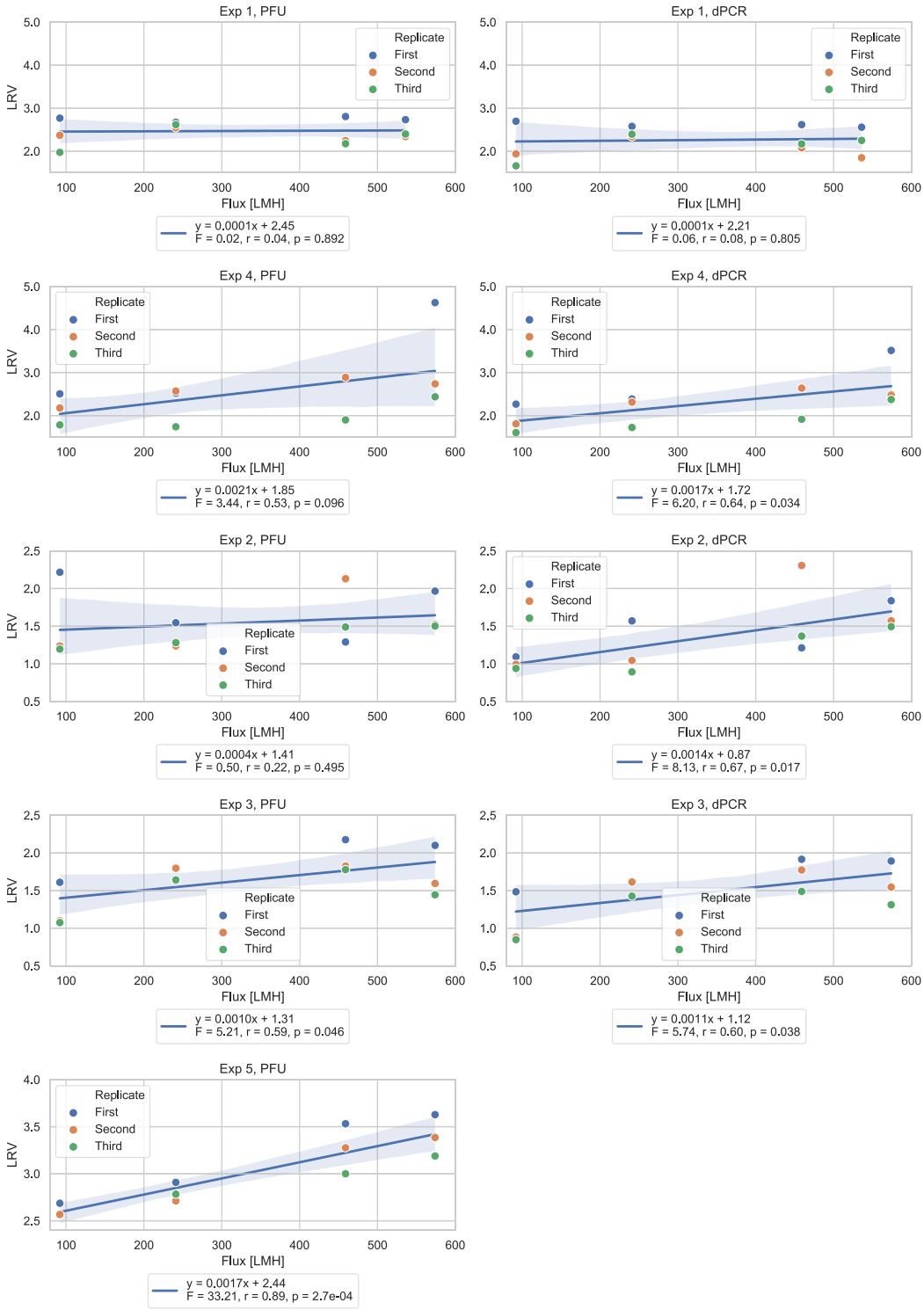

Figure 11-16: Linear regression models fitting the increasing LRVs of MS2 phages with increasing flux or TMP measured by dPCR as well as PFU for all individual experiments. The shaded areas around the fitted lines indicate the 95 % confidence interval of the regression lines. y describes the equation of the trend line equation. r represents the Pearson correlation coefficient. For $p < \alpha = 0.05$ the corresponding observed trend can be regarded as statistically significant. The underlying absolute values are displayed in section 11.4.12 (Figure 11-15). All values are included, no outlier's exclusion via Cook's distance was applied.

11.4.14 MS2 LRVs of different UF membranes reported in literature with the main experimental parameters applied

Table 11-22: MS2 LRVs of different UF membranes reported in literature with the main experimental parameters applied

UF membrane type	MWCO [kDa]	Pore size [nm]	LRV	Water matrix spiked with MS2	Reference
Ceramic: Al_2O_3 + TiO_2	100	30	1.5-3(median)	PBS, pH 7, TMP ranging between 1 to 8 bars, varying initial MS2 phage feed concentrations	Own study results
PVDF, DE	–	30	1.25	Pretreated river water, infectious MS2 were analyzed	Boudaud et al. (2012)
Modified PVDF, hollow fiber, DE	–	2 – 56 with median = 9	3.7 (average)	Deionized water	ElHadidy et al. (2013a)
PVDF, hollow fiber, DE	–	100	2.7 1.3 2.5 1.0 1.6 0.9	Secondary waste water effluent; Filtered secondary effluent; Sodium phosphate buffer (NaPi) NaPi + Ca/Na NaPi + Na NaPi + Ca	Huang et al. (2012)
Cellulosic esters, CF Polysulfone, CF	100 500	– –	> 6.8 ± 0.3* 1.5 ± 0.4*	Always deionized water + 0.0001 M phosphate buffer at pH 7;	Jacangelo et al. (1995)
Cellulose, DE PES, DE PES, DE	100 100 150	10 50 25	> 6 3.54 ± 0.56 > 4.89	Always 0.2 mM PBS	Langlet et al. (2009)
PES-20, DE	20-30	5-20	2.8-3.8	Sterile deionized water, observed decreasing retention with increasing TMP	Arkhangelsky and Gitis (2008)
Yttria stabilized Zirconia, DE	– – – – –	24.0 ± 2.6 35.0 ± 1.0 55.3 ± 3.2 96.0 ± 2.6 146 ± 4.4 (average)	9.2 ± 0.4 6 – 7 4.5 4 4	Always saline solutions (0.02M $MgCl_2$/0.15M NaCl) at pH 5.8	Werner et al. (2014)

DE = dead-end operation

CF = cross-flow operation

*Results for maximum pressure operation without any recirculation of the cross-flow concentrate

11.5 Supplementary information for Chapter 6

11.5.1 Wastewater parameter of WWTP Steinhäule

During MF and UF studies, wastewater parameters of the secondary and tertiary effluents of the full-scale WWTP Steinhäule were measured by online measurement devices. The range of measured dissolved organic fractions (UVA_{254}), total nitrogen and ortho-phosphate during the studies are illustrated in the Table 11-23.

Table 11-23: Secondary effluent (SE) and tertiary effluent (SE+PAC+SF) with arithmetic average of wastewater parameters measured during MF and UF studies.

values	TE	SE
UVA_{254} [m^{-1}]	4.73 ± 1.20	9.30 ± 1.14
N_{total} [mg/L]	4.47 ± 0.98	4.02 ± 0.92
PO_4-P [mg/L]	0.08 ± 0.05	0.37 ± 0.16

11.5.2 Role of the fouling layer for additional AMR removal

The data series of the Figure 6-4 were proved for significance mean values using pair samples T-tests (Table 11-24). The study results revealed that the correlation values for the pair samples T tests are moderate to significant at 0.57 to 1.00. The data series of 55 minutes' samples had lower but not significant lower *sul1* gene, *ermB* gene and TCC mean values than the data series of 5 minutes' samples. In contrast, *16S rRNA* gene and HNAC value had almost the same mean values comparing data series of 5 and 55 minutes' samples. Remarkable was the fact that *vanA* gene had significant lower abundances in the data series of 55 minutes' samples than the data series of 5 minutes samples.

Table 11-24: Results of pair samples T-Tests of sul1, ermB, vanA, 16S rRNA genes and HNAC, TCC values (experiment V

Parameter	sul1 [gene copies/100 mL]	ermB [gene copies/100 mL]	vanA [gene copies/100 mL]	16SrRNA [gene copies/100 mL]	HNAC [1/100 mL]	TCC [1/100 mL]
Mean value 5 min	4490	737	3844	113264	221600	6496467
Mean value 55 min	3384	500	500	133542	226833	4082933
Correlation	0.95	-	-	0.57	1	1
P-Value	0.166	0.356	0.004	0.548	0.629	0.187

11.5.3 Role of feed water quality for UF filtrate water quality

For statistical data analyses of the analyzed values of Figure 5 independent samples T-tests were conducted (Table 11-25). The data analyses demonstrated that *sul1*, *ermB*, *vanA* and *16S rRNA* genes as well as HNAC and TCC had significant different mean values comparing the feeds secondary and tertiary effluent. While all parameters of secondary effluent had significant higher mean values than tertiary effluent, mean values of *sul1*genes and TCC value were significant higher in ultrafiltered secondary effluent compared to ultrafiltered tertiary effluent ($p < 0.05$). Despite of significant HNAC and *16S rRNA* gene values in the feeds, the filtrates had almost the same mean values of HNAC and *16S rRNA* gene.

Table 11-25: Results of independent samples T-tests of sul1, ermB, vanA, 16S rRNA genes and HNAC, TCC values (experiment VI)

Parameter	sul1 [gene copies/100 mL]	ermB [gene copies/100 mL]	vanA [gene copies/100 mL]	16SrRNA [gene copies/100 mL]	HNAC [1/100 mL]	TCC [1/100 mL]
Mean value SE	1044646	149452.7	20012.2	330000000	410000000	1300000000
Mean value TE	215132	50258.4	6799.3	48846771	30816783	180000000
P-value	0.001	0.001	0.000	0.005	0.010	0.000
Mean value UF SE	3554	603.5	2244	128940	332900	4728115
Mean value UF TE	927	564.8	1285	162223	325800	940250
P-value	0.029	0.744	0.164	0.194	0.947	0.007

11.5.4 Absolute removal efficiencies of different parameters of the MF and UF process using secondary effluent as feed

To analyze the effect of different pore sizes leading to different AMR removal efficiencies, MF and UF with different pore sizes were employed. AMR analyzes were performed in the SE feed water as well as in the MF and UF filtrates, while MF and UF modules were operated in parallel using the same feed. The results are illustrated in Figure 11-17. While slightly higher TCC removals were analyzed by UF compared to MF, significantly higher HNAC and *16S rRNA* gene removals were observed using UF compared to MF. While MF and UF reduced *ermB* gene by about 2.7 and 2.8 log units, *sul1* gene removal was higher using UF (2.9 log units) compared to MF (2.1 log units). Significant lower *vanA* gene removal by MF (1.1 log units) and UF (1.2 log unit) were observed.

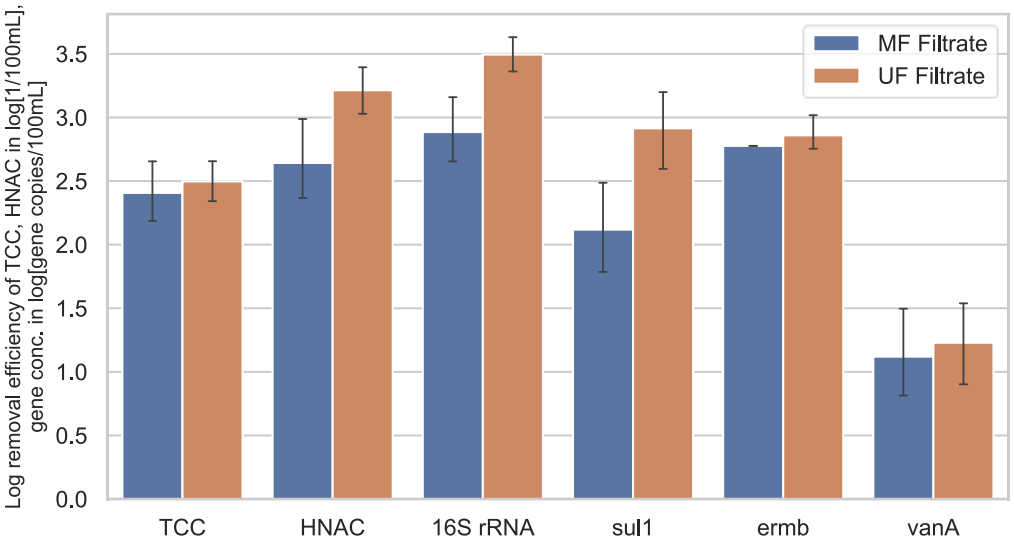

Figure 11-17: The absolute removal differentials of different parameters of the MF and UF process are illustrated while using secondary effluent from WWTP Steinhäule as feed water.

Independent samples T-tests of the analyzed values of Figure 6 were performed for significant mean value evaluation (Table 11-25). The data analyses in Table 11-26 illustrated that *ermB* and *vanA* genes had no significant different mean values. Indeed, *ermB* and *vanA* genes had almost the same abundances comparing MF and UF samples. In contrast, a clear trend in TCC mean values were observed whereas UF samples had about 37 % lower TCC values than MF samples. However, significant different mean values could be confirmed according to *sul1* gene, *16S rRNA* gene and HNAC value comparing MF and UF samples ($p < 0.05$).

Table 11-26: Results of independent samples T-tests of sul1, ermB, vanA, 16S rRNA genes and HNAC, TCC values (experiment VII)

Parameter	sul1 [gene copies/100 mL]	ermB [gene copies/100 mL]	vanA [gene copies/100 mL]	16SrRNA [gene copies/100 mL]	HNAC [1/100 mL]	TCC [1/100 mL]
Mean value MF SE	15136.8	500	2417.7	567215.9	1494257	7465050
Mean value UF SE	3605.3	603.5	1932.5	128939.9	332900	4728115
P-value	0.036	0.492	0.521	0.010	0.026	0.175

11.5.5 Comparison of TCC and HNAC abundance in Secondary effluent as well as in MF and UF filtrate

Flow cytometry measurements were performed in the SE feed water as well as the MF and UF filtrates, while MF and UF modules were operated in parallel using the same feed in order to compare retention of bacteria measured as HNAC. The results are illustrated in Figure 11-18. While MF reduced TCC values by about 2.6 log units, UF could reduce TCC values by about 3 log units.

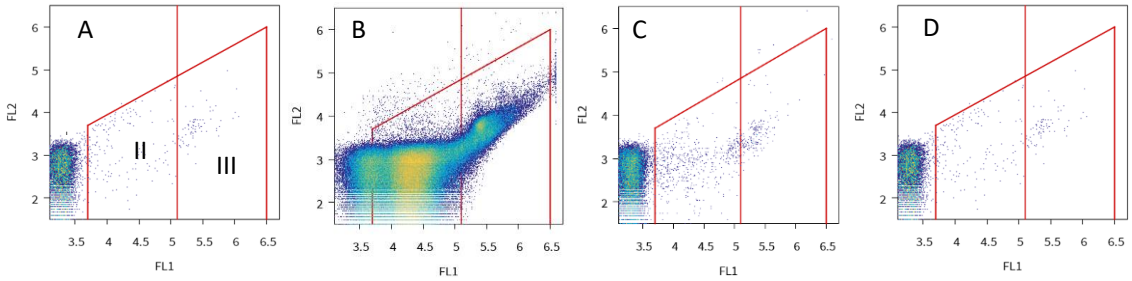

Example graph and description	Secondary effluent (SE) 1:3 dilution	MF effluent	UF effluent
TCC [1/100mL]	355,502,000	1,071,100	286,900
HNAC [%]	11.50	19.39	28.69

Figure 11-18: A: Structure of the flow cytometry diagram: x-axis: Fluorescence signal (FL1); y-axis: Fluorescence signal (FL2). Section I is the background signal; section II is the LNAC abundance and section III is the HNAC abundance. TCC is the sum of LNAC and HNAC. B: TCC and HNAC values of feed SE. C: TCC and HNAC values of corresponding MF filtrate. D: TCC and HNAC values of corresponding UF filtrate.

11.5.6 Live/Dead bacteria analyses

Live/dead bacteria analyses were undertaken to show living bacteria breakthrough the UF membrane. While in Figure 11-19A, the living bacteria are illustrated, the dead bacteria are presented in Figure 11-19B. The overall living and dead cells as well as 0.2 µm beads are shown in the graphical Figure 11-19C.

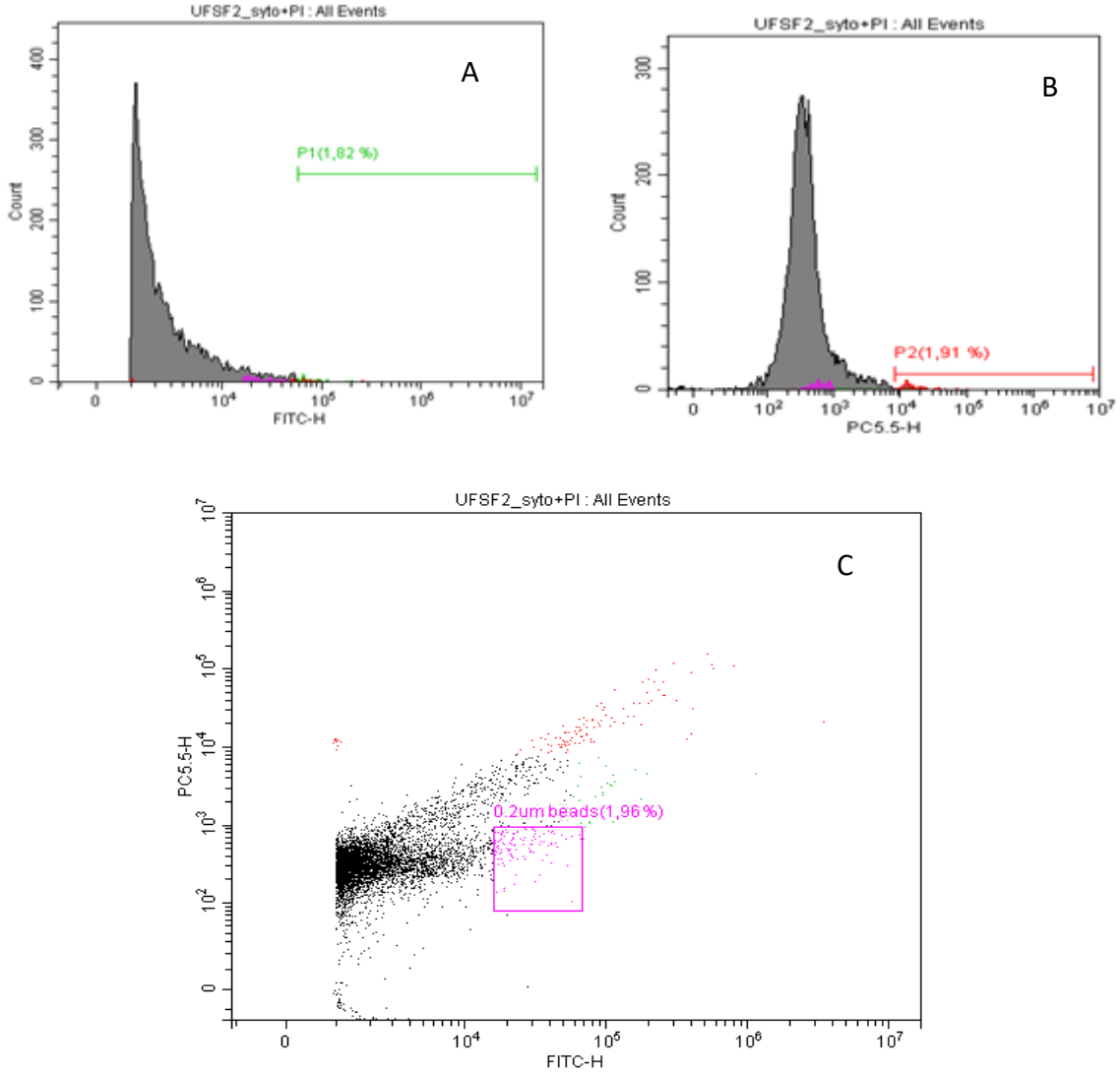

Figure 11-19: A: Living bacteria analysis of sample UF filtrate using feed tertiary effluent. Fluorescent channel FITC was applied. Sample was stained with Syto9. B: Dead bacteria analysis of sample UF filtrate using feed tertiary effluent. Fluorescent channel PC 5.5 was applied. Sample was stained with Propidiumiodide. C: graphical illustration of all detected DNA. Red dots are dead bacterial cells. Green dots are living bacterial cells. Purple dots are added 0.2 µm beads. Black dots are either LNAC or background noise.

11.5.7 Quantitative PCR standard curves

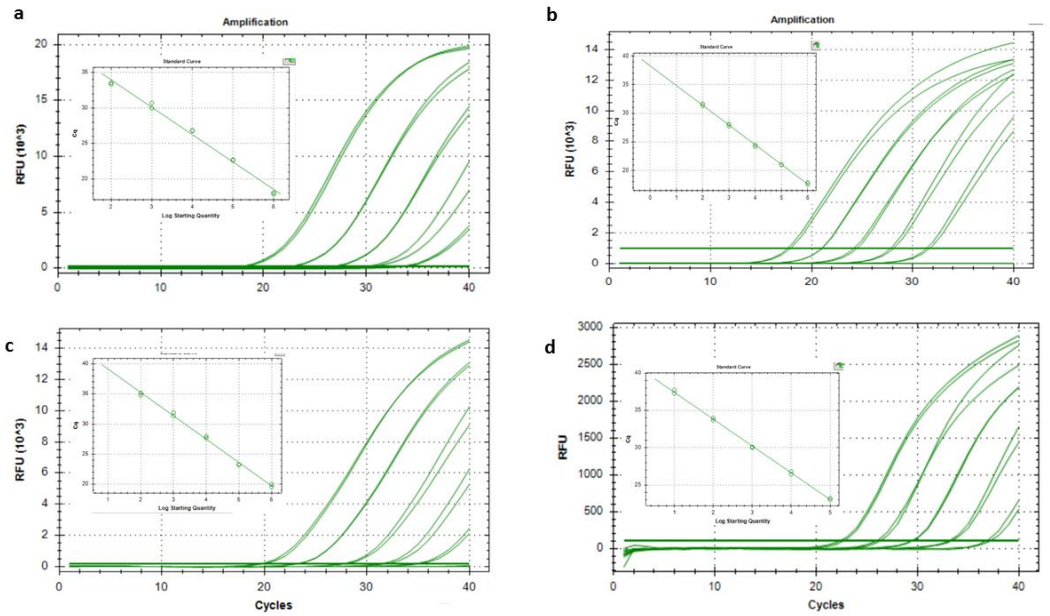

Figure 11-20: Standard curves for calibration of the quantitative PCR assays for the quantification of microbial genes. The above examples are extracted from the Bio-Rad CFX Manager (version 3.1) software for analyzing the qPCR results for a) 16S, b) ermB, c) sul1 and d) vanA gene copies. Inlets are showing the standard curves that resulted from the respective dilution series.

11.6 Supplementary information for Chapter 7

11.6.1 Figures

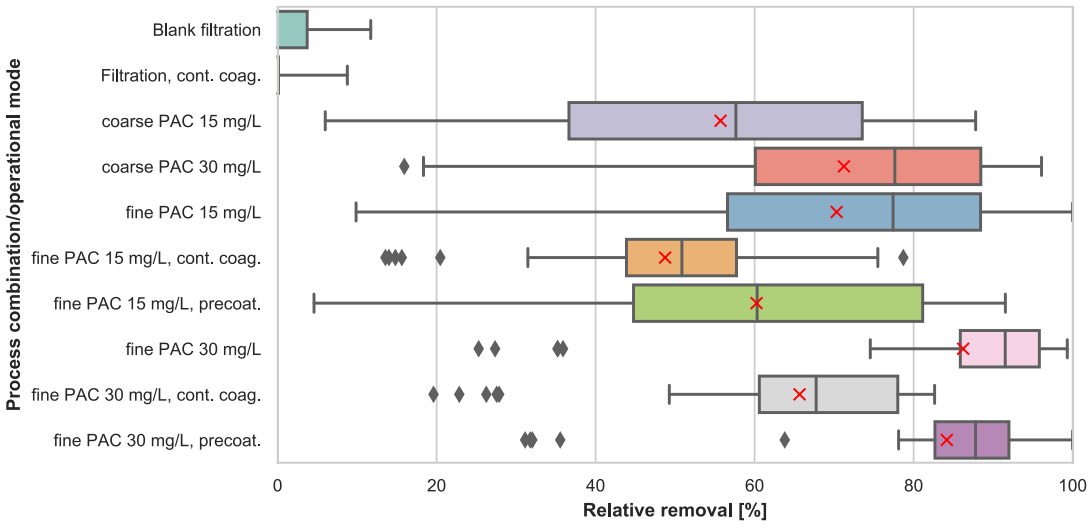

Figure 11-21: Box plots of overall removal efficiencies of TOrCs by operational modes tested in pilot scale, n = 56 per box plot. Each box shows the 25 %- and 75 %-quantiles of the dataset, while the whiskers extend to show the rest of the distribution, except for points that are determined to be ‘outliers’ using the method that is a function of the 1.5 inter-quartile range. The median is indicated by the vertical line within the box and the arithmetic mean is represented by the red cross.

11.6.2 Tables

Table 11-27: Specifications and typical properties of used PACs according to Chemviron Carbon.

Specifications and typical properties	PULSORB WP235		PULSORB WP260	
Iodine number, min. [mg/g]	850		1000	
Moisture, as packed, max. [wt%]	5		5	
Particle size analysis [%]	<75 µm	90	<45 µm	95
	<20 µm	50	<6 µm	50
Mean particle diameter [µm]	30		6–8	
Density, loose packed [kg/m^3]	350		-	

Table 11-28: Analytical methods for determining the water quality parameters.

	Parameter	Analytical method	Limit of quantitation (LOQ)
In-situ parameters	Electrical conductivity	EN ISO 10523, DEV C 5	-
	pH	EN ISO 10523, DEV C 5	-
Sum parameters	COD	DIN EN 38409, DEV H41	0.5 mg/L
	TOC	EN 1484, DEV H3	3 mg/L
	DOC	EN 1484, DEV H3	3 mg/L
	UV_{254}	DIN 38404-3	-
Anions	Nitrate NO_3^--N	DIN EN ISO 10304-1, DEV D19	0.05 mg/L
	ortho-Phosphate PO_4^{3-}-P		0.05 mg/L
TOrC	4-Formylaminoantipyrine	Müller et al. (2017)	10.0 ng/L
	Antipyrine		10.0 ng/L
	Atenolol		10.0 ng/L
	Benzotriazole		50.0 ng/L
	Caffeine		10.0 ng/L
	Carbamazepine		5.0 ng/L
	Citalopram		5.0 ng/L
	Climbazol		5.0 ng/L
	Diclofenac		5.0 ng/L
	Erythromycin		50.0 ng/L
	Gabapentin		2.5 ng/L
	Iopromid		50.0 ng/L
	Metoprolol		2.5 ng/L
	Phenytoin		5.0 ng/L
	Primidone		25.0 ng/L
	Sotalol		5.0 ng/L
	Sulfamethoxazole		5.0 ng/L
	TCEP		50.0 ng/L
	Tramadol		5.0 ng/L
	Trimethoprim		5.0 ng/L
	Valsartanic acid		5.0 ng/L
	Venlafaxine		2.5 ng/L

Table 11-29: Physicochemical quality parameters of the feed water for the tested HMP process (PAC and coagulant dosed prior to UF). Abbreviations stand for T = temperature, EC = electrical conductivity, COD = chemical oxygen demand, TOC = total organic carbon, DOC = dissolved organic carbon, UV_{254} = ultraviolet absorbance at 254 nm, NO_3^--N = nitrate measured as nitrogen, PO_4^{3-}-P = ortho-phosphate measured as phosphorus

Operational mode	**pH [-]**	**T [°C]**	**EC [µS/cm]**	**COD [mg/L]**	**TOC [mg/L]**	**DOC [mg/L]**	**UV_{254} [1/m]**	**NO_3^--N [mg/L]**	**PO_4^{3-}-P [mg/L]**
filtration, cont. coag.	7.4 ± 0.1	19.5 ± 0.1	754 ± 110	15.6 ± 0.9	5.4	4.6 ± 0.2	9.4 ± 0.4	2.2	0.4
blank filtration	7.1 ± 0.1	19.5 ± 0.1	500 ± 18	14.1 ± 1.4	5.6	4.1 ± 0.1	8.3 ± 0.1	1.8	0.4
coarse PAC 15 mg/L	7.4 ± 0.1	19.6 ± 0.1	774 ± 17	15.6 ± 0.9	5.4	4.2 ± 0.3	9.5 ± 0.1	4.0	0.6
coarse PAC 30 mg/L	7.3 ± 0.1	19.1 ± 0.2	755 ± 5	12.3 ± 0.6	4.6	4.1 ± 0.0	8.9 ± 0.1	4.0	0.4
fine PAC 15 mg/L	7.2 ± 0.1	19.4 ± 0.1	607 ± 9	13.4 ± 2.0	5.4	4.1 ± 0.1	9.2 ± 0.1	4.0	0.7
fine PAC 15 mg/L, cont. coag.	7.2 ± 0.1	18.4 ± 0.2	383 ± 4	11.3 ± 0.4	3.6	3.4 ± 0.3	7.0 ± 0.1	2.6	0.5
fine PAC 15 mg/L, precoat.	7.4 ± 0.1	19.2 ± 0.2	742 ± 4	14.2 ± 0.1	5.5	4.3 ± 0.2	9.6 ± 0.1	4.6	0.6
fine PAC 30 mg/L	7.2 ± 0.1	19.7 ± 0.2	502 ± 22	13.1 ± 0.4	4.3	4.0 ± 0.0	8.2 ± 0.0	2.0	0.7
fine PAC 30 mg/L, cont. coag	7.4 ± 0.1	18.5 ± 0.1	739 ± 4	13.6 ± 0.6	4.8	4.1 ± 0.0	9.0 ± 0.0	4.2	0.4
fine PAC 30 mg/L, precoat.	7.1 ± 0.1	18.6 ± 0.1	460 ± 27	9.6 ± 0.2	3.7	3.3 ± 0.1	6.9 ± 0.1	2.8	0.4
Total	7.3 ± 0.1	19.1 ± 0.4	621 ± 147	13.4 ± 2.0	4.8 ± 0.7	4.0 ± 0.4	8.6 ± 0.9	3.2 ± 1.0	0.5 ± 0.1

Table 11-30: Absolute arith. mean concentrations and corresponding standard deviations (std) of TOrCs in feed water and permeate water (n = 4) of the tested HMP process PAC and coagulant dosed prior to UF.

Process combination /operational mode	Name of TOrC	Feed water [ng/L]		Permeate/filtrate water [ng/L]	
		Mean	Std	Mean	Std
filtration, cont. coag.	4-Formylaminoantipyrine	1173	114	1218	146
	Benzotriazole	3415	260	3548	335
	Carbamazepine	220	18	232	18
	Citalopram	87	6	91	3
	Diclofenac	1119	150	1204	187
	Gabapentin	1089	107	1198	93
	Iopromide	945	111	1018	158
	Metoprolol	199	22	212	28
	Primidone	127	13	137	17
	Sulfamethoxazole	137	9	145	7
	Tramadol	116	12	123	11
	Trimethoprim	57	5	57	7
	Valsartanic acid	1266	115	1324	148
	Venlafaxine	208	18	218	25
blank filtration	4-Formylaminoantipyrine	991	20	1004	32
	Benzotriazole	3092	173	3190	132
	Carbamazepine	179	6	179	8
	Citalopram	79	5	79	7
	Diclofenac	820	28	831	48
	Gabapentin	1005	74	965	69
	Iopromide	693	69	693	27
	Metoprolol	160	4	165	6
	Primidone	103	3	106	5
	Sulfamethoxazole	106	9	111	6
	Tramadol	95	6	97	6
	Trimethoprim	48	2	47	2
	Valsartanic acid	935	96	966	94
	Venlafaxine	174	8	172	8
coarse PAC 15 mg/L	4-Formylaminoantipyrine	1746	52	990	30
	Benzotriazole	4282	234	1149	151
	Carbamazepine	202	5	60	7
	Citalopram	93	2	17	4
	Diclofenac	1256	10	600	13
	Gabapentin	1445	134	1208	68
	Iopromide	4135	415	2804	248
	Metoprolol	207	7	33	6
	Primidone	162	4	91	4
	Sulfamethoxazole	280	24	179	11
	Tramadol	143	4	45	2
	Trimethoprim	81	2	12	2
	Valsartanic acid	1636	8	1172	18
	Venlafaxine	239	5	83	6
coarse PAC 30 mg/L	4-Formylaminoantipyrine	1385	10	493	43
	Benzotriazole	4355	310	601	155
	Carbamazepine	247	7	30	12
	Citalopram	82	3	10	4
	Diclofenac	797	21	219	38
	Gabapentin	1505	92	1213	72
	Iopromide	3507	373	1630	258
	Metoprolol	190	10	14	8
	Primidone	133	3	49	3
	Sulfamethoxazole	260	9	103	7
	Tramadol	114	3	17	4
	Trimethoprim	82	2	7	2
	Valsartanic acid	1062	33	533	7
	Venlafaxine	197	4	35	8

Table 11-30 continued

Process combination/operational mode	Name of TOrC	Feed water [ng/L]		Permeate/filtrate water [ng/L]	
		Mean	Std	Mean	Std
fine PAC 15 mg/L	4-Formylaminoantipyrine	1390	39	524	53
	Benzotriazole	3389	171	551	185
	Carbamazepine	184	9	23	12
	Citalopram	79	2	20	19
	Diclofenac	906	45	236	100
	Gabapentin	1393	31	1232	25
	Iopromide	3416	393	1608	292
	Metoprolol	165	11	11	9
	Primidone	123	4	41	6
	Sulfamethoxazole	204	10	82	12
	Tramadol	113	5	13	5
	Trimethoprim	65	1	<5,0	<5,0
	Valsartanic acid	1068	52	563	32
	Venlafaxine	182	5	26	10
fine PAC 15 mg/L, cont. coag.	4-Formylaminoantipyrine	628	76	346	43
	Benzotriazole	2680	226	1039	91
	Carbamazepine	99	7	42	4
	Citalopram	57	4	35	11
	Diclofenac	482	57	262	38
	Gabapentin	769	123	643	101
	Iopromide	1179	657	491	484
	Metoprolol	102	11	45	7
	Primidone	62	5	32	6
	Sulfamethoxazole	109	6	57	2
	Tramadol	58	4	26	2
	Trimethoprim	49	5	20	4
	Valsartanic acid	451	38	275	17
	Venlafaxine	107	9	51	5
fine PAC 15 mg/L, precoat.	4-Formylaminoantipyrine	1783	96	850	175
	Benzotriazole	4565	292	1159	534
	Carbamazepine	197	8	47	28
	Citalopram	96	4	35	29
	Diclofenac	1245	76	484	194
	Gabapentin	1608	160	1420	52
	Iopromide	4727	450	2558	448
	Metoprolol	207	12	35	28
	Primidone	165	6	75	14
	Sulfamethoxazole	304	33	146	13
	Tramadol	133	7	35	20
	Trimethoprim	74	4	13	10
	Valsartanic acid	1515	52	916	97
	Venlafaxine	231	6	67	35
fine PAC 30 mg/L	4-Formylaminoantipyrine	972	26	100	34
	Benzotriazole	3821	120	303	123
	Carbamazepine	150	6	6	6
	Citalopram	72	4	18	19
	Diclofenac	1036	56	88	56
	Gabapentin	1195	23	825	59
	Iopromide	2205	127	290	64
	Metoprolol	165	2	5	4
	Primidone	92	4	<25	<25
	Sulfamethoxazole	92	12	11	4
	Tramadol	80	3	<5	<5
	Trimethoprim	51	2	<5	<5
	Valsartanic acid	614	19	105	37
	Venlafaxine	151	7	7	5

Table 11-30 continued

Process combination/operational mode	Name of TOrC	Feed water [ng/L]		Permeate/filtrate water [ng/L]	
		Mean	Std	Mean	Std
fine PAC 30 mg/L, cont. coag	4-Formylaminoantipyrine	1437	34	552	24
	Benzotriazole	5006	278	949	74
	Carbamazepine	239	2	51	2
	Citalopram	81	1	32	19
	Diclofenac	943	85	306	22
	Gabapentin	1736	99	1308	12
	Iopromide	4267	388	1943	106
	Metoprolol	207	13	42	2
	Primidone	131	6	48	3
	Sulfamethoxazole	210	25	75	13
	Tramadol	112	1	28	1
	Trimethoprim	84	1	17	2
	Valsartanic acid	963	21	412	34
	Venlafaxine	193	4	55	2
fine PAC 30 mg/L, precoat.	4-Formylaminoantipyrine	788	136	104	22
	Benzotriazole	2446	136	251	62
	Carbamazepine	106	7	<5	3
	Citalopram	59	3	11	7
	Diclofenac	423	32	63	14
	Gabapentin	895	186	604	132
	Iopromide	1500	543	244	144
	Metoprolol	98	18	6	2
	Primidone	66	9	<25	3
	Sulfamethoxazole	124	15	19	4
	Tramadol	61	5	<5	2
	Trimethoprim	48	2	<5	2
	Valsartanic acid	381	19	73	12
	Venlafaxine	111	7	11	3

11.7 Supplementary information for Chapter 8

11.7.1 Modelling flow in membrane systems

11.7.1.1 Mesoscale modelling

In UF, the small scales of feed channels and membrane pores usually result in laminar flows (Ghidossi et al. 2006b; Marcos et al. 2009). As a rough guideline, turbulence is widely considered to begin at Reynolds Numbers (Re) above 2300, with Re calculated based on average flow velocity, u, channel diameter, D, and kinematic viscosity, υ, according to equation (11-6).

$$Re = \frac{uD}{\upsilon} \tag{11-6}$$

Numerical solutions using the incompressible Navier-Stokes Equations are applied to flows in free-fluid regions (equations (11-7) and (11-8)) and Darcy's law (equation (11-9)) at the wall to determine filtration velocities (Oxarango et al. 2004; Ghidossi et al. 2006a; Marcos et al. 2009; Keir and Jegatheesan 2014; Lee et al. 2016).

$$\nabla \cdot \boldsymbol{u} = 0 \tag{11-7}$$

$$\frac{\partial \boldsymbol{u}}{\partial t} + (\boldsymbol{u} \cdot \nabla)\boldsymbol{u} = -\frac{1}{\rho}\nabla p + \nu\nabla^2\boldsymbol{u} + \boldsymbol{S} \tag{11-8}$$

$$\nabla p = -\frac{\mu}{\kappa}\mathbf{u} \tag{11-9}$$

Where **u** is flow velocity, t is time, ρ is fluid density, p is pressure, ν is kinematic viscosity, **S** is a source term, μ is dynamic viscosity, and κ is Darcy permeability.

As an extension to Darcy's law Brinkman's equation (equation (11-10)) provides an additional dissipative term to account for the significant viscous dissipation which can occur at the boundary between free and porous domains (Lu and Hwang 2020), where , μ̃ represents the effective viscosity.

$$\nabla p = -\frac{\mu}{\kappa}\mathbf{u} + \tilde{\mu}\nabla^2\boldsymbol{u} \tag{11-10}$$

In order to account for concentration polarization (CP) and fouling effects (Keir and Jegatheesan 2014) detailed modelling requires transient models. Since this study considered pure water, it not involved CP or fouling and modelling tasks were drastically simplified.

11.7.1.2 Nanoscale modelling

Since membrane module features are usually at the millimeter scale and the membrane surface features in UF are at the nanometer scale, the number of computation points required to simulate more than a small, representative section of a module quickly

becomes immense. An additional challenge with capturing fluid effects at the nanoscale is that additional physical effects become relevant. For this reason, flows at the micro to nanometer scale are considered under a subfield of fluid mechanics known as microfluidics (Rapp 2017).

11.7.1.3 Continuity

The Continuum Hypothesis typically holds as long as the Knudsen number, Kn, is much less than 1. The Knudsen number is most simply described as the ratio of the mean free path length of fluid particles, λ, to the characteristic length scale of the fluid domain, l_c, (equation (11-11)).

$$Kn = \frac{\lambda}{l_c} \tag{11-11}$$

The mean free path length of liquid water can be safely assumed to be about 0.31 nm (Rapp 2017). Though the mean free path length of liquids are not as predictable as with gases due to the very small spacing between molecules (Singh and Myong 2018), the assumption of 0.31 nm is based on the size of water molecules and the density of liquid water, so it should provide a fairly close estimate. Considering the size of UF pores in the 10 to 100 nm range, *Kn* at this scale is in the range of 0.0031 to 0.031. Since this is less than 1, continuum mechanics will still apply to fluid modelling at the membrane surface. This is supported by Borg et al. (2013), who noted that continuum mechanics assumptions such as the Navier-Stokes equations are still valid at the nano-scale.

11.7.1.4 Slip velocity

The magnitude of the tangential velocity at the wall is commonly modelled using the Navier-slip condition (Holland et al. 2015a; Holland et al. 2015b; Kobayashi 2020; Priezjev et al. 2005). This condition is given by equation (11-12), where the tangential velocity, u_R, is equal to a slip length, ζ, multiplied by the negative shear strain rate at the wall.

$$u_R = -\zeta \frac{du}{dr} \tag{11-12}$$

Hydrophobicity is the most important factor affecting the slip length (Wu et al. 2017a). Huang et al. (2008) performed an analysis of various studies and found that the slip length could be roughly approximated by the contact angle using equation (11-13):

$$\zeta \propto \frac{1}{(1 + cos\theta_c)^2} \tag{11-13}$$

An additional consideration when estimating the slip length is the effects of molecular layering near the wall, which restricts flows and has an effect similar to the slip length. According to Wu et al. (2017a) an Effective Slip Length was defined as an Apparent Slip

Length plus the slip length calculated in equation (11-13). The effective slip length is calculated as a function of empirical relationships of velocities near the wall and is given in Equation (11-14), where ζ_e is the Effective Slip Length, θ_c is the contact angle in degrees, A_i is the interfacial area, defined as the pore area within 0.7 nm of the wall, and A_t is the total pore area.

$$\zeta_e = \left[\frac{1}{(-0.018\theta_c + 3.25)\frac{A_i}{A_t} + \left(1 - \frac{A_i}{A_t}\right)}\right]\left(\frac{d}{8} + \zeta\right) + \zeta \qquad (11\text{-}14)$$

11.7.2 Set-up of the physical domains and boundary conditions

11.7.2.1 Pore scale simulations

The inlet BC was varied over 5 simulations to mimic the conditions over a range of fluxes summarized in Table 11-31. Normal velocities were obtained based on the flux velocities corresponding to each flux rate, and they were defined as negative to indicate flow in the negative z direction. Equation (6) was used to determine the tangential flow velocity, u_x. The axial distance used for calculations was 7 mm (two feed channel diameters), and the radial distance was 1.74994 mm (the radial distance to the top of the modelled flow domain). It will be seen that the tangential flow velocities had very little impact on the simulation outcomes, making it unnecessary to run additional simulations without tangential flow for comparison purposes.

Table 11-31: Inflow BC velocities for the pore scale simulations.

Flux (LMH)	**Normal Velocity, u_z (10^{-5} m/s)**	**Tangential Velocity, u_x (10^{-5} m/s)**
100	-2.778	0.1054
200	-5.556	0.2099
300	-8.333	0.3135
400	-11.11	0.4163
500	-13.89	0.5183

For a pore diameter of 30 nm, the *Kn* was approximately 0.01 (Equation (1), or 11.7.1.3), meaning that no-slip BCs could not initially be assumed at the walls. To estimate the slip length between TiO_2 and water, Equations (3) and (4) were used to estimate the actual and effective slip lengths. The exact wetting angle for the membrane material was not available from the manufacturer, so a range was estimated based on the knowledge that the material was strongly hydrophilic. Based on this, the upper estimate of the contact angle was assumed to be 50 degrees. As the lower estimate, Wang et al. (1997) found that the contact angle for TiO_2 can be as low as zero degrees when surface

treatments are applied. The resulting minimum and maximum slip length estimations based on this range are the provided in Table 11-32.

Table 11-32: Slip length estimations for membrane pores.

	Low	**High**	**units**
Contact Angle	**0**	**50**	**degrees**
A_i/A_t	4.61 x 10^{-2}		-
True Slip length	0.250	0.371	nm
Effective Slip length	-0.126	0.129	nm

With a known slip length, the analytical velocity profile could be derived as in 11.7.4.1. The result is Equation (11-15), where u_r is the velocity, Q is the flow through a single pore, ζ is the slip length, r is the radial distance, and R is the outer radius of the pore. The velocity profiles for varying slip lengths are shown in Figure 11-22, with velocities given normalized to the no-slip (0 nm slip length) maximum velocity. Since equations (3) and (4) could only provide a rough estimate of the slip length, a much larger range of slip lengths is plotted than what is estimated in Table 11-32. One can deduce that equation (11-15) will essentially become Hagen-Poiseuille flow when the slip length is small compared to the pore radius. This is reflected in Figure 11-22, where the slip lengths do not have a drastic effect on the flow profile in the pore. Since the estimated slip lengths in Table 11-32 are centred around zero and the magnitude of the slip length has a fairly minor effect on flow velocities, a no-slip condition was justifiably applied to the solid membrane surfaces.

$$u_r = \frac{Q}{\pi\left[R^2 - \frac{R^4}{2(R^2 + 2\zeta R)}\right]}\left(1 - \frac{r^2}{R^2 + 2\zeta R}\right) \tag{11-15}$$

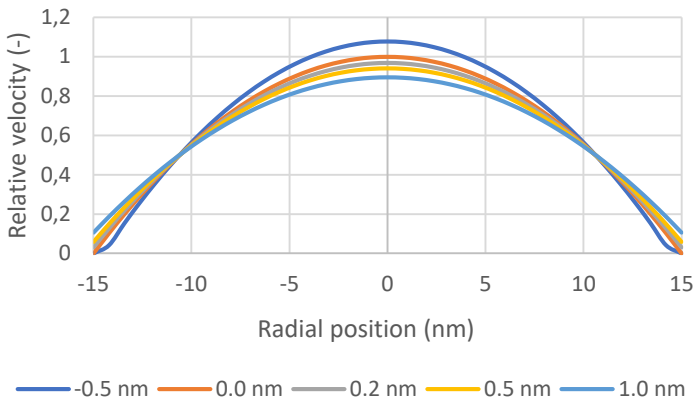

Figure 11-22: Velocity profile for 30 nm pore using different slip lengths.

11.7.2.2 Particle scale simulations

This domain presented a challenge for simulation due to the contact points where the spheres meet each other and the membrane. These points result in very narrow spaces, which would have caused issues when solving the simulations due to the very small cell dimensions and high cell skewing in these regions. Alkhalaf et al. (2018) proposed three solutions to this problem as follows:

1. Increase the particle size, creating an overlap between the particles
2. Decrease the particle size, creating a gap between the particles
3. Place cylindrical objects over the contact points to bridge over the narrow spaces

Alkhalaf et al. (2018) found that none of these methods were universally more accurate across all flow rates. All three methods were tested by constructing meshes in COMSOL's mesh generator, and it was determined that decreasing the particle size would produce the best results based on the mesh quality statistics and the resulting number of elements. The particles were reduced to 99 % of their original size, as recommended by Alkhalaf et al. (2018).

The porous membrane material was modelled in COMSOL by designating the membrane region as porous. The precise value of the membrane permeability was expected to have a significant impact on the flow field around the spherical particles. This is because of the additional viscous forces hindering flow into the confined spaces between the spheres and the membrane surface. If the forces required for additional flow to enter the membrane at less confined locations were less than the forces required to enter into a location underneath a particle, then additional flow would be allocated away from locations close to the contact point between the particles and the membrane surface.

A general estimate of the membrane permeability could be obtained by rearranging Darcy's law (equation (11-9)) to solve for permeability. Only the skin layer was considered for the thickness of the membrane, which the manufacturer reported to be about 75 µm. The pressure drop through the skin layer was not known, so it was assumed to be somewhere between 50 % and 90 % of the total pressure loss in the membrane. Simulations were run for 5 different values in this range (shown in Table 11-33) to observe whether the simulation output was sensitive to permeability values.

Table 11-33: Membrane permeabilities tested in particle scale simulations.

Pressure Drop in Skin Layer (%)	Permeability (10^{-17} m^2)
50	4.69
60	3.91
70	3.35
80	2.93
90	2.61

The permeability was assumed to be isotropic, though in reality the skin layer would likely have a lower permeability in the lateral directions. The modelled thickness only needed to be large enough to ensure that the flow became uniform before reaching the outlet. It was found that 3 µm was sufficient. The membrane permeability of 4.69 x 10^{-17} m^2 was used for all simulations except for the four simulations using the alternate permeabilities given in Table 11-33. This value was used because a higher permeability was expected to have a more pronounced effect on flow fields at the membrane surface.

The z velocities, u_z, at the inlet were assigned as the filtration velocities corresponding to the flux values that were used (cf. Table 11-34). The tangential velocities, u_x, were determined based on equation (6), considering an axial position 7 mm into the feed channel and a radial position of 1.73 mm (the feed channel radius minus the domain height). The tangential flow velocities were considerably greater than the normal flow velocities. For this reason, each simulation was repeated using zero tangential flow to observe the effects of the particle layer on tangential velocities at the membrane surface. Tangential flow velocities were overestimated, since the particle layer would extend no-slip boundary layer effects and reduce flow velocities in the region near the membrane surface. However, it will be seen that precise crossflow values are irrelevant for the purpose of this study.

Table 11-34: Particle scale simulation inlet velocities.

Flux (LMH)	Normal Velocity, u_z (10^{-5} m/s)	Tangential Velocity, u_x (10^{-5} m/s)
100	2.778	28.10
200	5.556	55.98
300	8.333	83.63
400	11.11	111.06
500	13.89	138.27

Effect of membrane permeability

As the exact membrane permeability was not known, it was necessary to observe the effects of permeability on the simulation outcomes within an expected range of permeability values. It was hypothesized that higher permeability would lead to increased filtration velocities at locations farther away from the particles. To evaluate this effect, Figure 11-23 shows the relationship between the membrane permeability and the increase in filtration velocities from the baseline at a flux of 500 LMH. In order to analyze the filtration velocity, flow velocities at the membrane surface were resampled onto a grid of 300 evenly spaced points along the x direction and 87 in the y direction. This created an approximately square grid and ensured that each point represented an equivalent area of the membrane. The statistics of the flow velocities were obtained from the resulting data points and compared with baseline filtration velocities. The average increase only included points on the membrane surface which experienced velocities greater than baseline velocity, which amounted to approximately 94 % of the membrane surface. As predicted, increasing the membrane permeability resulted in increased filtration velocities at some parts of the membrane. However, the maximum velocity increase was only about 1 % compared to the baseline, which is insignificant compared to the impacts on membrane flux from other operational variables.

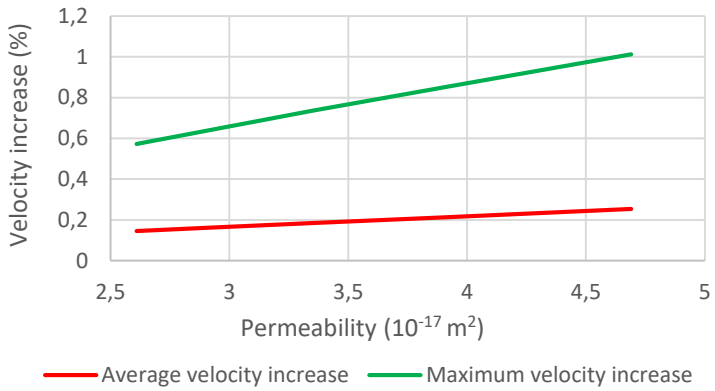

Figure 11-23: Relationship between membrane permeability and velocity at the membrane surface.

11.7.3 Meshing and convergence studies

One of the primary quality aspects of CFD solutions is ‘consistency’. Consistency is achieved when the simulated flow field quantities converge on an exact solution as the mesh spacing approaches zero (Slater 2008). Since decreasing the mesh size increases computational requirements exponentially, the true goal is to capture details at the smallest scales of interest (Borg et al. 2013). To ensure that a sufficiently fine mesh was used for each of the simulations, mesh convergence studies were conducted. Initial meshes were generated using COMSOL’s physics generated meshing feature, which

automatically refines the mesh in critical areas and applies boundary layers based on the geometry and physics being simulated. Tetrahedral/ triangular elements were used throughout the flow domains, except for the boundary layers where rectangular/ prismatic elements were used.

11.7.3.1 Pore scale simulations

The initial mesh was generated by COMSOL's physics induced mesh using the 'Finer' size setting. One coarsened and one refined mesh were created by scaling the element dimensions by 1.5 and $\frac{2}{3}$, respectively. A summary of the meshes is provided in Table 11-35. To evaluate the accuracy of shear and elongational strain rates at the pore entrance, the values were sampled and plotted for each mesh to allow easy comparison. Shear strain rate in the x-z plane was observed over a line of 101 evenly spaced points from coordinates (15, 0, 0) to (15, 0, 60). Elongational strain rate in the z direction was observed over 101 points, but from (0, 0, 0) to (0, 0, 60). The relative error of the two courser meshes (Mesh 5-1 and Mesh 5-2) with respect to the finest mesh (Mesh 5-3) were all calculated and plotted in box plots in Figure 11-24B. After examining the three meshes to obtain confidence about their accuracies, the finest mesh (Mesh 5-3) was used for the remainder of the simulations.

Table 11-35: Pore scale mesh summary.

Mesh Number	Mesh Description	Number of Elements	Simulation Time (s)
5-1	Coarsened	61046	19
5-2	'Finer'	244184	67
5-3	Refined	976736	405

The graphical results of the mesh refinement are shown in Figure 11-24. Results are only shown up to z=20 nm in order to better display the regions with the greatest error. It is clear in Figure 11-24A that shear strain rate values directly above the pore entrance had poor accuracy until about z=3 nm. This is likely due to inadequate resolution of the boundary layer where the outer membrane surface is located. Since the MGEs focused on in this study are at least an order of magnitude larger than 3 nm, this small region of inaccuracy did not warrant further refinement of the mesh. The elongational strain rate had the lowest accuracy around the peak at z=6 nm. However, even in this region the accuracy was considered sufficient. After about z=15 nm, results from the three grids became graphically indistinguishable.

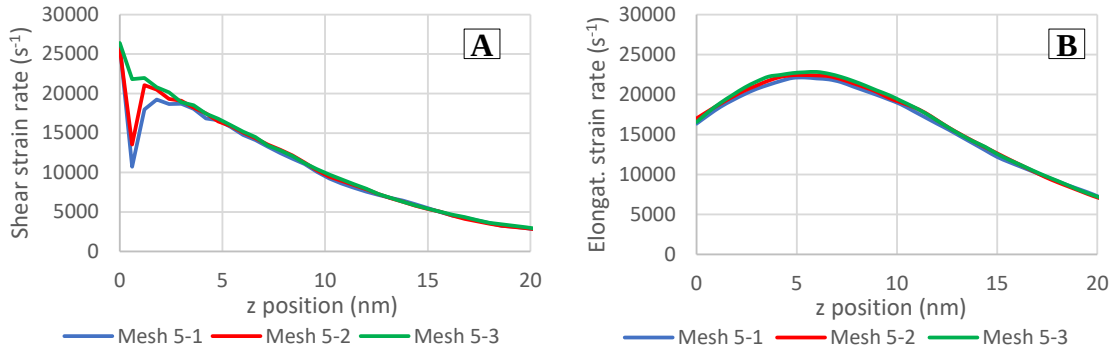

Figure 11-24: Graphical results of pore scale mesh study for (A) Shear strain rates along the Z axis at the edge of the pore and (B) elongational strain rates along the z axis at the center of the pore.

A summary of the relative errors between the courser meshes (Meshes 5-1 and 5-2) and the finest mesh (Mesh 5-3) is provided in Figure 11-25. The outer quartile range was slightly larger for observations of elongational strain rate than for shear strain rate, though the inner quartile ranges are similar for the two cases. Some of the outliers (not shown in these plots) include errors in shear stress very close to the pores, as well as error values very close to z=60 nm, where the very small strain rates mean that very small absolute errors can lead to large relative errors. It is seen that the refinement considerably decreased the magnitude of error. Given that the finest mesh was used for simulations, the magnitude of error in observed strain rates was generally less than 5 %, which was sufficient for the purpose of this study.

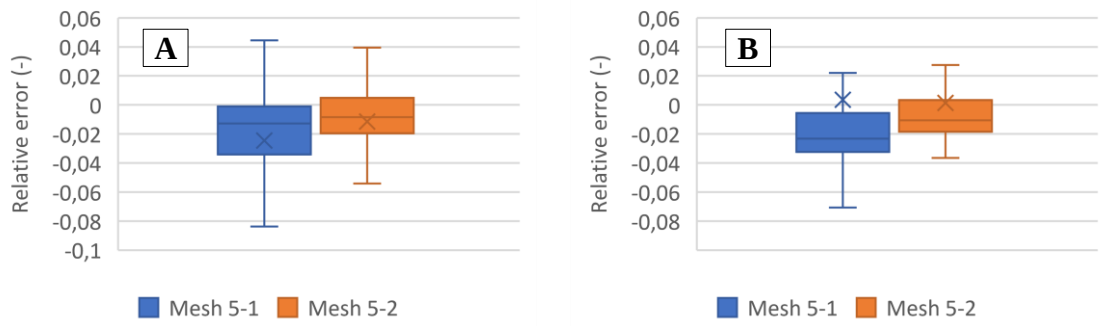

Figure 11-25: Relative error bands of courser meshes with respect to Mesh 5-3 for (A) Elongational strain rate along the z axis and (B) Shear strain rate along the z axis.

11.7.3.2 Particle scale simulations

The first mesh for the particle scale domain was generated using the 'Fine' size setting in COMSOL's mesh generator. A scaling function was used to multiply all cell dimensions by approximately 1.5 and $^2/_3$ to create one courser mesh and one finer mesh, respectively. It was attempted to perform an additional refinement using a scaling factor

of $^4/_9$, but this proved to be too computationally demanding for the available hardware. A summary of the three meshes is provided in Table 11-36.

Table 11-36: Particle scale mesh summary.

Mesh Number	Mesh Description	Number of Elements	Simulation Time (min)
6-1	Coarsened	65958	17
6-2	'Fine'	212692	49
6-3	Refined	732345	167

The accuracies of the meshes were estimated with respect to filtration velocities and the elongational strain rate in the z direction. Filtration velocities were observed along a line which followed the x axis from (0, 0, 0) to (13.856, 0, 0), allowing observations to be taken directly under the particle in the centre of the domain. Elongational strain rate in the z direction was observed along the z axis passing through the centre of the gap between spheres from (2.31, 0, -1) to (2.31, 0, 20). Analysis was performed graphically (Figure 11-26) using 101 evenly spaced points, then additional relative errors between the two course meshes, Mesh 6-1 and 6-2, and the finest mesh, Mesh 6-3 were calculated and analyzed using box plots (Figure 11-27).

The three meshes gave very similar results at most locations that were sampled. However, significant differences were observed in filtration velocities directly underneath the particles (Figure 11-26A), as well as in the elongational strain rate between the membrane surface and the top of the particle layer (Figure 11-26B). Mesh 6-1 was found to be inadequate, as it considerably underestimated magnitudes of velocities and strain rates. However, Mesh 6-2 and Mesh 6-3 gave very similar results, and it was not expected that additional mesh refinement would not have made a considerable difference in the obtained results.

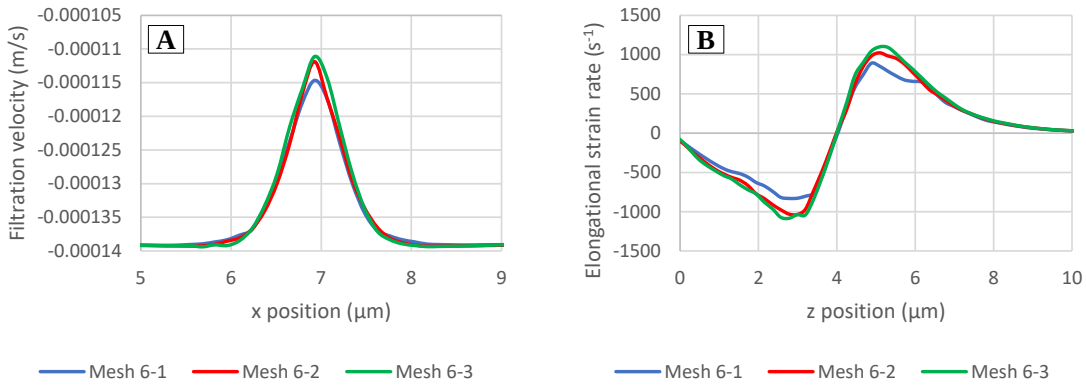

Figure 11-26: Graphical results of particle scale mesh study showing (A) Velocity at the membrane surface underneath a particle and (B) Elongational strain rates through the particle layer along the pore center. See Figure 8-2 for location descriptions.

Figure 11-27A shows the magnitude of errors with respect to membrane surface velocities for the different meshes. Despite the differences seen in Figure 11-26A, even the coarsest mesh (Mesh 6-1) had a very high accuracy, with a magnitude of relative error consistently less than 0.05 % (not including anomalies). Mesh 6-2 improved on the accuracy further, with a magnitude of relative error less than 0.03 %. With errors of this magnitude, it is evident that Mesh 6-3 was sufficiently fine to capture accurate filtration velocities. With respect to elongational strain rate, Figure 11-27B shows errors of more than 30 % for Mesh 6-1, which was unacceptable. Mesh 6-2 had errors which were generally less than 10 %. While this is still quite high, the uncertainty in the stiffness of MGEs is likely greater than this (see Section 5.2.2.1). The magnitudes of elongational strain rates are also much smaller than those seen in section 11.7.3.1, making their exact values somewhat insignificant. Given that the behavior of the strain rate seen in Figure 11-26B is very similar for the finest two meshes, errors within 10 % are unlikely to impact any final conclusions.

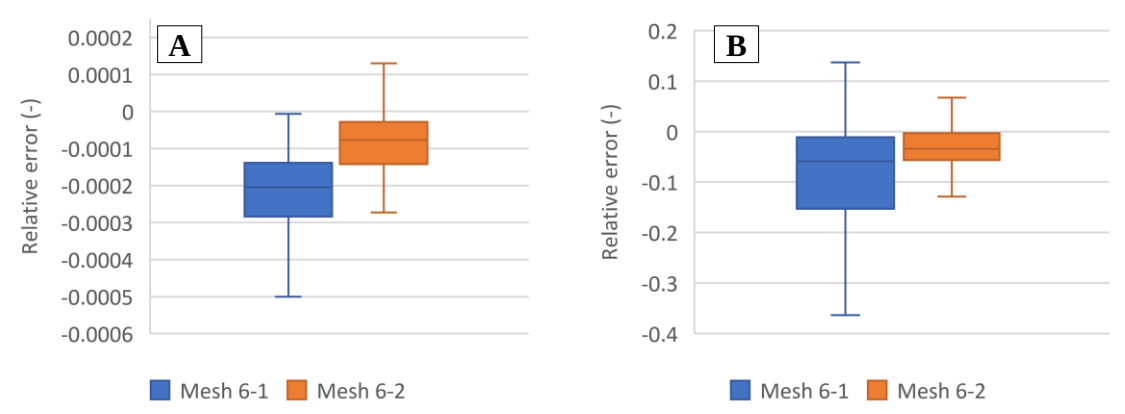

Figure 11-27: Relative error bands of courser meshes for (A) Flow velocities at the membrane surface and (B) Elongational strain rate along the z axis.

11.7.4 Calculations

11.7.4.1 Derivation of velocity profile for tube with partial slip condition at walls

Parameter	Units	Definition
u	m/s	Tangential velocity
$u(R)$	m/s	Tangential velocity at the wall (slip velocity)
U_{max}	m/s	Peak Velocity in the profile
r	m	Radial distance
R	m	Tube radius
R_{img}	m	Radius of velocity profile if it were Hagen-Poiseuille Flow
ζ	m	Slip length
Q	m^3/s	Flow

Navier Slip condition

$$u(R) = -\zeta \frac{du}{dr} \tag{11-16}$$

Hagen-Poiseuille Velocity Profile

$$u(r) = U_{max}\left(1 - \left(\frac{r}{R_{img}}\right)^2\right) \tag{11-17}$$

Derivation of U_{max}

$$Q = 2\pi U_{max}\int_0^R \left(1 - \left(\frac{r}{R_{img}}\right)^2\right) r dr \tag{11-18}$$

$$Q = 2\pi U_{max}\left[\frac{r^2}{2} - \frac{r^4}{4{R_{img}}^2}\right]\Bigg|_0^R \tag{11-19}$$

$$U_{max} = \frac{Q}{\pi\left[R^2 - \frac{R^4}{2{R_{img}}^2}\right]} \tag{11-20}$$

Derivation of R_{img}

$$-\zeta\frac{du}{dr} = \frac{Q}{\pi\left[R^2 - \frac{r^4}{2{R_{img}}^2}\right]}\left(1 - \left(\frac{R}{R_{img}}\right)^2\right), r = R \tag{11-21}$$

$$\frac{du}{dr} = -\frac{Q}{\left[R^2 - \frac{R^4}{2{R_{img}}^2}\right]}\frac{2R}{{R_{img}}^2} = -\frac{u}{\zeta} \tag{11-22}$$

$$-\frac{Q}{\left[R^2 - \frac{R^4}{2{R_{img}}^2}\right]}\frac{2R}{{R_{img}}^2} = -\frac{Q}{\zeta\pi\left[R^2 - \frac{R^4}{2{R_{img}}^2}\right]}\left(1 - \left(\frac{R}{R_{img}}\right)^2\right) \tag{11-23}$$

$$\frac{2R}{{R_{img}}^2} = \frac{1}{\zeta} - \frac{R^2}{\zeta{R_{img}}^2} \tag{11-24}$$

$$R_{img} = \sqrt{R^2 + 2\zeta R} \tag{11-25}$$

Final Velocity Profile

$$u(r) = \frac{Q}{\pi\left[R^2 - \frac{R^4}{2(R^2 + 2\zeta R)}\right]}\left(1 - \frac{r^2}{R^2 + 2\zeta R}\right) \tag{11-26}$$

11.7.4.2 Reynolds number calculations

Input Value	Calculated Value

Feed Channel Calculations

Parameter	Value	Unit	Notes
Membrane and Operation Parameters			
Flux	500	LMH	
Length	0.25	m	
Diameter	0.0035	m	
# of Channels	19		
Water Kinematic Viscosity	1.0023E-06	m^2/s	@ 20 °C
Water Density	998.19	kg/m^3	@ 20 °C
Flow Calculations			
Total membrane Area	0.05223	m^2	= π * Diameter * Length * # of Channels
Filtration Velocity	1.3889E-04	m/s	= Flux/($3.6*10^6$)
Total Flow	7.2540E-06	m^3/s	= Filtration Velocity * Total Membrane Area
Flow into Single Channel	3.8179E-07	m^3/s	= Total Flow/# of Channels
Channel Entrance Velocity	0.0039683	m/s	= Flow into Single Channel/(π * $Diameter^2/4$)
Feed Channel Reynolds Numbers			
Max Channel Reynolds Number	138.6		= Channel Entrance Velocity * Diameter/Water Kinematic Viscosity
Average Wall Reynolds Number	0.2425		= Filtration Velocity * (Diameter/2)/Water Kinematic Viscosity

Pore scale Calculations

Parameter	Value	Unit	Notes
Membrane Porosity	0.45		Skin Layer Porosity
Pore Diameter	3.00E-08	m	Average Pore Size
Domain Extents			
Domain Width/length	3.9633E-08	m	= sqrt(π * $(Pore\ Diameter)^2/4$/Membrane Porosity)
Domain Height	6.00E-08	m	2 * Pore Diameter
Pore Depth	3.00E-08	m	Pore Diameter
Feed Channel Reynolds Numbers			
Axial Velocity	5.1828E-06	m/s	Calculated from Oxarango et al. (2004)
Maximum Re_t	2.05E-07		Axial Velocity * Domain Width/Water Kinematic Viscosity
Average Re_n	5.49E-06		Filtration Velocity * Domain Width/Water Kinematic Viscosity

Particle scale Calculations

Particle Diameter	8.0E-6	m	
Average Re_p	1.11E-03		Particle Diameter * Domain Width/Water Kinematic Viscosity

11.7.4.3 Domain deflection calculations

Pore scale Flattening		
Parameter	**Value**	**Unit**
Number of Pores	1	
Outside Dimension	3.96E-08	m
Deflection of Membrane	1.122E-13	m
Percent Deflection	2.83E-04	%
Arc Angle	2.26E-05	rad
length of membrane surface	3.96E-08	m
length deviation	2.14E-09	%

Particle scale Flattening		
Parameter	**Value**	**Unit**
Number of Particles	0.5	
Outside Dimension	4.00E-06	m
Deflection of Membrane	1.143E-09	m
Percent Deflection	2.86E-02	%
Arc Angle	2.29E-03	rad
length of membrane surface	4.00E-06	m
length deviation	2.18E-05	%

****** All flattening values calculated based on circular geometry

11.7.4.4 Membrane permeability calculations

Feed Channel Membrane Permeability			
Parameter	**Value**	**Unit**	**Notes**
Membrane Inner Radius	0.00175	m	
Membrane Outer Radius	0.002	m	
Average Velocity	1.22E-04	m/s	= Filtration Velocity (1 + Membrane Inner Radius/(Membrane Inner Radius + Membrane Outer Radius))/2
Experimental Slope	0.008888	bar/LMH	From Membrane Data (Appendix C)
Transmembrane pressure (TMP)	4.4439	bar	
Membrane Permeability	7.329E-17	m^2	= Dynamic Viscosity * Average Velocity * (Membrane Outer Radius – Membrane Inner Radius)/TMP

Particle scale Membrane Permeability			
Parameter	**Value**	**Unit**	**Notes**
% Pressure Drop in Skin Layer	50	%	
Modelled Thickness	3.00E-06	m	
Modelled Permeability	4.690E-17	m^2	= Dynamic Viscosity * Filtration Velocity * (Modelled Thickness)/(% P Drop in Skin Layer * TMP)

11.7.5 Data from membrane pressure flux experiment

Membrane Area (m^2)	**0.05223**		
Flow [L/min]	**Flow [L/h]**	**Pressure [bar]**	**Flux [LMH]**
0	0	0	0.0
4.8	4.8	0.5	91.9
6	6	1	114.9
9	9	1.5	172.3
12.6	12.6	2	241.2
15.6	15.6	2.5	298.7
18.6	18.6	3	356.1
21.6	21.6	3.5	413.6
24.6	24.6	4	471.0
27	27	4.5	516.9
30	30	5	574.4
33	33	5.5	631.8
36	36	6	689.3
39	39	6.5	746.7
41.4	41.4	7	792.6

REFERENCES

2000/60/EC: Water Framework Directive 2000/60/EC of the european parliament and of the council of 23 october 2000 establishing a framework for Community action in the field of water policy. Available online at https://eur-lex.europa.eu/resource.html?uri=cellar:5c835afb-2ec6-4577-bdf8-756d3d694eeb.0004.02/DOC_1&format=PDF, checked on 6/17/2022.

2020/741/EU: EU Regulation 2020/741 of the European Parliament and of the Council on minimum requirements for water reuse. Available online at https://www.europarl.europa.eu/doceo/document/TA-8-2019-0071_EN.pdf, checked on 5/15/2020.

Abolafia-Rosenzweig, R.; Livneh, B.; Small, E. E.; Kumar, S. V. (2019): Soil Moisture Data Assimilation to Estimate Irrigation Water Use. In *Journal of advances in modeling earth systems* 11 (11), pp. 3670–3690. DOI: 10.1029/2019MS001797.

Acero, Juan L.; Benitez, F. Javier; Real, Francisco J.; Teva, Fernando (2016): Micropollutants removal from retentates generated in ultrafiltration and nanofiltration treatments of municipal secondary effluents by means of coagulation, oxidation, and adsorption processes. In *Chemical Engineering Journal* 289, pp. 48–58. DOI: 10.1016/j.cej.2015.12.082.

Acero, Juan L.; Javier Benitez, F.; Real, Francisco J.; Teva, Fernando (2012): Coupling of adsorption, coagulation, and ultrafiltration processes for the removal of emerging contaminants in a secondary effluent. In *Chemical Engineering Journal* 210, pp. 1–8. DOI: 10.1016/j.cej.2012.08.043.

Ad-hoc-AG Boden (2005): Bodenkundliche Kartieranleitung. In *Aufl., Hannover*.

Adomat, Yasmin; Orzechowski, Gerit-Hartmut; Pelger, Marc; Haas, Robert; Bartak, Rico; Nagy-Kovács, Zsuzsanna Ágnes et al. (2020): New Methods for Microbiological Monitoring at Riverbank Filtration Sites. In *Water* 12 (2), p. 584. DOI: 10.3390/w12020584.

Afonso, A.; Miranda, J. M.; Campos, J.B.L.M (2009): Numerical study of BSA ultrafiltration in the limiting flux regime — Effect of variable physical properties. In *Desalination* 249 (3), pp. 1139–1150. DOI: 10.1016/j.desal.2009.05.012.

Akinsemolu, Adenike A. (2020): The Principles of Green and Sustainability Science: Springer Nature.

Al Aani, Saif; Mustafa, Tameem N.; Hilal, Nidal (2020): Ultrafiltration membranes for wastewater and water process engineering: A comprehensive statistical review over the past decade. In *Journal of Water Process Engineering* 35, p. 101241. DOI: 10.1016/j.jwpe.2020.101241.

Al-Amoudi, Ahmed; Williams, Paul; Mandale, Steve; Lovitt, Robert W. (2007): Cleaning results of new and fouled nanofiltration membrane characterized by zeta potential and permeability. In *Separation and Purification Technology* 54 (2), pp. 234–240. DOI: 10.1016/j.seppur.2006.09.014.

Alcalde-Sanz, Laura; Gawlik, Bernd Manfred (2014): Water reuse in Europe. Relevant guidelines, needs for and barriers to innovation: a synoptic overview. Luxembourg: EUR-OP (JRC scientific and policy reports, 26947).

Alexander, Johannes; Bollmann, Anna; Seitz, Wolfram; Schwartz, Thomas (2015): Microbiological characterization of aquatic microbiomes targeting taxonomical marker genes and antibiotic resistance genes of opportunistic bacteria. In *The Science of the total environment* 512-513, pp. 316–325. DOI: 10.1016/j.scitotenv.2015.01.046.

Alkhalaf, Ali; Refaey, H. A.; Al-durobi, Nabeh; Specht, E. (2018): Influence of contact point treatment on the cross flow mixing in a simple cubic packed bed: CFD simulation and experimental validation. In *Granular Matter* 20 (2). DOI: 10.1007/s10035-018-0793-2.

Allen, Richard G.; Pereira, Luis S.; Raes, Dirk; Smith, Martin (1998): Crop evapotranspiration - Guidelines for computing crop water requirements-FAO Irrigation and drainage paper 56. In *Fao, Rome* 300 (9), D05109.

Altmann, Johannes; Massa, Lukas; Sperlich, Alexander; Gnirss, Regina; Jekel, Martin (2016): UV254 absorbance as real-time monitoring and control parameter for micropollutant removal in advanced wastewater treatment with powdered activated carbon. In *Water Research* 94, pp. 240–245. DOI: 10.1016/j.watres.2016.03.001.

Altmann, Johannes; Ruhl, Aki Sebastian; Zietzschmann, Frederik; Jekel, Martin (2014): Direct comparison of ozonation and adsorption onto powdered activated carbon for micropollutant removal in advanced wastewater treatment. In *Water Research* 55, pp. 185–193. DOI: 10.1016/j.watres.2014.02.025.

Altmann, Johannes; Zietzschmann, Frederik; Geiling, Eva-Linde; Ruhl, Aki Sebastian; Sperlich, Alexander; Jekel, Martin (2015): Impacts of coagulation on the adsorption of organic micropollutants onto powdered activated carbon in treated domestic wastewater. In *Chemosphere* 125, pp. 198–204. DOI: 10.1016/j.chemosphere.2014.12.061.

Altmayer, Michael; Belau, Michael; Foltyn, Maria (2017): Strategien zum Umgang mit Niedrigwasser in Zeiten des Klimawandels in Bayern. In *gwf Wasser/Abwasser* (158 (12)), pp. 29–37.

Amelung, Wulf; Blume, Hans-Peter; Fleige, Heiner; Horn, Rainer; Kandeler, Ellen; Kögel-Knabner, Ingrid et al. (2018): Scheffer/Schachtschabel Lehrbuch der Bodenkunde. With assistance of Thomas Gaiser, Jürgen Gauer, Nina Stoppe, Sören Thiele-Bruhn, Gerhard Welp. 17., überarbeitete und ergänzte Auflage. Berlin: Springer Spektrum.

Amy, Gary; Cho, Jaeweon (1999): Interactions between natural organic matter (nom) and membranes: Rejection and fouling. In *Water Science and Technology* 40 (9). DOI: 10.1016/S0273-1223(99)00649-6.

AQUASTAT (2016): Water withdrawal by sector, around 2010. Available online at https://firebasestorage.googleapis.com/v0/b/fao-aquastat.appspot.com/o/PDF%2FTABLES%2FWorldData-Withdrawal_eng.pdf?alt=media&token=02dec3dd-50fc-4d85-8ab7-521f376dedb0, checked on 1/6/2021.

Arkhangelsky, E.; Steubing, B.; Ben-Dov, E.; Kushmaro, A.; GITIS, V. (2008): Influence of pH and ionic strength on transmission of plasmid DNA through ultrafiltration membranes. In *Desalination* 227 (1-3), pp. 111–119. DOI: 10.1016/j.desal.2007.07.017.

Arkhangelsky, Elizabeth; Gitis, Vitaly (2008): Effect of transmembrane pressure on rejection of viruses by ultrafiltration membranes. In *Separation and Purification Technology* 62 (3), pp. 619–628. DOI: 10.1016/j.seppur.2008.03.013.

Arkhangelsky, Elizabeth; Sefi, Yossi; Hajaj, Barak; Rothenberg, Gadi; Gitis, Vitaly (2011): Kinetics and mechanism of plasmid DNA penetration through nanopores. In *Journal of Membrane Science* 371 (1-2), pp. 45–51. DOI: 10.1016/j.memsci.2011.01.014.

Asano, T.; Burton, F. L.; Leverenz, H. L.; Tsuchihashi, R.; Tchobanoglous, G. (2007): Water reuse: issue, technologies, and applications. With assistance of FAO of the UN.

Asano, Takashi (1991): Planning and Implementation of Water Reuse Projects. In *Water Science and Technology* 24 (9), pp. 1–10. DOI: 10.2166/wst.1991.0230.

Asano, Takashi; Mills, Richard A. (1990): Planning and Analysis for Water Reuse Projects. In *Journal - American Water Works Association* 82 (1), pp. 38–47. DOI: 10.1002/j.1551-8833.1990.tb06904.x.

Ashbolt, Nicholas; am Pruden; Miller, Jennifer; Riquelme, Maria V.; Maile-Moskowitz, A. (2018): Antimicrobal Resistance: Fecal Sanitation Strategies for Combatting a Global Public Health Threat. In *Global Water Pathogen Project*. Available online at https://www.waterpathogens.org/sites/default/files/Antimicrobal%20Resistance%20-%20Fecal%20Sanitation%20Strategies%20for%20Combatting%20a%20Global%20Public%20Health%20Threat_1.pdf, checked on 8/11/2020.

Bağcı, Özer; Dukhan, Nihad; Özdemir, Mustafa (2014): Flow Regimes in Packed Beds of Spheres from Pre-Darcy to Turbulent. In *Transp Porous Med* 104 (3), pp. 501–520. DOI: 10.1007/s11242-014-0345-0.

BBCH (2001): Biologische Bundesanstalt für Land und Forstwirtschaft: Entwicklungsstadien mono-und dikotyler Pflanzen. In *BBCH Scale*.

Bellona, Christopher; Drewes, Jörg E.; Xu, Pei; Amy, Gary (2004): Factors affecting the rejection of organic solutes during NF/RO treatment--a literature review. In *Water Research* 38 (12), pp. 2795–2809. DOI: 10.1016/j.watres.2004.03.034.

Bergamasco, Rosângela; Konradt-Moraes, Leila Cristina; Vieira, Marcelo Fernandes; Fagundes-Klen, Márcia Regina; Vieira, Angélica Marquetotti Salcedo (2011): Performance of a coagulation–ultrafiltration hybrid process for water supply treatment. In *Chemical Engineering Journal* 166 (2), pp. 483–489. DOI: 10.1016/j.cej.2010.10.076.

BGR-Geoviewer (2020): Bundesanstalt für Geowissenschaften und Rohstoffe - Geoviewer. Available online at https://www.bgr.bund.de/DE/Gemeinsames/Geoviewer/geoviewer_node.html, updated on 4/1/2020, checked on 4/1/2020.

Biel-Maeso, Miriam; Corada-Fernández, Carmen; Lara-Martín, Pablo A. (2018): Monitoring the occurrence of pharmaceuticals in soils irrigated with reclaimed wastewater. In *Environmental pollution (Barking, Essex : 1987)* 235, pp. 312–321. DOI: 10.1016/j.envpol.2017.12.085.

Bischel, Heather N.; Simon, Gregory L.; Frisby, Tammy M.; Luthy, Richard G. (2012): Management experiences and trends for water reuse implementation in Northern California. In *Environmental science & technology* 46 (1), pp. 180–188. DOI: 10.1021/es202725e.

Bixio, D.; Thoeye, C.; Koning, J. de; Joksimovic, D.; Savic, D.; Wintgens, T.; Melin, T. (2006): Wastewater reuse in Europe. In *Desalination* 187 (1-3), pp. 89–101. DOI: 10.1016/j.desal.2005.04.070.

BLZ (2017): Bundesinformationszentrum Landwirtschaft (BZL) in der Bundesanstalt für Landwirtschaft und Ernährung (BLE): Agrarmeteorologie. Available online at https://www.ble-medienservice.de/1651/agrarmeteorologie.

Böckelmann, Uta; Dörries, Hans-Henno; Ayuso-Gabella, M. Neus; Salgot de Marçay, Miquel; Tandoi, Valter; Levantesi, Caterina et al. (2009): Quantitative PCR monitoring of antibiotic resistance genes and bacterial pathogens in three European artificial groundwater recharge systems. In *Appl. Environ. Microbiol.* 75 (1), pp. 154–163. DOI: 10.1128/AEM.01649-08.

Bohonak, D.; Zydney, A. (2005): Compaction and permeability effects with virus filtration membranes. In *Journal of Membrane Science* 254 (1-2), pp. 71–79. DOI: 10.1016/j.memsci.2004.12.035.

Bonvin, Florence; Jost, Livia; Randin, Lea; Bonvin, Emmanuel; Kohn, Tamar (2016): Super-fine powdered activated carbon (SPAC) for efficient removal of micropollutants from wastewater treatment plant effluent. In *Water Research* 90, pp. 90–99. DOI: 10.1016/j.watres.2015.12.001.

Boretti, Alberto; Rosa, Lorenzo (2019): Reassessing the projections of the World Water Development Report. In *npj Clean Water* 2 (1). DOI: 10.1038/s41545-019-0039-9.

Borg, Matthew K.; Lockerby, Duncan A.; Reese, Jason M. (2013): A multiscale method for micro/nano flows of high aspect ratio. In *Journal of Computational Physics* 233, pp. 400–413. DOI: 10.1016/j.jcp.2012.09.009.

Bosch, Albert (1998): Human enteric viruses in the water environment: a minireview. In *International microbiology : the official journal of the Spanish Society for Microbiology* 1 (3), pp. 191–196.

Botzenhart, Konrad; Fleischer, Jens (2009): Abschätzung der Gesundheitsgefährdung durch Viren im Trinkwasser. In *Gas-und Wasserfach. Wasser, Abwasser* 150 (05), pp. 361–366.

Boudaud, Nicolas; Machinal, Claire; David, Fabienne; Fréval-Le Bourdonnec, Armelle; Jossent, Jérôme; Bakanga, Fanny et al. (2012): Removal of MS2, Qβ and GA bacteriophages during drinking water treatment at pilot scale. In *Water Research* 46 (8), pp. 2651–2664. DOI: 10.1016/j.watres.2012.02.020.

Bourrouet, A.; Garcia, J.; Mujeriego, R.; Peñuelas, G. (2001): Faecal bacteria and bacteriophage inactivation in a full-scale UV disinfection system used for wastewater reclamation. In *Water Science and Technology* 43 (10), pp. 187–194. DOI: 10.2166/wst.2001.0616.

Breazeal, Maria V. Riquelme; Novak, John T.; Vikesland, Peter J.; Pruden, Amy (2013): Effect of wastewater colloids on membrane removal of antibiotic resistance genes. In *Water Research* 47 (1), pp. 130–140. DOI: 10.1016/j.watres.2012.09.044.

Brown, M. R.; Camézuli, S.; Davenport, R. J.; Petelenz-Kurdziel, E.; Øvreås, L.; Curtis, T. P. (2015): Flow cytometric quantification of viruses in activated sludge. In *Water Research* 68, pp. 414–422. DOI: 10.1016/j.watres.2014.10.018.

Bui, X. T.; Vo, T. P. T.; Ngo, H. H.; Guo, W. S.; Nguyen, T. T. (2016): Multicriteria assessment of advanced treatment technologies for micropollutants removal at large-scale applications. In *The Science of the total environment* 563-564, pp. 1050–1067. DOI: 10.1016/j.scitotenv.2016.04.191.

Burek, Peter; Satoh, Yusuke; Fischer, Günther; Kahil, M. T.; Scherzer, A.; Tramberend, S. et al. (2016): Water futures and solution-fast track initiative. Available online at http://pure.iiasa.ac.at/id/eprint/13008/1/WP-16-006.pdf, checked on 1/6/2020.

Burgess, Jo (2015): Water re-use in South Africa. In *Water: Journal of the Australian Water Association* 42 (5), p. 42.

Bürgmann, Helmut; Frigon, Dominic; H Gaze, William; M Manaia, Célia; Pruden, Amy; Singer, Andrew C. et al. (2018): Water and sanitation: an essential battlefront in the war on antimicrobial resistance. In *FEMS microbiology ecology* 94 (9). DOI: 10.1093/femsec/fiy101.

BZfE (2016): Bundeszentrum für Ernährung: Kartoffeln richtig ernten und lagern - Nur reife Kartoffeln ins Lager. Available online at https://www.lfl.bayern.de/mam/cms07/publikationen/daten/informationen/p_19934.pdf, updated on 4/2/2020, checked on 4/3/2020.

BZfE (2019): Bundeszentrum für Ernährung: Kräuter: Erzeugung - Wild-, Topf- und Schnittkräuter. Available online at https://www.bzfe.de/inhalt/kraeuter-erzeugung-439.html, updated on 4/3/2020, checked on 4/3/2020.

Calderón-Franco, David; Seeram, Apoorva; Medema, G. J.; Loosdrecht, Mark C. M.; Weissbrodt, David G. (2020): Antibiotic resistance genes and mobile genetic elements removal from treated wastewater by sewage-sludge biochar and iron-oxide coated sand. Available online at https://www.biorxiv.org/content/10.1101/2020.09.17.302018v1.full.pdf, updated on 12/18/2020, checked on 12/18/2020.

Calero-Cáceres, William; Ye, Mao; Balcázar, José Luis (2019): Bacteriophages as Environmental Reservoirs of Antibiotic Resistance. In *Trends in microbiology* 27 (7), pp. 570–577. DOI: 10.1016/j.tim.2019.02.008.

Campinas, Margarida; Rosa, Maria João (2010): Removal of microcystins by PAC/UF. In *Separation and Purification Technology* 71 (1), pp. 114–120. DOI: 10.1016/j.seppur.2009.11.010.

Carducci, A.; Morici, P.; Pizzi, F.; Battistini, R.; Rovini, E.; Verani, M. (2008): Study of the viral removal efficiency in a urban wastewater treatment plant. In *Water Science and Technology* 58 (4), pp. 893–897. DOI: 10.2166/wst.2008.437.

Carroll, T.; King, S.; Gray, R.; Bolto, A.; Booker, N. A. (2000): The fouling of microfiltration membranes by NOM after coagulation treatment. In *Water Research* 34 (11), pp. 2861–2868. DOI: 10.1016/S0043-1354(00)00051-8.

Carter, Laura J.; Chefetz, Benny; Abdeen, Ziad; Boxall, Alistair B. A. (2019): Emerging investigator series: towards a framework for establishing the impacts of pharmaceuticals in wastewater irrigation systems on agro-ecosystems and human health. In *Environ. Sci.: Processes Impacts* 21 (4), pp. 605–622. DOI: 10.1039/C9EM00020H.

Chaudhry, Rabia M.; Nelson, Kara L.; Drewes, Jörg E. (2015): Mechanisms of pathogenic virus removal in a full-scale membrane bioreactor. In *Environ. Sci. Technol.* 49 (5), pp. 2815–2822. DOI: 10.1021/es505332n.

Che, You; Xia, Yu; Liu, Lei; Li, An-Dong; Yang, Yu; Zhang, Tong (2019): Mobile antibiotic resistome in wastewater treatment plants revealed by Nanopore metagenomic sequencing. In *Microbiome* 7 (1), p. 44. DOI: 10.1186/s40168-019-0663-0.

Chen, Lei; Xu, Yilu; Dong, Xuefang; Shen, Chaofeng (2020): Removal of Intracellular and Extracellular Antibiotic Resistance Genes in Municipal Wastewater Effluent by Electrocoagulation. In *Environmental Engineering Science* 37 (12), pp. 783–789. DOI: 10.1089/ees.2020.0189.

Chen, Weiping; Lu, Sidan; Jiao, Wentao; Wang, Meie; Chang, Andrew C. (2013a): Reclaimed water: A safe irrigation water source? In *Environmental Development* 8, pp. 74–83. DOI: 10.1016/j.envdev.2013.04.003.

Chen, Weiping; Xu, Jian; Lu, Sidan; Jiao, Wentao; Wu, Laosheng; Chang, Andrew C. (2013b): Fates and transport of PPCPs in soil receiving reclaimed water irrigation. In *Chemosphere* 93 (10), pp. 2621–2630. DOI: 10.1016/j.chemosphere.2013.09.088.

Cheng, Hong; Hong, Pei-Ying (2017): Removal of Antibiotic-Resistant Bacteria and Antibiotic Resistance Genes Affected by Varying Degrees of Fouling on Anaerobic Microfiltration Membranes. In *Environ. Sci. Technol.* 51 (21), pp. 12200–12209. DOI: 10.1021/acs.est.7b03798.

Cheswick, Ryan; Cartmell, Elise; Lee, Susan; Upton, Andrew; Weir, Paul; Moore, Graeme et al. (2019): Comparing flow cytometry with culture-based methods for microbial monitoring and as a diagnostic tool for assessing drinking water treatment processes. In *Environment international* 130, p. 104893. DOI: 10.1016/j.envint.2019.06.003.

Chew, Chun Ming; Aroua, Mohamed Kheireddine; Hussain, Mohd Azlan (2018): Advanced process control for ultrafiltration membrane water treatment system. In *Journal of Cleaner Production* 179, pp. 63–80. DOI: 10.1016/j.jclepro.2018.01.075.

Chhipi-Shrestha, Gyan; Hewage, Kasun; Sadiq, Rehan (2017): Microbial quality of reclaimed water for urban reuses: Probabilistic risk-based investigation and recommendations. In *The Science of the total environment* 576, pp. 738–751. DOI: 10.1016/j.scitotenv.2016.10.105.

Chiou, Ren-Jie (2008): Risk assessment and loading capacity of reclaimed wastewater to be reused for agricultural irrigation. In *Environmental monitoring and assessment* 142 (1-3), pp. 255–262. DOI: 10.1007/s10661-007-9922-9.

Clarridge III, Jill E. (2004): Impact of 16S rRNA gene sequence analysis for identification of bacteria on clinical microbiology and infectious diseases. In *Clinical microbiology reviews* 17 (4), pp. 840–862.

Cookson, John T.; North, Wheeler J. (1967): Adsorption of viruses on activated carbon. Equilibriums and kinetics of the attachment of Escherichia coli bacteriophage T4 on activated carbon. In *Environ. Sci. Technol.* 1 (1), pp. 46–52.

Cordier, Clémence; Stavrakakis, Christophe; Morga, Benjamin; Degrémont, Lionel; Voulgaris, Alexandra; Bacchi, Alessia et al. (2020): Removal of pathogens by ultrafiltration from sea water. In *Environment international* 142, p. 105809. DOI: 10.1016/j.envint.2020.105809.

Costán-Longares, Ana; Montemayor, Michel; Payán, Andrey; Méndez, Javier; Jofre, Joan; Mujeriego, Rafael; Lucena, Francisco (2008): Microbial indicators and pathogens: removal, relationships and predictive capabilities in water reclamation facilities. In *Water Research* 42 (17), pp. 4439–4448. DOI: 10.1016/j.watres.2008.07.037.

Courvalin, Patrice (1994): Transfer of antibiotic resistance genes between gram-positive and gram-negative bacteria. In *Antimicrobial agents and chemotherapy* 38 (7), pp. 1447–1451.

Criquet, Justine; Rodriguez, Eva M.; Allard, Sebastien; Wellauer, Sven; Salhi, Elisabeth; Joll, Cynthia A.; Gunten, Urs von (2015): Reaction of bromine and chlorine with phenolic compounds and natural organic matter extracts--Electrophilic aromatic substitution and oxidation. In *Water Research* 85, pp. 476–486. DOI: 10.1016/j.watres.2015.08.051.

Crittenden, John C.; Harza, Broomfield Montgomery Watson (2005): Water treatment: principles and design: Wiley.

Crittenden, John Charles; Trussell, R. Rhodes; Hand, David W.; Howe, Kerry J.; Tchobanoglous, George (2012): MWH's water treatment. Principles and design. 3rd ed. Hoboken, N.J: John Wiley and Sons. Available online at http://onlinelibrary.wiley.com/book/10.1002/9781118131473.

Cui, Bingjian; Hu, Chao; Fan, Xiangyang; Cui, Erping; Li, Zhongyang; Ma, Huanhuan; Gao, Feng (2020): Changes of endophytic bacterial community and pathogens in pepper (Capsicum annuum L.) as affected by reclaimed water irrigation. Applied Soil Ecology, 156, 103627. In *Applied Soil Ecology* 156, p. 103627. DOI: 10.1016/J.APSOIL.2020.103627.

Czekalski, Nadine; Gascón Díez, Elena; Bürgmann, Helmut (2014): Wastewater as a point source of antibiotic-resistance genes in the sediment of a freshwater lake. In *The ISME journal* 8 (7), pp. 1381–1390. DOI: 10.1038/ismej.2014.8.

Daigger, Glen T. (2009): Evolving Urban Water and Residuals Management Paradigms: Water Reclamation and Reuse, Decentralization, and Resource Recovery. In *water environ res* 81 (8), pp. 809–823. DOI: 10.2175/106143009X425898.

Daoudi, S.; Brochard, F. (1978): Flows of Flexible Polymer Solutions in Pores. In *Macromolecules* 11 (4), pp. 751–758. DOI: 10.1021/ma60064a027.

Debroas, Didier; Siguret, Cléa (2019): Viruses as key reservoirs of antibiotic resistance genes in the environment. In *The ISME journal* 13 (11), pp. 2856–2867. DOI: 10.1038/s41396-019-0478-9.

Di Zio, Alessia; Prisciandaro, Marina; Barba, Diego (2005): Disinfection of surface waters with UF membranes. In *Desalination* 179 (1-3), pp. 297–305. DOI: 10.1016/j.desal.2004.11.075.

DIN 19650: Bewässerung - Hygienische Belange von Bewässerungswasser - Februar 1999.

DIN 19684-10: Bodenbeschaffenheit - Chemische Laboruntersuchungen - Teil 10: Untersuchung und Beurteilung des Wassers bei Bewässerungsmaßnahmen - Januar 2009.

Dingemans, Milou; Smeets, Patrick; Medema, Gertjan; Frijns, Jos; Raat, Klaasjan; van Wezel, Annemarie; Bartholomeus, Ruud (2020): Responsible Water Reuse Needs an Interdisciplinary Approach to Balance Risks and Benefits. In *Water* 12 (5), p. 1264. DOI: 10.3390/w12051264.

Dobson, John; Kumar, Amit; Willis, Leon F.; Tuma, Roman; Higazi, Daniel R.; Turner, Richard et al. (2017): Inducing protein aggregation by extensional flow. In *Proceedings of the National Academy of Sciences of the United States of America*, pp. 4673–4678. DOI: 10.1073/pnas.1702724114.

Dodds, Walter K.; Perkin, Joshuah S.; Gerken, Joseph E. (2013): Human Impact on Freshwater Ecosystem Services: A Global Perspective. In *Environ. Sci. Technol.* 47 (16), pp. 9061–9068. DOI: 10.1021/es4021052.

Dong, Bingfeng; Kahl, Alandra; Cheng, Long; Vo, Hao; Ruehl, Stephanie; Zhang, Tianqi et al. (2015): Fate of trace organics in a wastewater effluent dependent stream. In *The Science of the total environment* 518-519, pp. 479–490. DOI: 10.1016/j.scitotenv.2015.02.074.

Drewes, J. E.; Khan, S.; Mujeriego, R. (2012): Water reuse: achievements and future challenges: IWA Publishing.

Drewes, J. E.; Khan, S. J. (2011): Water reuse for drinking water augmentation. In *Water Quality & Treatment: A Handbook on Drinking Water (Edzwald, JK, ed.). McGraw-Hill Professional, New York*, 16.1-16.48.

Drewes, J. E.; Khan, S. J. (2015): Contemporary design, operation, and monitoring of potable reuse systems. In *J Water Reuse Desalination* 5 (1), pp. 1–7. DOI: 10.2166/wrd.2014.148.

Drewes, J. E.; Schramm, E.; Ebert, B.; Mohr, M.; Beckett, M.; Krömer, K.; Jungfer, C. (2019): Potenziale und Strategien zur Überwindung von Hemmnissen für die Implementierung von Wasserwiederverwendungsansätzen in Deutschland. In *Korrespondenz Abwasser 66 (12) 995-1003*.

Drewes, Jörg E.; Becker, Dennis; Jungfer, Christina; Krömer, Kerstin; Mohr, Marius; Nahrstedt, Andreas et al. (2018): Mindestanforderungen an eine Wasserwiederverwendung: Hinweise aus Sicht der WavE Forschungsprojekte des Bundesministeriums für Bildung und Forschung (BMBF). Available online at https://www.gwf-wasser.de/fileadmin/GWF/Downloads/gwf_Wasser_Abwasser_Ausgabe_12_2018_WAVE.pdf.

Droogers, Peter; Allen, Richard G. (2002): Estimating reference evapotranspiration under inaccurate data conditions. In *Irrigation and drainage systems* 16 (1), pp. 33–45.

Du, Jing; Geng, Jinju; Ren, Hongqiang; Ding, Lili; Xu, Ke; Zhang, Yan (2015): Variation of antibiotic resistance genes in municipal wastewater treatment plant with A(2)O-MBR system. In *Environ Sci Pollut Res* 22 (5), pp. 3715–3726. DOI: 10.1007/s11356-014-3552-x.

Du, Xianjun; Shi, Yaoke; Jegatheesan, Veeriah; Haq, Izaz Ul (2020): A Review on the Mechanism, Impacts and Control Methods of Membrane Fouling in MBR System. In *Membranes* 10 (2). DOI: 10.3390/membranes10020024.

DWA-M 1200: Merkblatt DWA-M 1200 „Anwendung der Wasserwiederverwendung für landwirtschaftliche und urbane Zwecke“. Available online at https://de.dwa.de/de/regelwerksankuendigungen-volltext/merkblatt-dwa-m-

1200-anwendung-der-wasserwiederverwendung-fuer-landwirtschaftliche-und-urbane-zwecke.html, checked on 6/17/2022.

DWA-M 590: Grundsätze und Richtwerte zur Beurteilung von Anträgen zur Entnahme von Wasser für die Bewässerung.

DWD (2018a): Deutscher Wetterdienst: Schlagkonfiguration. Available online at https://www.dwd.de/DE/fachnutzer/landwirtschaft/dokumentationen/agrowetter/Schlagkonfiguration.pdf;jsessionid=3EAB093EE54D85903268C6431F4DBEA3.live21064?__blob=publicationFile&v=2, checked on 4/3/2020.

DWD (2018b): DWD Climate Data Center (CDC): Historical daily station observations (temperature, pressure, precipitation, sunshine duration, etc.) for Germany, version v006. Available online at https://opendata.dwd.de/climate_environment/CDC/observations_germany/climate/daily/kl/, updated on 5/5/2020, checked on 5/5/2020.

DWD (2018c): Wetter und Klima - Deutscher Wetterdienst - Our services - Climatological maps of Germany. Available online at https://www.dwd.de/EN/ourservices/klimakartendeutschland/klimakartendeutschland.html;jsessionid=7F0CB223FC89E845BC44B96B3630A4A6.live21073, updated on 4/16/2020, checked on 4/16/2020.

ElHadidy, Ahmed M.; Peldszus, Sigrid; van Dyke, Michele I. (2013a): An evaluation of virus removal mechanisms by ultrafiltration membranes using MS2 and φX174 bacteriophage. In *Separation and Purification Technology* 120, pp. 215–223. DOI: 10.1016/j.seppur.2013.09.026.

ElHadidy, Ahmed M.; Peldszus, Sigrid; van Dyke, Michele I. (2013b): Development of a pore construction data analysis technique for investigating pore size distribution of ultrafiltration membranes by atomic force microscopy. In *Journal of Membrane Science* 429, pp. 373–383. DOI: 10.1016/j.memsci.2012.11.054.

ElHadidy, Ahmed M.; Peldszus, Sigrid; van Dyke, Michele I. (2014): Effect of hydraulically reversible and hydraulically irreversible fouling on the removal of MS2 and φX174 bacteriophage by an ultrafiltration membrane. In *Water Research* 61, pp. 297–307. DOI: 10.1016/j.watres.2014.05.003.

Erel, Ran; Eppel, Amir; Yermiyahu, Uri; Ben-Gal, Alon; Levy, Guy; Zipori, Isaac et al. (2019): Long-term irrigation with reclaimed wastewater: Implications on nutrient management, soil chemistry and olive (Olea europaea L.) performance. In *Agricultural Water Management* 213, pp. 324–335. DOI: 10.1016/j.agwat.2018.10.033.

European Commission (2012): Water Scarcity & Droughts - 2012 Policy Review - Building Blocks. Available online at http://ec.europa.eu/environment/water/quantity/pdf/non-paper.pdf, checked on 2/4/2019.

Falsanisi, Dario; Liberti, Lorenzo; Notarnicola, Michele (2010): Ultrafiltration (UF) Pilot Plant for Municipal Wastewater Reuse in Agriculture: Impact of the Operation Mode on Process Performance. In *Water* 2 (4), pp. 872–885. DOI: 10.3390/w2040872.

Fan, Xiaojiang; Tao, Yi; Wang, Lingyun; Zhang, Xihui; Lei, Ying; Wang, Zhuo; Noguchi, Hiroshi (2014): Performance of an integrated process combining ozonation with ceramic membrane ultra-filtration for advanced treatment of drinking water. In *Desalination* 335 (1), pp. 47–54. DOI: 10.1016/j.desal.2013.12.014.

FAO-CROPWAT-Software 8.0: Default values: Default values.

FAO-CROPWAT-Software 8.0: Help: Help.

Farahbakhsh, K.; Smith, D. W. (2004): Removal of coliphages in secondary effluent by microfiltration-mechanisms of removal and impact of operating parameters. In *Water Research* 38 (3), pp. 585–592. DOI: 10.1016/j.watres.2003.10.018.

Feng, Yu; Jia, Yue; Cui, Ningbo; Zhao, Lu; Li, Chen; Gong, Daozhi (2017): Calibration of Hargreaves model for reference evapotranspiration estimation in Sichuan basin of southwest China. In *Agricultural Water Management* 181, pp. 1–9. DOI: 10.1016/j.agwat.2016.11.010.

Ferrer, O.; Casas, S.; Galvañ, C.; Lucena, F.; Bosch, A.; Galofré, B. et al. (2015): Direct ultrafiltration performance and membrane integrity monitoring by microbiological analysis. In *Water Research* 83, pp. 121–131. DOI: 10.1016/j.watres.2015.06.039.

Fiksdal, Liv; Leiknes, TorOve (2006): The effect of coagulation with MF/UF membrane filtration for the removal of virus in drinking water. In *Journal of Membrane Science* 279 (1-2), pp. 364–371. DOI: 10.1016/j.memsci.2005.12.023.

Fleig, Michael; Brauch, Heinz-Jürgen; Steinbach, Martina; Psot, Bernhard (2015): Sonderuntersuchungen auf organische Spurenstoffe im Längsprofil des Mains. Available online at https://epflicht.ulb.uni-bonn.de/periodical/titleinfo/301576.

Fleischer, J.; Hambsch, B. (2007): Enteropathogene Viren in Rohwässern (Oberflächenwässern) und in der Wasseraufbereitung. In *DVGW energie/wasserpraxis* 4, pp. 34–40.

Flörke, Martina; Schneider, Christof; McDonald, Robert I. (2018): Water competition between cities and agriculture driven by climate change and urban growth. In *Nat Sustain* 1 (1), pp. 51–58. DOI: 10.1038/s41893-017-0006-8.

Foster, T.; Gonçalves, I. Z.; Campos, I.; Neale, C. M. U.; Brozović, N. (2019): Assessing landscape scale heterogeneity in irrigation water use with remote sensing and in situ monitoring. In *Environ. Res. Lett.* 14 (2), p. 24004. DOI: 10.1088/1748-9326/aaf2be.

Frey, J. M.; Schmitz, P. (2000): Particle transport and capture at the membrane surface in cross-flow microfiltration. In *Chemical Engineering Science* 55 (19), pp. 4053–4065. DOI: 10.1016/S0009-2509(00)00071-3.

Frost, Laura S.; Leplae, Raphael; Summers, Anne O.; Toussaint, Ariane (2005): Mobile genetic elements: the agents of open source evolution. In *Nature reviews. Microbiology* 3 (9), pp. 722–732. DOI: 10.1038/nrmicro1235.

Furiga, Aurelie; Pierre, Gwenaelle; Glories, Marie; Aimar, Pierre; Roques, Christine; Causserand, Christel; Berge, Mathieu (2011): Effects of ionic strength on bacteriophage MS2 behavior and their implications for the assessment of virus retention by ultrafiltration membranes. In *Appl. Environ. Microbiol.* 77 (1), pp. 229–236. DOI: 10.1128/AEM.01075-10.

Furukawa, Takashi; Hashimoto, Reina; Mekata, Tohru (2015): Quantification of vancomycin-resistant enterococci and corresponding resistance genes in a sewage treatment plant. In *Journal of Environmental Science and Health, Part A* 50 (10), pp. 989–995. DOI: 10.1080/10934529.2015.1038150.

Galjaard, G.; Buijs, P.; Beerendonk, E.; Schoonenberg, F.; Schippers, J. C. (2001): Pre-coating (EPCE®) UF membranes for direct treatment of surface water. In *Desalination* 139 (1-3), pp. 305–316. DOI: 10.1016/S0011-9164(01)00324-1.

Gallegos, E.; Warren, A.; Robles, E.; Campoy, E.; Calderon, A.; Sainz, Ma. G. et al. (1999): The effects of wastewater irrigation on groundwater quality in Mexico. In *Water Science and Technology* 40 (2). DOI: 10.1016/S0273-1223(99)00429-1.

Gallichand, J.; Broughton, R. S.; Boisvert, J.; Rochette, P. (1991): Simulation of irrigation requirements for major crops in South Western Quebec. In *Canadian Agricultural Engineering* 33 (1), pp. 1–9.

Gao, Wei; Liang, Heng; Ma, Jun; Han, Mei; Chen, Zhong-lin; Han, Zheng-shuang; Li, Gui-bai (2011): Membrane fouling control in ultrafiltration technology for drinking water production: A review. In *Desalination* 272 (1-3), pp. 1–8. DOI: 10.1016/j.desal.2011.01.051.

Garrote, Luis (2017): Managing Water Resources to Adapt to Climate Change: Facing Uncertainty and Scarcity in a Changing Context. In *Water Resources Management* 31 (10), pp. 2951–2963. DOI: 10.1007/s11269-017-1714-6.

Gerba, Charles P.; Betancourt, Walter Q. (2017): Viral Aggregation: Impact on Virus Behavior in the Environment. In *Environ. Sci. Technol.* 51 (13), pp. 7318–7325. DOI: 10.1021/acs.est.6b05835.

Gerrity, Daniel; Gamage, Sujanie; Holady, Janie C.; Mawhinney, Douglas B.; Quiñones, Oscar; Trenholm, Rebecca A.; Snyder, Shane A. (2011): Pilot-scale evaluation of ozone and biological activated carbon for trace organic contaminant mitigation and disinfection. In *Water Research* 45 (5), pp. 2155–2165. DOI: 10.1016/j.watres.2010.12.031.

Gerrity, Daniel; Pecson, Brian; Trussell, R. Shane; Trussell, R. Rhodes (2013): Potable reuse treatment trains throughout the world. In *Journal of Water Supply: Research and Technology-Aqua* 62 (6), pp. 321–338. DOI: 10.2166/aqua.2013.041.

Ghidossi, R.; Daurelle, J. V.; Veyret, D.; Moulin, P. (2006a): Simplified CFD approach of a hollow fiber ultrafiltration system. In *Chemical Engineering Journal* 123 (3), pp. 117–125. DOI: 10.1016/j.cej.2006.07.007.

Ghidossi, R.; Veyret, D.; Moulin, P. (2006b): Computational fluid dynamics applied to membranes: State of the art and opportunities. In *Chemical Engineering and Processing: Process Intensification* 45 (6), pp. 437–454. DOI: 10.1016/j.cep.2005.11.002.

Gibson, John; Drake, Jennifer; Karney, Bryan (2017): UV disinfection of wastewater and combined sewer overflows. In *Ultraviolet light in human health, diseases and environment*, pp. 267–275.

Giedraitienė, Agnė; Vitkauskienė, Astra; Naginienė, Rima; Pavilonis, Alvydas (2011): Antibiotic resistance mechanisms of clinically important bacteria. In *Medicina* 47 (3), p. 19.

Gitis, Vitaly; Rothenberg, Gadi (2016): Ceramic membranes: new opportunities and practical applications: John Wiley & Sons.

Gómez, M.; La Rua, A. de; Garralón, G.; Plaza, F.; Hontoria, E.; Gómez, M. A. (2006): Urban wastewater disinfection by filtration technologies. In *Desalination* 190 (1-3), pp. 16–28. DOI: 10.1016/j.desal.2005.07.014.

González, O.; Bayarri, B.; Aceña, J.; Pérez, S.; Barceló, D. (2015): Treatment technologies for wastewater reuse: Fate of contaminants of emerging concern. In : Advanced Treatment Technologies for Urban Wastewater Reuse: Springer, pp. 5–37.

Goswami, Kakali Priyam; Pugazhenthi, G. (2020): Credibility of polymeric and ceramic membrane filtration in the removal of bacteria and virus from water: A review. In *Journal of environmental management* 268, p. 110583. DOI: 10.1016/j.jenvman.2020.110583.

Greve, P.; Kahil, T.; Mochizuki, J.; Schinko, T.; Satoh, Y.; Burek, P. et al. (2018): Global assessment of water challenges under uncertainty in water scarcity projections. In *Nat Sustain* 1 (9), pp. 486–494. DOI: 10.1038/s41893-018-0134-9.

GrwV (2010): Grundwasserverordnung: Verordnung zum Schutz des Grundwassers. Available online at http://www.gesetze-im-internet.de/grwv_2010/GrwV.pdf, checked on 9/10/2019.

Guo, Tianjiao; Englehardt, James; Wu, Tingting (2014): Review of cost versus scale: water and wastewater treatment and reuse processes. In *Water Science and Technology* 69 (2), pp. 223–234. DOI: 10.2166/wst.2013.734.

Hahn, Martin W. (2004): Broad diversity of viable bacteria in 'sterile' (0.2 microm) filtered water. In *Research in microbiology* 155 (8), pp. 688–691. DOI: 10.1016/j.resmic.2004.05.003.

Hallé, Cynthia (2010): Biofiltration in drinking water treatment: Reduction of membrane fouling and biodegradation of organic trace contaminants.

Hammes, Frederik; Salhi, Elisabeth; Köster, Oliver; Kaiser, Hans-Peter; Egli, Thomas; Gunten, Urs von (2006): Mechanistic and kinetic evaluation of organic disinfection by-product and assimilable organic carbon (AOC) formation during the ozonation of drinking water. In *Water Research* 40 (12), pp. 2275–2286. DOI: 10.1016/j.watres.2006.04.029.

Hassen, Abdennaceur; Mahrouk, Meryem; Ouzari, Hadda; Cherif, Mohamed; Boudabous, Abdellatif; Damelincourt, Jean Jacques (2000): UV disinfection of treated wastewater in a large-scale pilot plant and inactivation of selected bacteria in a laboratory UV device. In *Bioresource technology* 74 (2), pp. 141–150. DOI: 10.1016/S0960-8524(99)00179-0.

Heiberger, Richard M.; Burt Holland, Burt Holland (2015): Statistical Analysis and Data Display An Intermediate Course with Examples in R: Springer.

Helmreich, B.; Horn, H. (2009): Opportunities in rainwater harvesting. In *Desalination* 248 (1-3), pp. 118–124. DOI: 10.1016/j.desal.2008.05.046.

Hembach, Norman; Alexander, Johannes; Hiller, Christian; Wieland, Arne; Schwartz, Thomas (2019): Dissemination prevention of antibiotic resistant and facultative pathogenic bacteria by ultrafiltration and ozone treatment at an urban wastewater treatment plant. In *Scientific reports* 9 (1), pp. 1–12.

Hiller, C. X.; Hübner, U.; Fajnorova, S.; Schwartz, T.; Drewes, J. E. (2019): Antibiotic microbial resistance (AMR) removal efficiencies by conventional and advanced wastewater treatment processes: A review. In *The Science of the total environment* 685, pp. 596–608. DOI: 10.1016/j.scitotenv.2019.05.315.

Hirasaki, Tomoko; Noda, Toshiaki; Nakano, Hiroo; Ishizaki, Yoshiaki; Manabe, Sei-ichi; Yamamoto, Naoki (1994): Mechanism of Removing Japanese Encephalitis virus (JEV) and Gold Particles Using Cuprammonium Regenerated Cellulose Hollow Fiber (i-BMM or BMM) from Aqueous Solution Containing Protein. In *Polym J* 26 (11), pp. 1244–1256. DOI: 10.1295/polymj.26.1244.

Hirasaki, Tomoko; Sato, Tetsuo; Tsuboi, Takashi; Nakano, Hiroo; Noda, Toshiaki; Kono, Akira et al. (1995): Permeation mechanism of DNA molecules in solution through cuprammonium regenerated cellulose hollow fiber (BMMtm). In *Journal of Membrane Science* 106 (1-2), pp. 123–129. DOI: 10.1016/0376-7388(95)00082-N.

Hochschule Geisenheim (2019): Geisenheimer Bewässerungssteuerung 2019 - für Penman-Verdunstung -. Available online at https://www.hs-geisenheim.de/fileadmin/redaktion/FORSCHUNG/Institut_fuer_Gemuesebau/Ueberblick_Institut_fuer_Gemuesebau/Geisenheimer_Steuerung/kc-Werte_PENMAN_2019.pdf, checked on 12/20/2019.

Holland, David M.; Borg, Matthew K.; Lockerby, Duncan A.; Reese, Jason M. (2015a): Enhancing nano-scale computational fluid dynamics with molecular pre-simulations: Unsteady problems and design optimisation. In *Computers & Fluids* 115, pp. 46–53. DOI: 10.1016/j.compfluid.2015.03.023.

Holland, David M.; Lockerby, Duncan A.; Borg, Matthew K.; Nicholls, William D.; Reese, Jason M. (2015b): Molecular dynamics pre-simulations for nanoscale computational fluid dynamics. In *Microfluid Nanofluid* 18 (3), pp. 461–474. DOI: 10.1007/s10404-014-1443-6.

Holland, Robert Alan; Scott, Kate A.; Flörke, Martina; Brown, Gareth; Ewers, Robert M.; Farmer, Elizabeth et al. (2015c): Global impacts of energy demand on the freshwater resources of nations. In *Proceedings of the National Academy of Sciences of the United States of America* 112 (48), E6707-16. DOI: 10.1073/pnas.1507701112.

Hollender, Juliane; Zimmermann, Saskia G.; Koepke, Stephan; Krauss, Martin; McArdell, Christa S.; Ort, Christoph et al. (2009): Elimination of organic micropollutants in a municipal wastewater treatment plant upgraded with a full-scale post-ozonation followed by sand filtration. In *Environ. Sci. Technol.* 43 (20), pp. 7862–7869. DOI: 10.1021/es9014629.

Hong, Pei-Ying; Al-Jassim, Nada; Ansari, Mohd Ikram; Mackie, Roderick I. (2013): Environmental and Public Health Implications of Water Reuse: Antibiotics, Antibiotic Resistant Bacteria, and Antibiotic Resistance Genes. In *Antibiotics (Basel, Switzerland)* 2 (3), pp. 367–399. DOI: 10.3390/antibiotics2030367.

Howe, Kerry J.; Clark, Mark M. (2006): Effect of coagulation pretreatment on membrane filtration performance. In *Journal - American Water Works Association* 98 (4), pp. 133–146. DOI: 10.1002/j.1551-8833.2006.tb07641.x.

Hsieh, Chih-Chen; Balducci, Anthony; Doyle, Patrick S. (2007): An Experimental Study of DNA Rotational Relaxation Time in Nanoslits. In *Macromolecules* 40 (14), pp. 5196–5205. DOI: 10.1021/ma070570k.

Huang, Chihpin; Lin, Jr-Lin; Lee, Wen-Shan; Pan, Jill R.; Zhao, Bingqing (2011): Effect of coagulation mechanism on membrane permeability in coagulation-assisted microfiltration for spent filter backwash water recycling. In *Colloids and Surfaces A: Physicochemical and Engineering Aspects* 378 (1-3), pp. 72–78. DOI: 10.1016/j.colsurfa.2011.01.054.

Huang, David M.; Sendner, Christian; Horinek, Dominik; Netz, Roland R.; Bocquet, Lydéric (2008): Water slippage versus contact angle: a quasiuniversal relationship. In *Physical review letters* 101 (22), p. 226101. DOI: 10.1103/PhysRevLett.101.226101.

Huang, Haiou; Young, Thayer A.; Schwab, Kellogg J.; Jacangelo, Joseph G. (2012): Mechanisms of virus removal from secondary wastewater effluent by low pressure membrane filtration. In *Journal of Membrane Science* 409-410, pp. 1–8. DOI: 10.1016/j.memsci.2011.12.050.

Hübner, U.; Miehe, U.; Jekel, M. (2012): Optimized removal of dissolved organic carbon and trace organic contaminants during combined ozonation and artificial groundwater recharge. In *Water Research* 46 (18), pp. 6059–6068. DOI: 10.1016/j.watres.2012.09.001.

Hübner, U.; Seiwert, B.; Reemtsma, T.; Jekel, M. (2014): Ozonation products of carbamazepine and their removal from secondary effluents by soil aquifer treatment--indications from column experiments. In *Water Research* 49, pp. 34–43. DOI: 10.1016/j.watres.2013.11.016.

Iannelli, R.; Ripari, S.; Casini, B.; Buzzigoli, A.; Privitera, G.; Verani, M.; Carducci, A. (2014): Feasibility assessment of surface water disinfection by ultrafiltration. In *Water Science and Technology: Water Supply* 14 (4), pp. 522–531. DOI: 10.2166/ws.2014.003.

Iglesias, Ana; Garrote, Luis (2015): Adaptation strategies for agricultural water management under climate change in Europe. In *Agricultural Water Management* 155, pp. 113–124. DOI: 10.1016/j.agwat.2015.03.014.

Ikner, Luisa A.; Soto-Beltran, Marcela; Bright, Kelly R. (2011): New method using a positively charged microporous filter and ultrafiltration for concentration of viruses from tap water. In *Appl. Environ. Microbiol.* 77 (10), pp. 3500–3506. DOI: 10.1128/AEM.02705-10.

ISO 10705-1:2001: Water quality - Detection and enumeration of bacteriophages - Part 1: Enumeration of F-specific RNA bacteriophages.

ISO 10705-1:2001 (1995): Water Quality-Detection and Enumeration of Bacteriophages-Part 1: Enumeration of F-specific RNA Bacteriophages: ISO.

ISO 16075: Guidelines for treated wastewater use for irrigation projects 2015.

Ivancev-Tumbas, Ivana; Hobby, Ralph (2010): Removal of organic xenobiotics by combined out/in ultrafiltration and powdered activated carbon adsorption. In *Desalination* 255 (1-3), pp. 124–128.

Ivancev-Tumbas, Ivana; Hobby, Ralph; Küchle, Benjamin; Panglisch, Stefan; Gimbel, Rolf (2008): p-Nitrophenol removal by combination of powdered activated carbon adsorption and ultrafiltration–comparison of different operational modes. In *Water Research* 42 (15), pp. 4117–4124.

Ivancev-Tumbas, Ivana; Hoffmann, Grit; Hobby, Ralph; Kerkez, Đurđa; Tubić, Aleksandra; Babić-Nanić, Spomenka; Panglisch, Stefan (2018): Removal of diclofenac from water by in/out PAC/UF hybrid process. In *Environmental technology* 39 (18), pp. 2315–2320. DOI: 10.1080/09593330.2017.1354077.

Jacangelo, Joseph G.; Adham, Samer S.; Laîné, Jean-Michel (1995): Mechanism of Cryptosporidium, Giardia, and MS2 virus removal by MF and UF. In *Journal - American Water Works Association* 87 (9), pp. 107–121. DOI: 10.1002/j.1551-8833.1995.tb06427.x.

Jacob, Daniela; Göttel, Holger; Kotlarski, Sven; Lorenz, Philip; Sieck, Kevin (2008): Klimaauswirkungen und Anpassungen in Deutschland – Phase 1: Erstellung regionaler Klimaszenarien in Deutschland, Umweltbundesamt, Forschungsbericht 204 41 138. Available online at https://www.umweltbundesamt.de/sites/default/files/medien/publikation/long/3513.pdf, checked on 8/27/2018.

Jacquet, N.; Wurtzer, S.; Darracq, G.; Wyart, Y.; Moulin, L.; Moulin, P. (2021): Effect of concentration on virus removal for ultrafiltration membrane in drinking water production. In *Journal of Membrane Science* 634, p. 119417. DOI: 10.1016/j.memsci.2021.119417.

Jeirani, Zahra; Niu, Catherine Hui; Soltan, Jafar (2017): Adsorption of emerging pollutants on activated carbon. Reviews in Chemical Engineering, 33(5). In *Reviews in Chemical Engineering* 33 (5). DOI: 10.1515/REVCE-2016-0027.

Jekel, Martin; Dott, Wolfgang; Bergmann, Axel; Dünnbier, Uwe; Gnirß, Regina; Haist-Gulde, Brigitte et al. (2015): Selection of organic process and source indicator substances for the anthropogenically influenced water cycle. In *Chemosphere* 125, pp. 155–167. DOI: 10.1016/j.chemosphere.2014.12.025.

Johnston, Calum; Martin, Bernard; Fichant, Gwennaele; Polard, Patrice; Claverys, Jean-Pierre (2014): Bacterial transformation: distribution, shared mechanisms and divergent control. In *Nature reviews. Microbiology* 12 (3), pp. 181–196. DOI: 10.1038/nrmicro3199.

Jönsson, A-S; Jönsson, B.; Byhlin, H. (2006): A concentration polarization model for the ultrafiltration of nonionic surfactants. In *Journal of colloid and interface science* 304 (1), pp. 191–199. DOI: 10.1016/j.jcis.2006.08.030.

Jucker, Catherine; Clark, Mark M. (1994): Adsorption of aquatic humic substances on hydrophobic ultrafiltration membranes. In *Journal of Membrane Science* 97, pp. 37–52. DOI: 10.1016/0376-7388(94)00146-P.

Kalatur, Ekaterina; Buyakova, Svetlana; Kulkov, Sergey; Narikovich, Anton (2014): Porosity and mechanical properties of zirconium ceramics. In. INTERNATIONAL CONFERENCE ON PHYSICAL MESOMECHANICS OF MULTILEVEL SYSTEMS 2014. Tomsk, Russia, 3–5 September 2014: AIP Publishing LLC (AIP Conference Proceedings), pp. 225–228.

Kallioinen, M.; Pekkarinen, M.; Mänttäri, M.; Nuortila-Jokinen, J.; Nyström, M. (2007): Comparison of the performance of two different regenerated cellulose ultrafiltration membranes at high filtration pressure. In *Journal of Membrane Science* 294 (1-2), pp. 93–102. DOI: 10.1016/j.memsci.2007.02.016.

Kappell, Anthony D.; Kimbell, Lee K.; Seib, Matthew D.; Carey, Daniel E.; Choi, Melinda J.; Kalayil, Tino et al. (2018): Removal of antibiotic resistance genes in an anaerobic membrane bioreactor treating primary clarifier effluent at 20 °C. In *Environ. Sci.: Water Res. Technol.* 4 (11), pp. 1783–1793. DOI: 10.1039/C8EW00270C.

Keir, Greg; Jegatheesan, Veeriah (2014): A review of computational fluid dynamics applications in pressure-driven membrane filtration. In *Rev Environ Sci Biotechnol* 13 (2), pp. 183–201. DOI: 10.1007/s11157-013-9327-x.

Kennedy, M.; Zhizhong, L.; Febrina, E.; van Hoof, S.; Shippers, J. (2003): Effects of coagulation on filtration mechanisms in dead-end ultrafiltration. In *Water Science and Technology: Water Supply* 3 (5-6), pp. 109–116. DOI: 10.2166/ws.2003.0156.

Khadra, R.; Lamaddalena, N. (2006): A Simulation Model to generate the Demand Hydrographs in Large-scale Irrigation Systems. In *Biosystems Engineering* 93 (3), pp. 335–346. DOI: 10.1016/j.biosystemseng.2005.12.006.

Khan, Stuart J.; Walker, Troy; Stanford, Benjamin D.; Drewes, Jörg E. (2017): Advanced treatment for potable water reuse. In *wio* 16, pp. 581–605. DOI: 10.2166/9781780407197_0581.

Kim, Hyun-Chul; Hong, Jong-Hyun; Lee, Seockheon (2006): Fouling of microfiltration membranes by natural organic matter after coagulation treatment: A comparison of different initial mixing conditions. In *Journal of Membrane Science* 283 (1-2), pp. 266–272. DOI: 10.1016/j.memsci.2006.06.041.

Kobayashi, Motoyoshi (2020): An analysis on electrophoretic mobility of hydrophobic polystyrene particles with low surface charge density: effect of hydrodynamic slip. In *Colloid Polym Sci* 298 (10), pp. 1313–1318. DOI: 10.1007/s00396-020-04716-2.

Konieczny, Krystyna; Sąkol, Dorota; Płonka, Joanna; Rajca, Mariola; Bodzek, Michał (2009): Coagulation—ultrafiltration system for river water treatment. In *Desalination* 240 (1-3), pp. 151–159. DOI: 10.1016/j.desal.2007.11.072.

K'oreje, Kenneth Otieno; Okoth, Maurice; van Langenhove, Herman; Demeestere, Kristof (2020): Occurrence and treatment of contaminants of emerging concern in the African aquatic environment: Literature review and a look ahead. In *Journal of environmental management* 254, p. 109752. DOI: 10.1016/j.jenvman.2019.109752.

Kötzsch, S.; Alisch, S.; Egli, T.; Hammes, F.; Weilenmann, H. U.; Pfister, L.; Karmann, S. (2012): Durchflusszytometrische Analyse von Wasserproben. In *Bundesamt für Gesundheit, Schweizerisches Lebensmittelbuch, 46 S*.

Kötzsch, Stefan; Sinreich, Michael (2014): Zellzahlen zum Grundwasser: Bestimmung mittles Durchflusszytometrie: Wasserqualität. In *Aqua & Gas* 94 (3), pp. 14–21.

Kristiansson, Erik; Fick, Jerker; Janzon, Anders; Grabic, Roman; Rutgersson, Carolin; Weijdegård, Birgitta et al. (2011): Pyrosequencing of antibiotic-contaminated river sediments reveals high levels of resistance and gene transfer elements. In *PloS one* 6 (2), e17038. DOI: 10.1371/journal.pone.0017038.

Krzeminski, Pawel; Feys, Edward; Anglès d'Auriac, Marc; Wennberg, Aina Charlotte; Umar, Muhammad; Schwermer, Carsten Ulrich; Uhl, Wolfgang (2020): Combined membrane filtration and 265 nm UV irradiation for effective removal of cell free antibiotic resistance genes from feed water and concentrate. In *Journal of Membrane Science* 598, p. 117676. DOI: 10.1016/j.memsci.2019.117676.

Krzeminski, Pawel; Tomei, Maria Concetta; Karaolia, Popi; Langenhoff, Alette; Almeida, C. Marisa R.; Felis, Ewa et al. (2019): Performance of secondary wastewater treatment methods for the removal of contaminants of emerging concern implicated in crop uptake and antibiotic resistance spread: A review. In *The Science of the total environment* 648, pp. 1052–1081. DOI: 10.1016/j.scitotenv.2018.08.130.

Kulkarni, Prachi; Olson, Nathan D.; Paulson, Joseph N.; Pop, Mihai; Maddox, Cynthia; Claye, Emma et al. (2018): Conventional wastewater treatment and reuse site practices modify bacterial community structure but do not eliminate some opportunistic pathogens in reclaimed water. In *The Science of the total environment* 639, pp. 1126–1137. DOI: 10.1016/j.scitotenv.2018.05.178.

Kumar, Awanish; Pal, Dharm (2018): Antibiotic resistance and wastewater: Correlation, impact and critical human health challenges. In *Journal of Environmental Chemical Engineering* 6 (1), pp. 52–58. DOI: 10.1016/j.jece.2017.11.059.

Lan, Lihua; Kong, Xianwang; Sun, Haoxiang; Li, Changwei; Liu, Dezhao (2019): High removal efficiency of antibiotic resistance genes in swine wastewater via nanofiltration and reverse osmosis processes. In *Journal of environmental management* 231, pp. 439–445. DOI: 10.1016/j.jenvman.2018.10.073.

Langlet, J.; Gaboriaud, F.; Gantzer, C. (2007): Effects of pH on plaque forming unit counts and aggregation of MS2 bacteriophage. In *Journal of applied microbiology* 103 (5), pp. 1632–1638. DOI: 10.1111/j.1365-2672.2007.03396.x.

Langlet, Jérémie; Gaboriaud, Fabien; Duval, Jérôme F. L.; Gantzer, Christophe (2008): Aggregation and surface properties of F-specific RNA phages: implication for membrane filtration processes. In *Water Research* 42 (10-11), pp. 2769–2777. DOI: 10.1016/j.watres.2008.02.007.

Langlet, Jérémie; Ogorzaly, Leslie; Schrotter, Jean-Christophe; Machinal, Claire; Gaboriaud, Fabien; Duval, Jérôme F.L.; Gantzer, Christophe (2009): Efficiency of MS2 phage and Qβ phage removal by membrane filtration in water treatment: Applicability of real-time RT-PCR method. In *Journal of Membrane Science* 326 (1), pp. 111–116. DOI: 10.1016/j.memsci.2008.09.044.

Larson, Jonathan W.; Yantz, Gregory R.; Zhong, Qun; Charnas, Rebecca; D'Antoni, Christina M.; Gallo, Michael V. et al. (2006): Single DNA molecule stretching in sudden mixed shear and elongational microflows. In *Lab on a chip* 6 (9), pp. 1187–1199. DOI: 10.1039/b602845d.

Lata, Pushpa; Ram, Siya; Agrawal, Madhoolika; Shanker, Rishi (2009): Real time PCR for the rapid detection of vanA gene in surface waters and aquatic macrophyte by molecular beacon probe. In *Environ. Sci. Technol.* 43 (9), pp. 3343–3348. DOI: 10.1021/es803635y.

Latulippe, D. R.; Zydney, A. L. (2009): Elongational flow model for transmission of supercoiled plasmid DNA during membrane ultrafiltration. In *Journal of Membrane Science* 329 (1-2), pp. 201–208. DOI: 10.1016/j.memsci.2008.12.045.

Latulippe, David R.; Ager, Kimberly; Zydney, Andrew L. (2007): Flux-dependent transmission of supercoiled plasmid DNA through ultrafiltration membranes. In *Journal of Membrane Science* 294 (1-2), pp. 169–177. DOI: 10.1016/j.memsci.2007.02.033.

Latulippe, David R.; Zydney, Andrew L. (2011): Separation of plasmid DNA isoforms by highly converging flow through small membrane pores. In *Journal of colloid and interface science* 357 (2), pp. 548–553. DOI: 10.1016/j.jcis.2011.02.029.

LAWA (2017): Bund/Länder-Arbeitsgemeinschaft Wasser: Auswirkungen des Klimawandels auf die Wasserwirtschaft. Bestandsaufnahme, Handlungsoptionen und strategische Handlungsfelder 2017. Available online at http://www.laenderfinanzierungsprogramm.de/cms/WaBoAb_prod/WaBoAb/Vorhaben/Sonstige/K_1.17/20171221_lawa-bericht_hydron.pdf, checked on 8/30/2018.

LAWA (2021): Bund/Länder-Arbeitsgemeinschaft Wasser - Jahresbericht 2020. Available online at https://www.lawa.de/documents/jahresbericht_der_lawa_2020_1629700570.pdf, checked on 5/3/2022.

Le Page, Michel; Fakir, Younes; Jarlan, Lionel; Boone, Aaron; Berjamy, Brahim; Khabba, Saïd; Zribi, Mehrez (2020): Projection of irrigation water demand based on the simulation of synthetic crop coefficients and climate change. In *Hydrology and Earth System Sciences*. DOI: 10.5194/hess-2020-301.

Lebaron, Philippe; Servais, Pierre; Agogué, Helene; Courties, Claude; Joux, Fabien (2001): Does the high nucleic acid content of individual bacterial cells allow us to discriminate between active cells and inactive cells in aquatic systems? In *Appl. Environ. Microbiol.* 67 (4), pp. 1775–1782.

Lebleu, Nathalie; Roques, Christine; Aimar, Pierre; Causserand, Christel (2009): Role of the cell-wall structure in the retention of bacteria by microfiltration membranes. In *Journal of Membrane Science* 326 (1), pp. 178–185. DOI: 10.1016/j.memsci.2008.09.049.

Leclerc, H.; Edberg, S.; Pierzo, V.; Delattre, J. M. (2000): Bacteriophages as indicators of enteric viruses and public health risk in groundwaters. In *Journal of applied microbiology* 88 (1), pp. 5–21. DOI: 10.1046/j.1365-2672.2000.00949.x.

Lee, Anna; Elam, Jeffrey W.; Darling, Seth B. (2016): Membrane materials for water purification: design, development, and application. In *Environ. Sci.: Water Res. Technol.* 2 (1), pp. 17–42. DOI: 10.1039/C5EW00159E.

Lee, Jeong-Dae; Lee, Sang-Ho; Jo, Min-Ho; Park, Pyung-Kyu; Lee, Chung-Hak; Kwak, Jong-Woon (2000): Effect of Coagulation Conditions on Membrane Filtration Characteristics in Coagulation−Microfiltration Process for Water Treatment. In *Environ. Sci. Technol.* 34 (17), pp. 3780–3788. DOI: 10.1021/es9907461.

Lee, Suntae; Hata, Akihiko; Yamashita, Naoyuki; Tanaka, Hiroaki (2017): Evaluation of Virus Reduction by Ultrafiltration with Coagulation-Sedimentation in Water Reclamation. In *Food Environ Virol* 9 (4), pp. 453–463. DOI: 10.1007/s12560-017-9301-9.

Lengsfeld, C. S.; Anchordoquy, T. J. (2002): Shear-induced degradation of plasmid DNA. In *Journal of Pharmaceutical Sciences* 91 (7), pp. 1581–1589. DOI: 10.1002/jps.10140.

Lerch, André (2008): Fouling layer formation by flocs in inside-out driven capillary ultrafiltration membranes. In *Universität Duisburg-Essen, Fakultät für Ingenieurwissenschaften, Abteilung Maschinenbau*.

Lewis, Roger J.; Pecora, R. (1986): Comparison of predicted Rouse-Zimm dynamics with observations for a 2311 base pair DNA fragment. In *Macromolecules* 19 (7), pp. 2074–2075. DOI: 10.1021/ma00161a049.

LfL (2006): Bayerische Landesanstalt für Landwirtschaft: Sonnenblumen zur Kornnutzung. Available online at https://www.lfl.bayern.de/mam/cms07/publikationen/daten/informationen/p_19934.pdf, checked on 4/3/2020.

LfL (2008): Bayerische Landesanstalt für Landwirtschaft: Bewässerung im Ackerbau und in gärtnerischen Freilandkulturen. In *LfL, Freising*.

LfU (2009): Bayerisches Landesamt für Umwelt: Klimawandel im Süden Deutschlands. Ausmaß – Folgen – Strategien, Auswirkungen auf die Wasserwirtschaft. Available online at http://kliwa.de/download/Klimawandel_im_Sueden_Deutschlands.pdf.

LfU (2020): Mittelwerte des Gebietsniederschlags - LfU Bayern. Available online at https://www.lfu.bayern.de/wasser/klima_wandel/bayern/niederschlag/index.htm, checked on 10/6/2020.

Li, Baoguang; Vellidis, George; Liu, Huanli; Jay-Russell, Michele; Zhao, Shaohua; Hu, Zonglin et al. (2014a): Diversity and antimicrobial resistance of Salmonella enterica isolates from surface water in Southeastern United States. In *Appl. Environ. Microbiol.* 80 (20), pp. 6355–6365. DOI: 10.1128/AEM.02063-14.

Li, Jianan; Cheng, Weixiao; Xu, Like; Strong, P. J.; Chen, Hong (2015): Antibiotic-resistant genes and antibiotic-resistant bacteria in the effluent of urban residential areas, hospitals, and a municipal wastewater treatment plant system. In *Environmental science and pollution research international* 22 (6), pp. 4587–4596. DOI: 10.1007/s11356-014-3665-2.

Li, Jingsi; Fei, Liangjun; Li, Shan; Xue, Cai; Shi, Zhongxing; Hinkelmann, Reinhard (2020a): Development of "water-suitable" agriculture based on a statistical analysis of factors affecting irrigation water demand. In *The Science of the total environment* 744, p. 140986. DOI: 10.1016/j.scitotenv.2020.140986.

Li, W. C. (2014b): Occurrence, sources, and fate of pharmaceuticals in aquatic environment and soil. In *Environmental pollution (Barking, Essex : 1987)* 187, pp. 193–201. DOI: 10.1016/j.envpol.2014.01.015.

Li, Yinbo; Wang, Hongwei; Chen, Yun; Deng, Mingjiang; Li, Qian; Wufu, Adiliai et al. (2020b): Estimation of regional irrigation water requirements and water balance in Xinjiang, China during 1995–2017. In *PeerJ* 8, e8243. Available online at https://peerj.com/articles/8243/#.

Libutti, Angela; Gatta, Giuseppe; Gagliardi, Anna; Vergine, Pompilio; Pollice, Alfieri; Beneduce, Luciano et al. (2018): Agro-industrial wastewater reuse for irrigation of a vegetable crop succession under Mediterranean conditions. In *Agricultural Water Management* 196, pp. 1–14. DOI: 10.1016/j.agwat.2017.10.015.

Lin, Yen-Ching; Lai, Webber Wei-Po; Tung, Hsin-hsin; Lin, Angela Yu-Chen (2015): Occurrence of pharmaceuticals, hormones, and perfluorinated compounds in groundwater in Taiwan. In *Environmental monitoring and assessment* 187 (5), p. 256. DOI: 10.1007/s10661-015-4497-3.

Liu, Jie; Li, Bing; Wang, Yingying; Zhang, Guijuan; Jiang, Xiaotao; Li, Xiaoyan (2019): Passage and community changes of filterable bacteria during microfiltration of a surface water supply. In *Environment international* 131, p. 104998. DOI: 10.1016/j.envint.2019.104998.

Liu, Qiong; Nie, Yihan; Zhan, Haifei; Zhu, Huaiyong; Sun, Ziqi; Bell, John et al. (2020): Atomistic Mechanisms of Ultralarge Bending Deformation of Single-Crystalline TiO 2 –B Nanowires. In *J. Phys. Chem. C* 124 (20), pp. 11174–11182. DOI: 10.1021/acs.jpcc.0c01614.

Liu, Shan-Shan; Qu, Hong-Mei; Yang, Dong; Hu, Hui; Liu, Wei-Li; Qiu, Zhi-Gang et al. (2018): Chlorine disinfection increases both intracellular and extracellular antibiotic resistance genes in a full-scale wastewater treatment plant. In *Water Research* 136, pp. 131–136. DOI: 10.1016/j.watres.2018.02.036.

Long, Ying; Yu, Genying; Dong, Lu; Xu, Yanchao; Lin, Hongjun; Deng, Ying et al. (2021): Synergistic fouling behaviors and mechanisms of calcium ions and polyaluminum chloride associated with alginate solution in coagulation-ultrafiltration (UF) process. In *Water Research* 189, p. 116665. DOI: 10.1016/j.watres.2020.116665.

Lonigro, Antonio; Rubino, Pietro; Lacasella, Vita; Montemurro, Nicola (2016): Faecal pollution on vegetables and soil drip irrigated with treated municipal wastewaters. In *Agricultural Water Management* 174, pp. 66–73. DOI: 10.1016/j.agwat.2016.02.001.

López-Gutiérrez, Juan C.; Henry, Sonia; Hallet, Stéphanie; Martin-Laurent, Fabrice; Catroux, Gérard; Philippot, Laurent (2004): Quantification of a novel group of nitrate-reducing bacteria in the environment by real-time PCR. In *Journal of microbiological methods* 57 (3), pp. 399–407.

López-Lambraño, Alvaro Alberto; Martínez-Acosta, Luisa; Gámez-Balmaceda, Ena; Medrano-Barboza, Juan Pablo; Remolina López, John Freddy; López-Ramos, Alvaro (2020): Supply and Demand Analysis of Water Resources. Case Study: Irrigation Water Demand in a Semi-Arid Zone in Mexico. In *Agriculture* 10 (8), p. 333. DOI: 10.3390/agriculture10080333.

Löwenberg, Jonas; Zenker, Armin; Baggenstos, Martin; Koch, Gerhard; Kazner, Christian; Wintgens, Thomas (2014): Comparison of two PAC/UF processes for the removal of micropollutants from wastewater treatment plant effluent: process performance and removal efficiency. In *Water Research* 56, pp. 26–36. DOI: 10.1016/j.watres.2014.02.038.

Lu, Jin Gang; Hwang, Wook Ryol (2020): On the Interfacial Flow Over Porous Media Composed of Packed Spheres: Part 2-Optimal Stokes–Brinkman Coupling with Effective Navier-Slip Approach. In *Transp Porous Med* 132 (2), pp. 405–421. DOI: 10.1007/s11242-020-01398-w.

Maczulak, Anne Elizabeth (2010): Environmental engineering. Designing a sustainable future. New York: Facts On File (Green technology, / Anne Maczulak ; 4).

Madaeni, S.S (1999): The application of membrane technology for water disinfection. In *Water Research* 33 (2), pp. 301–308. DOI: 10.1016/S0043-1354(98)00212-7.

Mahjoub, O.; Escande, A.; Rosain, D.; Casellas, C.; Gomez, E.; Fenet, H. (2011): Estrogen-like and dioxin-like organic contaminants in reclaimed wastewater: transfer to irrigated soil and groundwater. In *Water Science and Technology* 63 (8), pp. 1657–1662. DOI: 10.2166/wst.2011.322.

Maniak, Ulrich (2016): Hydrologie und Wasserwirtschaft. Eine Einführung für Ingenieure. 7., neu bearbeitete Auflage. Berlin, Heidelberg: Springer Vieweg (Lehrbuch).

Mansour, Hani A.; El Sayed Mohamed, Salwa; Lightfoot, David A. (2020a): Molecular studies for drought tolerance in some Egyptian wheat genotypes under different irrigation systems. In *Open Agriculture* 5 (1), pp. 280–290. DOI: 10.1515/opag-2020-0030.

Mansour, Hani A.; Gaballah, Maybelle S.; Nofal, Osama A. (2020b): Evaluating the water productivity by Aquacrop model of wheat under irrigation systems and algae. In *Open Agriculture* 5 (1), pp. 262–270. DOI: 10.1515/opag-2020-0029.

Mantovani, P.; Abu-Orf, M.; O'Connor, T. (2001): Bridging the Gap: Meeting the World's Water and Environmental Resources Challenges. In *Nonpotable Water Reuse Management Practices*.

Marcos, Bernard; Moresoli, Christine; Skorepova, Jana; Vaughan, Brandi (2009): CFD modeling of a transient hollow fiber ultrafiltration system for protein concentration. In *Journal of Membrane Science* 337 (1-2), pp. 136–144. DOI: 10.1016/j.memsci.2009.03.036.

Marcotullio, Peter J. (2007): Urban water-related environmental transitions in Southeast Asia. In *Sustain Sci* 2 (1), pp. 27–54. DOI: 10.1007/s11625-006-0019-0.

Margot, Jonas; Kienle, Cornelia; Magnet, Anoÿs; Weil, Mirco; Rossi, Luca; Alencastro, Luiz Felippe de et al. (2013): Treatment of micropollutants in municipal wastewater: ozone or powdered activated carbon? In *The Science of the total environment* 461-462, pp. 480–498. DOI: 10.1016/j.scitotenv.2013.05.034.

Mariño, Miguel A.; Tracy, John C.; Taghavi, S.Alireza (1993): Forecasting of reference crop evapotranspiration. In *Agricultural Water Management* 24 (3), pp. 163–187. DOI: 10.1016/0378-3774(93)90022-3.

Marti, Elisabet; Monclús, Hector; Jofre, Juan; Rodriguez-Roda, Ignasi; Comas, Joaquim; Balcázar, José Luis (2011): Removal of microbial indicators from municipal wastewater by a membrane bioreactor (MBR). In *Bioresource technology* 102 (8), pp. 5004–5009. DOI: 10.1016/j.biortech.2011.01.068.

Marx, Andreas (2019): Dürre 2018 - Helmholtz-Zentrum für Umweltforschung UFZ. Available online at https://www.ufz.de/index.php?de=44429, updated on 2/8/2019, checked on 4/4/2020.

Mastel, K. (2002): Beregnung und Bewässerung landwirtschaftlicher und gärtnerischer Kulturen. In *Merkblätter für die Umweltgerechte Landbewirtschaftung* 24, pp. 1–12.

Matsui, K.; Honjo, M.; Kawabata, Z. (2001): Estimation of the fate of dissolved DNA in thermally stratified lake water from the stability of exogenous plasmid DNA. In *Aquat. Microb. Ecol.* 26, pp. 95–102. DOI: 10.3354/ame026095.

Matsui, Kazuaki; Ishii, Nobuyoshi; Kawabata, Zen'ichiro (2003): Release of extracellular transformable plasmid DNA from Escherichia coli cocultivated with algae. In *Applied and environmental microbiology* 69 (4), pp. 2399–2404. DOI: 10.1128/aem.69.4.2399-2404.2003.

Matsushita, Taku; Suzuki, Hideaki; Shirasaki, Nobutaka; Matsui, Yoshihiko; Ohno, Koichi (2013): Adsorptive virus removal with super-powdered activated carbon. In *Separation and Purification Technology* 107, pp. 79–84. DOI: 10.1016/j.seppur.2013.01.017.

McDonald, Robert I.; Weber, Katherine; Padowski, Julie; Flörke, Martina; Schneider, Christof; Green, Pamela A. et al. (2014): Water on an urban planet: Urbanization and the reach of urban water infrastructure. In *Global Environmental Change* 27, pp. 96–105. DOI: 10.1016/j.gloenvcha.2014.04.022.

Meacle, F. J.; Zhang, H.; Papantoniou, I.; Ward, J. M.; Titchener-Hooker, N. J.; Hoare, M. (2007): Degradation of supercoiled plasmid DNA within a capillary device. In *Biotechnology and bioengineering* 97 (5), pp. 1148–1157. DOI: 10.1002/bit.21275.

Mehta, Amit; Zydney, Andrew L. (2005): Permeability and selectivity analysis for ultrafiltration membranes. In *Journal of Membrane Science* 249 (1-2), pp. 245–249. DOI: 10.1016/j.memsci.2004.09.040.

Meng, Bo-Yang; Li, Xiao-Yan (2019): In Situ Visualization of Concentration Polarization during Membrane Ultrafiltration Using Microscopic Laser-Induced Fluorescence. In *Environ. Sci. Technol.* 53 (5), pp. 2660–2669. DOI: 10.1021/acs.est.8b05741.

Metzner, A. B.; Metzner, A. P. (1970): Stress levels in rapid extensional flows of polymeric fluids. In *Rheol Acta* 9 (2), pp. 174–181. DOI: 10.1007/BF01973476.

Miklos, D. B.; Wang, W.-L.; Linden, K. G.; Drewes, J. E.; Hübner, U. (2019): Comparison of UV-AOPs (UV/H2O2, UV/PDS and UV/Chlorine) for TOrC removal from municipal wastewater effluent and optical surrogate model evaluation. In *Chemical Engineering Journal* 362, pp. 537–547. DOI: 10.1016/j.cej.2019.01.041.

Miklos, David B.; Remy, Christian; Jekel, Martin; Linden, Karl G.; Drewes, Jörg E.; Hübner, Uwe (2018): Evaluation of advanced oxidation processes for water and wastewater treatment - A critical review. In *Water Research* 139, pp. 118–131. DOI: 10.1016/j.watres.2018.03.042.

Miller, Wade G. (2006): Integrated concepts in water reuse: managing global water needs. In *Desalination* 187 (1-3), pp. 65–75. DOI: 10.1016/j.desal.2005.04.068.

Morales-Morales, Hugo A.; Vidal, Guadalupe; Olszewski, John; Rock, Channah M.; Dasgupta, Debanjana; Oshima, Kevin H.; Smith, Geoffrey B. (2003): Optimization of a reusable hollow-fiber ultrafilter for simultaneous concentration of enteric bacteria, protozoa, and viruses from water. In *Appl. Environ. Microbiol.* 69 (7), pp. 4098–4102.

Morrison, Jim (2009): Statistics for engineers: an introduction: John Wiley & Sons.

Müller, Johann; Drewes, Jörg E.; Hübner, Uwe (2017): Sequential biofiltration - A novel approach for enhanced biological removal of trace organic chemicals from wastewater treatment plant effluent. In *Water Research* 127, pp. 127–138. DOI: 10.1016/j.watres.2017.10.009.

Munir, Mariya; Wong, Kelvin; Xagoraraki, Irene (2011): Release of antibiotic resistant bacteria and genes in the effluent and biosolids of five wastewater utilities in Michigan. In *Water Research* 45 (2), pp. 681–693. DOI: 10.1016/j.watres.2010.08.033.

Myers, Samuel S. (2017): Planetary health: protecting human health on a rapidly changing planet. In *The Lancet* 390 (10114), pp. 2860–2868. DOI: 10.1016/S0140-6736(17)32846-5.

Nakamoto, M. (2010): Watsonville recycled water project story: Preserving agriculture in the Pajaro Valley. In *WateReuse California Annual Conference*.

Nasser, A. M.; Tchorch, Y.; Fattal, B. (1993): Comparative Survival of E. Coli, F+Bacteriophages, HAV and Poliovirus 1 in Wastewater and Groundwater. In *Water Science and Technology* 27 (3-4), pp. 401–407. DOI: 10.2166/wst.1993.0381.

National Research Council (2012): Water reuse: Potential for expanding the nation's water supply through reuse of municipal wastewater: National Academies Press.

NCBI (2021): Phage MS2 genome. National Center for biotechnology Information. Rockville Pike. Available online at https://www.ncbi.nlm.nih.gov/nuccore/176120924, checked on 2/20/2022.

Ng, Isaac; Shorney-Darby, Holly; Zheng, Jumeng; Galjaard, Gilbert (2018): Ceramic membranes for reuse. In *Water Practice and Technology* 13 (2), pp. 414–423. DOI: 10.2166/wpt.2018.053.

Nguyen, Anh H.; Tobiason, John E.; Howe, Kerry J. (2011): Fouling indices for low pressure hollow fiber membrane performance assessment. In *Water Research* 45 (8), pp. 2627–2637. DOI: 10.1016/j.watres.2011.02.020.

Nguyen, Quang Trong; Neel, Jean (1983): Characterization of ultrafiltration membranes. In *Journal of Membrane Science* 14 (2), pp. 111–127. DOI: 10.1016/S0376-7388(00)80098-8.

Nikolaou, Anastasia; Meric, Sureyya; Fatta, Despo (2007): Occurrence patterns of pharmaceuticals in water and wastewater environments. In *Analytical and bioanalytical chemistry* 387 (4), pp. 1225–1234. DOI: 10.1007/s00216-006-1035-8.

NSF/ANSI 55 (2019): Ultraviolet Microbiological Water Treatment Systems. NSF International Standard / American National Standard for Drinking Water Treatment Units.

O'Neill, Brian C.; Oppenheimer, Michael; Warren, Rachel; Hallegatte, Stephane; Kopp, Robert E.; Pörtner, Hans O. et al. (2017): IPCC reasons for concern regarding climate change risks. In *Nature Clim Change* 7 (1), pp. 28–37. DOI: 10.1038/nclimate3179.

Osundeko, Olumayowa; Ansolia, Preeti; Gupta, Sanjay Kumar; Bag, Pushan; Bajhaiya, Amit K. (2019): Promises and Challenges of Growing Microalgae in Wastewater. In : Water Conservation, Recycling and Reuse: Issues and Challenges: Springer, Singapore, pp. 29–53. Available online at https://link.springer.com/chapter/10.1007/978-981-13-3179-4_2.

Ottoson, J.; Hansen, A.; Björlenius, B.; Norder, H.; Stenström, T. A. (2006): Removal of viruses, parasitic protozoa and microbial indicators in conventional and membrane processes in a wastewater pilot plant. In *Water Research* 40 (7), pp. 1449–1457. DOI: 10.1016/j.watres.2006.01.039.

OWID (2020): Our World in Data. Available online at https://ourworldindata.org/, checked on 1/15/2021.

Oxarango, Laurent; Schmitz, Philippe; Quintard, Michel (2004): Laminar flow in channels with wall suction or injection: a new model to study multi-channel filtration systems. In *Chemical Engineering Science* 59 (5), pp. 1039–1051. DOI: 10.1016/j.ces.2003.10.027.

Pan, Long; Matsui, Yoshihiko; Matsushita, Taku; Shirasaki, Nobutaka (2016): Superiority of wet-milled over dry-milled superfine powdered activated carbon for adsorptive 2-methylisoborneol removal. In *Water Research* 102, pp. 516–523. DOI: 10.1016/j.watres.2016.06.062.

Panglisch, Stefan (2001): Zur Bildung und Vermeidung schwer entfernbarer Partikelablagerungen in Kapillarmembranen bei der Dead-End Filtration. IWW.

Panglisch, Stefan; Gimbel, Rolf (2004): Formation of layers of non-Brownian particles in capillary membranes operated in dead-end mode. In *Journal of the Chinese Institute of Chemical Engineers* 35 (1), pp. 77–85.

Park, Pyung-Kyu; Lee, Chung-Hak; Choi, Sang-June; Choo, Kwang-Ho; Kim, Seung-Hyun; Yoon, Cho-Hee (2002): Effect of the removal of DOMs on the performance of a coagulation-UF membrane system for drinking water production. In *Desalination* 145 (1-3), pp. 237–245. DOI: 10.1016/S0011-9164(02)00418-6.

Park, Soohyung; Lee, Wontae (2018): Removal of selected pharmaceuticals and personal care products in reclaimed water during simulated managed aquifer recharge. In *The Science of the total environment* 640-641, pp. 671–677. DOI: 10.1016/j.scitotenv.2018.05.221.

Paschold, Peter-Jürgen; Beltz, Heinrich (2010): Bewässerung im Gartenbau. 38 Tabellen. Stuttgart: Ulmer (Gartenbau). Available online at http://www.content-select.com/index.php?id=bib_view&ean=9783800190898.

Pedrero, Francisco; Kalavrouziotis, Ioannis; Alarcón, Juan José; Koukoulakis, Prodromos; Asano, Takashi (2010): Use of treated municipal wastewater in irrigated agriculture—Review of some practices in Spain and Greece. In *Agricultural Water Management* 97 (9), pp. 1233–1241. DOI: 10.1016/j.agwat.2010.03.003.

Pei, Ruoting; Kim, Sung-Chul; Carlson, Kenneth H.; Pruden, Amy (2006): Effect of river landscape on the sediment concentrations of antibiotics and corresponding antibiotic resistance genes (ARG). In *Water Research* 40 (12), pp. 2427–2435. DOI: 10.1016/j.watres.2006.04.017.

Persson, Kenneth M.; Gekas, Vassilis; Trägårdh, Gun (1995): Study of membrane compaction and its influence on ultrafiltration water permeability. In *Journal of Membrane Science* 100 (2), pp. 155–162. DOI: 10.1016/0376-7388(94)00263-X.

Petrie, Bruce; Barden, Ruth; Kasprzyk-Hordern, Barbara (2015): A review on emerging contaminants in wastewaters and the environment: current knowledge, understudied areas and recommendations for future monitoring. In *Water Research* 72, pp. 3–27. DOI: 10.1016/j.watres.2014.08.053.

Polaczyk, Amy L.; Narayanan, Jothikumar; Cromeans, Theresa L.; Hahn, Donghyun; Roberts, Jacqueline M.; Amburgey, James E.; Hill, Vincent R. (2008): Ultrafiltration-based techniques for rapid and simultaneous concentration of multiple microbe classes from 100-L tap water samples. In *Journal of microbiological methods* 73 (2), pp. 92–99. DOI: 10.1016/j.mimet.2008.02.014.

Powell, Traci; Brion, Gail M.; Jagtoyen, Marit; Derbyshire, Frank (2000): Investigating the Effect of Carbon Shape on Virus Adsorption. In *Environ. Sci. Technol.* 34 (13), pp. 2779–2783. DOI: 10.1021/es991097w.

Priezjev, Nikolai V.; Darhuber, Anton A.; Troian, Sandra M. (2005): Slip behavior in liquid films on surfaces of patterned wettability: comparison between continuum and molecular dynamics simulations. In *Physical review. E, Statistical, nonlinear, and soft matter physics* 71 (4 Pt 1), p. 41608. DOI: 10.1103/PhysRevE.71.041608.

QIAGEN: QIAcuity® One-Step Viral RT-PCR Kit. Quick-Start Protocol. Available online at https://www.qiagen.com/us/resources/download.aspx?id=1f29fe9f-8983-4a27-af2a-202a0cc94058&lang=en, checked on 2/22/2022.

QIAGEN (2021): QIAcuity User Manual. Available online at https://www.qiagen.com/us/resources/resourcedetail?id=ad681197-cdf1-401c-89c7-2db518129e86&lang=en, checked on 2/22/2022.

Qin, Qin; Chen, Xijuan; Zhuang, Jie (2015): The Fate and Impact of Pharmaceuticals and Personal Care Products in Agricultural Soils Irrigated With Reclaimed Water. In *Critical Reviews in Environmental Science and Technology* 45 (13), pp. 1379–1408. DOI: 10.1080/10643389.2014.955628.

Rapp, Bastian E. (2017): Microfluidics: Modeling, mechanics, and mathematics. Kidlington, United Kingdom: William Andrew (Micro & nano technologies series).

Ren, Shaojie; Boo, Chanhee; Guo, Ning; Wang, Shuguang; Elimelech, Menachem; Wang, Yunkun (2018): Photocatalytic Reactive Ultrafiltration Membrane for Removal of Antibiotic Resistant Bacteria and Antibiotic Resistance Genes from Wastewater Effluent. In *Environ. Sci. Technol.* 52 (15), pp. 8666–8673. DOI: 10.1021/acs.est.8b01888.

Reungoat, J.; Escher, B. I.; Macova, M.; Argaud, F. X.; Gernjak, W.; Keller, J. (2012): Ozonation and biological activated carbon filtration of wastewater treatment plant effluents. In *Water Research* 46 (3), pp. 863–872. DOI: 10.1016/j.watres.2011.11.064.

Revetta, Randy P.; Pemberton, Adin; Lamendella, Regina; Iker, Brandon; Santo Domingo, Jorge W. (2010): Identification of bacterial populations in drinking water using 16S rRNA-based sequence analyses. In *Water Research* 44 (5), pp. 1353–1360. DOI: 10.1016/j.watres.2009.11.008.

Rizzo, L.; Manaia, C.; Merlin, C.; Schwartz, T.; Dagot, C.; Ploy, M. C. et al. (2013): Urban wastewater treatment plants as hotspots for antibiotic resistant bacteria and genes spread into the environment: a review. In *The Science of the total environment* 447, pp. 345–360. DOI: 10.1016/j.scitotenv.2013.01.032.

Rizzo, Luigi; Gernjak, Wolfgang; Krzeminski, Pawel; Malato, Sixto; McArdell, Christa S.; Perez, Jose Antonio Sanchez et al. (2020): Best available technologies and treatment trains to address current challenges in urban wastewater reuse for irrigation of crops in EU countries. In *The Science of the total environment* 710, p. 136312. DOI: 10.1016/j.scitotenv.2019.136312.

Rizzo, Luigi; Malato, Sixto; Antakyali, Demet; Beretsou, Vasiliki G.; Đolić, Maja B.; Gernjak, Wolfgang et al. (2019): Consolidated vs new advanced treatment methods for the removal of contaminants of emerging concern from urban wastewater. In *The Science of the total environment* 655, pp. 986–1008. DOI: 10.1016/j.scitotenv.2018.11.265.

Rodriguez, Elena; Campinas, Margarida; Acero, Juan Luis; Rosa, Maria João (2016): Investigating PPCP Removal from Wastewater by Powdered Activated Carbon/Ultrafiltration. In *Water Air Soil Pollut* 227 (6), p. 139. DOI: 10.1007/s11270-016-2870-7.

Rodriguez-Mozaz, Sara; Chamorro, Sara; Marti, Elisabet; Huerta, Belinda; Gros, Meritxell; Sànchez-Melsió, Alexandre et al. (2015): Occurrence of antibiotics and antibiotic resistance genes in hospital and urban wastewaters and their impact on the receiving river. In *Water Research* 69, pp. 234–242. DOI: 10.1016/j.watres.2014.11.021.

Rosa, Lorenzo; Rulli, Maria Cristina; Davis, Kyle Frankel; Chiarelli, Davide Danilo; Passera, Corrado; D'Odorico, Paolo (2018): Closing the yield gap while ensuring water sustainability. In *Environ. Res. Lett.* 13 (10), p. 104002. DOI: 10.1088/1748-9326/aadeef.

RUF (2006): Regierung von Unterfranken: Trinkwasserversorgung in Unterfranken.

RUF (2010): Regierung von Unterfranken: Wasserversorgungsbilanz Unterfranken 2025 - I Bericht. Available online at https://www.regierung.unterfranken.bayern.de/assets/6/3/wvb_unterfranken_teil_i_bericht_klein.pdf, checked on 8/30/2018.

Rusiñol, Marta; Hundesa, Ayalkibet; Cárdenas-Youngs, Yexenia; Fernández-Bravo, Ana; Pérez-Cataluña, Alba; Moreno-Mesonero, Laura et al. (2020): Microbiological contamination of conventional and reclaimed irrigation water: Evaluation and management measures. In *The Science of the total environment* 710, p. 136298. DOI: 10.1016/j.scitotenv.2019.136298.

Santos, Martha; Oliveira, Helena; Pereira, Joana L.; Pereira, Mário J.; Gonçalves, Fernando J.M.; Vidal, Tânia (2019): Flow cytometry analysis of low/high DNA content (LNA/HNA) bacteria as bioindicator of water quality evaluation. In *Ecological Indicators* 103, pp. 774–781. DOI: 10.1016/j.ecolind.2019.03.033.

Sanz, Laura Alcalde; Gawlik, Bernd Manfred (2014): Water reuse in Europe. In *Relevant guidelines, needs for and barriers to innovation. A synoptic overview, European Commission, Joint Research Centre and Institute for Environment and Sustainability, Ispra*.

Savva, A. P.; Frenken, K.; Sunguro, S.; Tirivamwe, L. (2002): Irrigation manual: planning, development monitoring and evaluation of irrigated agriculture with farmer participation. Available online at ftp://ftp.fao.org/docrep/fao/010/ai596e/ai596e.pdf.

Scheurer, Marco; Godejohann, Markus; Wick, Arne; Happel, Oliver; Ternes, Thomas A.; Brauch, Heinz-Jürgen et al. (2012): Structural elucidation of main ozonation products of the artificial sweeteners cyclamate and acesulfame. In *Environmental science and pollution research international* 19 (4), pp. 1107–1118. DOI: 10.1007/s11356-011-0618-x.

Schijven, Jack F.; Hassanizadeh, S. Majid (2000): Removal of Viruses by Soil Passage: Overview of Modeling, Processes, and Parameters. In *Critical Reviews in Environmental Science and Technology* 30 (1), pp. 49–127. DOI: 10.1080/10643380091184174.

Schmitz, Philippe; Prat, Marc (1995): 3-D Laminar stationary flow over a porous surface with suction: Description at pore level. In *AIChE J.* 41 (10), pp. 2212–2226. DOI: 10.1002/aic.690411005.

Schüßler, Walter (2017): Arzneimittelwirkstoffe, Metaboliten und polare Spurenstoffe in Abwasser, Oberflächengewässern und Uferfiltrat: Ergebnisse 2004–2015. Available online at https://www.bestellen.bayern.de/application/eshop_app000000?SID=1338668297&ACTIONxSESSxSHOWPIC(BILDxKEY:%27lfu_all_00145%27,BILDxCLASS:%27Artikel%27,BILDxTYPE:%27PDF%27).

Schwaller, Christoph; Fokkens, Kevin; Helmreich, Brigitte; Drewes, Jörg E. (2022): CFD simulations of flow fields during ultrafiltration: Effects of hydrodynamic strain rates with and without a particle cake layer on the permeation of mobile genetic elements. In *Chemical Engineering Science* 254, p. 117606. DOI: 10.1016/j.ces.2022.117606.

Schwaller, Christoph; Helmreich, Brigitte; Gerdes, H.; Drewes, Jörg E. (2020): Abschlussbericht: Forschungsvorhaben „Nutzwasser – Gewinnung und Einsatzmöglichkeiten am Beispiel der Schweinfurter Trockenplatte" (AZ: 52-4429-10).

Schwaller, Christoph; Hoffmann, Grit; Hiller, Christian X.; Helmreich, Brigitte; Drewes, Jörg E. (2021): Inline dosing of powdered activated carbon and coagulant prior to ultrafiltration at pilot-scale – Effects on trace organic chemical removal and operational stability. In *Chemical Engineering Journal* 414, p. 128801. DOI: 10.1016/j.cej.2021.128801.

Seidel, S. J.; Barfus, K.; Gaiser, T.; Nguyen, T. H.; Lazarovitch, N. (2019): The influence of climate variability, soil and sowing date on simulation-based crop coefficient curves and irrigation water demand. In *Agricultural Water Management* 221, pp. 73–83. DOI: 10.1016/j.agwat.2019.02.007.

Seis, W.; Lesjean, B.; Maaßen, S.; Balla, D.; Hochstrat, R.; Düppenbecker, B. (2016): Rahmenbedingungen für die umweltgerechte Nutzung von behandeltem Abwasser zur landwirtschaftlichen Bewässerung. In *Umweltforschungsplan des Bundesministeriums für Umwelt, Naturschutz, Bau und Reaktorsicherheit*, p. 196. Available online at https://www.umweltbundesamt.de/sites/default/files/medien/378/publikationen/texte_34_2016_rahmenbedingungen_fuer_die_umweltgerechte_nutzung_von_behandeltem_abwasser_0.pdf, checked on 6/19/2020.

Selinka, H-C; Botzenhart, K.; Feuerpfeil, I.; Puchert, W.; Schmoll, O.; Szewzyk, R.; Willmitzer, H. (2011): Nachweis von Viren im Rohwasser als Grundlage einer Risikoabschätzung. In *Bundesgesundheitsblatt, Gesundheitsforschung, Gesundheitsschutz* 54 (4), pp. 496–504. DOI: 10.1007/s00103-011-1249-6.

Sharma, Priyamvada; Poustie, Andrew; Verburg, Paul; Pagilla, Krishna; Yang, Yu; Hanigan, David (2020): Trace organic contaminants in field-scale cultivated alfalfa, soil, and pore water after 10 years of irrigation with reclaimed wastewater. In *The Science of the total environment* 744, p. 140698. DOI: 10.1016/j.scitotenv.2020.140698.

Shen, Yanjun; Li, Shuo; Chen, Yaning; Qi, Yongqing; Zhang, Shuowei (2013): Estimation of regional irrigation water requirement and water supply risk in the arid region of Northwestern China 1989–2010. In *Agricultural Water Management* 128, pp. 55–64. DOI: 10.1016/j.agwat.2013.06.014.

Sheng, Chenguang; Nnanna, A. AgwuG.; Liu, Yanghe; Vargo, John D. (2016): Removal of Trace Pharmaceuticals from Water using coagulation and powdered activated carbon as pretreatment to ultrafiltration membrane system. In *Science of The Total Environment* 550, pp. 1075–1083. DOI: 10.1016/j.scitotenv.2016.01.179.

Shi, Yan; Yang, Guofu; Du, Yuanyuan; Ren, Yuan; Lu, Yijun; Fan, Likun et al. (2018): Estimating irrigation water demand for green spaces in humid areas: seeking a sustainable water management strategy. In *Urban Water Journal* 15 (1), pp. 16–22. DOI: 10.1080/1573062X.2017.1363255.

Shishkina, Natalia; Hannelly, Toni; Rodriguez, Clemencia (2012): Water recycling in Western Australia: analysis of 2003–2009 water quality monitoring programme. In *Journal of Water Supply: Research and Technology-Aqua* 61 (8), pp. 463–472. DOI: 10.2166/aqua.2012.046.

Sigala, J.; Unc, A. (2012): A PCR-DGGE approach to evaluate the impact of wastewater source on the antibiotic resistance diversity in treated wastewater effluent. In *Water Science and Technology* 65 (7), pp. 1323–1331. DOI: 10.2166/wst.2012.024.

Simon, S.; Krause, H. J.; Weber, C.; Peukert, W. (2011): Physical degradation of proteins in well-defined fluid flows studied within a four-roll apparatus. In *Biotechnology and bioengineering* 108 (12), pp. 2914–2922. DOI: 10.1002/bit.23257.

Singh, Harpreet; Myong, Rho Shin (2018): Critical Review of Fluid Flow Physics at Micro- to Nano-scale Porous Media Applications in the Energy Sector. In *Advances in Materials Science and Engineering* 2018, pp. 1–31. DOI: 10.1155/2018/9565240.

Singh, Rajindar (2015): Introduction to Membrane Technology. In : Membrane Technology and Engineering for Water Purification: Elsevier, pp. 1–80.

Slater, J. W. (2008): Tutorial on CFD Verification & Validation. Available online at https://www.grc.nasa.gov/WWW/wind/valid/tutorial/tutorial.html, updated on 4/20/2021, checked on 4/20/2021.

Slipko, Katarzyna; Reif, Daniela; Wögerbauer, Markus; Hufnagl, Peter; Krampe, Jörg; Kreuzinger, Norbert (2019): Removal of extracellular free DNA and antibiotic resistance genes from water and wastewater by membranes ranging from microfiltration to reverse osmosis. In *Water Research* 164, p. 114916. DOI: 10.1016/j.watres.2019.114916.

Smith, D. E.; Babcock, H. P.; Chu, S. (1999): Single-polymer dynamics in steady shear flow. In *Science (New York, N.Y.)* 283 (5408), pp. 1724–1727. DOI: 10.1126/science.283.5408.1724.

Smith, Martin (1992): CROPWAT: A computer program for irrigation planning and management: Food & Agriculture Org (46). Available online at https://books.google.it/books?id=p9tB2ht47NAC&pg=PP1&source=kp_read_button&redir_esc=y#v=onepage&q&f=false.

Snoeyink, V. L.; Campos, C.; Mariñas, B. J. (2000): Design and performance of powdered activated carbon/ultrafiltration systems. In *Water Science and Technology* 42 (12), pp. 1–10. DOI: 10.2166/wst.2000.0228.

Snyder, Shane A.; Adham, Samer; Redding, Adam M.; Cannon, Fred S.; DeCarolis, James; Oppenheimer, Joan et al. (2007): Role of membranes and activated carbon in the removal of endocrine disruptors and pharmaceuticals. In *Desalination* 202 (1-3), pp. 156–181. DOI: 10.1016/j.desal.2005.12.052.

Spieler, Martin; Muffler, Lukas; Drewes, Jörg E. (2021a): Wasserrechtliche Rahmenbedingungen der Wasserwiederverwendung in Deutschland - Teil 2: Rechtliche Anforderungen 68. DOI: 10.3242/kae2020.12.004.

Spieler, Martin; Muffler, Lukas; Drewes, Jörg E. (2021b): Wasserrechtliche Rahmenbedingungen der Wasserwiederverwendung in Deutschland - Teil 3: Gewässerveränderungen des Grundwassers 68. DOI: 10.3242/kae2021.03.005.

Stoll, C.; Sidhu, J. P. S.; Tiehm, A.; Toze, S. (2012): Prevalence of clinically relevant antibiotic resistance genes in surface water samples collected from Germany and Australia. In *Environ. Sci. Technol.* 46 (17), pp. 9716–9726. DOI: 10.1021/es302020s.

Stoquart, Céline; Servais, Pierre; Bérubé, Pierre R.; Barbeau, Benoit (2012): Hybrid Membrane Processes using activated carbon treatment for drinking water: A review. In *Journal of Membrane Science* 411-412, pp. 1–12. DOI: 10.1016/j.memsci.2012.04.012.

Strudgeon, George E.; Lewis, Brian J.; Albury, W. W.; Clinger, R. C. (1980): Safety considerations in handling activated carbon. In *Journal (Water Pollution Control Federation)*, pp. 2516–2522.

Suchecka, Teresa; Biernacka, Elzbieta; Piatkiewicz, Wojciech (2003): Microorganism Retention on Microfiltration Membranes. In *Filtration & Separation* 40 (8), pp. 50–55. DOI: 10.1016/S0015-1882(03)00830-9.

Sui, Qian; Cao, Xuqi; Lu, Shuguang; Zhao, Wentao; Qiu, Zhaofu; Yu, Gang (2015): Occurrence, sources and fate of pharmaceuticals and personal care products in the groundwater: A review. In *Emerging Contaminants* 1 (1), pp. 14–24. DOI: 10.1016/j.emcon.2015.07.001.

Sun, Lihua; He, Ning; Yu, Tianmin; Duan, Xi; Feng, Cuimin; Zhang, Yajun (2017): The removal of typical pollutants in secondary effluent by the combined process of powdered activated carbon-ultrafiltration. In *Water Science and Technology* 75 (5-6), pp. 1485–1493. DOI: 10.2166/wst.2017.016.

Sun, Wen; Liu, Junxia; Chu, Huaqiang; Dong, Bingzhi (2013): Pretreatment and membrane hydrophilic modification to reduce membrane fouling. In *Membranes* 3 (3), pp. 226–241. DOI: 10.3390/membranes3030226.

Szczepanowski, Rafael; Linke, Burkhard; Krahn, Irene; Gartemann, Karl-Heinz; Gützkow, Tim; Eichler, Wolfgang et al. (2009): Detection of 140 clinically relevant antibiotic-resistance genes in the plasmid metagenome of wastewater treatment plant bacteria showing reduced susceptibility to selected antibiotics. In *Microbiology (Reading, England)* 155 (Pt 7), pp. 2306–2319. DOI: 10.1099/mic.0.028233-0.

Ternes, T. (2007a): The occurrence of micopollutants in the aquatic environment: a new challenge for water management. In *Water Science and Technology* 55 (12), pp. 327–332. DOI: 10.2166/wst.2007.428.

Ternes, Thomas A.; Bonerz, Matthias; Herrmann, Nadine; Teiser, Bernhard; Andersen, Henrik Rasmus (2007b): Irrigation of treated wastewater in Braunschweig, Germany: an option to remove pharmaceuticals and musk fragrances. In *Chemosphere* 66 (5), pp. 894–904. DOI: 10.1016/j.chemosphere.2006.06.035.

Thomas, Christopher M.; Nielsen, Kaare M. (2005): Mechanisms of, and barriers to, horizontal gene transfer between bacteria. In *Nature reviews. Microbiology* 3 (9), pp. 711–721. DOI: 10.1038/nrmicro1234.

Thompson, Kyle A.; Shimabuku, Kyle K.; Kearns, Joshua P.; Knappe, Detlef R. U.; Summers, R. Scott; Cook, Sherri M. (2016): Environmental Comparison of Biochar and Activated Carbon for Tertiary Wastewater Treatment. In *Environ. Sci. Technol.* 50 (20), pp. 11253–11262. DOI: 10.1021/acs.est.6b03239.

Trinh, Long Thi; Duong, Chinh Cong; van der Steen, Peter; Lens, Piet N.L. (2013): Exploring the potential for wastewater reuse in agriculture as a climate change adaptation measure for Can Tho City, Vietnam. In *Agricultural Water Management* 128, pp. 43–54. DOI: 10.1016/j.agwat.2013.06.003.

Trinkwasserverordnung (2020): Verordnung über die Qualität von Wasser für den menschlichen Gebrauch. Available online at https://www.gesetze-im-internet.de/trinkwv_2001/TrinkwV.pdf, checked on 7/10/2020.

Tsurumi, Takashi; Sato, Tetsuo; Osawa, Naoki; Hitaka, Hidetoshi; Hirasaki, Tomoko; Yamaguchi, Kazuhito et al. (1990): Structure and Filtration Performances of Improved Cuprammonium Regenerated Cellulose Hollow Fiber (Improved BMM Hollow Fiber) for Virus Removal. In *Polym J* 22 (12), pp. 1085–1100. DOI: 10.1295/polymj.22.1085.

UBA (2021a): Neue EU-Verordnung zu Wasserwiederverwendung. Available online at https://www.umweltbundesamt.de/themen/wasser/wasser-bewirtschaften/wasserwiederverwendung/neue-eu-verordnung-zu-wasserwiederverwendung#undefined, checked on 5/3/2022.

UBA (2021b): New EU Regulation on Minimum Requirements for Water Reuse. Available online at https://www.umweltbundesamt.de/en/topics/water/water-resource-management/water-reuse/new-eu-regulation-on-minimum-requirements-for-water#objectives-and-core-elements-of-the-eu-regulation, checked on 6/17/2022.

UBA (2021c): Wasserwiederverwendung. Available online at https://www.umweltbundesamt.de/themen/wasser/wasser-bewirtschaften/wasserwiederverwendung#nutzung-aufbereiteten-wassers-zur-ressourcenschonung-in-der-europaischen-union, checked on 5/3/2022.

UN (2015): Transforming our world: the 2030 Agenda for Sustainable Development. Resolution adopted by the General Assembly on 25 September 2015. Available online at https://www.un.org/en/development/desa/population/migration/generalassembly/docs/globalcompact/A_RES_70_1_E.pdf, checked on 10/6/2020.

UN (2021): Summary Progress Update 2021: SDG 6 — water and sanitation for all. Available online at https://www.unwater.org/app/uploads/2021/12/SDG-6-Summary-Progress-Update-2021_Version-July-2021a.pdf, checked on 5/10/2022.

UN Programme, International Resource Panel (2015): Options for Decoupling Economic Growth from Water Use and Water Pollution: A Report of the Water Working Group of the International Resource Panel - Summary for Policy Makers. Available online at https://wedocs.unep.org/20.500.11822/7539, checked on 5/10/2022.

UNESCO (2020): United Nations World Water Development Report 2020: Water and Climate Change: UNESCO, Paris https://en. unesco. org/themes/water-security/wwap/wwdr.

Urkiaga, A.; las Fuentes, L. de; Bis, B.; Chiru, E.; Balasz, B.; Hernández, F. (2008): Development of analysis tools for social, economic and ecological effects of water reuse. In *Desalination* 218 (1-3), pp. 81–91. DOI: 10.1016/j.desal.2006.08.023.

US EPA 600-R-12-618: US Environmental Protection Agency: Guidelines for Water Reuse.

van den Berg, G. B.; Smolders, C. A. (1990): Flux decline in ultrafiltration processes. In *Desalination* 77, pp. 101–133. DOI: 10.1016/0011-9164(90)85023-4.

van der Bruggen, Bart; Vandecasteele, Carlo; van Gestel, Tim; Doyen, Wim; Leysen, Roger (2003): A review of pressure-driven membrane processes in wastewater treatment and drinking water production. In *Environ. Prog.* 22 (1), pp. 46–56. DOI: 10.1002/ep.670220116.

van Houtte, Emmanuel; Verbauwhede, Johan (2012): Sustainable groundwater management using reclaimed water: the Torreele/St-André case in Flanders, Belgium. In *Journal of Water Supply: Research and Technology-Aqua* 61 (8), p. 473.

van Vliet, Michelle T.H.; Flörke, Martina; Wada, Yoshihide (2017): Quality matters for water scarcity. In *Nature Geosci* 10 (11), pp. 800–802. DOI: 10.1038/ngeo3047.

Velten, Silvana (2008): Adsorption capacity and biological activity of biological activated carbon filters in drinking water treatment. Available online at https://www.research-collection.ethz.ch/bitstream/handle/20.500.11850/151230/1/eth-41845-01.pdf.

Vieno, Niina M.; Härkki, Heli; Tuhkanen, Tuula; Kronberg, Leif (2007): Occurrence of pharmaceuticals in river water and their elimination in a pilot-scale drinking water treatment plant. In *Environ. Sci. Technol.* 41 (14), pp. 5077–5084. DOI: 10.1021/es062720x.

Vollmer, Derek; Shaad, Kashif; Souter, Nicholas J.; Farrell, Tracy; Dudgeon, David; Sullivan, Caroline A. et al. (2018): Integrating the social, hydrological and ecological dimensions of freshwater health: The Freshwater Health Index. In *The Science of the total environment* 627, pp. 304–313. DOI: 10.1016/j.scitotenv.2018.01.040.

Vörösmarty, C. J.; McIntyre, P. B.; Gessner, M. O.; Dudgeon, D.; Prusevich, A.; Green, P. et al. (2010): Global threats to human water security and river biodiversity. In *Nature* 467 (7315), pp. 555–561. DOI: 10.1038/nature09440.

Wachendorf, Michael; Buerkert, Andreas; Graß, Rüdiger (Eds.) (2018): Ökologische Landwirtschaft. Uni-Taschenbücher GmbH. Stuttgart: Verlag Eugen Ulmer (UTB Agrarwissenschaften Forstwissenschaften Ökologie, 4863).

Wada, Yoshihide; van Beek, L. P. H.; Bierkens, Marc F. P. (2012): Nonsustainable groundwater sustaining irrigation: A global assessment. In *Water Resour. Res.* 48 (6), p. 219. DOI: 10.1029/2011WR010562.

Wang, Rong; Hashimoto, Kazuhito; Fujishima, Akira; Chikuni, Makota; Kojima, Eiichi; Kitamura, Atsushi et al. (1997): Light-induced amphiphilic surfaces. In *Nature* 388 (6641), pp. 431–432. DOI: 10.1038/41233.

Wang, Rongxuan; Matsuura, Norihisa; Hara-Yamamura, Hiroe; Watanabe, Toru; Honda, Ryo (2021): Initial behaviors and removal of extracellular plasmid gene in membrane bioreactor. In *Journal of environmental management* 298, p. 113541. DOI: 10.1016/j.jenvman.2021.113541.

Wang, Z.; Chang, A.C; Wu, L.; Crowley, D. (2003): Assessing the soil quality of long-term reclaimed wastewater-irrigated cropland. In *Geoderma* 114 (3-4), pp. 261–278. DOI: 10.1016/S0016-7061(03)00044-2.

Wang, Zhen; Li, Jiusheng; Li, Yanfeng (2017): Using Reclaimed Water for Agricultural and Landscape Irrigation in China: a Review. In *Irrig. and Drain.* 66 (5), pp. 672–686. DOI: 10.1002/ird.2129.

Water Reuse Europe (2018): Water Reuse Europe Review. Available online at https://www.water-reuse-europe.org/wp-content/uploads/2018/08/wre_review2018_final.pdf, checked on 6/23/2020.

Watts, Darrell G. (1968): Consumptive use and net irrigation requirements for Oregon.

Werner, Julia; Besser, Benjamin; Brandes, Christoph; Kroll, Stephen; Rezwan, Kurosch (2014): Production of ceramic membranes with different pore sizes for virus retention. In *Journal of Water Process Engineering* 4, pp. 201–211. DOI: 10.1016/j.jwpe.2014.10.007.

WHO (2006): Guidelines for the Safe Use of Wastewater, Excreta and Greywater, Volume 4. Excreta and Greywater Use in Agriculture. Geneva: World Health Organization. Available online at http://gbv.eblib.com/patron/FullRecord.aspx?p=284771.

WHO (2014): Antimicrobial resistance: global report on surveillance: World Health Organization.

WHO (2015): Antimicrobial resistance: An emerging water, sanitation and hygiene issue. Available online at http://www.who.int/water_sanitation_health/publications/antimicrobial-resistance/en/, checked on 10/19/2018.

WHO (2017): Guidelines for drinking-water quality. Fourth edition incorporating the first addendum. Geneva: World Health Organization.

WHO (2020): Antimicrobial resistance. Available online at https://www.who.int/news-room/fact-sheets/detail/antimicrobial-resistance, updated on 3/30/2021, checked on 4/20/2021.

Wick, Charles; Patrick, McCubbin (1999a): Passage of MS2 bacteriophage through various molecular weight filters. In *Toxicology Methods* 9 (4), pp. 265–273. DOI: 10.1080/105172399242618.

Wick, Charles; Patrick, McCubbin (1999b): Passage of MS2 bacteriophages through various molecular weight filters. In *Toxicology Methods* 9 (4), pp. 265–273. DOI: 10.1080/105172399242618.

Wirtschaftliche Vereinigung Zucker e.V. (2020): Aussaat und Wachstum. Available online at https://www.zuckerverbaende.de/ruebe-zucker/von-der-ruebe-zum-zucker/die-zuckerruebe/aussaat-und-wachstum.html, updated on 4/3/2020, checked on 4/3/2020.

Worch, Eckhard (2012): Adsorption technology in water treatment: fundamentals, processes, and modeling: Walter de Gruyter. Available online at https://vancuaphai.com/pic/FileLibrary/Adsorptio_636815213382331503.pdf, checked on 7/13/2020.

WRI (2019): World Resources Institute: WIR-Aquaduct. Washington, D.C. Available online at https://www.wri.org/blog/2019/08/17-countries-home-one-quarter-world-population-face-extremely-high-water-stress, checked on 5/2/2022.

Wriedt, Gunter; van der Velde, Marijn; Aloe, Alberto; Bouraoui, Fayçal (2009): Estimating irrigation water requirements in Europe. In *Journal of Hydrology* 373 (3-4), pp. 527–544. DOI: 10.1016/j.jhydrol.2009.05.018.

Wright, James L.; Jensen, Marvin E. (1972): Peak water requirements of crops in southern Idaho. In *Proceedings of the American Society of Civil Engineers, Journal of the Irrigation and Drainage Division* 98 (IR2), pp. 193–201.

Wu, Chenxi; Witter, Jason D.; Spongberg, Alison L.; Czajkowski, Kevin P. (2009): Occurrence of selected pharmaceuticals in an agricultural landscape, western Lake Erie basin. In *Water Research* 43 (14), pp. 3407–3416. DOI: 10.1016/j.watres.2009.05.014.

Wu, Keliu; Chen, Zhangxin; Li, Jing; Li, Xiangfang; Xu, Jinze; Dong, Xiaohu (2017a): Wettability effect on nanoconfined water flow. In *Proceedings of the National Academy of Sciences of the United States of America* 114 (13), pp. 3358–3363. DOI: 10.1073/pnas.1612608114.

Wu, Ray-Shyan; Liu, Jih-Shun; Chang, Sheng-Yu; Hussain, Fiaz (2017b): Modeling of Mixed Crop Field Water Demand and a Smart Irrigation System. In *Water* 9 (11), p. 885. DOI: 10.3390/w9110885.

Xu, Jian; Wu, Laosheng; Chang, Andrew C.; Zhang, Yuan (2010): Impact of long-term reclaimed wastewater irrigation on agricultural soils: a preliminary assessment. In *Journal of Hazardous Materials* 183 (1-3), pp. 780–786. DOI: 10.1016/j.jhazmat.2010.07.094.

Yan, Zhongsen; Liu, Bin; Qu, Fangshu; an Ding; Liang, Heng; Zhao, Yan; Li, Guibai (2017): Control of ultrafiltration membrane fouling caused by algal extracellular organic matter (EOM) using enhanced Al coagulation with permanganate. In *Separation and Purification Technology* 172, pp. 51–58. DOI: 10.1016/j.seppur.2016.07.054.

Yavich, Alex A.; Lee, Kyung-Hyuk; Chen, Kuan-Chung; Pape, Lars; Masten, Susan J. (2004): Evaluation of biodegradability of NOM after ozonation. In *Water Research* 38 (12), pp. 2839–2846. DOI: 10.1016/j.watres.2004.03.040.

Yoo, Sung (2018): Operating Cost Reduction of In-line Coagulation/Ultrafiltration Membrane Process Attributed to Coagulation Condition Optimization for Irreversible Fouling Control. In *Water* 10 (8), p. 1076. DOI: 10.3390/w10081076.

Yoon, Yeomin; Westerhoff, Paul; Snyder, Shane A.; Wert, Eric C. (2006): Nanofiltration and ultrafiltration of endocrine disrupting compounds, pharmaceuticals and personal care products. In *Journal of Membrane Science* 270 (1-2), pp. 88–100. DOI: 10.1016/j.memsci.2005.06.045.

Yoon, Yeomin; Westerhoff, Paul; Snyder, Shane A.; Wert, Eric C.; Yoon, Jaekyung (2007): Removal of endocrine disrupting compounds and pharmaceuticals by nanofiltration and ultrafiltration membranes. In *Desalination* 202 (1-3), pp. 16–23.

Yu, Chenghui; Gao, Baoyu; Wang, Wenyu; Xu, Xing; Yue, Qinyan (2019): Alleviating membrane fouling of modified polysulfone membrane via coagulation pretreatment/ultrafiltration hybrid process. In *Chemosphere* 235, pp. 58–69. DOI: 10.1016/j.chemosphere.2019.06.146.

Yu, Wenzheng; Xu, Lei; Qu, Jiuhui; Graham, Nigel (2014): Investigation of pre-coagulation and powder activate carbon adsorption on ultrafiltration membrane fouling. In *Journal of Membrane Science* 459, pp. 157–168. DOI: 10.1016/j.memsci.2014.02.005.

Yu, Wen-zheng; Graham, Nigel; Liu, Hui-juan; Qu, Jiu-hui (2013): Comparison of FeCl3 and alum pre-treatment on UF membrane fouling. In *Chemical Engineering Journal* 234, pp. 158–165. DOI: 10.1016/j.cej.2013.08.105.

Yuan, S. W.; Finkelstein, A. (1955): Laminar pipe flow with injection and suction through a porous wall. Fort Belvoir, VA. Available online at https://apps.dtic.mil/dtic/tr/fulltext/u2/058831.pdf, checked on 4/20/2021.

Yuan, Wei; Zydney, Andrew L. (2000): Humic Acid Fouling during Ultrafiltration. In *Environ. Sci. Technol.* 34 (23), pp. 5043–5050. DOI: 10.1021/es0012366.

Zambrano-Vaca, Carlos; Zotarelli, Lincoln; Beeson, Richard C.; Morgan, Kelly T.; Migliaccio, Kati W.; Chaparro, José X.; Olmstead, Mercy A. (2020): Determining water requirements for young peach trees in a humid subtropical climate. In *Agricultural Water Management* 233, p. 106102. DOI: 10.1016/j.agwat.2020.106102.

Zarei-Baygi, Ali; Smith, Adam L. (2021): Intracellular versus extracellular antibiotic resistance genes in the environment: Prevalence, horizontal transfer, and mitigation strategies. In *Bioresource technology* 319, p. 124181. DOI: 10.1016/j.biortech.2020.124181.

Zemann, M.; Majewsky, M.; Wolf, L. (2016): Accumulation of pharmaceuticals in groundwater under arid climate conditions - Results from unsaturated column experiments. In *Chemosphere* 154, pp. 463–471. DOI: 10.1016/j.chemosphere.2016.03.136.

Zhang, Jianan; Lin, Tao; Chen, Wei (2017): Micro-flocculation/sedimentation and ozonation for controlling ultrafiltration membrane fouling in recycling of activated carbon filter backwash water. In *Chemical Engineering Journal* 325, pp. 160–168. DOI: 10.1016/j.cej.2017.05.077.

Zhang, Qinqin; Jia, Ai; Wan, Yi; Liu, Hong; Wang, Kunping; Peng, Hui et al. (2014): Occurrences of three classes of antibiotics in a natural river basin: association with antibiotic-resistant Escherichia coli. In *Environ. Sci. Technol.* 48 (24), pp. 14317–14325. DOI: 10.1021/es503700j.

Zheng, Xing; Plume, Stephan; Ernst, Mathias; Croué, Jean-Philippe; Jekel, Martin (2012): In-line coagulation prior to UF of treated domestic wastewater – foulants removal, fouling control and phosphorus removal. In *Journal of Membrane Science* 403-404, pp. 129–139. DOI: 10.1016/j.memsci.2012.02.051.

Zhuang, Yao; Ren, Hongqiang; Geng, Jinju; Zhang, Yingying; Zhang, Yan; Ding, Lili; Xu, Ke (2015): Inactivation of antibiotic resistance genes in municipal wastewater by chlorination, ultraviolet, and ozonation disinfection. In *Environmental science and pollution research international* 22 (9), pp. 7037–7044. DOI: 10.1007/s11356-014-3919-z.

Zietzschmann, Frederik; Worch, Eckhard; Altmann, Johannes; Ruhl, Aki Sebastian; Sperlich, Alexander; Meinel, Felix; Jekel, Martin (2014): Impact of EfOM size on competition in activated carbon adsorption of organic micro-pollutants from treated wastewater. In *Water Research* 65, pp. 297–306. DOI: 10.1016/j.watres.2014.07.043.

Zimmerman, Julie Beth; Mihelcic, James R.; Smith, James (2008): Global stressors on water quality and quantity. In *Environ. Sci. Technol.* 42 (12), pp. 4247–4254. DOI: 10.1021/es0871457.

Zinkernagel, Jana; Weinheimer, Sebastian; Mayer, Norbert (2017): Wasserbedarf von Freilandgemüsekulturen. Available online at https://www.hortigate.de/bericht?nr=73862, checked on 4/20/2020.

Ziska, Austin D.; Park, Minkyu; Anumol, Tarun; Snyder, Shane A. (2016): Predicting trace organic compound attenuation with spectroscopic parameters in powdered activated carbon processes. In *Chemosphere* 156, pp. 163–171. DOI: 10.1016/j.chemosphere.2016.04.073.

Zucker, I.; Mamane, H.; Cikurel, H.; Jekel, M.; Hübner, U.; Avisar, D. (2015): A hybrid process of biofiltration of secondary effluent followed by ozonation and short soil aquifer treatment for water reuse. In *Water Research* 84, pp. 315–322. DOI: 10.1016/j.watres.2015.07.034.